



Aramco  
Journal  
of Technology

SUMMER 20  
21

---

page 2 /

**A Novel Approach to Improve Acid Diversion Utilizing  
In Situ Foam Generating Fluids**

*Ayman R. Al-Nakhli, Ibrahim M. El-Zefzafy, Danish Ahmed and  
Wassim Kharat*

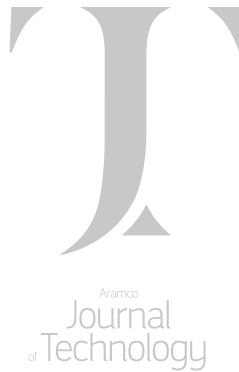
---

page 15 /

**A New Methodology for Calculating Wellbore  
Pressure of Shut-in Wells in Numerical Reservoir  
Simulation**

*Babatope O. Kayode and Dr. Mahmoud Jamiolamahdi*





The *Aramco Journal of Technology* is published quarterly by the Saudi Arabian Oil Company, Dhahran, Saudi Arabia, to provide the company's scientific and engineering communities a forum for the exchange of ideas through the presentation of technical information aimed at advancing knowledge in the hydrocarbon industry.

#### **Management**

##### **Amin Nasser**

President & CEO, Saudi Aramco

##### **Nabeel A. Al-Jama'**

Senior Vice President, HR and Corporate Services

##### **Fahad K. Al Dhubaib**

General Manager, Public Affairs

#### **Editorial Advisors**

##### **Ahmad O. Al-Khowaiter**

Vice President, Technology Oversight and Coordination

##### **Abdullah M. Al-Ghamdi**

Vice President, Gas Operations

##### **Abdul Hameed A. Al-Rushaid**

Vice President, Drilling and Workover

##### **Khalid M. Al-Abdulqader**

Vice President, Unconventional Resources

##### **Khaled A. Al Abdulgader**

Chief Drilling Engineer

##### **Omar S. Al-Husaini**

General Manager, Drilling and Workover Operations

##### **Jamil J. Al-Bagawi**

Chief Engineer

##### **Waleed A. Al Mulhim**

Chief Petroleum Engineer

##### **Ammar A. Al-Nahwi**

Manager, Research and Development Center

##### **Ashraf M. Al-Tahini**

Manager, EXPEC ARC

#### **Editor**

##### **William E. Bradshaw**

[william.bradshaw.1@aramco.com.sa](mailto:william.bradshaw.1@aramco.com.sa)

tel: +966-013-876-0498

#### **Production Coordination**

##### **Richard E. Doughty**

Corporate Publications, Aramco Americas

#### **Design**

##### **Graphic Engine Design Studio**

Austin, Texas, U.S.A.

No articles, including art and illustrations, in the *Aramco Journal of Technology* except those from copyrighted sources, may be reproduced or printed without the written permission of Saudi Aramco. Please submit requests for permission to reproduce items to the editor.

The *Aramco Journal of Technology* gratefully acknowledges the assistance, contribution and cooperation of numerous operating organizations throughout the company.

ISSN 1319-2388

© Copyright 2021 Aramco Services Company, all rights reserved.





# Contents

---

- p. **2** **A Novel Approach to Improve Acid Diversion Utilizing In Situ Foam Generating Fluids**

*Ayman R. Al-Nakhli, Ibrahim M. El-Zefzafy, Danish Ahmed and Wassim Kharrat*

---

- p. **9** **A Deep Learning WAG Injection Method for CO<sub>2</sub> Recovery Optimization**

*Dr. Klemens Katterbauer, Dr. Alberto F. Marsala and Dr. Abdulaziz S. Al Qasim  
Lena Petrozziello, Dr. Christoph Kayser, Dr. Cyril Okocha, Dr. Tao Chen and Dr. Qiwei Wang*

---

- p. **15** **A New Methodology for Calculating Wellbore Pressure of Shut-in Wells in Numerical Reservoir Simulation**

*Babatope O. Kayode and Dr. Mahmoud Jamiolahmady*

---

- p. **24** **Rock Mechanical Characterization of Shale Drilling Fluid Interactions to Mitigate Borehole Instability Problems**

*Dr. Mohammad H. Alqam, Dr. Md. Amanullah, Antonio Santagati, Salem H. Al-Garni,  
Adnan H. Al-Makrami, and Dr. Sinan Caliskan*

---

- p. **34** **Thermochemical Acid Fracturing of Tight and Unconventional Rocks: Experimental and Modeling Investigations**

*Dr. Zeeshan Tariq, Dr. Murtada S. Al-Jawad, Dr. Mohamed Mahmoud,  
Dr. Abdulazeez Abdulraheem and Ayman R. Al-Nakhli*

---

- p. **50** **New Catalyst-free Polycrystalline Diamond with Industry Record Wear Resistance**

*Dr. Guodong Zhan, Dr. Bodong Li, Timothy E. Moellendick, Dr. Duanwei He  
and Dr. Jianhui Xu*

---

- p. **57** **Design Optimization for Hydraulically Driven Agitation Tool in Extended Coiled Tubing Reach Application**

*Hussain A. Al-Saood, Laurie S. Duthie, Ahmed H. Albaqshi and Muhammad Ahsan*

---

- p. **66** **A New Aramco Record in Patents**

*Michael J. Ives*

# A Novel Approach to Improve Acid Diversion Utilizing In Situ Foam Generating Fluids

Ayman R. Al-Nakhli, Ibrahim M. El-Zefzafy, Danish Ahmed and Wassim Kharrat

## Abstract /

Acidizing is a common stimulation treatment in carbonate reservoirs. Acid distribution over all layers and areas around a treated well is crucial for the matrix stimulation success. Effective acidizing, especially for long horizontal wells, requires an acid diverting technique to ensure uniform distribution along the wellbore intervals. Mechanical diversion is costly, while chemical diversion using in situ gelled acid and viscoelastic surfactants (VES) have been widely applied during matrix stimulation. These chemical methods showed not only limited efficiency, but can introduce damage to the treated formation. Several chemical additives and complex formulations are usually used to ensure stability and success of diverting the fluid application. This exercise greatly increases the treatment cost.

This study introduces a novel solution to improve acid diversion using in situ foam generation. Thermochemical fluid is used to generate foam in situ at downhole conditions, which will divert acid stages into non-treated sections of the reservoirs. In this article, two field treatments of two water injector wells — a vertical and a horizontal — were demonstrated using the new system. The in situ foam generating fluid was used to divert acid in several pumping stages to ensure homogenous treatment. The pumping sequence and treatment mechanisms are described.

The results showed that the in situ foam generation approach has a very effective performance in diverting acid, with superior results compared to conventional diversion using a VES. As the new system generates foam downhole, it showed very practical operation procedures. No pumping difficulties are experienced, compared with surface pumping to the foam. Having the reaction activated downhole made the whole treatment safe and user-friendly to apply. Foam can occupy large areas, so less fluid is required to divert the acid stage. No complex formulation was required with several additives to ensure fluid activation downhole, which significantly reduced the overall treatment cost.

The novel method will enable effective and homogenous acidizing of carbonate reservoirs and eliminate the need for VES, which is expensive, and provides a limited effect. This work presents an effective method to place acid uniformly across a treated well using in situ foam generation.

## Introduction

Effective acidizing of carbonate reservoirs requires a diversion mechanism to have a uniform acid treatment along the stimulated interval<sup>1-5</sup>. This is crucial, especially for long horizontal wells. Ineffective diversion will let acid stimulate and propagate into only one area, leaving most of the horizontal section untreated.

There are two types of diversion mechanisms in the industry, either mechanical or chemical. One of the chemical diverting mechanisms is the application of viscoelastic surfactants (VES), which had widely been used as an acid diverter during stimulation treatments. The concept of this application is that VES can chelate with metal ions, such as calcium ions, once neutralized, and when the acidic hydrogen is removed<sup>6-9</sup>.

Figure 1 shows the titration of cationic and amphoteric surfactants in an acidic solution, using hydroxide. When the pH is plotted against the change of pH, the graph will show the neutralization of the VES, and the removal of acidic hydrogen. The titration curve showed that the amphoteric VES had two peaks, as the surfactant actually had two functional groups. The cationic VES had one dominant peak, as the surfactant had only one acidic hydrogen. During actual field application, this neutralization process takes place inside the reservoir, as the acid is spent when reacting with calcium carbonate, and generates calcium chloride (CaCl<sub>2</sub>). The calcium ion (Ca<sup>2+</sup>) will chelate with the VES, and will form a solidified gel<sup>10</sup>.

In actual field treatments, the VES is mixed with hydrochloric (HCl) acid during pumping, with low viscosity. As the acid reacts with carbonate formations, CaCl<sub>2</sub> will be generated, and the pH will increase above 5.0, Fig. 1. As the pH increases, the VES starts to bond to the calcium ions and form a viscous gel, to divert the acid to untreated areas, Fig. 2.

One of the drawbacks of applying a VES is that they can chelate with ferric ions (Fe<sup>3+</sup>) and form sludge, which is a damaging material during pumping. This phenomenon can happen even at acidic solution with a zero

Fig. 1 The acid-based titration of the amphoteric and cationic surfactants<sup>10</sup>.

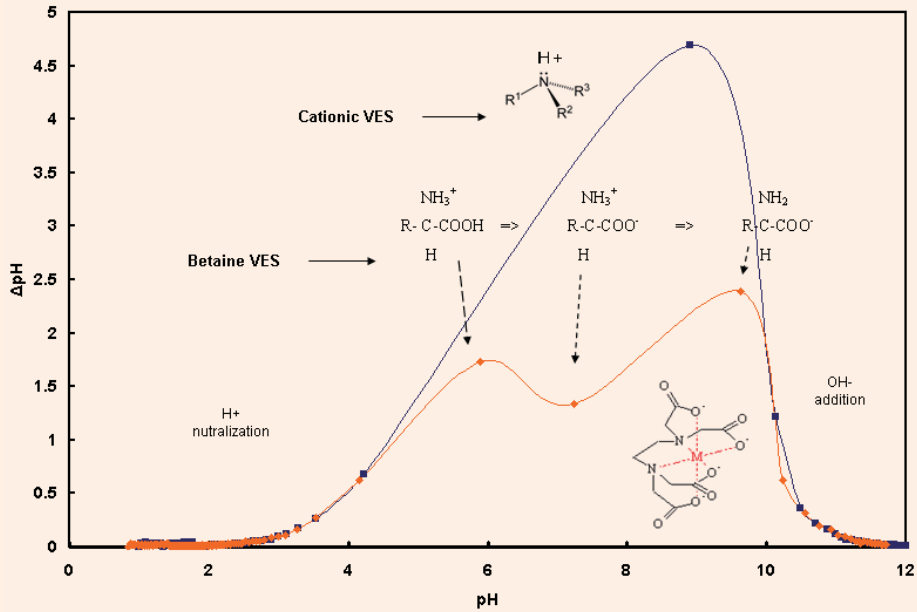


Fig. 2 The cross-linking of the amphoteric VES with calcium carbonate forms a gel.

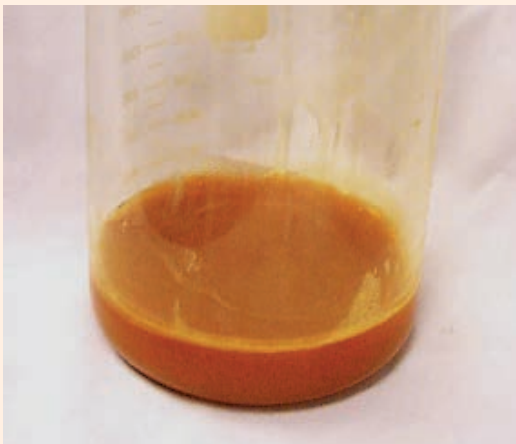


Fig. 3 The cross-linking of the amphoteric VES with corrosion products, Fe (III) forms sludge<sup>10</sup>.



pH. So, corrosion products, such as iron, can chelate with the VES to form a gel, even before spending the acid, at zero pH.

Figure 3 shows the sludge formation out of the VES chelating with Fe<sup>3+</sup>. As a result, not only will no diversion take place, but also the formed sludge material will plug and damage the formation. Several field applications of VES, during acidizing, show limited results. The VES are quite expensive chemicals, and increases the overall stimulation cost<sup>10</sup>.

## Discussion

### In situ Foam Diversion

This study introduces a novel acid diversion method using in situ foam generation chemicals. Thermochemical fluids are pumped with very low viscosity, as a diverting agent, at the end of each acid stage, Fig. 4. A reaction will be activated downhole to generate in situ foam and create high viscous contrast, which will divert new acid stages into the untreated areas, Fig. 5.

Foam can expand, fill, and block large fractures after acidizing, and effectively divert the acid. The VES

**Fig. 4** In situ foam generating system pre-activation.

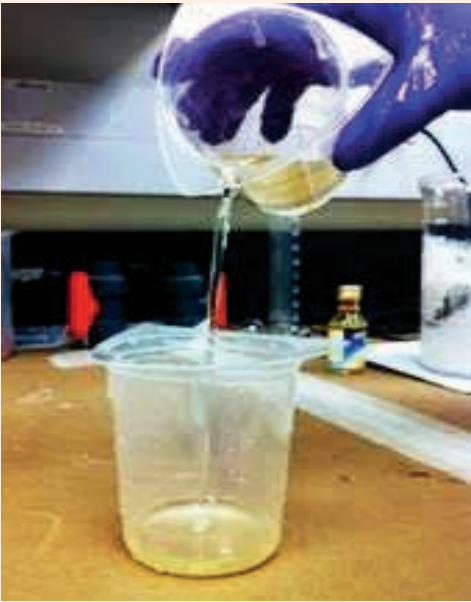


**Fig. 5** Generation of the in situ foam by an activating reaction.



requires large chemical volumes to block the fracture, which is usually unpractical and expensive. One advantage of this method is that foam is not a damaging material and can completely collapse, post-acid treatment. So, neither damaging material nor leftovers are expected, compared to the use of a VES.

Pumping foam from service is also a challenge and not a very practical treatment for service companies. Pumping foam requires high pumping pressure, which sometimes exceeds pumping limitations, as the foam has very low hydrostatic pressure. Therefore, squeezing the foam into a fracture is a challenge. When a thermochemical fluid is used to generate in situ foam, hydrostatic pressure will help with the pumping pressure to squeeze the foam into placed fractures. Not only that, but foam can also be generated inside the fracture. So, from field applications, this method is very practical and showed superior results.

Recording of the distributed temperature sensing (DTS) — during actual well treatment — showed an in situ generation of foam, which forced fluid flow diversion into another interval, Fig. 6. DTS was useful and used as the in situ foam generation system that generated heat, which is detectable by the DTS. The gray lines show the fluid's flow progress — pre-reaction on the left and post-reaction on the right. It is shown that as foam was generated, fluid was diverted from the upper to the lower interval.

#### Treatment of a Vertical Well (Well-A)

Well-A is a water injector in a carbonate formation, which was damaged and requires acidizing. The well is located far from oil producers, in a high-pressurized area. The application of conventional acidizing for 20 years, using VES, showed the injection rate increase

by onefold to twofold, maximum.

When the in situ foam generation system was applied, the well injectivity increased by fivefold, which was unprecedented. During the treatment, a preflush stage was conducted to remove any corrosion products, and organic and inorganic damages. Then, HCl acid was injected in the well, in four stages. After each acid stage, in situ foam generation fluid was injected to provide a uniform distribution of the acid along the vertical well. The injection of an in situ foam system was to divert the new acid stage to a new well interval, Fig. 7.

In situ foam generation was indicated from a slight increase in wellhead pressure. No difficulties were faced during the pumping of the in situ foam generating system. Not only was the stimulation treatment more effective, but also the cost was reduced by 65% compared to the VES applications.

#### Well-A Treatment Sequence

The treatment sequence for Well-A consisted of the following:

A: The pumping of the preflush stage of organic dissolver, HCl acid, and displacement with treated water.

B-1: First stage of pumping in situ foam generation system.

B-2: Second stage of pumping in situ foam generation system.

B-3: Third stage of pumping in situ foam generation system.

C: Pumping three stages of HCl acid.

#### Treatment of a Horizontal Well (Well-B)

Well-B is a horizontal water injection well. Conventional acidizing using VES did not show significant

**Fig. 6** The DTS of in situ foam generation downhole.

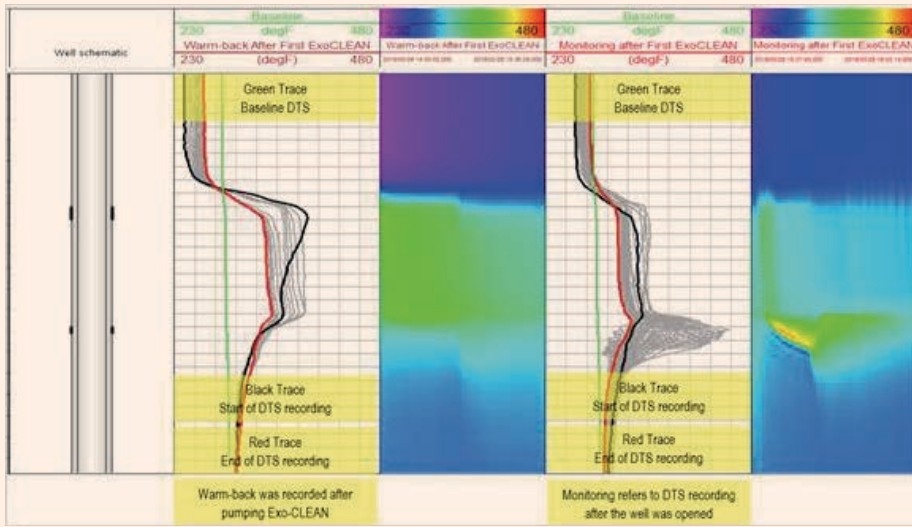


**Fig. 7** The matrix acidizing of a vertical well (Well-A) using an in situ foam generation system.

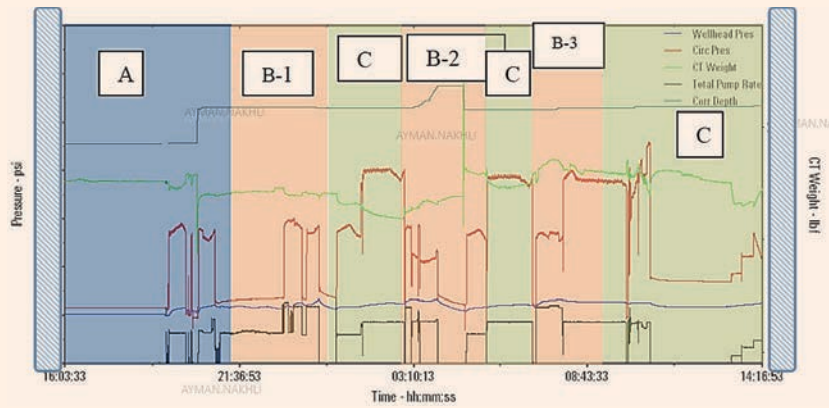


**Fig. 8** The preflush stage of matrix acidizing of a horizontal well (Well-B) using an in situ foam generation system.

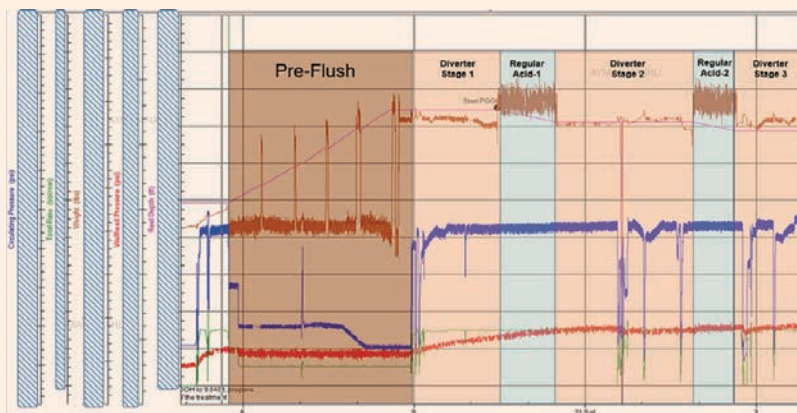
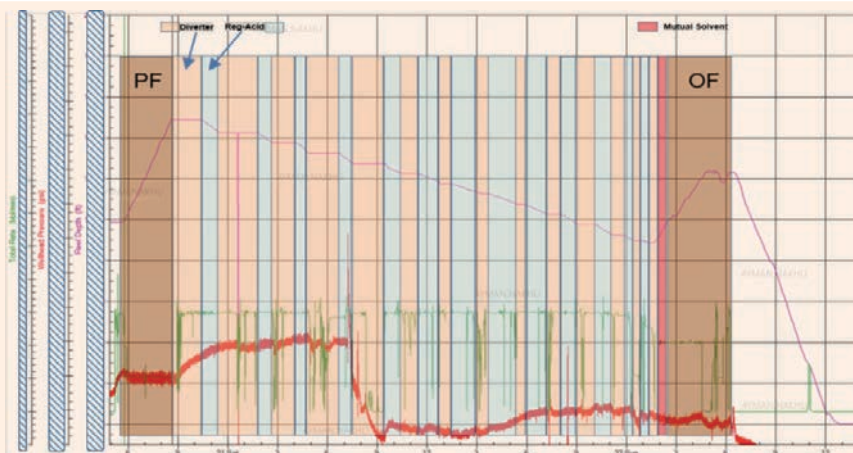




**Fig. 9** The matrix acidizing of a horizontal well (Well-B) using an in situ foam generation system.



improvement to stimulate the well. So, it was decided to apply an in situ foam generating system, as a diverting agent during acidizing. The treatment consisted of 15 stages, including preflush and post-flush. During the preflush, a weak acid was pumped for pickling, and an organic dissolver was pumped for well conditioning, Fig. 8.

Then, alternating stages of acid and an in situ foam generating system were pumped in 13 stages. At each stage, a slight increase in wellhead pressure indicated to the operators the generation of in situ foam, and acid diversion to a new interval, Fig. 9. As shown in Fig. 9, the overall wellhead pressure is decreasing with the progress of the treatment, which indicates the effectiveness of acidizing.

Post-treatment, well injectivity was increased by more

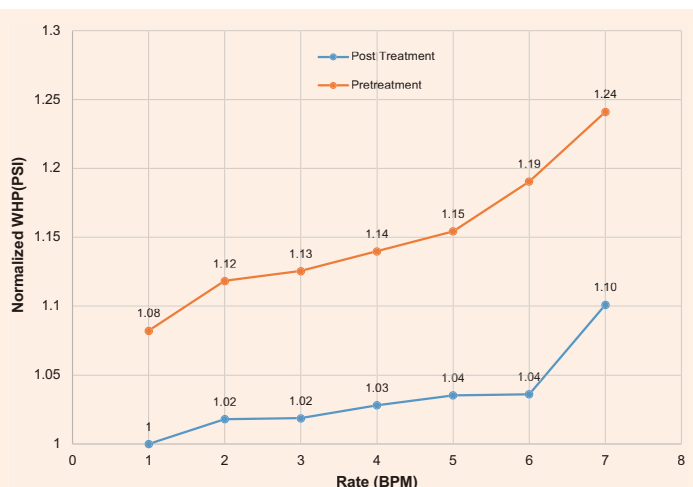
than sevenfold, which is relatively high in horizontal wells. Figure 10 shows normalized injectivity tests pre- and post-treatment. The cost was also reduced by 65% compared to conventional VES acidizing.

## Conclusions

In this study, in situ foam generation fluid was developed as an acid diverter and applied in two water injectors. Based on the results achieved, the following conclusions can be drawn:

- Application of an in situ foam generating system — as a diverting agent — during acidizing was very successful in a vertical and a horizontal well. Well injectivity of the vertical and horizontal wells were increased by fivefold and sevenfold, respectively.
- The new system is friendly without any pumping issues. The treatment is also more cost-effective compared to applying conventional VES as a diverting agent.
- The in situ foam generation fluid generates down-hole foam that invades acidized and high permeability areas, allowing the next acid stage to treat new areas.
- Gas and foam form an excellent diversion mechanism as the foam expands up to 10 times of the original fluid volume. Therefore, less volume will be required to divert the acid fluid to new areas and a uniform stimulation will be achieved.
- Neither damaging material nor residual is left after the foam collapse, leaving an effective stimulated area.
- Generating foam in situ is more practical from an operational point of view compared to the surface pumping of foam. When foam is pumped from the service, high back pressure will be observed in the surface pump. Squeezing foam into the formation is not a very practical step, as foam has a very low hydrostatic pressure. When generating foam downhole, the wellbore is filled with liquid

**Fig. 10** The pretreatment and post-matrix stimulation using an in situ foam generation system.



fluid, where foam is generated downhole. The hydrostatic pressure of the liquid will provide an extra pressure that supports the pumping pressure, which will make it practical to squeeze foam into the stimulated area.

- The in situ generation of foam will eliminate the use of chemical and mechanical diverters, and will significantly reduce treatment cost.
- The application of DTS is practical to monitor acid diversion during in situ foam generation, as the fluid generates heat.

## References

1. Taylor, K.C. and Nasr-El-Din, H.A.: "Laboratory Evaluation of in Situ Gelled Acids for Carbonate Reservoirs," *SPE Journal*, Vol. 8, Issue 4, December 2005, pp. 426-434.
2. MaGee, J., Buijse, M.A. and Pongratz, R.: "Method for Effective Fluid Diversion when Performing a Matrix Acid Stimulation in Carbonate Formations," SPE paper 57756, presented at the Middle East Oil Show and Conference, Manama, Kingdom of Bahrain, March 15-18, 1997.
3. Chang, F., Qu, Q. and Frenier, W.: "A Novel Self-Diverting Acid Developed for Matrix Stimulation of Carbonate Reservoirs," SPE paper 65053, presented at the SPE International Symposium on Oil Field Chemistry, Houston, Texas, February 15-16, 2001.
4. Lungwitz, B., Fredd, C., Brady, M., Miller, M., et al.: "Diversion and Cleanup Studies of Viscoelastic Surfactant-Based Self-Diverting Acid," SPE paper 86504, presented at the SPE International Symposium and Exhibition on Formation Damage Control, Lafayette, Louisiana, February 18-20, 2004.
5. Nasr-El-Din, H.A., Al-Ghamdi, A.H., Al Qahtani, A.A. and Samuel, M.M.: "Impact of Acid Additives on the Rheological Properties of a Viscoelastic Surfactant and their Influence on Field Application," *SPE Journal*, Vol. 15, Issue 1, March 2008, pp. 35-47.
6. Buijse, M.A. and van Domelen, M.S.: "Novel Application of Emulsified Acids to Matrix Stimulation of Heterogeneous Formations," *SPE Production and Facilities*, Vol. 15, Issue 5, August 2000, pp. 208-215.
7. Fadele, O., Zhu, D. and Hill, A.D.: "Matrix Acidizing in Gas Wells," SPE paper 59771, presented at the SPE/CERI Gas Technology Symposium, Calgary, Alberta, Canada, April 5-5, 2000.
8. Nasr-El-Din, H.A., Al-Dirweesh, S. and Samuel, M.M.: "Development and Field Application of a New, Highly Stable Emulsified Acid," SPE paper 115926, presented at the SPE Annual Technical Conference and Exhibition, Denver, Colorado, September 21-24, 2008.
9. Hill, A.D. and Rossen, W.R.: "Fluid Placement and Diversion in Matrix Acidizing," SPE paper 27982, presented at the University of Tulsa Centennial Petroleum Engineering Symposium, Tulsa, Oklahoma, August 29-31, 1994.
10. Al-Nakhli, A.R., Nasr-El-Din, H.A. and Al-Baiyat, I.A.: "Interactions of Iron and Viscoelastic Surfactants: A New Formation Damage Mechanism," SPE paper 112465, presented at the SPE International Symposium and Exhibition on Formation Damage Control, Lafayette, Louisiana, February 15-15, 2008.

---

### About the Authors

#### **Ayman R. Al-Nakhli**

*M.S. in Entrepreneurship for New Business Development, Open University Malaysia*

Ayman R. Al-Nakhli is a Petroleum Scientist in Saudi Aramco's Exploration and Petroleum Engineering Center – Advanced Research Center (EXPEC ARC), where he leads the research program on thermochemicals and develops technologies related to conventional and unconventional reservoirs such as pulse fracturing, stimulation, diverting agents, and heavy oil.

Ayman has developed and field deployed several novel technologies, with four of them being commercialized with international service

companies. He received the World Oil Award for Best Production Chemical in 2015.

Ayman has filed more than 20 patents, published 35 journal papers, and 40 conference papers.

He received his B.S. degree in Industrial Chemistry from King Fahd University of Petroleum and Minerals (KFUPM), Dhahran, Saudi Arabia, and an M.S. degree in Entrepreneurship for New Business Development from Open University Malaysia, Bahrain.

#### **Ibrahim M. El-Zefzafy**

*B.S. in Petroleum Engineering, Al-Azhar University*

Ibrahim M. El-Zefzafy is a Petroleum Engineering Specialist with Saudi Aramco's South Ghawar Production Engineering Division of the Southern Area Production Engineering Department.

He has 26 years of experience in the oil and gas industry in rigless well intervention, oil artificial lift design, well performance and production optimization, well completion and testing, and workover interventions. Ibrahim also has comprehensive well services and production enhancement experience in onshore and offshore operations.

Since joining Saudi Aramco in 2006, he has been involved in a wide variety of technical projects and planning activities as part of oil development and enhanced oil recovery projects. Ibrahim manages a team responsible

for the introduction and implementation of new technology applications, including developing engineered solutions to improve productivity, in collaboration with Saudi Aramco's Exploration and Petroleum Engineering Center – Advanced Research Center (EXPEC ARC) and the Research and Development Center (R&DC).

Prior to joining Saudi Aramco, he worked as a District Production Engineer with Gulf of Suez Petroleum Company's joint venture with BP in Egypt.

Ibrahim is a registered member of the Society of Petroleum Engineers (SPE), and he has authored and coauthored numerous SPE papers.

In 1995, Ibrahim received his B.S. degree in Petroleum Engineering from Al-Azhar University, Cairo, Egypt.

#### **Danish Ahmed**

*M.S. in Petroleum Engineering, Heriot-Watt Institute of Petroleum Engineering*

Danish Ahmed has been working at Saudi Arabia Schlumberger since 2007. He is the technical expert currently working with Schlumberger Well Services – Coiled Tubing Services. Danish's experience involves working as a Field Engineer with Well Production Services (Fracturing and Pumping Services) based in 'Udhailiyah, where he designed, executed and evaluated the proppant/acid

fracturing and matrix acidizing jobs. Danish also worked as a Production Technologist with Petro-Technical Services (formerly called Data and Consulting Services) in Dhahran, Saudi Arabia.

In 2007, he received his M.S. degree in Petroleum Engineering from the Heriot-Watt Institute of Petroleum Engineering, Edinburgh, Scotland, U.K.

#### **Wassim Kharrat**

*M.S. in Mechanical and Industrial Engineering, École Nationale Supérieure d'Arts et Métiers*

Wassim Kharrat has been working with Schlumberger since September 1998 in several countries around the world, including Tunisia, Germany, Libya, the United States and Saudi Arabia. He built his technical and operational expertise in coiled tubing and matrix stimulation. Currently, Wassim is working as a Coiled Tubing District Technical Engineer in 'Udhailiyah

with a focus on introducing and implementing ACTIVE new technology (real-time monitoring with fiber optics) for all types of coiled tubing jobs.

In 1998, he received his M.S. degree in Mechanical and Industrial Engineering from École Nationale Supérieure d'Arts et Métiers (ENSAM), Paris, France.



# A Deep Learning WAG Injection Method for CO<sub>2</sub> Recovery Optimization

*Dr. Klemens Katterbauer, Dr. Alberto F. Marsala and Dr. Abdulaziz S. Al Qasim*

## Abstract /

Carbon dioxide (CO<sub>2</sub>) has some critical technical and economic reasons for its use as an injection gas for oil recovery. CO<sub>2</sub> is very soluble in crude oil at reservoir pressures; it contributes to sweep efficiency enhancement as it swells the oil and significantly reduces its viscosity. Although the mechanism of CO<sub>2</sub> flooding is the same as that for other gases, CO<sub>2</sub> is easier to handle, it is cheaper, and it is an environmentally better candidate than other gases.

The low density of CO<sub>2</sub> relative to the reservoir fluid (oil and water) results in gravity override, whereby the injected CO<sub>2</sub> gravitates toward the top of the reservoir, leaving the bulk of the reservoir uncontacted. This may lead to poor sweep efficiency and poor oil recovery; this criticality can be minimized by alternating CO<sub>2</sub> injection with water or similar chase fluids. This process is known as water alternating gas (WAG).

A major challenge in the optimization of the WAG process is to determine the cycle periods and the injection levels to optimize recovery and production ranges. In this work we present a data-driven approach to optimizing the WAG process for CO<sub>2</sub> enhanced oil recovery (EOR).

The framework integrates a deep learning technique for estimating the output levels of the producer wells from the injection parameters set at the injector wells. The deep learning technique is incorporated into a stochastic nonlinear optimization framework for optimizing the overall oil production over various WAG cycle patterns and injection levels.

The framework was examined on a realistic synthetic field test case with several producer and injection wells. The results were promising, allowing to efficiently optimize various injection scenarios. The results outline a process to optimize CO<sub>2</sub> EOR from the reservoir formation via the utilization of CO<sub>2</sub> as compared to sole water injection.

The novel framework presents a data-driven approach to the WAG injection cycle optimization for CO<sub>2</sub> EOR. The framework can be easily implemented and assists in the pre-selection of various injection scenarios to validate their impact with a full feature reservoir simulation. A similar process may be tailored for other improved oil recovery mechanisms.

## Introduction

Developments in deep learning have profoundly impacted the oil and gas industry, allowing the accurate analyses and interpretation of reservoir data<sup>1,2</sup>. Deep learning and machine learning concern a computers' ability to learn without being explicitly programmed and represents a core area of modern computational techniques. Machine learning can generally be classified into three major categories that distinguish themselves in terms of the response signal available to them.

The three major categories are supervised and unsupervised learning as well as reinforcement learning. Supervised learning is the broadest category and implies that both input and target data may consist of numerical values or string labels, and the responses are known<sup>3</sup>. Nwachuku et al. (2018)<sup>4</sup> presented a supervised XGBoost-based framework for optimizing water alternating gas (WAG) injection and adjusting both controls and injection simultaneously. This allowed them to optimize the economics of the pilot based on adjusting the well location, water and gas injection rates, and production rates. The study's main conclusion was that the data-driven proxy models can capture the dynamics of the reservoir simulation, which provided certainty about the quality of the optimization results.

Supervised learning allows the comparison of the responses to the target labels and learn from the difference to improve the models. Unsupervised learning learns from the data without having available any associated response. The algorithms try to cluster the data to related features and provide more in-depth analysis and correlations between them. The challenge of unsupervised learning is that the feature extraction may depend strongly on the underlying algorithm given the lack of ground truth. Reinforcement learning is a significant area for improving unsupervised learning via providing positive or negative feedback for decisions the algorithms take<sup>5</sup>.

This approach is similar to trial and error and penalizes the estimates for errors. For example, this may be the utilization of different strategies for the choke size opening to optimize production from reservoirs. Recently, semi-supervised learning has attracted significant attention, as there are ways to utilize incomplete training data where some of the target outputs are missing. Machine learning problems may be differentiated into classification, regression, and clustering approaches. Classification requires that the inputs are subdivided into different classes, and the classes have to be known in advance. Regression problems focus on the continuous estimate of outputs from inputs, and clustering requires the division of input into separate groups<sup>6</sup>.

For the challenge of optimizing carbon dioxide (CO<sub>2</sub>) assisted recovery optimization, conventional approaches are to develop a reservoir model and history match the reservoir to the existing production and injection data. While such an approach allows us to accurately model the reservoir structure, the computational time required to run a simulation makes an automatic optimization approach with several hundreds of simulations an infeasibility.

Data-driven approaches utilizing machine learning and artificial intelligence have the advantage of capturing the dynamics in the well production data, while being efficient to be executed. A significant advantage for data-driven approaches is that the biases incorporated by false subsurface modeling or interpretations significantly affecting reservoir simulation results are avoided, and the algorithms solely base their learning on the collected data.

## Methodology

The developed advanced deep learning framework for WAG injection optimization consists of a feedforward neural network that is connected to a genetic algorithm-based integer optimization framework. As displayed in Fig. 1, the framework takes the historical well and reservoir data and then incorporates them into a delay network for the estimation of production

from the producer wells. The arising estimates are then utilized to optimize switching cycles and injection quantities.

The deep learning framework consists of hundreds of fully connected layers and a sigmoid activation function for the forecasting of the production of single wells. The input data for the framework are time series production and injection data, as well as indicator variables for the switching cycle length. A crucial part of the framework is the feedback loop incorporated into the forecasted estimates as the input features' weight factors. To optimize the WAG injection with respect to the deep learning provided — a highly nonlinear objective function — we utilized a modified version of a genetic algorithm for global optimization.

Genetic algorithms are a class of global optimization methods that model the search for a global optimum via a natural evolution process. The optimization process is similar to natural evolution, where the fittest individual is selected for reproduction to produce an offspring of the next generation. The offspring inherits the characteristics of the parent and will be added to the next generation. If the parents' fitness is high, then the offspring will have even better fitness and a better chance at surviving. The process is iterated until a generation is found with the fittest individual.

The algorithm follows five phases that start with the initial population that is evaluated on the fitness function. Based on the results of the fitness function, the selection of the population is then performed, and crossover and mutations are generated to create a new population from it. A crucial part of genetic algorithms is the crossover and mutation that is by its design similar to genes mutating where some of the genes are interchanged. In the framework's case, the mutation is the modification of the injectors' injection quantities and switching cycle.

We examined the framework on a realistic field case with four injector and four producer wells as outlined in Fig. 2. The four injector wells are either gas or water injecting with a maximum capacity of 20,000 bbl or 50 MMscf per day. The maximum injection

**Fig. 1** A framework illustration of the deep learning optimization framework.

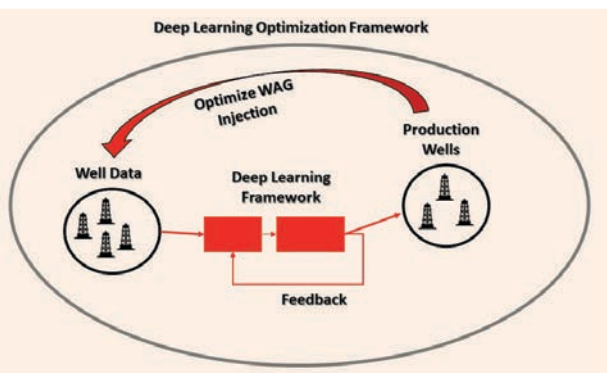
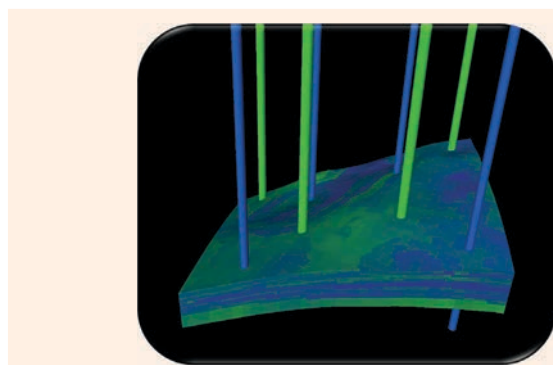


**Fig. 2** A graphical representation of the reservoir and the four injector wells (blue) and the four producer wells (green).



quantities for both CO<sub>2</sub> and water injection are in line with conventionally maximum reachable well limits without experiencing massive well damage even when the well choke is opened 100%. All four producers may produce oil, water, and gas.

A crucial step for optimizing the WAG injection process is developing an accurate deep learning model for relating injection patterns to their corresponding production levels of the producer wells. We employed a neural network for the estimation of production given the injection quantities.

The neural network consists of 100 hidden layers that are fully connected and utilize sigmoid activation functions to estimate production levels. Oil, water, and gas production from all four producer wells are estimated simultaneously, ensuring consistency between the estimates and avoiding potential biases that may occur during the training process. The input layer consists of the injection quantities for CO<sub>2</sub> and water for each of the four injector wells.

The framework is then connected to a genetic algorithm that optimizes the cycle length and injection quantities for each of the injector wells to maximize overall oil production from the reservoir.

## Results

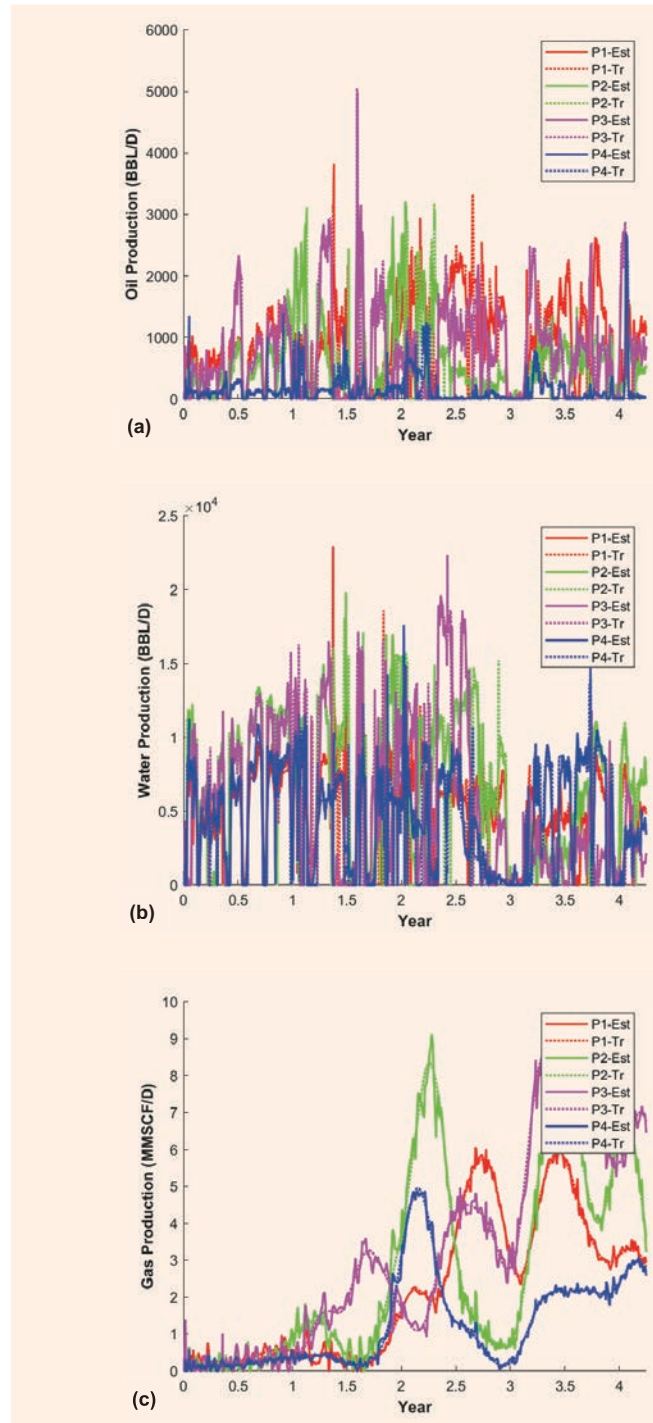
The framework was trained on production and injection data for the reservoir from the last 4.5 years, and the objective is to estimate the WAG injection for the next five years. Production and injection rates were recorded on a daily level and incorporated into the training process data set. For the neural network training, the neural network was trained on 80% of the data and then validated and tested on the remaining 20%.

As outlined in Fig. 3, the deep learning framework is well reproducing the production patterns from the four producer wells, which provides a strong confidence in the model's quality for optimizing the WAG injection process. Comparing the estimates to the actual production data, one observes that the framework deals well with the noise in the production data and follows the major trends for gas production. Similarly, on-off patterns with sharp rises in the water and oil production are realized as well.

To investigate in greater detail the dependency of the injection setup on the overall oil production, we compared two different optimization scenarios. In the first scenario, we assumed that operational constraints require that each of the injection wells funnel the same amount of injection quantities, which implies that the injection rates are identical for each of the wells. The number of optimization variables then reduces necessarily to four variables, which are the injection cycle length and the daily rates for water, CO<sub>2</sub>, and natural gas liquids for each of the injector wells.

While this reduces the number of variables and thereby improves the optimization routine's performance, it restricts the flexibility to adapt the injection patterns across the different injector wells via the adjustment of the inflow. For the study's sake, we did not take into

**Fig. 3** A comparison of the training data and the framework estimates for (a) water, (b) oil, and (c) gas production rates for the producer wells.



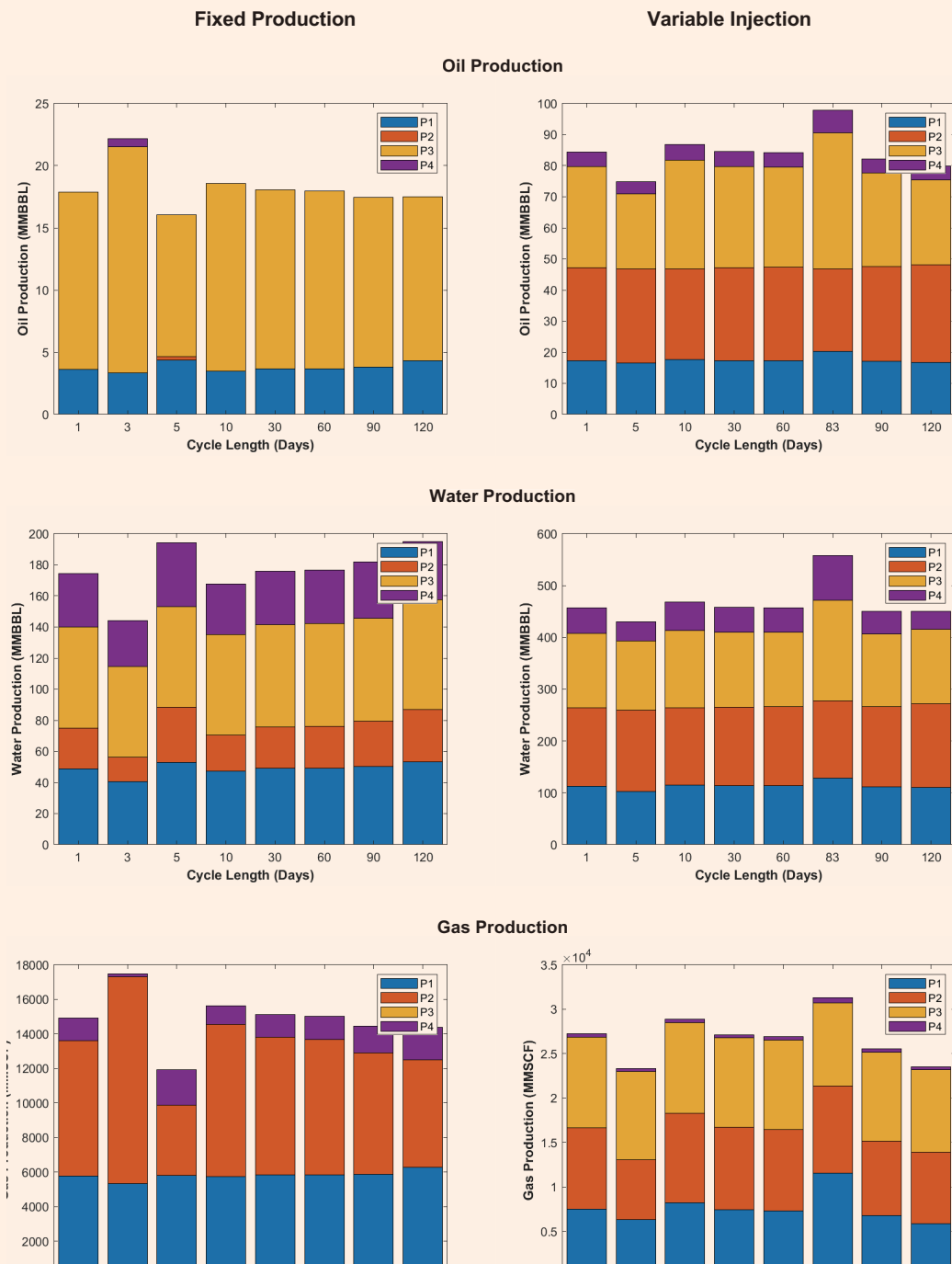
account different cycle lengths for the different wells or simultaneous injection of water and CO<sub>2</sub> into the field via different injection amounts. The reasoning behind this is that this may be rather challenging to be executed in practice or may be prohibitive in terms of its cost. We will refer this to a fixed injection pattern when the injection quantities are equal for all the wells,

while variable injection patterns allow for the variation in injection between the wells.

We performed an optimization of the framework for both scenarios. For the fixed injection scenario, the optimal cycle length is three days. This corresponds to the general assumption that without utilizing the optimization of injection to take advantage of the reservoir geometry, the lower the cycle length, the better

the hydrocarbon recovery will be. On the other hand, allowing for the different injection quantities for each of the wells enables us to increase the cycle length as the impact of each well on the production can be adjusted and optimized. This leads to a cycle length of 83 days when the injection is variable among the different wells. A major question arises as to what extent that a change in the cycle leads to a change in

**Fig. 4** A comparison of the total production of oil, water, and gas for the fixed and variable injection patterns for each well.



the overall recovery. In other words, how sensitive the solution is to changes in the cycle length.

Figure 4 displays a comparison of the total production for oil, gas, and water for various cycle lengths for a fixed injection and variable injection pattern. The optimal cycle length for fixed injection is three days, while for a variable injection it is 83 days. Comparing the production levels for cumulative oil, water, and gas production for every single well, one observes a great difference in the effectiveness of different cycle lengths. Specifically, production levels from the third producer well may differ significantly between the different wells for the fixed injection system, contributing the most in terms of cumulative oil production with a cycle length of three days.

A comparison between the different cycle lengths outlines the trend that the optimization of the cycle is crucial to minimize water production while maximizing hydrocarbon extraction for fixed injection scenarios. An exciting trend is that a slight variation from the optimum cycle for fixed injection may lead to lower performance, while this is less of a challenge for a variable injection approach. An exciting data behavior is that a variable injection leads to a more even distribution of production across the different wells. In contrast, for a fixed injection technique, there may be substantial differences, with some wells being solely gas producing while others are primarily oil producing.

## Conclusions

We have developed a new framework for the optimization of WAG injection and demonstrated it on a realistic eight well reservoir case. The framework incorporates a deep learning network approach to forecast well production levels from injection levels, which is subsequently incorporated into a mixed integer optimization problem to optimize the cycle length and injection quantities. The results demonstrate the importance of WAG optimization via allowing to significantly increase oil production from the reservoir while minimizing water production from the reservoir.

## Acknowledgments

This article was prepared for presentation at the Middle East Oil and Gas Show and Conference, Manama, Kingdom of Bahrain, November 28-December 1, 2021.

## References

1. Gu, Y., Bao, Z., Song, X., Wei, M., et al.: "Permeability Prediction for Carbonate Reservoir Using a Data-Driven Model Comprising Deep Learning Network, Particle Swarm Optimization, and Support Vector Regression: A Case Study of the LULA Oil Field," *Arabian Journal of Geosciences*, Vol. 12, Issue 20, October 2019.
2. Cheung, C.M., Goyal, P., Prasanna, V.K. and Tehrani, A.S.: "OReONet: Deep Convolutional Network for Oil Reservoir Optimization," paper presented at the IEEE International Conference on Big Data (Big Data), Boston, Massachusetts, December 11-14, 2017.
3. Singh, H., Seol, Y. and Myshakin, E.M.: "Automated Well-Log Processing and Lithology Classification by Identifying Optimal Features through Unsupervised and Supervised Machine Learning Algorithms," *SPE Journal*, Vol. 25, Issue 5, October 2020, pp. 2778-2800.
4. Nwachukwu, A., Jeong, H., Sun, A., Pycz, M., et al.: "Machine Learning-Based Optimization of Well Locations and WAG Parameters under Geologic Uncertainty," SPE paper 190259, presented at the SPE Improved Oil Recovery Conference, Tulsa, Oklahoma, April 14-18, 2018.
5. Katterbauer, K., Al-Yousif, A.A. and Marsala, A.F.: "Intelligent Reconciliation of Well Logs — A Pathway toward 4IR Assisted Log Interpretation," SPE paper 202621, presented at the Abu Dhabi International Petroleum Exhibition and Conference, Abu Dhabi, UAE, November 9-12, 2020.
6. Katterbauer, K. and Marsala, A.F.: "A Novel Sparsity Deploying Reinforcement Deep Learning Algorithm for Saturation Mapping of Oil and Gas Reservoirs," *Arabian Journal for Science and Engineering*, October 2020.



---

## About the Authors

### Dr. Klemens Katterbauer

Ph.D. in Petroleum Engineering,  
King Abdullah University of  
Science and Technology

Dr. Klemens Katterbauer is a Petroleum Scientist working in the Reservoir Engineering Technology Division of Saudi Aramco's Exploration and Petroleum Engineering Center – Advanced Research Center (EXPEC ARC), where he uses his experience as a Petroleum Engineer and software developer to focus on the development of the latest Fourth Industrial Revolution IR 4.0 technologies for reservoir engineering applications.

Klemens has a proven track record having developed data driven uncertainty frameworks for enhancing oil recovery and strengthening sustainability of existing oil and gas reservoirs. A strong focus was laid on solar and wind energy and providing dedicated solutions for optimizing grid transfer rates, reduce downtime, and enhance efficiency in the power transmission.

He has in recent years developed some major technologies, such as enhanced artificial intelligence technologies for tracking water-

fronts in subsurface reservoirs, and forecasting their movements. Furthermore, Klemens has developed robotics systems for enabling real-time logging while drilling, as well as subsurface sensing and logging operations.

Having been an experienced young professional member in several energy related societies, he has been an active member and heavily focused on mentoring young students that may dream to go into the oil and gas industry. In doing so, Klemens has advised several students and assisted them in broadening their expertise to focus on learning about new digital technologies, code development, as well as robotics.

He received his M.S. degree in Petroleum Engineering from Heriot-Watt University, Edinburgh, Scotland, U.K. Klemens received his Ph.D. degree in Petroleum Engineering from King Abdullah University of Science and Technology, Thuwal, Saudi Arabia.

### Dr. Alberto F. Marsala

Ph.D. in Nuclear Physics,  
University of Milan

Dr. Alberto F. Marsala has more than 29 years of oil industry experience. For the last 15 years, he has been working in Saudi Aramco's Exploration and Petroleum Engineering Center – Advanced Research Center (EXPEC ARC) as the Deep Diagnostics Focus Area Champion, with responsibilities covering R&D and innovation in formation evaluation and deep reservoir characterization.

Alberto previously work with Eni and Agip, where he had technical and managerial responsibilities in geoscience, including 4D seismic, reservoir characterization, petrophysics, geomechanics, core analysis, drilling, and construction in environmentally sensitive areas. Alberto worked in the Technology Planning and R&D committee of Eni. He was also the Head of Performance Improvement of the KCO Joint

Venture (Shell, ExxonMobil, Total, and others) for the development of giant fields in the northern Caspian Sea.

Alberto has authored a book on *Value of Innovation*, 100+ papers, and 30+ patents.

In 1991, Alberto received his Ph.D. degree in Nuclear Physics from the University of Milan, Milan, Italy, and in 1996, he received an MBA in Quality Management from the University of Pisa, Pisa, Italy. He also holds a Specialization in Innovation Management, received in 2001.

Some of Alberto's recent recognitions are the Society of Petrophysics and Well Log Analysts (SPWLA) Meritorious Award, the Society of Petroleum Engineers (SPE) Regional Formation Evaluation Award, Hart's E&P Engineering Innovation Award, and the World Oil Award for Best Exploration Technology.

### Dr. Abdulaziz S. Al-Qasim

Ph.D. in Petroleum Engineering,  
University of Tulsa

Dr. Abdulaziz S. Al-Qasim is a Petroleum Engineer and a Champion of Enhanced Oil Recovery Monitoring and Surveillance on the Reservoir Engineering Technology team of Saudi Aramco's Exploration and Petroleum Engineering Center – Advanced Research Center (EXPEC ARC). Since joining Saudi Aramco in 2007, he has been involved in enhanced oil recovery and improved oil recovery projects, reservoir management, field development, and production related challenges. Abdulaziz's experience includes working in a variety of departments within Saudi Aramco.

He has more than 40 patents, disclosed and granted, with many providing innovative sustainability and decarbonization solutions. Abdulaziz has written more than 30 technical papers and journals, and deployed many technologies.

He was selected to serve as a member of the Saudi Ministry of Energy (MoE) and King Abdulaziz City for Science and Technology (KACST) joint CCUS committee. Abdulaziz was selected as one of the Hart Energy E&P's "40

under Forty" 2021 honoree for his contributions to advancing E&P innovations. He was selected to join the CERAWEEK 2021 Future Energy Leaders program.

Abdulaziz is a member of the World Energy Council Future Energy Leaders (FEL-100) Board. He was named as one of Standard & Poors 2020 Global Platts Energy Rising stars and as one of the "World Oil" innovative thinkers of the year.

In 2020, Abdulaziz was recognized by the Energy Institute in 2019 as one of the young energy professionals of the year. He previously served as a Vice Chairman of the Society of Petroleum Engineers-Young Professionals (SPE-YP) regional symposium held in Oman in February 2009. Abdulaziz has also served in numerous SPE events at different levels.

He received his B.S. degree in 2007 from King Fahd University of Petroleum and Minerals (KFUPM), Dhahran, Saudi Arabia; his M.S. degree in 2011 from the University of Texas at Austin, Austin, TX; and his Ph.D. degree in 2016 from the University of Tulsa, Tulsa, OK, all in Petroleum Engineering.

# A New Methodology for Calculating Wellbore Pressure of Shut-in Wells in Numerical Reservoir Simulation

Babatope O. Kayode and Dr. Mahmoud Jamiolahmady

## Abstract /

In low permeability reservoirs, the pressure transient response of the buildup takes a long time to stabilize. During the history matching process, the observed non-stabilized buildup pressure cannot be compared to simulated well block pressure. This challenge arises because most reservoir simulators convert the well block pressure of flowing wells to wellbore pressure using Peaceman's equation, but do not perform this conversion for buildup pressure data. Such conversion is particularly important for low permeability reservoirs. This article discusses a new method to calculate the wellbore pressure of shut-in wells and highlights its benefits.

A full superposition equation for analytical wellbore pressure, without the usual logarithmic approximation of an  $Ei$  function, is the basis of the mathematical formulation proposed here. A modified equivalent radius concept, together with the superposition principle, are used to arrive at an expression to calculate the wellbore pressure from simulated well block pressure. To verify the validity of the approach, the calculated wellbore pressure is compared with analytical wellbore pressure described by the Horner function.

The results show that this calculated wellbore pressure is in better agreement with the non-stabilized observed pressure data than well block pressure. The well block pressure, which is currently used, is an average pressure over a spatial distance in which theoretical pressure varies as a logarithmic function of distance. Therefore, when the grid size is large and the spatial pressure gradient is significant (as the case in low permeability reservoirs), the simulated shut-in well block pressure may be very different from the observed shut-in wellbore pressure measured by a downhole gauge. Our results demonstrate that this difference increases with increasing grid size. If, during numerical well testing, the calculated wellbore pressure is used for the log-log pressure derivative plot instead of the well block pressure, the early distortions of infinite acting radial flow stabilization, which has been observed by some investigators is eliminated.

The presented methodology to calculate shut-in wellbore pressure is practically attractive to complement existing simulator capabilities for relating wellbore pressure to well block pressure. The use of the wellbore pressure, calculated using the method proposed here, instead of well block pressure, eliminates the need to apply the time-shift proposed by some investigators to correct the infinite acting radial flow signature deviation, and observe the true flow regime.

## Introduction

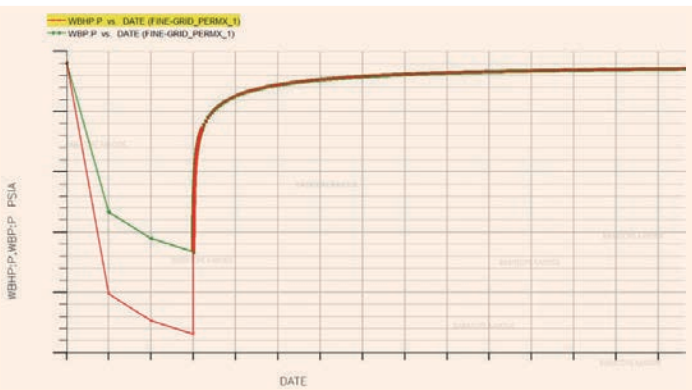
When we lower a pressure gauge into a well, it measures the wellbore bottom-hole pressure (BHP), which may be flowing or shut-in wellbore pressure. For flowing wells, numerical simulators explicitly calculate, in general, well block pressure at each time step. Simulators then use Peaceman's equation<sup>1,2</sup> to convert simulated well block pressure to equivalent wellbore pressure. During shut-in, most numerical simulators continue to calculate well block pressure, and report it as the wellbore pressure.

Figure 1 is an example of the Eclipse simulation results of pressure vs. time data from a synthetic model. It shows that during the flow period, the well block pressure is different from the wellbore pressure.

As shown in Fig. 1, the Eclipse simulator sets the wellbore pressure to well block pressure during well shut-in, because the wellbore pressure is assumed to be applicable only to flowing wells<sup>3</sup>. In this article, we will propose a methodology for calculating the wellbore pressures during the shut-in period following a numerical simulation exercise. We will denote this wellbore pressure during shut-in as static BHP (SBHP); it is the wellbore equivalent of well block pressure during shut-in, which can be used for history matching purposes.

A key objective of history matching is to calibrate a model to historical datum pressures. If the final gauge reading during buildup stabilizes, the measured pressure represents the average drainage area pressure and is comparable to well block pressure.

**Fig. 1** The comparison of well block pressure and wellbore BHP from an Eclipse simulation of a synthetic model.

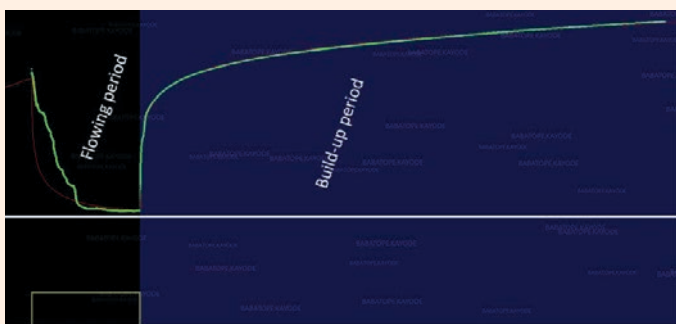


If gauge pressure is still building up at the end of the pressure survey, the final shut-in gauge pressure is not an average drainage area pressure. Simulated well block pressure is an average grid block pressure, and we should only compare it to stabilized historical pressure. For non-stabilized historical pressure, the rigorous numerical equivalent for history matching is the numerical wellbore pressure. We will show in this work that the simulated well block pressure in low permeability and large simulation grid block may differ from the theoretical wellbore pressure.

Figure 2 is an example of pressure vs. time, showing non-stabilized gauge pressure within the pressure survey duration.

Building on this concept, we will propose a methodology for calculating SBHP, a parameter that most reservoir simulator packages currently do not calculate. SBHP can be used for history matching purposes, and is most helpful for low permeability cases where stabilized historical pressure cannot be archived. The SBHP will help to eliminate the need for perhaps unrealistic geomodel modifications during history matching, which would otherwise be based on unrealistic pressure values.

**Fig. 2** The non-stabilized pressure buildup in a low permeability reservoir after 400 hours of well shut-in.



## Literature Review

Numerical simulators explicitly calculate well block pressure at each time step during both flowing and shut-in conditions. Poolen et al. (1968)<sup>4</sup> and Peaceman (1977)<sup>1</sup> have highlighted that well block pressure is not directly comparable with wellbore pressure. The difference between the two increases with increasing spatial discretization size,  $\Delta x$ . According to Ding et al. (1995, 2007)<sup>5, 6</sup>, this difference is because simulators compute average pressure within a well block that is usually many times larger than the wellbore size.

The wellbore radius would be in the order of 0.5 ft to 1.5 ft, while simulation grid sizes would range from 50 ft to 500 ft. There is a significant areal pressure gradient in low permeability reservoirs, such that the average volumetric pressure around the well is higher than the wellbore pressure. We illustrate this in Fig. 3, which shows that in the simulation model of a low permeability reservoir using 300 ft grid size, simulated well block pressure ( $P_{avg}$ ) is different from the wellbore pressure ( $P_{ws}$ ).

During flowing conditions, Peaceman's formula, i.e., Eqn. 1, is used to convert well block pressure into equivalent wellbore pressure.

$$P_o = P_{wf} + \frac{q\mu}{2\pi kh} \ln \frac{r_o}{r_w} \quad 1$$

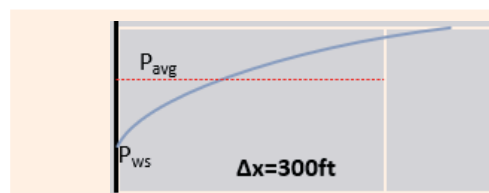
$P_o$  is the simulated well block pressure,  $r_o$  is the equivalent radius defined by Peaceman as  $r_o = 0.2\Delta x$ . Therefore, flowing BHP is calculated by Eqn. 2, which states that wellbore flowing pressure is the simulated well block pressure minus a correction term.

$$P_{wf} = P_o - \frac{q\mu}{2\pi kh} \ln \frac{0.2\Delta x}{r_w} \quad 2$$

Ding et al. (1995, 2007)<sup>5, 6</sup> and Sharpe et al. (1992)<sup>7</sup> have questioned the application of Peaceman's approach and the value of 0.2 in Eqn. 2. Peaceman (1983)<sup>2</sup> remarked that his expression  $r_o = 0.2\Delta x$  is a rule of thumb based on simulation experiments and may not be a universal expression. In this work, we propose a modified equivalent radius for calculating SBHP.

According to Poolen et al. (1968)<sup>4</sup>, we should compare well block pressure to the average pressure within the reservoir portion represented by the well block size during history matching. When we measure a single point pressure data from a well, the drainage area

**Fig. 3** A comparison of the wellbore and well block pressure in a low permeability large grid block simulation model.





associated with the observed pressure is unknown. Therefore, contrary to the requirement proposed by Poolen et al. (1968)<sup>4</sup>, simulated well block pressure could correspond to a larger reservoir area — depending on the well block size — than that associated with the non-stabilized single point pressure.

To make a historical non-stabilized pressure usable, Miller et al. (1949)<sup>8</sup>, Dietz (1965)<sup>9</sup>, and Kazemi (1974)<sup>10</sup> proposed methodologies to convert it to an equivalent drainage area pressure. These approaches require assumptions about the drainage area and geometrical location of the well. They also require continuous pressure buildup data to determine  $P^*$  — required for  $P_{avg}$  calculation — from Horner's semi-log plot. Therefore, when only a single point of pressure data is available, non-stabilized pressure data cannot be converted to an equivalent drainage area pressure using any of these approaches.

Poolen et al. (1968)<sup>4</sup> proposed a shut-in duration equation, Eqn. 3, at which theoretical buildup pressure would be comparable to simulated well block pressure. They defined the corresponding buildup pressure at this time as the dynamic pressure.

$$\Delta t = \frac{\varphi \mu c r_b^2}{0.001582k} \quad 3$$

This approach has the advantage that when continuous pressure buildup data are available, we can extract the appropriate dynamic pressure corresponding to the simulation grid size. The limitation is that when only a single point of pressure is available, we cannot compare that piece of historical pressure data with simulated well block pressure for history matching if the historical data's shut-in duration is different from the shut-in duration computed from Eqn. 3.

Peaceman (1983)<sup>2</sup> and Eaulougher (1972)<sup>11</sup> attempted to resolve the limitation pointed out about the Poolen et al. (1968)<sup>4</sup> methodology by deriving Eqn. 4 to calculate dynamic pressure when only single point pressure data is available.

$$P_{dyn} = (P_{ws})_{obs} + \frac{162.6q\beta}{kh/\mu} * \log_{10} \left( \frac{200\varphi\mu c\Delta x^2}{k\Delta t_{obs}} \right) \quad 4$$

This approach does not require continuous pressure buildup data, which are not routinely available. It has the limitation that dynamic pressure may be laborious to calculate for every historical pressure in a typical history matching project that comprises hundreds of wells, each having several (non-stabilized) single point pressures ( $P_{ws})_{obs}$ .

Another limitation of the Peaceman (1983)<sup>2</sup> and Ear-lougher (1972)<sup>11</sup> approach is that Eqn. 4 is only valid on the assumption that  $(P_{ws})_{obs}$  be on the straight line portion of Horner's semi-log plot. We cannot know in advance if  $(P_{ws})_{obs}$  meets the required condition unless continuous pressure buildup data is available.

Instead of applying these correction procedures on historical, non-stabilized pressure to make it comparable to simulated well block pressure, a different approach taken by the current work is to simulate the historical data's numerical equivalent and directly

compare both. The numerical wellbore pressure at  $\Delta t$  corresponds to  $\Delta t_{obs}$  of the historical pressure data.

## Methodology Description

For infinite acting well producing at a rate of  $q$  bbl/d for  $t_p$  hours and then shut-in, we can write the superposition equation as shown in Eqn. 5:

$$P_i - P_{(r,\Delta t)} = \theta \left( -Ei \left( \frac{-\alpha r^2}{(t_p + \Delta t)} \right) \right) - \theta \left( -Ei \left( \frac{-\alpha r^2}{\Delta t} \right) \right) \quad 5$$

$$\theta = 70.6 \frac{q\beta\mu}{kh}$$

$$\alpha = \left( \frac{948\varphi\mu c_t}{\kappa} \right)$$

Equation 5 can then be written for distances  $r_o^*$  (radius corresponding to the pressure for a grid block) and  $r_w$  as:

$$P_{(r_o^*,\Delta t)} = P_i - \theta \left( -Ei \left( \frac{-\alpha r_o^{*2}}{(t_p + \Delta t)} \right) \right) + \theta \left( -Ei \left( \frac{-\alpha r_o^{*2}}{\Delta t} \right) \right) \quad 6$$

$$P_{(r_w,\Delta t)} = P_i - \theta \left( -Ei \left( \frac{-\alpha r_w^2}{(t_p + \Delta t)} \right) \right) + \theta \left( -Ei \left( \frac{-\alpha r_w^2}{\Delta t} \right) \right) \quad 7$$

where the SBHP =  $P_{(r_w, \Delta t)}$ .

Subtracting Eqn. 6 from Eqn. 7 allows us to eliminate  $P_i$  and obtain:

$$P_{(r_o^*,\Delta t)} - P_{(r_w,\Delta t)} = \theta \left( -Ei \left( \frac{-\alpha r_o^{*2}}{(\Delta t)} \right) \right) - \theta \left( -Ei \left( \frac{-\alpha r_o^{*2}}{t_p + \Delta t} \right) \right) - \theta \left( -Ei \left( \frac{-\alpha r_w^2}{(\Delta t)} \right) \right) + \theta \left( -Ei \left( \frac{-\alpha r_w^2}{t_p + \Delta t} \right) \right) \quad 8$$

Finally, we can compute the SBHP by re-arranging Eqn. 8 as:

$$P_{(r_w,\Delta t)} = P_{(r_o^*,\Delta t)} - \left[ \theta \left( -Ei \left( \frac{-\alpha r_o^{*2}}{(\Delta t)} \right) \right) - \theta \left( -Ei \left( \frac{-\alpha r_o^{*2}}{t_p + \Delta t} \right) \right) - \theta \left( -Ei \left( \frac{-\alpha r_w^2}{(\Delta t)} \right) \right) + \theta \left( -Ei \left( \frac{-\alpha r_w^2}{t_p + \Delta t} \right) \right) \right] \quad 9$$

The first term on the right-hand side of Eqn. 9 is simulated grid pressure, while the remaining terms on the right-hand side are the rock, fluid, rate, and time data, which are readily available during the simulation run time. Therefore, the strategy for computing the SBHP is the application of a correction term to the simulated pressure for a chosen grid block.

We would ordinarily expect that the simulated grid pressure to be corrected is the well grid pressure.

Subsequently, as discussed in Appendix A, the well grid is prone to a double-dip phenomenon, making its simulated pressure considerably deviate from theoretical results. Therefore, Eqn. 9 is solved for the grid block immediately adjacent to the well grid.  $P_{(r_o^*, \Delta x)}$  in Eqn. 9 is the simulated pressure in grid(i + 1). Equation 9 is solved using the value of  $r_o^*$ , table of  $-Ei(-x)$ , and the simulated grid(i + 1) pressures at each time step.

Calculating the SBHP from Eqn. 9, requires  $r_o^*$  first to be calculated.  $r_o^*$  is the distance from the mid-point of the grid (i) to a point inside the grid(i + 1), where the theoretical pressure in the grid is equal to the simulated grid pressure as illustrated in Fig. 4 for a well in the center of a grid block with size  $\Delta x$ .

The pressure distance curve is described by Eqn. 10:

$$P(r) = P_{wf} + \frac{141.2q\beta\mu}{kh} \ln \frac{r}{r_w} \quad 10$$

At the distance,  $r_o$ , the theoretical pressure ( $P_r$ ) is equal to the simulated grid(i + 1) pressure ( $P_o$ ), and  $r_o^* = 0.5\Delta x + r_o$ . Appendix B shows the derivation of  $r_o^*$ .

It is noted that under certain conditions, Eqn. 7 can be rewritten for  $r_o$ , using the natural logarithm approximation of the  $Ei$  function as:

$$P_{(r_w, \Delta t)} = P_i - 70.6 \frac{q\beta\mu}{kh} \ln \left( \frac{t_p + \Delta t}{\Delta t} \right) \quad 11$$

where  $-Ei(-x) = \ln(1.78x)$

Equation 11 is known as Horner's equation, and it is the analytical solution to be used for validating the results from the proposed methodology. In the following sections, we will demonstrate the reliability of the proposed formulations using some single well simulations.

### Data Set Description

We constructed a coarse black oil Eclipse model having  $N_x = N_y = 20$  and  $N_z = 1$ . The model is homogeneous, having a connate water saturation of 22%, the porosity of 25%, the permeability of 100 mD, and a grid block size of  $\Delta x = \Delta y = 100$  ft and  $\Delta z = 20$  ft.

This coarse model was then refined to dimensions of  $N_x = N_y = 200$  and  $N_z = 1$  where each grid block is of size  $\Delta x = \Delta y = 10$  ft and  $\Delta z = 20$  ft. We have divided each of the original coarse grids into 100 fine grids. All properties of the fine grids remain the same

as that of the coarse grid.

We also created a low permeability scenario for the same coarse and fine grid cases where we set model permeability to 0.5 mD. Therefore, there are four models in all, described as:

1. Coarse\_Grid\_Permx\_100: coarse grid model with a permeability of 100 mD
2. Coarse\_Grid\_Permx\_05: coarse grid model with a permeability of 0.5 mD
3. Fine\_Grid\_Permx\_100: fine grid model with a permeability of 100 mD
4. Fine\_Grid\_Permx\_05: fine grid model with a permeability of 0.5 mD

A single producing well, Well-P1, was defined in each of the models, flowed for 72 hours, and followed with an extended shut-in for pressure buildup. For the coarse grid models, Well-P1 was defined at the grid location (10, 10), whereas for the fine grid models, we defined Well-P1 at the (100, 100) grid location.

As earlier described, the presented methodology requires grid(i + 1) simulated grid block pressure as input. To obtain this grid(i + 1) simulated grid block pressure, an observation well, Well-P2, was defined at the grid location (10, 11) for the coarse grid models and at (100, 101) for the fine grid models. Since Well-P2 is an observation well, the simulated well block pressure of Well-P2 is the grid(i + 1) pressure of Well-P1.

## Discussion of Results

### Calculation of SBHP (Coarse\_Grid\_Permx\_05 model)

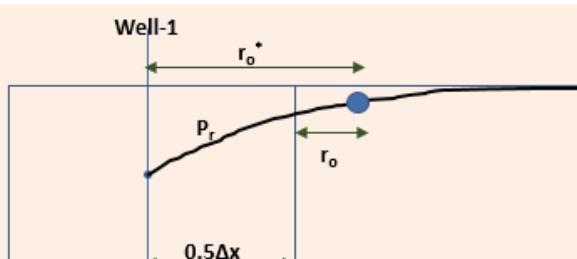
Figure 5 is a plot of pressure vs. time for the data of the coarse grid model. In this figure, the well block pressure is the simulated well block pressure of Well-P1, the SBHP is the wellbore pressure calculated based on the proposed methodology and using a computer code that solves Eqn. 9 at every time step, and  $P_{ws}$  (Horner) is the theoretical buildup calculated from Eqn. 11. We observe that the SBHP gives similar results with the theoretical results, whereas the simulated well block pressure of Well-P1 does not.

If we had measured pressure in Well-P1, say after 5 hours of shut-in, the measured pressure would be on the theoretical pressure curve, Fig. 6, which is a zoom in of the early-time pressure data of Fig. 5.

Using SBHP adequately matches the data in this 0.5 mD reservoir example to within 50 psi. The mismatch of well block pressure compared to historical data is around 500 psi.

As discussed in Appendix A, the error associated with the well block pressure is reduced, as the grid size is reduced. Figure 7 is a plot of pressure vs. time for data of the fine grid model. In this figure, the well block pressure of Well-P1 matches the theoretical results adequately, confirming that when grid blocks are small, the well block pressure results are reliable and consistent with the theoretical results. Fine grid simulation comes at a high runtime cost. Therefore, there would be a need for SBHP, which is always consistent with

Fig. 4 An illustration of the concept of the modified equivalent radius.



theoretical results regardless of the grid block size.

**Calculation of SBHP (Coarse\_Grid\_Permx\_100 model)**

As discussed in Appendix A, the difference between average drainage area pressure and wellbore pressure is small in a large permeability reservoir owing to the minimal areal pressure gradient. The same conclusion is supported by looking at Fig. 8, which is a plot of pressure vs. time for the coarse grid model having a permeability of 100 mD. In this figure, the well block pressure of Well-P1 becomes consistent with the theoretical buildup and SBHP within 2 hours of well shut-in.

These results could be summarized as:

1. In high permeability reservoirs (and regardless of grid block size), the well block pressure is consistent with theoretical wellbore pressure after a few hours of shut-in.
2. In low permeability reservoirs, the well block pressure is consistent with the theoretical wellbore pressure only if simulation uses finely gridded blocks.
3. Regardless of permeability and grid block size, the SBHP is consistent with the theoretical wellbore pressure.

**Practical Application**

This section tests the proposed method’s application on a simulation model’s history matching process of a low permeability reservoir. Several pieces of pressure transient data acquired on this reservoir indicate a slow buildup, where pressure is still increasing after 400 hours of well shut-in. The shut-in duration for most of the acquired single point shut-in pressure data is 72 hours. A coarse grid single well numerical simulation model of the reservoir, which was available, is used here.

Pressure in the grid(i + 1) was extracted through a dummy well defined in that location. We extracted average permeability, porosity, viscosity, and formation volume factor from the simulation model and calculated the numerical SBHP using Eqn. 9. The parameter, pseudo-producing time ( $t_p$ ) in Eqn. 9 was obtained by dividing the cumulative production by the most recent average production rate.

Figure 9 is a plot of pressure vs. date. This figure shows the comparison between the simulated well block pressure, grid(i + 1) pressure, and the SBHP. In this particular example, while the well block pressure is higher than the observed pressure, the SBHP matches the observed data.

If history matching precedes using the well block pressure data, then the engineer would need to make an adjustment like reducing either the geomodel aquifer size/strength or the geomodel hydrocarbon pore volume or other possibly unsubstantiated corrections to calibrate the well block pressure data to the observed pressure data. Consequently, by using the SBHP, it can be concluded that no geomodel adjustment is necessary around this particular well because the SBHP is matching the observed pressure data adequately. Therefore,

**Fig. 5** A comparison of the well block, the SBHP, and the theoretical pressure buildup for the coarse grid low permeability model.

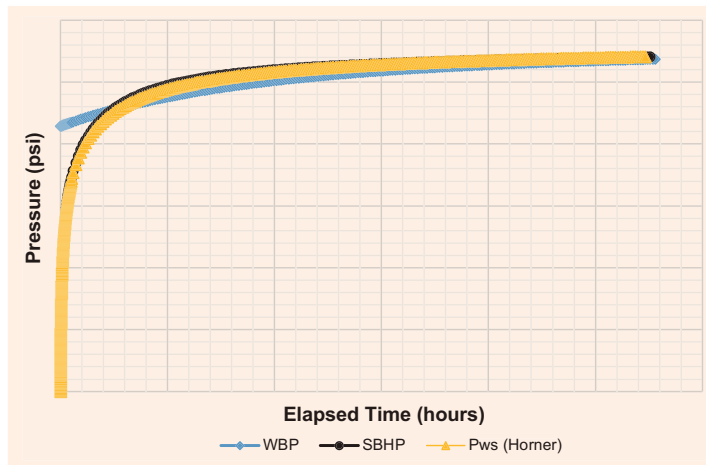


**Fig. 6** The zoom of the early-time region of data shown in Fig. 5.

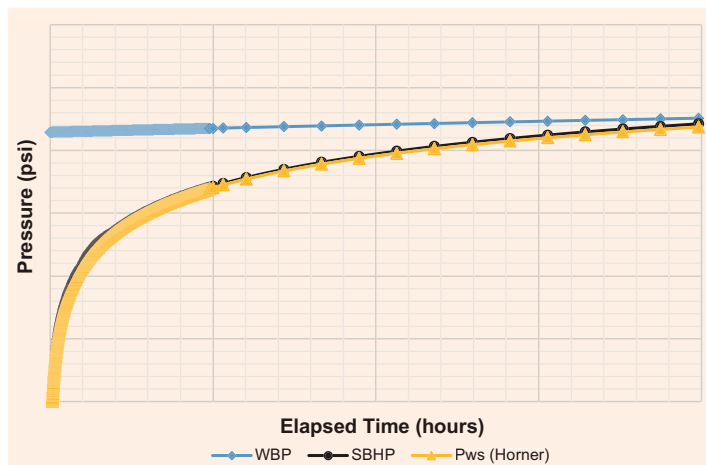


**Fig. 7** The comparison of the well block, SBHP, and theoretical pressure buildup in the fine grid low permeability model.

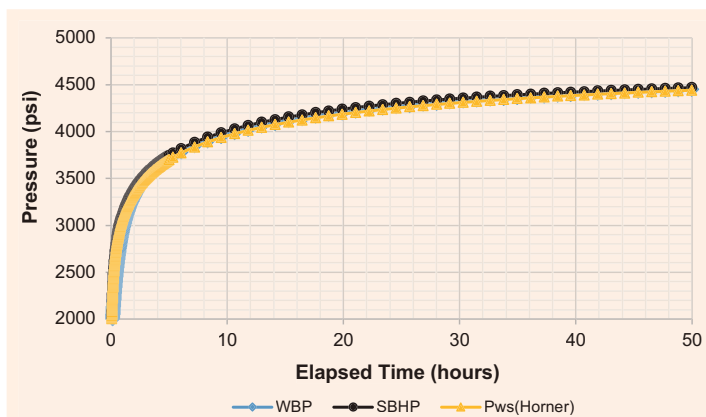


**Fig. 8** The comparison of the well block, SBHP, and theoretical pressure buildup for the coarse grid high permeability model.

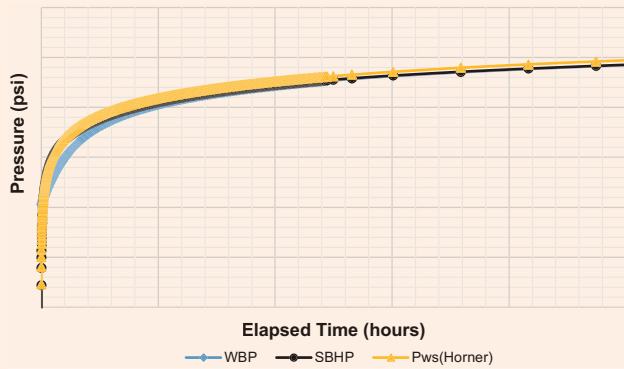
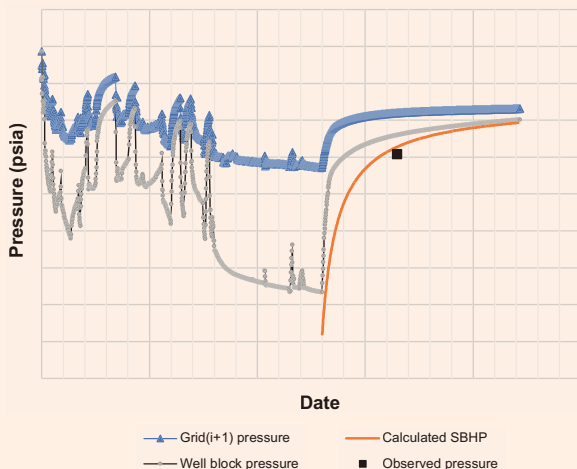


**Fig. 9** The comparison between the well block pressure and the SBHP on a producing well of a low permeability reservoir.



the use of SBHP will help avoid using unnecessary geomodel modifications during history matching.

## Conclusions and Recommendations

1. In this article, a methodology was described to obtain wellbore pressure of shut-in wells and SBHP, a parameter not reported by most numerical reservoir simulators.
2. In coarse grid simulation models of the two considered low permeability reservoirs, we showed that the well block pressure is not consistent with theoretical results. Although, the calculation of the SBHP using the presented methodology gives results that are consistent with theoretical results. In a 0.5 mD reservoir example, the mismatch of well block pressure compared to historical data is approximately 500 psi while SBHP was matching to within 50 psi.

3. The methodology presented in this article is also applicable to injectors (wellbore pressure fall-off).
4. Subsequently, the presented methodology's backbone equations contain an inherent assumption that wells are vertical and pressure transient is infinite acting. Further work would be required to adopt this methodology to other scenarios, including deviated and horizontal wells, which are currently under investigation.

## Nomenclature

$P_o$ : simulated grid-block pressure

$P_{wf}$ : flowing bottom-hole pressure

$P_i$ : initial reservoir pressure

$P_{avg}$ : average reservoir pressure

$r_w$ : wellbore radius

$r_o$ : equivalent radius

$r_o^*$ : modified equivalent radius

$r$ : distance from wellbore

$q$ : surface flow rate

$k$ : reservoir permeability

$h$ : reservoir thickness

$t_p$ : pseudo-producing time

$\Delta t$ : shut-in time

$\mu$ : viscosity

$\beta$ : formation volume factor

$\phi$ : porosity

$c$ : compressibility

$r_b$ : grid block equivalent radius

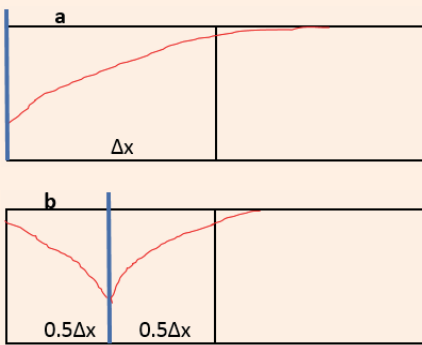
$kh$ : permeability-thickness

### Appendix A: Limitation of Comparing Historical Single Point Shut-in Pressure to Well Block Pressure

As previously noted by Ding et al. (1995)<sup>2</sup>, simulated well block pressure during flow is not consistent with the theoretical results. The authors attributed the inconsistency to the large size of the simulation grid block wellbore size. This section shows that the simulated well block pressure during shut-in is not consistent with the theoretical results. The inconsistency is pronounced at low permeability and large grid size.

We show in Fig. A-1a the reservoir well configuration used to develop the theoretical solution. The well is at the grid block's outer face, and pressure varies away from the wellbore as a logarithmic function of distance.

**Fig. A-1** (a) The reservoir well configuration in theoretical solution, and (b) the reservoir well configuration in the numerical solution.



Equation A1 gives the average volumetric pressure of the well block in Fig. A-1a:

$$P_{avg} = \frac{\int P(r)dv}{\Delta v} \tag{A1}$$

If we assume steady-state flow of single-phase, slightly compressible fluids, then:

$$P(r) = P_{wf} + \frac{141.2q\beta\mu}{kh} \ln \frac{r}{r_w} \tag{A2}$$

According to Dakes<sup>12</sup>, Eqn. A1, and Eqn. A2 can be solved to give Eqn. A3:

$$P_{avg} = P_{wf} + \frac{141.2q\beta\mu}{kh} \left[ \ln \frac{r}{r_w} - 0.5 \right] \tag{A3}$$

Based on Fig. A-1a, Eqn. A4 is an expression for the theoretically calculated average pressure within the well block.

$$P_{avg}^A = P_{wf} + \frac{141.2q\beta\mu}{kh} \left[ \ln \frac{\Delta x}{r_w} - 0.5 \right] \tag{A4}$$

In the numerical simulator, Fig. A-1b shows the well and reservoir model configuration for a case where the

well is at the center of the well block, thereby giving rise to two equal wings of pressure-distance profiles within the well block. By applying Eqn. A3 to each wing of the pressure-distance curve, we obtain:

$$P_{avg} = P_{wf} + \frac{141.2q\beta\mu}{kh} \left[ \ln \frac{0.5\Delta x}{r_w} - 0.5 \right] \tag{A5}$$

Therefore, the average pressure in the well block would be the sum of each wing's average pressure divided by two, resulting in Eqn. A6:

$$P_{avg}^N = P_{wf} + \frac{141.2q\beta\mu}{kh} \left[ \ln \frac{0.5\Delta x}{r_w} - 0.5 \right] \tag{A6}$$

For a fixed simulation grid size, we can show the impact of permeability by taking a difference of Eqn. A4 and Eqn. A6 to obtain Eqn. A7:

$$P_{avg}^A - P_{avg}^N = \frac{97.8q\beta\mu}{kh} \tag{A7}$$

Equation A7 shows that the difference between the numerical average block pressure and the average analytical pressure increases at low permeability.

### Appendix B: Derivation of the Modified Equivalent Radius

For a steady-state radial flow of slightly compressible fluid in a circular reservoir, the equation governing the pressure distribution around a well is given as:

$$P_r = P_{wf} + \frac{q\mu}{2\pi kh} \ln \frac{r}{r_w} \tag{B1}$$

The average volumetric pressure is the integral of the pressure distribution over the entire reservoir and given by Eqn. 2:

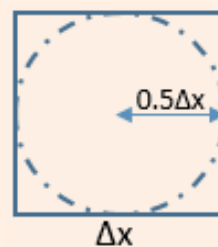
$$P_{avg} = P_{wf} + \frac{q\mu}{2\pi kh} \left[ \ln \frac{r_e}{r_w} - 0.5 \right] \tag{B2}$$

#### Appendix B-1: Maximum Reservoir Radius Assumption

Suppose we assume  $r_e$  in Eqn. B2 represents the maximum radius of the circle that we can inscribe within a square simulation grid of sides  $\Delta x$ , then  $r_e = 0.5\Delta x$  and Eqn. B2 becomes:

$$P_{avg} = P_{wf} + \frac{q\mu}{2\pi kh} \left[ \ln \frac{\Delta x}{2r_w} - 0.5 \right] \tag{B3}$$

**Fig. B-1** An illustration of a circular reservoir having a radius to boundary equal to the minimum distance to the boundary of a well in the center of a square grid block.



In the numerical simulator, Fig. A-1b shows the well and reservoir model configuration for a case where the

From Eqn. B1, we can write an expression for the theoretical pressure at distance  $r_o$  within the well block as:

$$P_o = P_{wf} + \frac{q\mu}{2\pi kh} \ln \frac{r_o}{r_w} \quad \text{B4}$$

Now we seek to determine the distance  $r_o$ , such that  $P_o = P_{avg}$  by equating Eqn. B3 to Eqn. B4 and solving for  $r_o$ :

$$\ln \frac{r_o}{r_w} = \ln \frac{\Delta x}{2r_w} - 0.5 \quad \text{B5}$$

The analogy used to obtain Eqn. B5 is not exact because from Fig. B-1; the radial area is less than the grid block area. Therefore, the average pressure within the circular reservoir assumption is less than the well block pressure

## Appendix B-2: Equivalent Reservoir Area Assumption

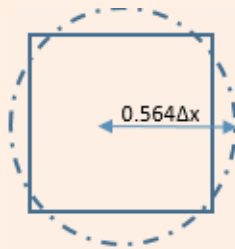
The second assumption is to take  $r_e$  in Eqn. B2 as the radius of a circle having an equivalent area as the simulation grid block:

$$\pi r_e^2 = \Delta x^2 \quad \text{B6}$$

$$r_e = \frac{\Delta x}{\sqrt{\pi}}$$

$$r_e = 0.564\Delta x$$

**Fig. B-2** An illustration showing that the distance to the boundary of a circular reservoir having the same area as a square grid block is larger than the radius to the boundary of a well centered in the square grid block.



We can rewrite Eqn. B2 by substituting for  $r_e$ :

By equating Eqn. B4 to Eqn. B6 and solving for  $r_o$  gives:

$$\ln \frac{r_o}{r_w} = \ln \frac{\Delta x}{\sqrt{\pi} r_w} - 0.5 \quad \text{B7}$$

$$r_o = \text{Exp}(-0.5) * \frac{\Delta x}{\sqrt{\pi}}$$

$$r_o = 0.342\Delta x$$

This answer is also an approximation. As seen from Fig. B-2, the distance to the boundary of a circular reservoir with the same area as a square simulation

grid block is larger than the grid block, and has a larger average pressure than well block pressure.

A final and philosophical approach is to consider that since pressure follows a logarithmic function of distance, then, strictly speaking,  $r_o$  should be the centroid of a logarithmic scale, that is,  $\text{Antilog}(0.5) = 0.32$ . This value is exactly midway between the two earlier derived approximate values.

Therefore, the current work proposes a new definition for equivalent radius as  $r_o = 0.32\Delta x$ .

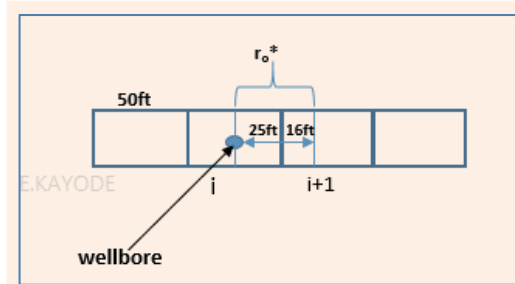
When this is applied to grid  $(i + 1)$ , the modified equivalent radius becomes:

$$r_o^* = 0.5\Delta x + r_o$$

$$r_o^* = 0.5\Delta x + 0.32\Delta x$$

Figure B-3 illustrates the concept for a grid block the size of 50 ft \* 50 ft \* 5 ft.

**Fig. B-3** An illustration of the modified equivalent radius.





## References

1. Peaceman, D.W.: "Interpretation of Well Block Pressures in Numerical Reservoir Simulation," *Society of Petroleum Engineers Journal*, Vol. 18, Issue 3, June 1978, pp. 183-194.
2. Peaceman, D.W.: "Interpretation of Well Block Pressure in Numerical Reservoir Simulation with non-Square Grid Blocks and Anisotropic Permeability," *Society of Petroleum Engineers Journal*, Vol. 25, Issue 3, June 1983, pp. 551-545.
3. ECLIPSE Reference Manual, ver. 2014.1, Schlumberger, 2014, 2831 p.
4. Van Poolen, H.K., Breitenbach, E.A. and Thurnau, D.H.: "Treatment of Individual Wells and Grids in Reservoir Modeling," *Society of Petroleum Engineers Journal*, Vol. 8, Issue 4, December 1968, pp. 541-546.
5. Ding, Y., Renard, G. and Weill, L.: "Representation of Wells in Numerical Reservoir Simulation," *SPE Reservoir Evaluation and Engineering*, Vol. 1, Issue 1, February 1998, pp. 18-25.
6. Ding, Y. and Renard, G.: "A New Representation of Wells in Numerical Reservoir Simulation," *SPE Reservoir Engineering*, Vol. 9, Issue 2, May 1994, pp. 140-144.
7. Sharpe, H.N. and Ramesh, B.A.: "Development and Validation of a Modified Well Model Equation for Non-uniform Grids with Application to Horizontal Well and Coning Problems," SPE paper 24896, presented at the SPE Annual Technical Conference and Exhibition, Washington, D.C., October 4-7, 1992.
8. Miller, C.C., Dyes, A.B. and Hutchinson Jr., C.A.: "The Estimation of Permeability and Reservoir Pressure from Bottom-hole Pressure Buildup," paper presented at the Petroleum Branch Meeting, San Antonio, Texas, October 5-7, 1949.
9. Dietz, D.N.: "Determination of Average Reservoir Pressure from Buildup Surveys," *Journal of Petroleum Technology*, Vol. 17, Issue 8, August 1965, pp. 955-959.
10. Kazemi, H.: "Determining Average Reservoir Pressure from Pressure Buildup Tests," *Society of Petroleum Engineers Journal*, Vol. 14, Issue 1, February 1974, pp. 55-62.
11. Earlougher, R.C.: "Comparing Single Point Pressure Buildup Data with Reservoir Simulator Results," *Journal of Petroleum Technology*, Vol. 24, Issue 6, June 1972, pp. 711-712.
12. Dake, L.P.: *Fundamentals of Reservoir Engineering*, Elsevier Sciences B.V., Netherlands, 1983, 464 p.

---

### About the Authors

#### **Babatope O. Kayode**

*M.S. in Petroleum Engineering,  
Heriot-Watt University*

Babatope O. Kayode is a Senior Reservoir Engineer working in Saudi Aramco's Reservoir Description & Simulation Department, where he works as a Simulation Engineer.

Babatope has 20 years of oil and gas industry experience primarily devoted to reservoir simulation studies. His research interests include methodologies for improved reservoir characterization and workflows for faster and better history matching.

Babatope is the author of 10 conference and

journal papers. He has filed 12 U.S. patents in his research areas, of which three have been granted.

Babatope received his B.S. degree in Petroleum Engineering from the University of Ibadan, Ibadan, Nigeria, and his M.S. degree in Petroleum Engineering from Heriot-Watt University, Edinburgh, Scotland, U.K. Babatope is currently working on his Ph.D., researching methodologies for history matching.

---

#### **Prof. Mahmoud Jamiolahmady**

*Ph.D. in Petroleum Engineering,  
Heriot-Watt University*

Prof. Mahmoud Jamiolahmady is a Professor of Petroleum Engineering at Heriot-Watt University Institute of Geo-energy Engineering, where he leads gas condensate recovery and well test activities and delivers a number of petroleum engineering courses.

Mahmoud is also the Director of the Heriot-Watt University Petroleum Engineering M.S. program, a fellow member of the U.K. Higher Education Academy, and the Technical Director of Petroc Technologies.

He has over 25 years of experience studying fluid flow in porous media with more than 140 conference and technical papers to his name.

Mahmoud received his B.S. degree and M.S. degree in Reservoir Engineering from the Petroleum University of Technology and University of Tehran, Iran. He received his Ph.D. degree in Petroleum Engineering from Heriot-Watt University, Edinburgh, Scotland, U.K.

# Rock Mechanical Characterization of Shale Drilling Fluid Interactions to Mitigate Borehole Instability Problems

*Dr. Mohammad H. Alqam, Dr. Md. Amanullah, Antonio Santagati, Salem H. Al-Garni, Adnan H. Al-Makrami and Dr. Sinan Caliskan*

## Abstract /

Borehole instability is one of the biggest problems faced by the oil and gas industry when drilling shale formations, mud rocks, marl, or a combination of them using water-based muds (WBM).

The physiochemical interaction of WBMs and the rock formations along with their micro- and macro-scale mechanical degradation are some of the root causes for instantaneous and time-dependent borehole instability problems. Though there are comprehensive studies of the physiochemical aspect of shale drilling fluid interactions, only a few studies are available that describe the rock mechanical aspect of shale drilling fluid interactions. This R&D will concentrate on the testing and evaluation of the geomechanical aspect of shale drilling fluid interactions by conducting rock mechanical testing of original shale cores, water-saturated shale cores, and two WBM saturated shale cores to develop a comparative assessment of the rock-fluid interaction's effect on the mechanical properties of reactive shales/mud rocks.

This article describes the rock mechanical diagnostic signatures of rock-fluid interactions that were related to instantaneous and time-dependent borehole instability problems. This study will provide a tool for field engineers to predict the nature of the borehole instability problems and provide appropriate technical guidelines to the mud engineers and drilling fluid consultants to reduce the probability and the likelihood of creating instantaneous and time-dependent borehole instability problems.

## Introduction

The terminology "shale" is a driller's term<sup>1</sup> that is obsolete and was used to describe fissile claystones. Similarly, mud rock is a general term that focuses on the grain-size of the lithified sediment. Although both terms are still used, their use is inaccurate in describing the rocks. "Shale" is primarily used to mud rocks that are fissile irrespective of their mineralogical composition. The more accurate nomenclature of a rock that is composed mud-sized (clay and silt) siliciclastics is "claystone (> 66% clay)," "siltstone" (> 66% silt), or "mudstone" (mixture of clay- and silt-sized particles). In the case of carbonate, the mud-sized carbonates are termed "mudstone," or may be used with a prefix, e.g., lime mudstone to discriminate different types of mudstones if they exist in the context of the study. The samples used in this study are mostly an argillaceous mudstone with mainly calcite and dolomite as components, with minor percentages of kaolinite and pyrite.

Drilling mud is an inseparable part of the rotary drilling process and was routinely used to drill boreholes for exploration of oil and gas resources. These muds are nontoxic, of an eco-friendly nature, and high biodegradation characteristics<sup>2</sup>. Also, the preparation and handling of both in the field and the lab are low-cost compared to oil-based mud (OBM) systems. Commonly freshwater or salt water-based muds (WBMs) were used in drilling onshore and offshore.

These drilling mud systems were used for both drilling operations to explore and exploit oil and gas resources without causing any damage or degradation to other valuable resources. Moreover, due to the high affinity of the water molecules of WBMs to clay containing subsurface rocks such as shales, mud rocks and marls, they often create various time independent and time-dependent drilling problems such as borehole collapse, hole enlargement, heaving, shale sloughing, hole reduction, mud quality degradation, etc.<sup>3-5</sup>.

This is why the industry often switches to OBM for trouble-free drilling operations in the presence of shales, mud rocks, marls and other troublesome formations. Although, due to the negative environmental impact, poor biodegradation, and an undesirable effect on the occupational health and safety of workers and rig site professionals, and the virtually toxic nature of OBMs<sup>6</sup>, the industry is very interested to replace the OBMs and develop high performance WBMs to be in the forefront of the best drilling practices.

Mud engineers, mud chemists, and mud consultants often evaluate the physiochemical effect of shale drilling



mud interactions by evaluating the shale swelling potential<sup>7,9</sup>, cuttings dispersion tendency<sup>10</sup> and capillary suction time<sup>11</sup>, membrane generating capacity<sup>12</sup> and mud pressure penetration, and petrographic aspects of rock-fluid interactions, etc. These experimental results are used for chemical treatment of the mud systems to reduce or neutralize the chemical interactions of the water molecules with the reactive clays of the shales/mud rocks, and thereby stabilize the near wellbore shale formations. The results are also used to design superior and high performance WBM, evaluate the strength of rock-fluid interactions, and provide technical guidelines for trouble-free drilling operations.

Root cause analyses of various drilling problems encountered while drilling using non-inhibitive or poor quality WBMs highlighted the major factors triggering the problems. Scientists and the mud engineers found that the problems arise when the reactive water molecules of the mud systems interact with the water loving clays of shale and the mud rock matrix. Due to the high water affinity of the clays of the shale formations, the water phase of non-inhibitive or poorly inhibitive WBMs was easily attracted. This can lead to the WBMs inundating the clay surfaces, leading to high swelling, interparticle bond weakening, and the softening of the clays, and finally, the shale formation.

It creates not only a physiochemical effect with changes, but also rock mechanical degradation such as the strength reduction, a decrease in load-bearing capacity, a drop in interparticle adhesion and cohesion, and also the tensile, compressive and shear strength of the shale matrix. Due to these changes, there is a dramatic reduction in mechanical properties and biaxial and triaxial load behavior of the near wellbore formations. This is why shale formations frequently create drilling problems in the presence of WBMs.

The mechanical properties of subsurface rocks are very important for geomechanical modeling and mechanical stabilization of near wellbore formations for safe and trouble-free drilling operations<sup>13</sup>. Typically, the original rock mechanical properties such as the virgin unconfined compressive strength (UCS), Young's modulus and Poisson's ratios were used for modeling and the prediction of mechanical stability without considering the geomechanical effect of rock-fluid interactions.

As reactive WBM can cause significant damage and degradation of subsurface rocks — especially reactive shale and mud rocks — the use of the rock mechanical properties of the original non-damaged rock may lead to misleading information with disastrous consequences. Therefore, evaluation of the geomechanical aspect of rock-fluid interactions is very important for modeling, borehole stabilization, and safe drilling operations. This highlights the importance of the evaluation of the geomechanical aspects of rock-fluid interactions for safe and trouble-free drilling operations.

A review of published literature shows the abundance of publications related to physiochemical and mineralogical aspects of rock-fluid interactions to control

borehole instability problems, design superior WBMs to reduce nonproductive time and the operational cost. Only limited studies were conducted by the industry to evaluate the rock mechanical aspect of shale drilling fluid interactions<sup>14,15</sup> to use as a design tool for high performance and highly efficient WBMs.

This article describes the effect of shale drilling mud interactions on the rock mechanical properties of several shales/mud rock samples in the presence of water and two WBMs frequently used in drilling operations to highlight the degree of mechanical degradation of the shale samples, due to shale drilling mud interactions. The experimental data will provide valuable input parameters for the mechanical stabilization of near wellbore formations by a combination of physiochemical and mechanical approaches of wellbore stabilization by designing a new generation of WBM for current and future drilling operations.

WBMs that can prevent physiochemical interactions and enhance rock mechanical properties simultaneously will be highly effective in the stabilization of near wellbore formations, especially the reactive and vulnerable shale and mud rock formations for safe and trouble-free operations. The findings of this study will also help design superior inhibitive mud systems due to the consideration of the physiochemical and mechanical factors associated with shale drilling mud interactions.

## Experimental Study

### Drilling Mud Systems

Freshwater, potassium chloride (KCl) polymer, and low solids non-dispersed (LSND) mud systems were used in this study to evaluate the effect of water molecule interactions on UCS, angle of friction, and interparticle cohesion force. Freshwater was selected to represent the most aggressive environment. KCl-polymer and LSND muds are two common inhibitive mud systems that have some inhibition potential to prevent physiochemical and mechanical damage of the reactive shale samples. The addition of salt in the mud enhanced the shale inhibition potential of other inhibitors. Each mud was prepared by mixing the components in the proportions given in the formulation, Table 1. The components were used to match the field formulation and create a functional mud system with good rheological, filtration, and thixotropic properties and fulfill their various functional requirements in drilling reactive shales/mud rocks. It was assumed that the high-density solid phase of the drilling mud would have no significant effect in changing the mechanical properties of the rock. Therefore, no high-density materials were included in preparing the mud systems.

### Core and Plug Preparation

**Core Preservation:** Mineral oil was used for coring and core preservation. The preservation of the core was made on the rig by removing the shale from the core barrel, cut it, put in tubes, fill the tube with same coring fluid, then seal the tube. The methodology was adapted to minimize exposure to the atmosphere and

**Table 1** Formulations of the KCl-polymer and LSND mud systems used in the study.

KCl-polymer Composition	
Materials	Quantity
Water (ml)	332
Soda Ash (g)	0.25
Bentonite (g)	5
PAC LV (g)	3
XC Polymer (g)	1
KCl (g)	20
pH	9.5

LSND Mud Composition	
Materials	Quantity
Water (ml)	332
Soda Ash (g)	0.3
Bentonite (g)	6
PAC L (g)	3
XC Polymer (g)	1
KCl (g)	20
Soltex (g)	3
Sodium Sulfite (g)	1

sufficiently seal the core under controlled conditions.

**Plug Preparation:** Six samples, with a diameter of 1.5" and a length of 3", were plugged horizontally from a full core diameter (4"). These samples were drilled from a reactive shale section, Figs. 1 and 2.

The end faces of the plugged samples underwent grinding on the surface to become parallel and flat to within 0.001".

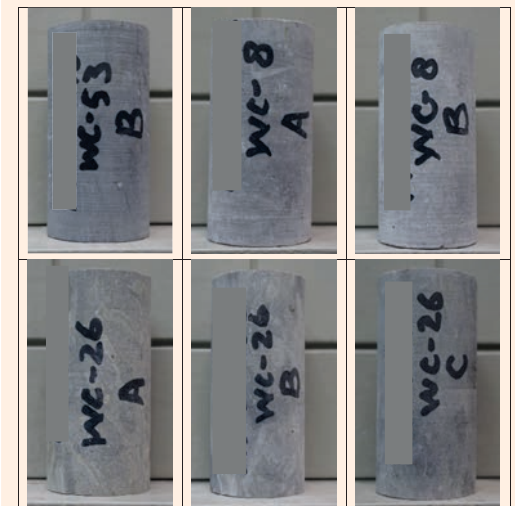
**Vacuum Saturation of Shale Samples:** Four shale samples of the same geological formations with roughly a similar mineralogical composition and physical condition were selected for the test. One sample was tested without any saturation to use as the benchmark sample for comparative evaluation of the interaction effect of the selected mud systems. Three samples were used to saturate with water, KCl-polymer mud, and LSND mud to simulate the interaction effect of a real borehole environment. A vacuum pump was used periodically to allow the infiltration of the mud into the shale matrix.

**CT Scan Analysis:** The analysis were carried out by computerized tomography (CT). Table 2 summarizes the details of the core samples and the parameters of

**Fig. 1** Images of the reactive shale sections where the plugs were drilled horizontally to be used as samples.



**Fig. 2** Images of the plugs drilled from the full core sample.




scanning.

The whole core samples listed in Table 2 were scanned in a nondestructive manner using a medical-type X-ray CT scanner at continuous mode starting from the top end of the sample. This CT scanning report of the overall core samples provides the following deliverables:

- CT scanning of the whole core samples to produce slice images at a close spacing of 1 mm in continuous mode.
- Analysis (histogram for each slice) and the images (slice and vertical/horizontal reconstructed slabs) have been reported.
- Additionally, high resolution CT slice images for the fracture detection purposes have also been prepared and presented in this report.

**Table 2** Summary of the CT scanning of the whole core samples.

1	Core size and state	4" diameter, 6" long Partial brine saturated
2	3 full diameter core samples: 8, 26, and 35	
3	CT slice thickness and space	1 mm in continuous mode
4	X-ray energy	135 kV/100 mA
5	CT scanner used	Toshiba RXL (medical type)
6	Pixel size	 0.234 × 0.234 mm
7	CT scale	Min: 1,000, Max: 3,000

Color-coding has been adopted to differentiate among minerals present in the scanned samples based on the variation of the densities. Based on the CT scale number, any cracks, vugs, or minerals on these slices smaller than a minimum CT number would be seen as black, and minerals higher than the maximum CT number would be seen as dark red.

To enable a direct comparison between all the scanned rock samples and to highlight the various minerals of different densities as well as vugs with a different color representation, a minimum CT number and maximum CT number given in Table 2 were determined and used. This means that the color code represents the CT numbers (Hounsfield units) based on the density of the sample, i.e., samples with a higher density produce higher CT numbers.

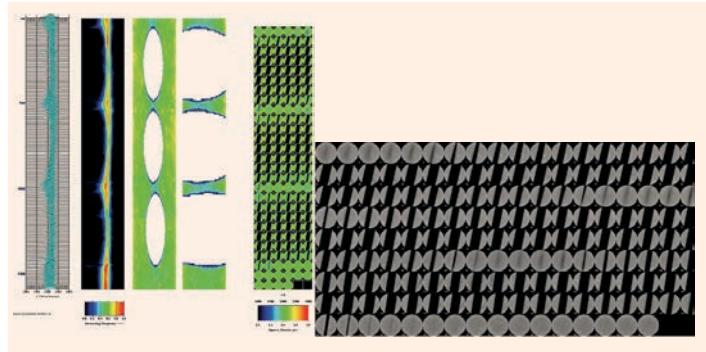
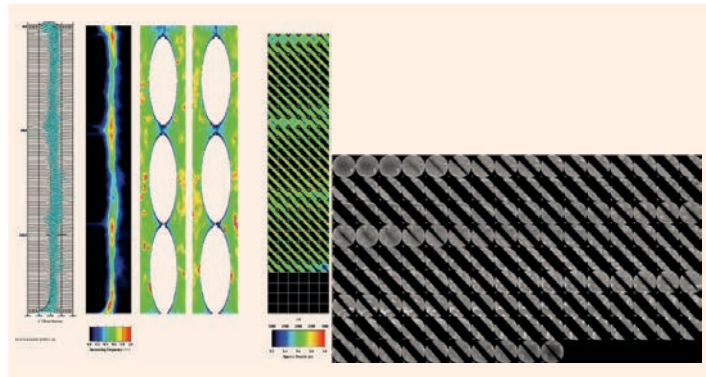
It helps to understand and interpret the definitions of the colors over the slices and slab images. For example, the blue color blended with black on a slice image indicates the lower density, while a yellow color blended with red indicates the higher density. A single color on a slice image indicates the higher homogeneity.

On the other hand, a combination of different colors, e.g., blue, green, yellow, and red, or combination of two or three colors on the same slice image indicates the higher heterogeneity, i.e., different densities. Subsequently, it is essential that when interpretations were made based on the CT slice images; color codes should always be used as a reference. Figures 3, 4, and 5 are the CT images for the scanned samples.

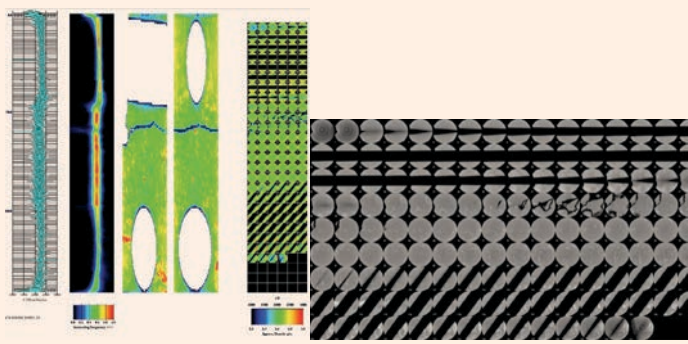
**Samples Preparation:** The samples were crushed to fine powder using a McCrone Micronizing Mill. The clay size fractions of the sample are separated and dried in air on the glass slide. The air-dried glass slide was glycolated in a desiccator containing ethylene glycol at 60 °C in an oven.

**Shale Mineralogy:** The X-ray powder diffraction (XRD) technique was used to determine the composition of core samples from Well-X. The result showed the analyzed samples consisted of sandstone (quartz) and carbonate minerals (calcite/dolomite) with minor quantities of clay minerals (kaolinite, halite), and iron sulfide (pyrite), Table 3.

The three samples indicate a carbonate rock, in which samples 8 and 53 are calcite (limestone), whereas sample 26 is dolomite. The minor quartz and phyllosilicates (kaolinite, palygorskite), rutile and pyrite may have environmental information such as the site of deposition, sedimentation processes, etc., but the entire sedimentology and geochemistry need to be looked at in parallel to draw any conclusions in that regard.

**Fig. 3** The CT scan image, Sample 8.**Fig. 4** The CT scan image, Sample 26.

**Fig. 5** The CT scan image, Sample 53.



### Rock Mechanics Testing

After completing the sample preparation as per the procedure, the plug is equipped and loaded onto the testing frame of a rock mechanical testing apparatus as follows:

- The jacket is clamped to the transducers from both ends to allow for hydraulic application of the confining pressure around the sample, Fig. 6.
- Radial and axial linear variable differential transformers (LVDTs) are positioned around and along the sample to measure radial and axial strains, respectively, Fig. 6.
- Confining pressure is applied hydrostatically around the sample. The confining pressures were selected to simulate the approximate stress condition found in the wellbore.

A series of multistage triaxial tests were performed on the selected samples.

For multistage testing, at first the sample is loaded hydrostatically to a specific confining pressure. Then the differential axial stress was increased slowly until a nonlinear stress-strain relationship was reached. At

this point, correspondent to the onset of plastic deformation, yield point ( $Y_p$ ), the axial load acting on the sample is released and a new confining pressure ( $P_{c-i}$ ) is applied before going through a new loading stage with the same procedure.

In the final cycle, the axial load was increased until full sample failure was reached to determine the difference between the  $Y_p$  and the peak stress at failure for this plug and then define the failure envelope for the tested sample. For this project, the Mohr-Coulomb failure envelope was constructed from three loading cycles according to the following procedure:

1. First, the difference between the differential peak stress ( $P_{dev-3}$ ) and the differential yield stress for stage 3 ( $Y_{dev-3}$ ) is calculated.
2. The result is then added to the differential yield stress for each of the other  $i$ -stages (stage 1 and stage 2):  $P_{dev-i} = Y_{dev-i} + (P_{dev-3} - Y_{dev-3})$ .
3. The total peak stress ( $P_{tot}$ ) at each stage was calculated adding the  $P_{c-i}$  to  $P_{dev-i}$ , where  $-i$  stands for the stage number.

**Fig. 6** Experimental setup for the triaxial tests.

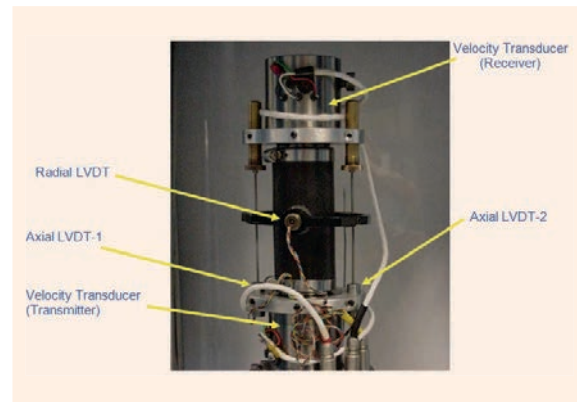


**Table 3** The XRD semi-quantitative phase analysis results for the samples.

Mineral	Sample #8 (wt%)	Sample #26 (wt%)	Sample #53 (wt%)
Calcite ( $\text{CaCO}_3$ )	91	1	89
Kaolinite ( $\text{Al}_2\text{Si}_2\text{O}_5(\text{OH})_4$ )	7	6	1
Quartz ( $\text{SiO}_2$ )	1	26	6
Pyrite ( $\text{FeS}_2$ )	1	1	—
Dolomite ( $\text{CaMg}(\text{CO}_3)_2$ )	—	66	2
Halite ( $\text{NaCl}$ )	—	traces	—
Rutile ( $\text{TiO}_2$ )	—	traces	—
Palygorskite ( $\text{MgAlSi}_4\text{O}_{10}(\text{OH})(\text{H}_2\text{O})_4$ )	—	—	2



The following data was collected during each test:

- Vertical stress: The vertical stress was applied axially at an axial displacement rate of 3 mm/hour to 6 mm/hour (4% to 8% strain). The loading rate was applied in such a way that full failure or near failure was reached within 5 to 15 minutes.
- Axial strain: The axial strain was measured from the two LVDTs positioned on two locations 180° apart along the axis of the sample.
- Radial strain as measured from the radial LVDT.
- Confining pressure as provided by the confining fluid.
- $V_p$  and  $V_s$  velocity from an ultrasonic signal propagated axially through the sample.

The static elastic properties are determined from the stress-strain curve of the multistage test. In addition, ultrasonic compressional and shear velocities were measured on each sample during the three steps of the multistage test phases under triaxial loading. A final average is derived for the dynamic and static moduli (Young's modulus and Poisson's ratio) representing the elastic properties of the specific plug.

The UCS, cohesion ( $C_p$ ) and friction angle ( $\phi$ ) were also computed for each plug. These parameters were used to determine the Mohr-Coulomb yield envelope of the rock samples.

## Results and Discussion

### Testing and Evaluation Method

Shale samples were prepared from the same core of a reactive shale section. These core samples were taken from the same section of the core that has nearly similar mineralogical composition and physical characteristics. Six core samples were selected for interactions with a highly reactive WBM and two inhibitive mud systems (KCl-polymer and LSND mud).

A vacuum pump was used for quick saturation and interaction with the mud systems. Two samples were tested without any interaction with a WBM. Here, water was selected to represent the most aggressive WBM. After saturation for 16 hours, the UCS of virgin, water interacted, KCl-polymer mud interacted, and the LSND mud interacted rock samples were determined using rock mechanical loading frame.

### Dry Samples

Samples WC-53-B and WC-8-A were tested in a dry state, Figs. 7 to 10. Data from these tests were used as a baseline to evaluate the effect of exposure of the samples to different drilling fluids on the mechanical properties of the study rock. A CT scan was conducted on the core samples. The uniaxial compressive strength of the dry samples is higher than those of the samples exposed to the selected mud systems by as much as 50% (WC-8-A). The mechanical behavior of the two samples is markedly different: WC-53-B has a higher stiffness and friction angle, while WC-8-A presents an extensive plastic deformation zone and higher cohesion resulting in a higher UCS in spite of lower yield and peak strengths measured in the three test cycles.

Fig. 7 The triaxial test results for plug WC-53-B.

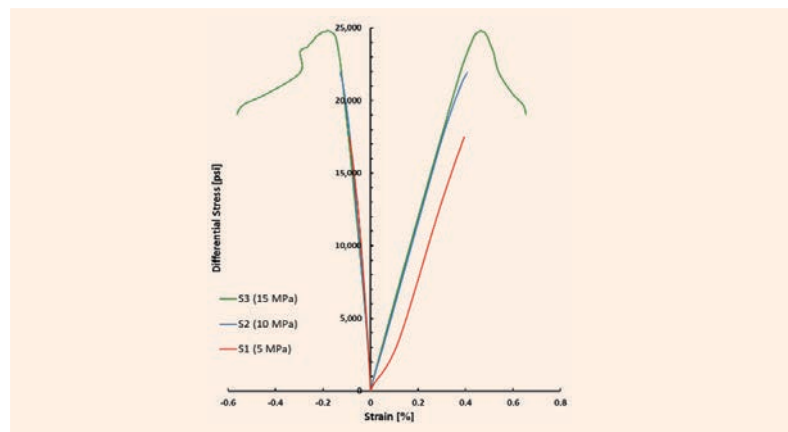


Fig. 8 The triaxial test results for plug WC-8-A.

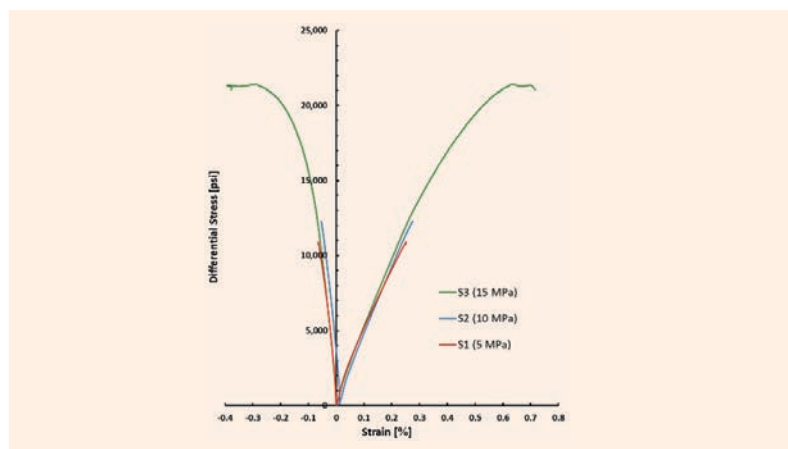
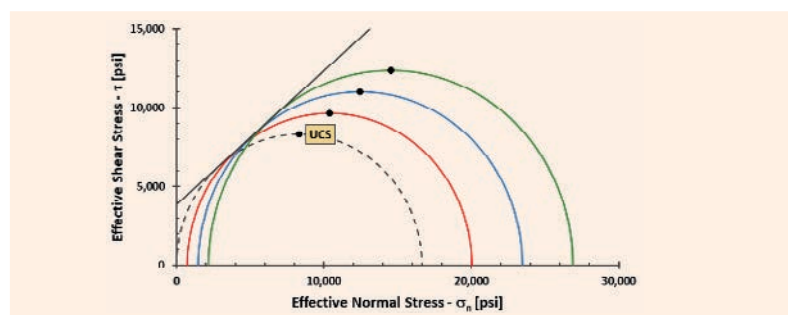


Fig. 9 The Mohr-Coulomb interpretation for plug WC-53-B.



### Saturated Samples: Water

Samples WC-8-C and WC-26-A were tested in a water-saturated state, Figs. 11 to 14. Water was selected to represent the most aggressive WBM. Plugs saturated in water show the lowest UCS of the series, similar to

Fig. 10 The Mohr-Coulomb interpretation for plug WC-8-A.

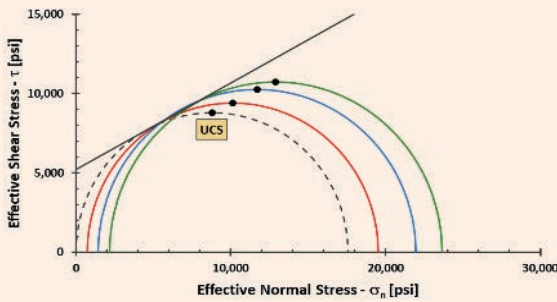


Fig. 11 The triaxial test results for plug WC-8-C.

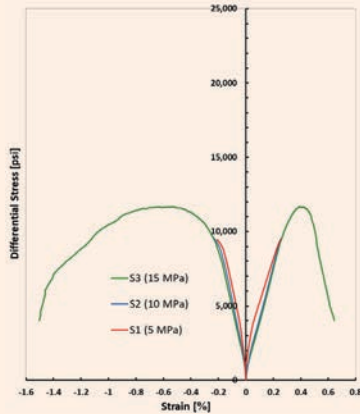


Fig. 12 The triaxial test results for plug WC-26-A.

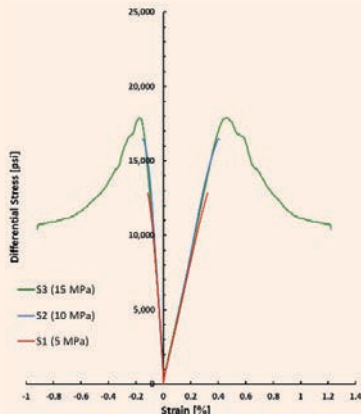


Fig. 13 The Mohr-Coulomb interpretation for plug WC-8-C.

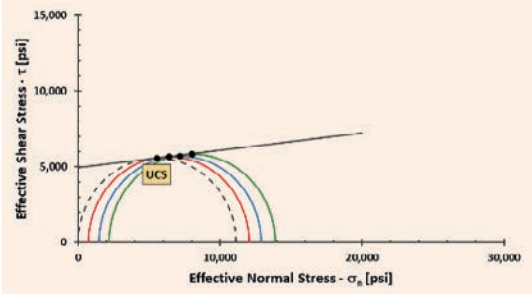


Fig. 14 The Mohr-Coulomb interpretation for plug WC-26-A.

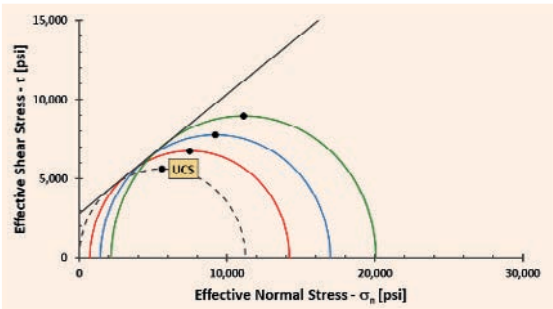
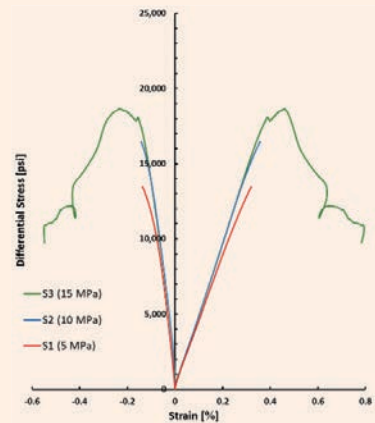


Fig. 15 The triaxial test results for plug WC-26-B.



the strength of the KCl saturated samples, but lower than that of LSND saturated samples. Plug WC-8-C exhibits a very low friction angle; it is possible that the test results are affected by the possible presence of a discontinuity not detected before the test. The same feature may also cause the large value in Poisson's ratio.

**Saturated Samples: KCl and LSND**

Sample WC-26-B was tested in a KCl saturated state. Sample WC-26-C was tested in an LSND saturated state. Exposure to different mud systems is affecting the shale rock in different fashions, with the KCl-polymer brine having an effect on the strength of the rock similar to that of water, and the LSND brine displaying a somehow intermediate effect on the plug strength,

Fig. 16 The triaxial test results for plug WC-26-C.

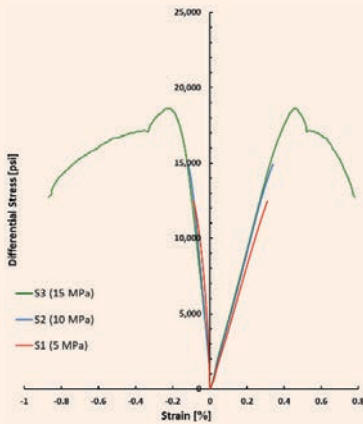
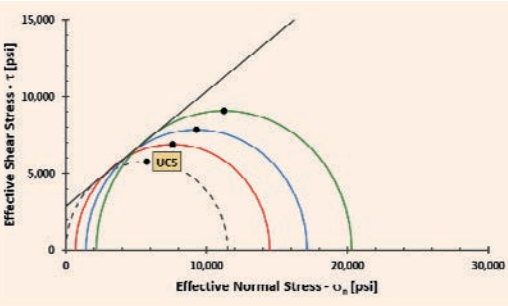


Fig. 17 The Mohr-Coulomb interpretation for plug WC-26-B.

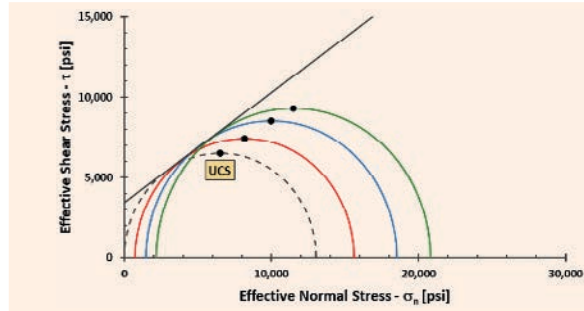


Figs. 15 to 18.

In all the cases, the stiffness of the plugs do not seem to be affected by exposure to different mud systems as compared to the dry sample (WC-53-B), except in the case of plugs originated from the WC-8 whole core sample. Table 4 provides a summary of all tests.

In general, the data indicates the mechanical degradation of the rocks, especially clay containing rocks due

Fig. 18 The Mohr-Coulomb interpretation for plug WC-26-C.



to the interactions of water molecules with the clays and other reactive and water sensitive components of the rock samples. Subsequently, the strength of the interactions varies depending on the sample quality, sample characteristics, and the inhibition potential of the WBM.

### Conclusions

1. The rock mechanical testing shows that simple water or non-inhibitive WBM represents the most aggressive fluids compared to the KCl-polymer and the LSND muds.
2. All WBM cause some degradation and damage of subsurface rock formations, especially the clay containing shales and mud rocks. Although, the degradation amount varies depending on the inhibition potential of the WBM.
3. In this study, the traditional KCl-polymer mud showed lower performance than the LSND mud, probably due to the reduced infiltration of the inhibitors into the sample matrix.
4. The LSND mud showed the least degradation of the rock mechanical properties compared to water and the KCl-polymer mud. Therefore, it is a better alternative to drill formations that have similar mineralogical composition and geomechanical characteristics.

Table 4 A summary of the triaxial test results.

Sample #	Saturating Fluid	E <sub>stat</sub> (psi)	E <sub>dyn</sub> (psi)	v <sub>stat</sub>	v <sub>dyn</sub>	UCS (psi)	Φ (deg)	C <sub>0</sub> (psi)
WC-53-B	Dry	5.65E+06	8.01E+06	0.301	0.295	16,644	40.3	3,850
WC-8-A	Dry	4.14E+06	7.12E+06	0.289	0.276	17,575	28.6	5,216
WC-26-A	Water	4.38E+06	8.67E+06	0.346	0.287	11,226	37.0	2,799
WC-26-B	KCl	4.35E+06	8.77E+06	0.355	0.274	11,500	36.8	2,882
WC-26-C	LSND	4.62E+06	8.23E+06	0.363	0.292	13,047	34.4	3,440

5. A comprehensive study using cores containing low, high, very high, and extremely high clays and various shale inhibitors can provide very useful data about the mechanical aspect of rock-fluid interactions.

## Acknowledgments

The authors would like to acknowledge the support provided by the Drilling Technology Division Lab technicians in preparing the mud samples, and the Petrophysics Department personal in testing and evaluating the rock samples.

## References

1. Holmes, A.: *The Age of the Earth*, 2<sup>nd</sup> edition, Thomas Nelson & Sons Ltd., London, 1957, 277 p.
2. Amanullah, M. and Yu, L.: "Environment Friendly Fluid Loss Additives to Protect the Marine Environment from the Detrimental Effect of Mud Additives," *Journal of Petroleum Science and Engineering*, Vol. 48, Issues 3-4, September 2005, pp. 199-208.
3. Chenevert, M.E. and Osisanya, S.O.: "Shale/Mud Inhibition Defined with Rig Site Methods," *SPE Drilling Engineering*, Vol. 4, Issue 3, September 1989, pp. 261-268.
4. Lomba, R.F.T., Chenevert, M.E. and Sharma, M.M.: "The Role of Osmotic Effects in Fluid Flow through Shales," *Journal of Petroleum Science and Engineering*, Vol. 25, Issues 1-2, January 2000, pp. 23-25.
5. Maury, V.M. and Sauzay, J.-M.: "Borehole Instability: Case Histories, Rock Mechanics Approach, and Results," SPE/IADC paper 16051, presented at the SPE/IADC Drilling Conference, New Orleans, Louisiana, March 15-18, 1987.
6. Amanullah, M.: "Physiochemical Characterization of Vegetable Oils and Preliminary Test Results of Vegetable Oil-Based Muds," SPE/IADC paper 97008, presented at the Middle East Drilling Technology Conference and Exhibition, Dubai, UAE, September 12-14, 2005.
7. O'Brien, D.E. and Chenevert, M.E.: "Stabilizing Sensitive Shales with Inhibited, Potassium-Based Drilling Fluids," *Journal of Petroleum Technology*, Vol. 25, Issue 9, September 1975.
8. Amanullah, M., Marsden, J.R. and Shaw, H.F.: "An Experimental Study of the Swelling Behavior of Mud Rocks in the Presence of Drilling Mud Systems," *Canadian Journal of Petroleum Technology*, Vol. 36, No. 3, March 1997, pp 45-50.
9. Berry, S.L., Boles, J.L., Brannon, H.D. and Beall, B.B.: "Performance Evaluation of Ionic Liquids as a Clay Stabilizer and Shale Inhibitor," SPE paper 112540, presented at the SPE International Symposium and Exhibition on Formation Damage Control, Lafayette, Louisiana, February 15-15, 2008.
10. Emmanuel, O.E. and Dosunmu, A.: "Experimental Analysis of Shale for Evaluating Shale Drilling Fluid Interaction in Agbada Formation," *British Journal of Applied Science & Technology*, Vol. 4, Issue 35, 2014, pp. 4878-4907.
11. Sethi, R., Hinkel, J.J. and Mackay, B.: "An Alternative to the Capillary Suction Time Test," SPE paper 173789, presented at the SPE International Symposium on Oil Field Chemistry, The Woodlands, Texas, April 13-15, 2015.
12. Tan, C.P., Amanullah, M., Mody, F.K. and Tare, U.M.: "Novel High Membrane Efficiency Water-Based Drilling Fluids for Alleviating Problems in Troublesome Shale Formations," SPE paper 77192, presented at the IADC/SPE Asia Pacific Drilling Technology, Jakarta, Indonesia, September 9-11, 2002.
13. Amanullah, M., Marsden, J.R. and Shaw, H.F.: "Effects of Rock-Fluid Interactions on the Petrofabric and Stress-Strain behavior of Mud Rocks," SPE paper 28050, presented at the Rock Mechanics in Petroleum Engineering, Delft, the Netherlands, August 29-31, 1994.
14. Mody, F.K. and Hale, A.H.: "Borehole Stability Model to Couple the Mechanics and Chemistry of Drilling Fluid Shale Interaction," *Journal of Petroleum Technology*, Vol. 45, Issue 11, November 1993, pp. 1093-1101.
15. Lal, M.: "Shale Stability: Drilling Fluid Interaction and Shale Strength," SPE paper 54356, presented at the SPE Asia Pacific Oil and Gas Conference, Jakarta, Indonesia, April 20-22, 1999.

---

### About the Authors

#### Dr. Mohammad H. Alqam

Ph.D. in Petroleum Engineering,  
King Fahd University of Petroleum  
and Minerals

Dr. Mohammad H. Alqam is currently a Research Consultant in the Rock Mechanics Laboratory in the Advanced Technical Services Division within Saudi Aramco's Exploration and Petroleum Engineering Center – Advanced Research Center (EXPEC ARC).

He has more than 35 years of experience with Saudi Aramco and has been involved in an emulsion study, formation damage, hydraulic

fracturing studies and rock mechanics studies.

In 1991, Mohammad received his B.S. degree in Chemistry from California State University, Fresno, CA, and in 1997, he received his M.S. degree in Chemistry from King Fahd University of Petroleum and Minerals (KFUPM), Dhahran, Saudi Arabia. Mohammad received his Ph.D. degree in Petroleum Engineering from KFUPM.



**Dr. Md. Amanullah**

*Ph.D. in Petroleum Engineering,  
Imperial College*

Dr. Md. Amanullah was a Senior Petroleum Engineering Consultant working at Saudi Aramco's Exploration and Petroleum Engineering Center – Advanced Research Center (EXPEC ARC) before his retirement. Prior to joining Saudi Aramco, he worked as a Principal Research Scientist at CSIRO in Australia.

Aman is the lead inventor of a vegetable oil-based dielectric fluid (patented) that led to the formation of a spinoff company in Australia for commercialization of the product.

He has published more than 100 technical papers and filed more than 75 patents, with 30

already granted. He is a member of the Society of Petroleum Engineers (SPE). In 2018, Aman received the Middle East Oil and Gas Technical Innovation of the Year Award, and he also received the Board of Engineers Recognition Certificate for Date Seed-based ARC Plug development.

Aman received his M.S. degree (First Class) in Mechanical Engineering from the Moscow Oil and Gas Institute, Moscow, Russia, and his Ph.D. degree in Petroleum Engineering from Imperial College, London, U.K.

**Antonio A. Santagati**

*M.S. in Geological Engineering,  
University of Oklahoma*

Antonio A. Santagati is a Geological Specialist leading the Rock Mechanics Team in the Advanced Technical Services Division within Saudi Aramco's Exploration and Petroleum Engineering Center – Advanced Research Center (EXPEC ARC). His operational focus is with the expansion of the Rock Mechanics Laboratory productivity and service portfolio.

Currently, Antonio is collaborating in operational and research efforts with the Reservoir Management Department, the Unconventional Resources Department, and

other EXPEC ARC teams.

He has almost 25 years of global experience in geomechanics and geotechnical engineering across Europe, North America, the Middle East, India, and Southeast Asia.

Antonio's main interests lie in the analysis of fracture behavior under a triaxial state of stress and in the development of quality control procedures for rock mechanical data.

He received his M.S. degree in Geological Engineering from the University of Oklahoma, Norman, OK.

**Salem H. Algarni**

*B.S. in Mechanical Engineering,  
King Fahd University of Petroleum  
and Minerals*

Salem H. Algarni is a Geomechanics Scientist working in the Advanced Technical Services Division within Saudi Aramco's Exploration and Petroleum Engineering Center – Advanced Research Center (EXPEC ARC). He is currently leading the hydraulic fracturing testing area in the RM laboratory, where he is working on developing a lab workflow and testing procedure for geomechanical property modeling for hydraulic fracturing.

In 2013, Salem received his B.S. degree in Mechanical Engineering from King Fahd University of Petroleum and Minerals (KFUPM), Dhahran, Saudi Arabia. He is currently studying for his M.S. degree in Petroleum Engineering at KFUPM as a part time student.

Salem received his Society of Petroleum Engineers (SPE) certification and became a certified Petroleum Engineer in 2019.

**Adnan H. Al-Makrami**

*B.S. in Petroleum and Natural Gas  
Engineering,  
Pennsylvania State University*

Adnan H. Al-Makrami is an Engineer working at the Rock Mechanics Laboratory in the Advanced Technical Services Division within Saudi Aramco's Exploration and Petroleum Engineering Center – Advanced Research Center (EXPEC ARC). His focus is on stress dependent permeability testing on low permeability samples.

As part of Adnan's development program in

geomechanics, he completed two years of training during his assignments with the Production Engineering Department and the Unconventional Resources Department.

In 2013, Adnan received his B.S. degree in Petroleum and Natural Gas Engineering from Pennsylvania State University, State College, PA.

**Dr. Sinan Caliskan**

*Ph.D. in Civil Engineering,  
Cardiff University*

Dr. Sinan Caliskan is a Petroleum Engineering Specialist working in the Petrophysics Unit within Saudi Aramco's Exploration and Petroleum Engineering Center – Advanced Research Center (EXPEC ARC). Since joining Saudi Aramco in 2007, he has been the Group Leader of the Computerized Tomography Unit.

During his postgraduate studies, Sinan investigated fracture properties of composite materials, by means of experimental, numerical

as well as visualization techniques. He then moved to academia and worked for six years in Dundee University, Dundee, Scotland, later earning an Associate Professor title.

Sinan received his M.S. degree (1997) and his Ph.D. degree (2001) in Civil Engineering from Cardiff University, Cardiff, U.K.

He has been granted several patents, published more than 40 technical articles and edited two books.

# Thermochemical Acid Fracturing of Tight and Unconventional Rocks: Experimental and Modeling Investigations

*Dr. Zeeshan Tariq, Dr. Murtada S. Al-Jawad, Dr. Mohamed Mahmoud, Dr. Abdulazeez Abdulraheem and Ayman R. Al-Nakhli*

## Abstract /

The exploitation of unconventional formations requires propped hydraulic fracturing treatments. Propped fracturing is an expensive process that usually suffers from operational challenges. In this study, a new technology is proposed, which targets implementing thermochemical fluids to stimulate unconventional formations. These fluids release large pressure pulses upon a reaction that creates networks of cracks along the fracture. Triggering thermochemical fluids with acid creates differential etching along the fracture surfaces due to the acid/rock dissolution.

The new technology was tested experimentally through coreflooding on Indiana limestone and Kentucky sandstone samples, and through breakdown pressure experiments on Eagle Ford shale samples. The breakdown pressure of the Eagle Ford shale samples was reduced from 2,400 psia to 900 psia using thermochemical fluids triggered with acid. It was also observed that the acid triggered thermochemical fluids could maintain the permeability of the fractures at high closure stresses due to the acid/rock dissolution.

Laboratory and field-scale models were also developed in this study to understand the thermochemical reactions. The laboratory-scale model could capture the pressure pulses generated experimentally and the system temperature. The field-scale model was then used to understand the thermochemical reactive transport in a hydraulic fracture. The model showed that thermochemical concentration is the most significant parameter in controlling the temperature and pressure magnitudes in the field.

## Introduction

Unconventional reservoirs are those that need special methods to produce hydrocarbons economically. Horizontal drilling combined with multistage hydraulic fracturing is one of the best stimulation methods to produce from tight unconventional reservoirs. Hydrocarbon reserves trapped within these types of low permeability formations exhibit little to negligible production. Accessing these reserves requires large fracture networks with high conductivity to maximize well performance when implementing existing conventional recovery methods. Recovery from these unconventional reservoirs requires assertive and expensive solutions, such as hydraulic fracturing stimulation methods<sup>1</sup>. Some of the examples of unconventional reservoirs may include tight sands, coal bed methane, tar sands, heavy oil, gas hydrates, and oil-rich shales<sup>2-4</sup>.

Production from unconventional formations require special techniques to enhance the stimulated reservoir volume. Stimulated reservoir volume is a term used to quantify the stimulated area in an unconventional reservoir by the creation of multiple complex fracture networks. The combination of horizontal drilling and hydraulic fracturing has allowed access to previously inaccessible hydrocarbon sources. Consequently, stimulation of the unconventional hydrocarbon resources with horizontal drilling and conventional hydraulic fracturing methods could be challenging, due to several reasons such as high breakdown pressure of the rock, huge reservoir compaction, high rock integrity, large rock stiffness, huge overburden pressure, etc.<sup>5,6</sup>.

To address the difficulties and challenges associated with conventional fracturing methods, an alternative way to treat unconventional resources is by generating synthetic hotspots — pockets of high porosity and high permeability regions — using pulse fracturing treatments. Pulse fracturing is a relatively new technique, in which the injection pressure rises in a fraction of seconds to create multiple microfractures. Pulse fracturing, also called dynamic loading, can be executed by several methods such as explosive shooting, impact loading, by the release of high-energized gases, and by means of thermochemical fluids<sup>7-9</sup>.

Thermochemical fluids are those fluids upon which reaction can cause a strong exothermic reaction. The reaction can simultaneously generate high-pressure and high temperature (HPHT). For the past many years, the oil and gas industry has witnessed many thermochemical fluid applications in different areas. The first application of thermochemical reaction in the petroleum industry appeared in 1986 when McSpadden et al.

(1986)<sup>10</sup> utilized them to dissolve the paraffin waxes from the tubing of producing wells. Khalil et al. (1994)<sup>11</sup> used thermochemical fluids to dissolve paraffin deposited in subsea production lines.

Amin et al. (2007)<sup>12</sup> and Singh and Saidu Mohamed (2013)<sup>13</sup> found a huge increment in the production profiles of the wells treated with thermochemical fluids for wax and organic scale removal. Al-Nakhli (2015)<sup>14</sup> used thermochemical fluids to enhance the stimulated reservoir volume by in situ generations of localized pressure and temperature. They found that due to chemically induced pressure pulses, the stimulated reservoir volume of the reservoir increased tremendously. Wang et al. (2018)<sup>15</sup> used thermochemical fluids for the first time in the application of enhanced oil recovery.

They generated the in situ foams by mixing surfactants with thermochemical fluids, and carried out oil recovery experiments using coreflooding setup. Through their experiments, they reported a 20% to 34% increment in oil recovery. The other areas of petroleum engineering where thermochemical reactions have been investigated included thermochemical fracturing<sup>16,17</sup>, wax removal<sup>15,18</sup>, paraffin removal<sup>10,11</sup>, filter cake removal<sup>19</sup>, organic scale removal<sup>12</sup>, foam flooding by mixing thermochemical fluids with surfactants<sup>15</sup>, heavy oil recovery<sup>20</sup>, sludge removal<sup>21</sup>, stimulated reservoir volume enhancement<sup>14, 22, 23</sup>, and in situ steam generation<sup>24</sup>.

Acid induced thermochemical fracturing is a unique stimulation technique in which any low pH acid type such as acetic acid or hydrochloric (HCl) acid are used to trigger the thermochemical reaction. The thermochemical reaction needs a medium or source for the reaction to start. First, acid is injected to saturate the rock sample. After the acid injection is completed, a slug of thermochemical fluids is injected to start the reaction.

Figure 1 shows the conceptual diagram of the new method. Due to acid injection, an etched surface is created, which helps the fracture to remain open under closure stresses.

Therefore, in this research, thermochemical reagents are used to fracture the unconventional rock samples. The goal of this research work is to study the impact and potential of different thermochemical fluids in

reducing the breakdown pressure of the unconventional tight rocks. The proposed study also explored the advantage of thermochemical fluids in eliminating the need for injecting large volumes of proppants. Both experimental and numerical studies are presented and discussed. The results of coreflooding and breakdown pressure experiments on different rock samples such as shale, tight sands, and tight carbonates are discussed. The numerical study presents the laboratory and field-scale models to understand the phenomenon of the pressure pulse in thermochemical reactions and reactive transport in the hydraulic fracturing.

## Experiment Methodology

### Experimental Apparatus

The process flow diagram of the breakdown pressure/hydraulic fracturing experimental setup, Fig. 2. The experimental setup was mainly comprised of a HPHT special core holder, two piston transfer cells, two injection pumps, an electric oven, pressure sensors, a data acquisition system, and several HPHT valves and fittings. The special core holder used could accommodate a cylindrical core sample with a 2" diameter and a length up to 12".

The core specimen tested in this study had an outside diameter and length of 2". The length of the specimen inside the core holder was fixed by adding several spacers between the upper and lower end caps. A cylindrical core sample was fitted in a viton sleeve and mounted onto a fixed platen at one end while the floating platen was at the other end, through which the fluid passes via a 1/4" diameter tubing. Each thermochemical reagent was stored in a separate piston accumulator. Each accumulator had a capacity of 1,000 ml. An electric oven with a maximum heating capacity of 150 °C was used in the study. A core holder was fitted inside the electric oven.

An ISCO pump with a maximum pumping rate

**Fig. 1** A conceptual diagram of the new method for acid induced thermochemical fracturing.

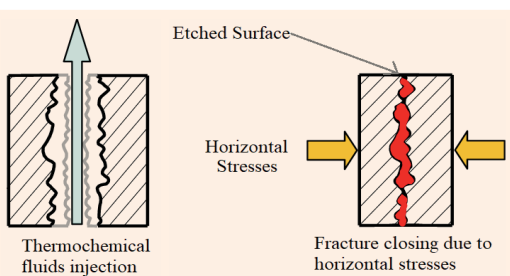
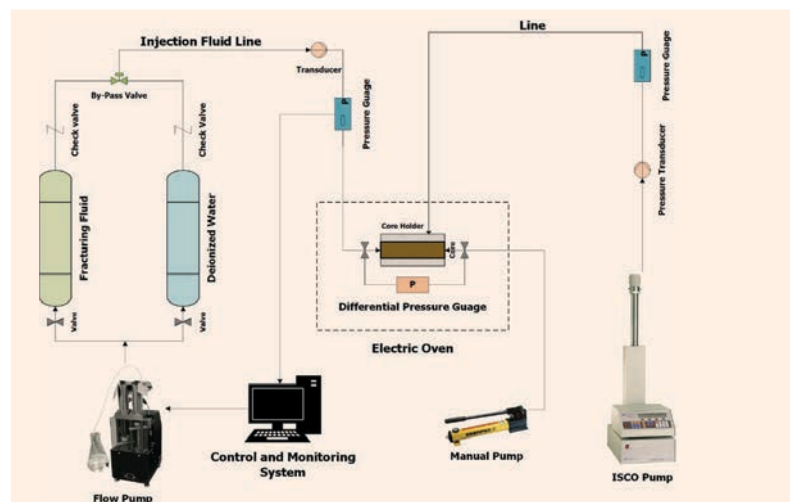


**Fig. 2** A schematic of the breakdown pressure/hydraulic fracturing experimental setup.

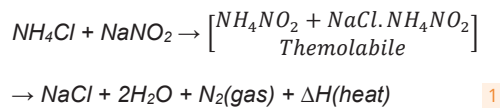


capacity of 50 ml/min was used to transfer fracturing fluid from the piston transfer cell to the core holder. The maximum injection pressure of the ISCO pump was 10,000 psi. All HPHT connections and fittings were used in the experimental setup. The overburden pressure and the injection pressure were applied from independent lines; therefore, the injection pressure was assumed not to interfere with the overburden pressure. To record the overburden and injection pressures, a high-resolution pressure sensor was installed at the inlet of the core holder. The pressure sensor could record 10 readings/sec. The data was then processed at the computer operating software.

A similar setup was used for the coreflooding experiments. The coreflooding experimental setup consists of an ISCO injection pump, two transfer cells, a core holder, a back pressure regulator, an overburden pressure pump, pressure transducers, and an electric oven.

### Thermochemical Fluids

In this study, the thermochemical fluids used were comprised of salts of nitrogen, such as sodium nitrite ( $\text{NaNO}_2$ ) and ammonium chloride ( $\text{NH}_4\text{Cl}$ ). The two reagents were used in the proportion of one to one. The solution mixture was prepared at an ambient temperature and pressure conditions. When one mole of  $\text{NaNO}_2$  reacts with one mole of  $\text{NH}_4\text{Cl}$ , a strong exothermic chemical reaction happened and sodium chloride salt, water (steam), and nitrogen gas is released. The release of nitrogen gas is the reason for high-pressure generation. This thermochemical reaction can be defined by Eqn. 1:



This reaction resulted in the generation of an intermediate product named Themolabile, which immediately transformed into sodium chloride (brine), nitrogen gas, and steam. Comprehensive reaction kinetics of thermochemical fluids were investigated and the reaction parameters, such as enthalpy change, thermal conductivity, and specific heat capacity, were determined in the laboratory, which are listed in Table 1. These parameters were determined to produce the thermal energy required to dissolve filter cake formed with water-based and oil-based drilling fluids.

This reaction could generate HPHTs as recorded

from laboratory experiments and field practices. The thermochemical reaction was studied under a batch system in an insulated HPHT micro-reactor. The setup for the monitoring progress of a thermochemical reaction consists of a heater, a nitrogen gas cylinder for pressure control, a HPHT batch micro-reactor, and the pressure and temperature sensors coupled with a data acquisition system. The advancement of the reaction was followed by collecting data for the increase in pressure and temperature at equal intervals of time.

Figure 3 shows the effect of the molar concentration on achieving the pressure peak vs. time. With one molar concentration of thermochemical fluid, the reaction could generate a pressure peak of up to 3,500 psi in 40 seconds while with two molar concentration of thermochemical fluids, the reaction could generate a pressure peak of up to 5,500 psi in 30 seconds. The experiment was conducted in an aging cell with a 20 cc volume. The experiment began with an initial pressure of 1,000 psi and the preheated temperature of 100 °C. The figure essentially shows that increasing the molar concentration of the reactants could enhance the pressure generation.

The pressure pulse was generated due to the liberation of nitrogen gas. The pressure pulse declined due to the fluid conversion to hot water and gas. The curve was declined because nitrogen gas was dissolved as the reaction product. After declination of the pressure curve, it became flattened and aligned with an

**Fig. 3** The effect of one and two molar concentrations on the pressure pulse generation, due to thermochemical fluids.

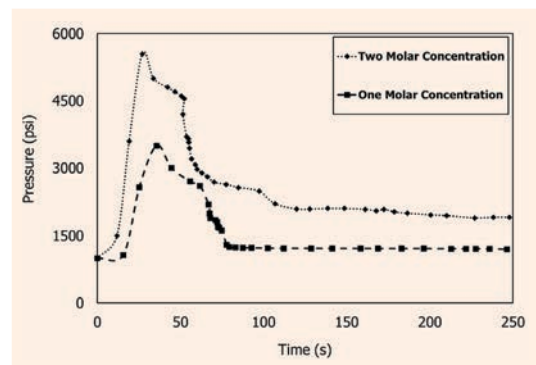


**Table 1** Reaction parameters obtained from the thermochemical reaction when one molar concentration of reagents was utilized.

Reaction Parameters	Values	Units
Enthalpy change ( $\Delta H$ )	369	$\text{kJ/mol}$
Thermal conductivity ( $\lambda$ )	0.1 – 0.6	$\text{W/m.K}$
Specific heat capacity ( $C$ )	85 – 110	$\text{J/mol.K}$

approximate initial cell pressure. The pressure pulse was generated a few seconds after the reaction. In the rock, this pulse could create microfractures, and that would reduce the breakdown pressure of the rock.

This figure essentially shows that increasing the molar concentration of the reactants could enhance the pressure generation. The thermochemical reaction could be initiated by preheating a cell to 100 °C or by using any low pH acid. This generated pressure pulse from the release of nitrogen gas was logged in an aging cell with a capacity of 20 cc.

### Rock Characterization

Shale, sandstone, and limestone rock samples were tested in this study. Specifically, Eagle Ford shale, Indiana limestone, and Kentucky sandstone were collected and characterized in the laboratory. X-ray diffraction (XRD) analysis was utilized in the laboratory to determine the mineralogical composition of the studied samples.

The Eagle Ford shale and Indiana limestone were predominantly composed of calcite content, 82% and 99.29%, respectively, whereas the Kentucky sandstone comprised mainly of quartz content (61%). A moderate amount of Illite was present in the Kentucky sandstone (14%) while a very small amount of 1.4% of Illite was found in the Eagle Ford shale.

Table 2 lists the complete XRD analysis of the Eagle Ford shale, the Indiana limestone, and the Kentucky sandstone samples. Routine core analysis was conducted on the rock samples and the petrophysical properties such as porosity, permeability, and density

were measured.

Table 3 shows the petrophysical properties of the three samples.

### Samples Preparation

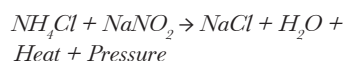
The Kentucky sandstone and Indiana limestone samples had a length of 3" and a diameter of 1½". The Eagle Ford shale sample had a length of 2" and a diameter of 2". A 6 mm diameter hole was drilled at the center of the shale sample to a depth of 0.75". A stainless steel casing was inserted inside the drilled hole to a depth of 0.5", leaving an open hole section of 0.25", and then cemented to the rock sample using epoxy. Figure 4 is an image of the prepared shale rock sample with the steel tubing fixed with epoxy.

## Experimental Results and Discussion

### Coreflooding Experiments

Coreflooding experiments with two types of thermochemical fluids were conducted on the Kentucky sandstone and Indiana limestone. An overburden pressure between 500 psi to 2,500 psi was applied in all coreflooding experiments. The two types of thermochemical fluids were thermochemical fluid A and thermochemical fluid B. Thermochemical fluid A was triggered with a heat mechanism and thermochemical fluid B was triggered with acid.

Thermochemical A presents the following compositions:



2

**Table 2** The complete XRD analysis of the Eagle Ford shale, the Indiana limestone, and the Kentucky sandstone samples.

Mineral Name	Chemical Formula	Weight Percentage (%)		
		Eagle Ford Shale	Indiana Limestone	Kentucky Sandstone
Calcite	CaCO <sub>3</sub>	82.7	99.29	—
Quartz	SiO <sub>2</sub>	5.1	—	61
Gypsum	CaSO <sub>4</sub> ·2H <sub>2</sub> O	4	—	—
Dolomite	CaMg(CO <sub>3</sub> ) <sub>2</sub>	4	—	—
Kaolinite	Al <sub>4</sub> [Si <sub>4</sub> O <sub>10</sub> ](OH) <sub>8</sub>	2.4	—	—
Illite	(K <sub>1-1.5</sub> Al <sub>4</sub> )[Si <sub>7-6.5</sub> Al <sub>1-1.5</sub> O <sub>20</sub> ](OH) <sub>4</sub>	1.4	—	14
Potassium Feldspar	KAlSi <sub>3</sub> O <sub>8</sub>	—	—	3
Plagioclase	(Na, Ca)(Si, Al) <sub>4</sub> O <sub>8</sub>	—	—	5
Sodium Feldspar	NaAlSi <sub>3</sub> O <sub>8</sub>	—	—	17
Ankerite	Ca(Fe <sup>2+</sup> , Mg, Mn)(CO <sub>3</sub> ) <sub>2</sub>	—	0.1	—
Biotite	K(Mg, Fe <sup>2+</sup> ) <sub>3</sub> (Al, Fe <sup>3+</sup> )Si <sub>3</sub> O <sub>10</sub> (OH, F) <sub>2</sub>	—	0.1	—
Muscovite	KAl <sub>2</sub> (Si <sub>3</sub> Al)O <sub>10</sub> (OH, F) <sub>2</sub>	—	0.5	—
Anhydrite	CaSO <sub>4</sub>	—	0.01	—

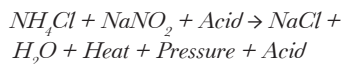


**Table 3** The petrophysical properties of the three studied rock samples.

Samples	Sample IDs	Diameter (in)	Length (in)	Porosity (%)	Permeability (mD)	Bulk Volume (ml)	PV
Eagle Ford Shale	Sh-3	2.01	1.998	8.7	0.07	103.90	9.04
	Sh-4	1.997	2.002	8.5	0.03	102.77	8.74
	Sh-5	1.991	2.012	9.01	0.056	102.66	9.25
Indiana Limestone	LS	1.5	3.01	11	1	87.18	9.59
Kentucky Sandstone	SS	1.5	3	14	0.12	86.89	12.16

**Fig. 4** A view of the prepared shale rock sample.

Thermochemical B presents the following compositions:



The acid could be HCl acid, citric acid, acetic acid, formic acid, L-glutamic acid-N,N-diacetic acid tetrasodium (GLDA) chelating agent, ethylene-di-amine-tetra-acetic acid (HEDT), nitrilo-tri-acetic acid (NTA), methyl-glycine-di-acetic acid (MGDA), ethylene-di-amine-tetra-acetic acid (EDTA), or any low pH chelant. The pH of the latter reaction should be below 4, and the acid concentration range could be from 3 wt% to 10 wt%. The pressure pulse will create the fracture and the heat will increase the acid reactivity with the rock surface and create a newly etched surface.

Coreflooding experiments were conducted to measure the permeability under different overburden pressure

with a different type of thermochemical fluid (A and B). All coreflooding experiments were conducted at a pore pressure of 1,000 psi and at a temperature of 26 °C. In all experiments, an initial permeability was measured with the thermochemical fluids at three different flow rates: 0.5 cc/min, 0.75 cc/min, and 1.00 cc/min.

The pressure drop readings were recorded when the flow rates stabilized. Permeability measurements were repeated with different overburden pressures. In each flooding period, the fluid was injected with a constant flow rate until the stabilized pressure drop is achieved. Then values of the stabilized pressure drop with the corresponding flow rate values were plotted and the slope was calculated. The permeability to the fluid was calculated using the Darcy law, Eqn. 4:

$$k = 14,700 \frac{q\mu L}{A\Delta P}$$

where  $k$  is the permeability in mD,  $q$  is the flow rate in cc/min,  $L$  is the length of the sample in cm,  $A$  is the cross-sectional area in  $\text{cm}^2$ ,  $\Delta P$  is the pressure drop (inlet pressure minus outlet pressure) in psi. Once the stabilized pressure drop was achieved with the final flow rate, the overburden pressure was increased.

Figures 5 and 6 show the effect of overburden pressure on the core permeability, which resulted from thermochemical fracturing. When the pressure is released, the rock permeability is maintained, due to the etched surface for thermochemical B. From thermochemical A the reaction created a fracture with no etching, due to the absence of the acid, and the resulting permeability is due to the fracturing decrease due to the overburden. The original permeability of tight sandstone was 0.12 mD, and after the acid fracturing, it increased to 280 mD in the case of thermochemical B (with acid). The permeability increased from 0.12 mD to 180 mD in the case of thermochemical A. Similar trends were observed in the case of tight carbonate (Indiana limestone) in which the original rock permeability of the sample was 1 mD.

#### Breakdown Pressure Experiments

Breakdown pressure experiments were conducted on the Eagle Ford shale samples. Three breakdown pressure experiments were conducted. The first one was



**Fig. 5** The effect of thermochemicals A and B on the fracture permeability in tight sandstone rocks (Kentucky sandstone).

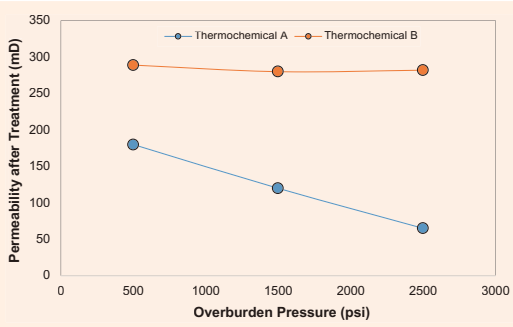
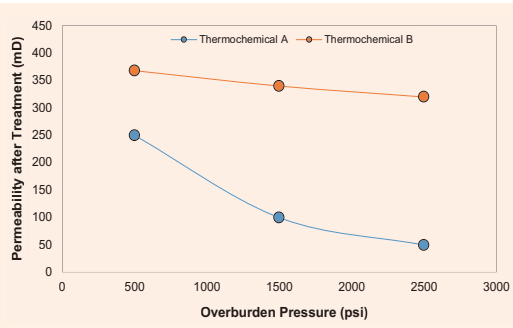


**Fig. 6** The effect of thermochemicals A and B on the fracture permeability in tight carbonate rocks (Indiana limestone).



a reference base case experiment with conventional hydraulic fracturing, the second breakdown pressure experiment was using temperature activating thermochemical fluid A, and the third experiment was with acid triggering thermochemical fluid B. The breakdown pressure experiments with thermochemical fluid B was conducted with citric acid as an activating agent. The performance of the thermochemical fluid experiments were compared with each other and with the conventional hydraulic fracturing technique.

**Hydraulic Fracturing with Conventional Fluid:** A base case experiment was conducted at a room temperature of 26 °C with distilled water as the fracturing fluid. The experiment was conducted on the Eagle Ford shale sample with a 6 mm drilled hole. The pH of the distilled water was 7.0. A constant injection rate of 5 cc/min was maintained throughout the experiment. The overburden pressure used was 1,000 psia.

Figure 7 shows the injection pressure profile with respect to time. The breakdown pressure observed for the base case experiment was 2,167 psia.

**Fracturing with Thermochemical Fluid A:** The fracturing experiment with thermochemical fluid A proceeded with a constant injection rate of 0.1 ml/min.

The whole experiment was completed in three phases: injection, soaking, and reaction. A constant overburden pressure of 1,000 psi was maintained throughout the experiment, at an ambient temperature of 26 °C. The initial pressure during the injection phase was 10 psi. The injection of thermochemical fluid A continued for 40 minutes until it reached an injection pressure of 100 psi. During that phase, a 0.45 pore volume (PV) of thermochemical fluid A was injected. Once the pressure reached 100 psi, the injection of the thermochemical fluid was stopped, and the soaking period was started in which the fluid was allowed to soak inside the core sample.

An electric oven was used to heat the sample; set to a reaction triggering temperature of 90 °C for the soaking phase. The soaking period lasted for approximately 60 minutes. During the soaking period, the pressure inside the core sample was increased from 100 psi to 285 psi, due to the heating. Once the sample reached 90 °C (at 101.01 minutes), a strong exothermic reaction happened and the pressure inside the core sample increased from 285 psi to the pressure at which the sample was fractured (992 psi) instantaneously. When the reaction happened, it took the pressure 1 minute to reach to the rock breakdown pressure of 992 psi.

Figure 8 shows the complete injection pressure profile obtained from the breakdown pressure experiment with the thermochemical fluid A.

**Fracturing with Thermochemical Fluid B:** The fracturing with an acid triggering thermochemical fluid B proceeded with the pre-injection of the citric acid. Citric acid was selected to trigger the thermochemical reaction because it is a weak acid, an excellent chelating agent, and easy to handle in the laboratory. A constant injection rate of 0.1 ml/min was implemented to initially flood the core sample. The injection was conducted at an ambient temperature of 26 °C under a constant overburden pressure of 1,000 psi. Approximately 0.3 PVs of citric acid was injected.

**Fig. 7** The injection pressure profile with respect to time and the breakdown pressure from conventional hydraulic fracturing with water.

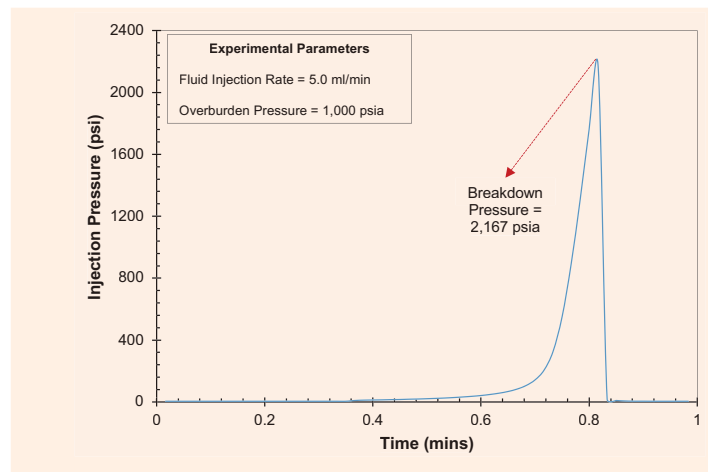
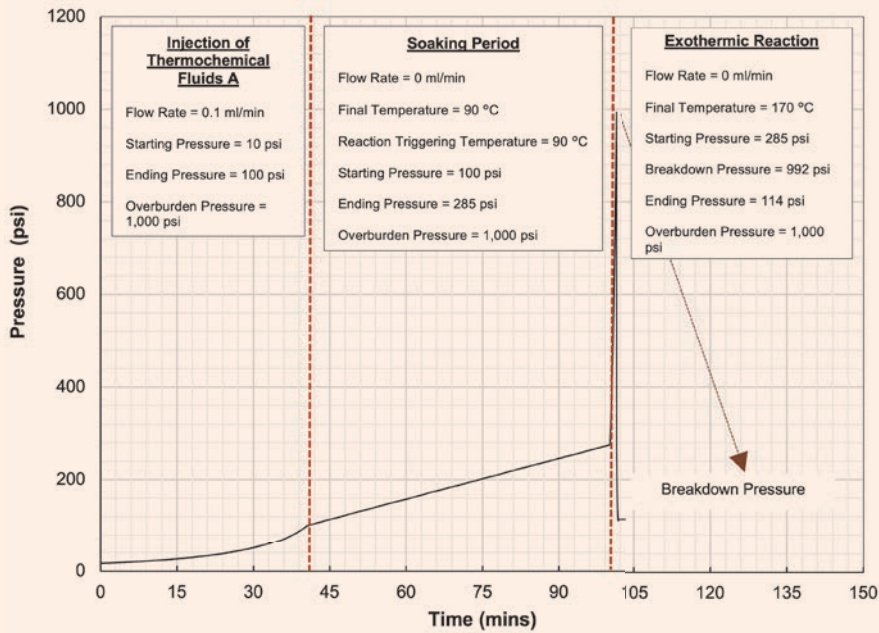


**Fig. 8** The injection pressure profile obtained from the breakdown pressure of thermochemical fluid A in the Eagle Ford shale sample.



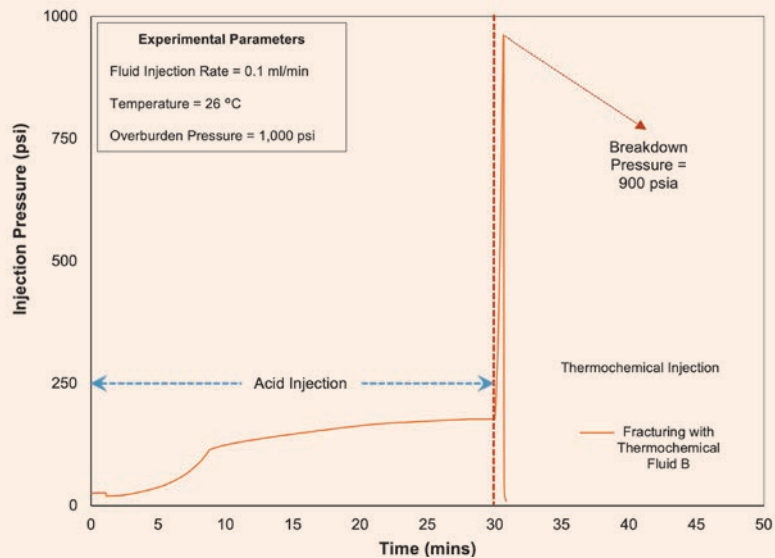
After injecting 0.3 PVs of citric acid, the thermochemical fluid was injected inside the core sample. As soon as the thermochemical fluid mixed with citric acid on the surface of the rock sample, a strong in situ exothermic reaction took place. Due to this exothermic reaction, the pressure started rising rapidly until the rock fractured. When the reaction happened, it took pressure 0.65 minutes to reach to the rock breakdown

pressure of 900 psi. The breakdown pressure recorded for an acid-induced thermochemical fracturing was 900 psi, which was 92 psi lower than what was observed with thermochemical fluid A.

Figure 9 shows the complete injection pressure profile of thermochemical fluid B.

**Comparative Analysis:** The thermochemical fluids were injected through a borehole inside the core

**Fig. 9** The injection pressure profile obtained from the injection of thermochemical fluid B in the Eagle Ford shale sample.



samples of Eagle Ford shale to create the in situ chemical reaction. Due to the in situ chemical reaction, an exothermic reaction took place and a pressure pulse was generated, due to the liberation of nitrogen gas. This nitrogen gas created several microfractures, which resulted in the significant reduction of breakdown pressure when compared to the base case experiment with conventional hydraulic fracturing with distilled water.

Figure 10 shows the fracture pattern obtained from conventional hydraulic fracturing, thermochemical fracturing with fluid A, and thermochemical fracturing with fluid B. The images show extensive fractures and complete fracture paths. Figure 10a shows a single tiny axial channel created due to an ordinary hydraulic fracturing experiment, whereas Figs. 10b and 10c show of a thick major fracture after use of a thermochemical fluid.

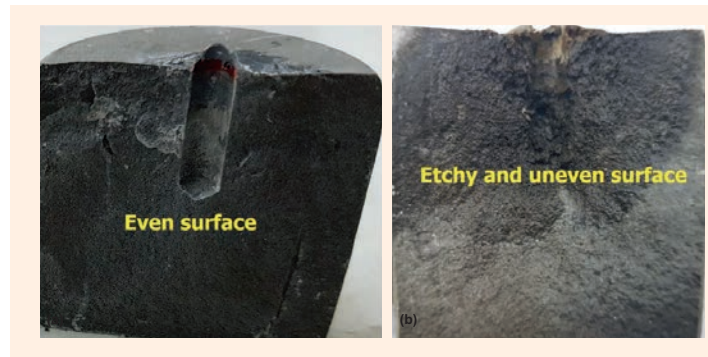
Figure 11 shows cross-sectional views of the core sample after fracturing with heat triggering thermochemical fluid (type A), and an acid triggering thermochemical fluid (type B). Figure 11a shows the regular plane after fracturing with thermochemical fluid A while Fig. 11b shows that the thermochemical fluid B creates differential etching along the fracture surface due to the acid/rock dissolution after pre-injection of a citric acid. Thermochemical fluid B resulted in an uneven surface on the fracture plane.

The new technique, if applied on the real reservoir, could result in an irregular pattern of etched surfaces. Therefore, this could prevent the fracture closure due to the formation of minimum horizontal stress. In addition to that, the thermochemical injection could result in the generation of synthetic sweet spots by creating multiple microfractures around the region of the wellbore, which helped in the reduction of breakdown pressure.

## Reactive Modeling of Thermochemical Fluids

This section provides insight regarding modeling thermochemical reactions at lab-scale and field-scale. The lab-scale model shows how to capture the pressure pulses, temperature, and concentration profiles at a static condition. The matched parameters from the

**Fig. 11** Fractures created due to fracturing with thermochemical fluids, (a) Type A, and (b) Type B.



lab-scale were used in the field-scale study. The purpose of the field study was to show the penetration length of thermochemical fluids within the hydraulic fracture, temperature magnitude, and heat propagation distance.

### Methodology

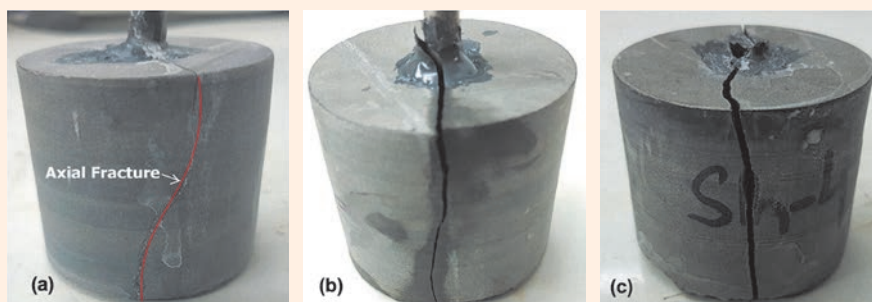
**Lab-Scale Model:** The thermochemical fluids stimulate the reservoir by generating high-pressure pulses. Predicting the magnitude of pulse generation as a function of concentration and temperature of the thermochemical fluid is an essential parameter for field operations. Based on the lab provided data, the pressure pulses previously shown in Fig. 3 were matched to a good extent.

The thermochemical fluids generate pluses by producing a large quantity of nitrogen gas and heat. The rate of thermochemical reaction in the closed aging cell can be defined as:

$$\frac{dC_{TC}}{dt} = -k_r C_{TC} \quad 5$$

where  $C_{TC}$  is the concentration of thermochemical fluids,  $k_r$  is the reaction rate constant, and  $t$  is time. The reaction is assumed to be first-order based on the study provided<sup>20</sup>. Notice that the reaction rate “constant” is a strong function of temperature according to the Arrhenius equation:

**Fig. 10** The fracture pattern obtained from three different methods: (a) conventional hydraulic fracturing, (b) thermochemical fluid A, and (c) thermochemical fluid B.



$$k_r = k_r^0 \exp\left(-\frac{\Delta E}{RT}\right) \quad 6$$

where  $k_r^0$  is the pre-exponential factor,  $\Delta E$  is the activation energy,  $R$  is the universal gas constant, and  $T$  is the absolute temperature. Therefore, the reaction rate depends strongly on the cell temperature, which can be obtained based on the following equation:

$$\overline{\rho \hat{c}_p} V_c \frac{dT}{dt} = k_r C_{TC} \Delta H_{r,TC} V_c - S_c U (T - T_b) \quad 7$$

where  $\overline{\rho \hat{c}_p}$  is the average density and specific heat capacity for the two-phase system,  $V_c$  is the cell volume,  $T$  is the system temperature,  $\Delta H_{r,TC}$  is the thermochemical fluid heat of reaction,  $S_c$  is the cell surface area,  $T_b$  is the room temperature, and  $U$  is the overall heat transfer coefficient. The equation states that the increase in the system temperature is equal to the heat generated due to the exothermic reaction minus the heat loss to the surroundings.

Predicting the system pressure might require two-phase equilibrium calculations. Nevertheless, the following assumptions, made in this study, proved to be reasonable for predicting the pressure pulses:

1. All the generated nitrogen molecules will be in the gaseous phase assuming negligible nitrogen solubility in the liquid phase.
2. The sudden pressure pulse results in negligible water content in the vapor phase.
3. The pressure in the liquid phase is equivalent to that of the vapor phase.

Based on these assumptions, the change in the liquid phase volume can be estimated based on the integrated liquid compressibility equation, defined as:

$$V_L - V_{L,i} = -c_L V_{L,i} (P - P_i) \quad 8$$

where  $V_L$  is the liquid phase volume,  $P$  is the system pressure,  $c_L$  is the liquid phase compressibility, and the subscript  $i$  stands for the initial value. The system pressure can be estimated through the real gas law as:

$$P = znRT/V_g \quad 9$$

where  $z$  is the gas compressibility,  $n$  is the number of gas moles, and  $V_g$  is the volume of the gas phase, which can be obtained as:

$$V_g = V_c - V_L \quad 10$$

The reaction generates nitrogen where the number of moles can be estimated as:

$$n = (C_{TC,i} - C_{TC}) V_c \quad 11$$

where  $C_{TC,i}$  is the initial thermochemical concentration. The ordinary differential equations, Eqns. 5 and 7, is solved using the forward Euler method. The system of Eqns. 8 to 10 are solved using Newton's method. The solver estimates the thermochemical fluids concentration, temperature, and amount of nitrogen generated by solving Eqns. 5, 6, 7, and 11, sequentially. Then, Eqns. 8 to 10 are solved simultaneously to find the system pressure.

**Field-Scale:** A dynamic model was built to understand the impact of thermochemical reaction on acid fracturing. The input data produced a good match with the lab experiments that were used for the field model. The model integrates flow dynamics, mass conservation, and heat transfer in the wellbore, hydraulic fracture, and reservoir. The reaction is assumed to take place inside the hydraulic fracture, i.e., no reaction is triggered in the wellbore. The model is based on the work done by Aljawad et al. (2020)<sup>25</sup>; nevertheless, thermochemical reactive transport was added in this study. Subsequently, only a description of thermochemical reactive transport within the hydraulic fracture was provided.

A fracture propagation model was used to determine the size of the hydraulic fracture at each time step. To obtain the thermochemical fluid's concentration profile, the thermochemical fluid's mass balance is solved, which can be written as:

$$\left(\frac{\partial C_{TC}}{\partial t} + \mathbf{u} \cdot \nabla C_{TC}\right) = \nabla \cdot (D_{TH} \nabla C_{TC}) + k_r C_{TC} \quad 12$$

where  $C_{TC}$  is the reactant concentration,  $D_{TH}$  is the diffusion coefficient of thermochemical fluids, and  $u$  is velocity vector. The first term represents the transient accumulation of the thermochemical fluids, the second term is the convection due to flow, the third term is the diffusion, and the last term is the reaction. The model assumed that there is no concentration gradient,  $\left.\frac{\partial C_{TC}}{\partial t}\right|_w$ , at the fracture walls. This is a reasonable assumption in an unconventional formation as the fluid loss is limited. It is also assumed that the reaction takes place inside the fracture where the inlet concentration is the initial  $TC$  concentration,  $C_{TC}|_{inlet} = C_{TC,i}$ , Fig. 12. It should be noted that the thermochemical diffusion term has no impact on the solution; therefore, knowledge of a thermochemical diffusion is of negligible importance.

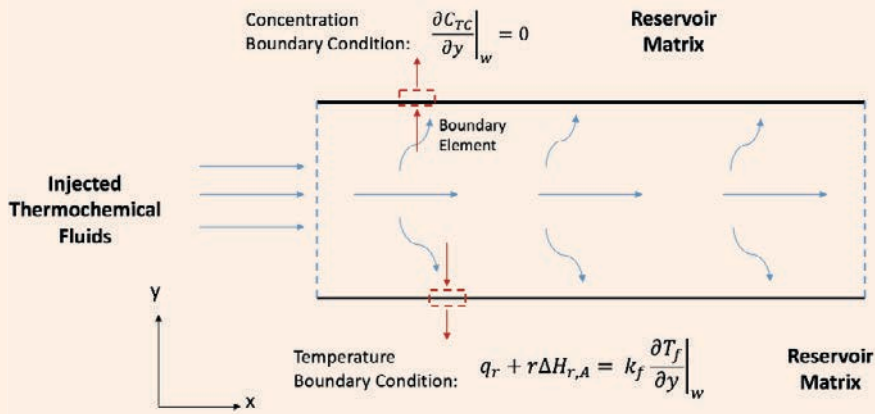
A heat transfer model was coupled, as the reaction term in Eqn. 12 is temperature dependent. Equation 13 defines the energy balance in the hydraulic fracture:

$$\rho_f \hat{c}_p \left(\frac{\partial T_f}{\partial t} + \mathbf{u} \cdot \nabla T_f\right) = \nabla \cdot (k_f \nabla T_f) + k_r C_{TC} \Delta H_{r,TC} \quad 13$$

where  $T_f$  is the fracture temperature,  $\hat{c}_p$  is the fluid specific heat capacity,  $k_f$  is the fluid thermal conductivity, and  $\Delta H_{r,TC}$  is the thermochemical heat of reaction. Observe that the first term accounts for the heat storage, the second term is the convection of heat, the third term is the heat conduction, and the last term is the heat of reaction released within the fracture. When the thermochemical reaction is triggered with acid, its impact should be coupled. For instance, the HCl acid reaction with the minerals releases heat; therefore, it mathematically appears in the boundary of the domain. Equation 14 defines the wall boundary condition for the heat transfer:

$$-k_f \left.\frac{\partial T_f}{\partial y}\right|_w = |r(\Delta H_{r,A})| + q_r \quad 14$$

**Fig. 12** A schematic showing the boundary conditions of the thermochemical fluid concentration and temperature in the hydraulic fracture domain.



where  $\Delta H_{r,A}$  is the acid heat of reaction (if acid is used to trigger the reaction), and  $q_r$  is the heat lost to the reservoir.

The boundary illustrates that the heat lost from the fracture is equal to the acid/rock heat of reaction and heat lost to the formation. Obtaining the heat lost from the fracture to the reservoir requires a reservoir heat transfer model, which is implemented in this research. Details of coupling the hydraulic fracture and reservoir heat transfer models were provided by Aljawad (2020)<sup>26</sup>. A finite volume scheme is implemented to obtain the temperature and concentration profiles.

**Model Match with Experiments**

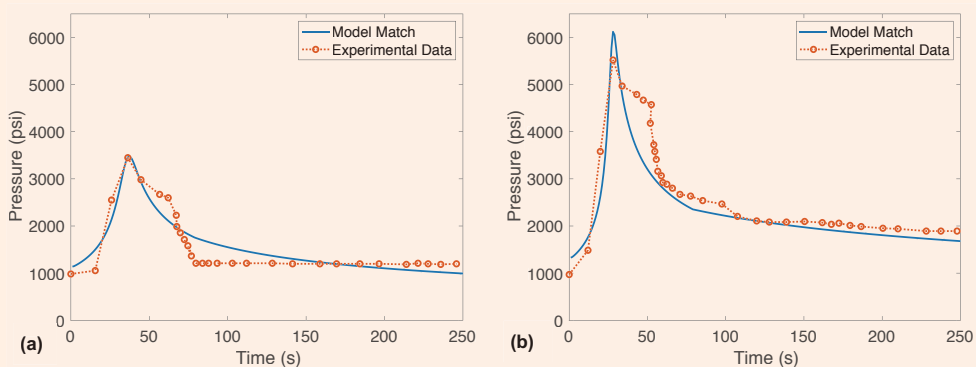
Figure 13 shows that the proposed static model could capture the experimentally generated pulse in the aging cell shown in Fig. 3. Tables 4 and 5 shows the data used in the model to capture the pulses given; the reaction kinetics were obtained from<sup>20</sup>. Liquid compressibility is used as a matching parameter for the pressure magnitude. Notice that the compressibility is a function of the pressure, temperature, and salinity. The compressibility range produced from the model was

from  $1 \times 10^{-6}$  to  $2.5 \times 10^{-6}$  1/psi, which is a reasonable range for water compressibility. The sudden sharp increase in the pressure is due to the sudden release of a large amount of nitrogen gas and heat.

Figure 14a shows the predicted concentration profile as a function of time. One might observe that the thermochemical fluids were consumed within 50 seconds. The two molar thermochemical fluids were consumed faster as higher concentrations speed the reaction and release larger heat magnitudes. Notice that the peaks of the pulses in Fig. 13 correspond to the moment where the thermochemical fluids were completely consumed. This is logical as no more nitrogen was released to pressurize the cell.

Figure 14b shows the temperature response produced from the model. As expected, a higher concentration resulted in higher temperature magnitude. These simulations agree with the average temperature magnitudes recorded in the lab even though a continuous profile was not generated. The temperature peak also corresponds to the time where the thermochemical fluids were completely consumed. The sharp increase in

**Fig. 13** The static model match with the pressure pluses obtained from the experiments for (a) one molar, and (b) two molar cases.



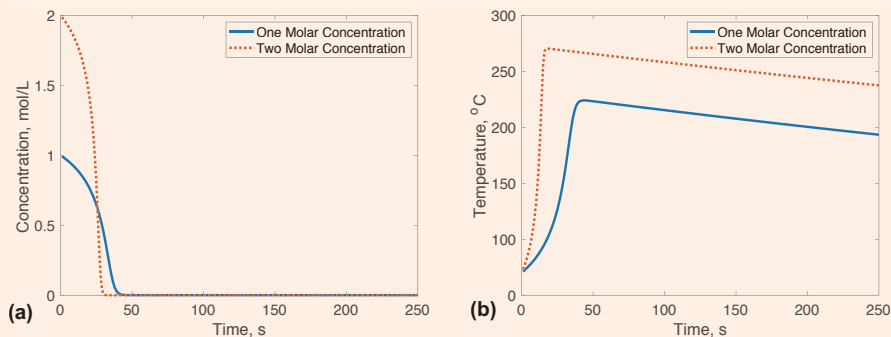


**Table 4** The reaction kinetics constants and heat of reaction for TC.

Reaction	$n_r$	$k_r^0$ (1/s)	$\frac{\Delta E}{R}$ (K)	$\Delta H_r$ ( $\frac{KJ}{mol}$ )
$NH_4Cl + NaNO_2$	1	$9.99 \times 10^3$	$4.58 \times 10^3$	369

**Table 5** The fluid and rock's thermal properties.

Input Data	SI Unit	Field Unit
Overall heat transfer coefficient ( $U_o$ )	0.1 KJ/(s.m <sup>2</sup> °C)	0.0048 Btu/(hr.ft <sup>2</sup> .°F)
Ambient temperature ( $T_p$ )	25 °C	77 °F
Fluid specific heat capacity ( $C_p$ )	4.13 KJ/(Kg °C)	0.964 Btu/(lbm °F)
Fluid thermal conductivity ( $k_f$ )	$6 \times 10^{-4}$ KJ/(s.m °C)	0.347 Btu/(hr.ft °F)
Formation specific heat capacity ( $C_{ma}$ )	0.879 KJ/(Kg °C)	0.2099 Btu/(lb °F)
Formation thermal conductivity ( $k_{ma}$ )	$1.57 \times 10^{-3}$ KJ/(s.m °C)	0.907 Btu/(hr.ft °F)

**Fig. 14** For the one and two molar cases as simulated by the model: (a) The predicted concentration profile as a function of time, and (b) the temperature response produced from the model.

temperature corresponds to the fast generation of heat upon reaction while the relatively flat curve thereafter represents the temperature decline due to heat loss to the surroundings.

#### Field-Scale Analysis

A sensitivity analysis was performed to evaluate the performance of thermochemical fluids at the field-scale. Temperature, concentration, injection rate, and acid impact were investigated. The base case for this study assumes an injection of 210 gal/ft of 3 molar concentrated thermochemical fluids at 25 bbl/min. Such a treatment volume and injection rate are suitable for hydraulic fracturing operations as the purpose is to extend a hydraulic fracture. The reservoir temperature was assumed to be 100 °C, while the injected fluid temperature was 25 °C.

**Temperature.** Both thermochemical fluids and reservoir temperatures have a significant impact on the reactivity. This is a major parameter that determines how long the thermochemical fluids can penetrate inside a hydraulic fracture. Figure 15 shows that the thermochemical fluids could reach 12 ft inside the hydraulic fracture when injected at 25 °C, while only reaching 5 ft when the fluid temperature was 100 °C. Remember that the reaction rate constant depends exponentially on temperature as described by the Arrhenius equation.

Figure 16a shows a sound relationship between the fluid temperature and concentration profile. A rule of thumb is that a longer penetration could be achieved at lower fluid injection temperatures. It is interesting that the injected fluids' temperature also has an impact



**Fig. 15** The impact of the temperature of the thermochemical fluids on their penetration inside a hydraulic fracture.

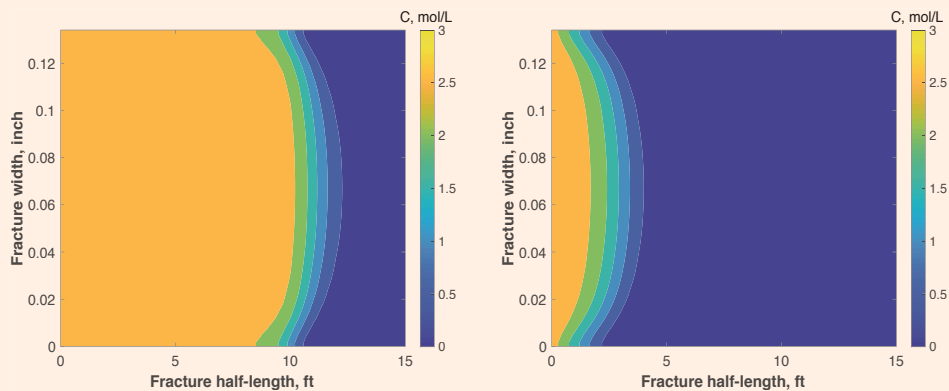
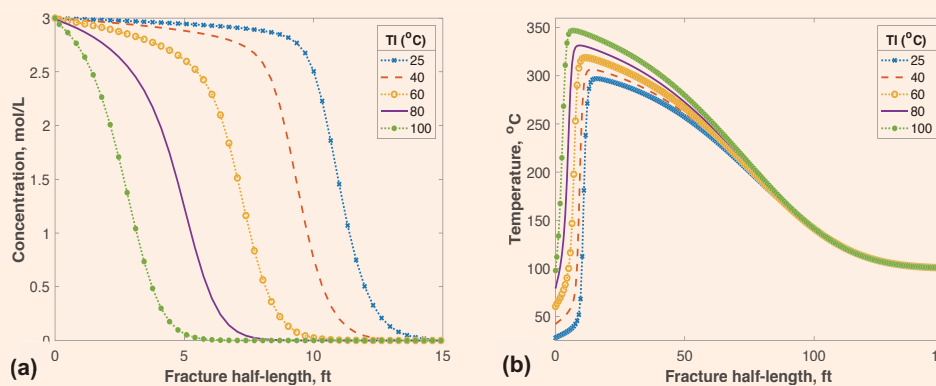


**Fig. 16** (a) The concentration profile, and (b) the temperature profile along the hydraulic fracture at different injected thermochemical temperatures.



on the maximum temperature magnitude inside the fracture as indicated in Fig. 16b. For instance, 300 °C was achieved when the thermochemical fluids were injected at 25 °C while 350 °C was reached when the fluid temperature was 100 °C. Notice that the heat provided by the exothermic reaction could reach to more than 100 ft inside the hydraulic fracture, providing advantage in terms of hydraulic fracture clean up during flow back operations.

Though the thermochemical fluids could penetrate only a couple of feet within the hydraulic fracture, the heat of reaction reached an order of magnitude longer distance. The location of the temperature peak coincides with the location of the thermochemical fluid consumption and probably is the location of the peak of pressure pulse. This observation is similar to the one obtained from lab experiments, Figs. 13 and 14.

The impact of the reservoir temperature, Fig. 17, was also investigated assuming a constant injected fluid temperature of 35 °C. The same conclusion was perceived for reservoir temperature impacts as colder temperatures allowed for longer thermochemical penetration,

Fig. 17a. Nevertheless, the reservoir temperature did not affect the temperature peak magnitude as it was 300 °C for all studied cases in Fig. 17b.

**Concentration.** The concentration of thermochemical fluids is the most significant parameter in controlling the pressure pulse and temperature magnitudes. Figure 18a shows that the thermochemical penetration could range from 7 ft to 50 ft based on the concentration magnitude. Higher concentrations surge the reaction rate and result in a larger amount of heat released, which also speeds the reaction. For instance, a 4 molar of thermochemical fluids could increase the temperature close to 400 °C, while the 1 molar could only increase the temperature to 150 °C, Fig. 18b. The thermochemical concentration should be carefully designed based on the required temperature and pressure magnitudes.

**Injection Rate.** The injection rate is significant in determining the penetration length of thermochemical fluids within the hydraulic fracture. Figure 19a shows that a higher injection rate leads to a higher penetration within the fracture. In addition, the injection rate controls the efficiency of heat transfer within

Fig. 17 (a) The concentration profile, and (b) the temperature profile along the hydraulic fracture at different reservoir temperatures.

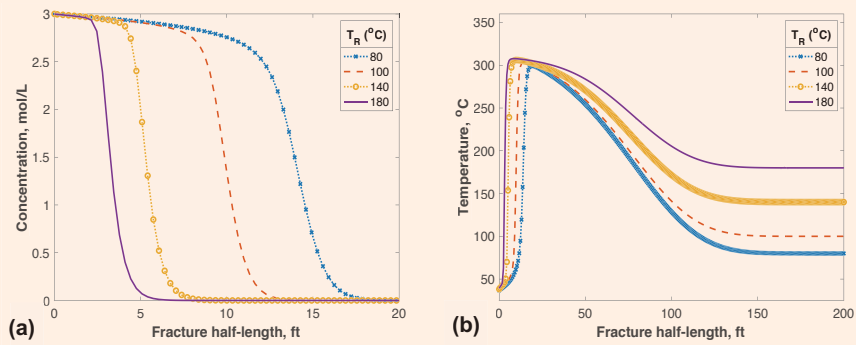


Fig. 18 (a) The concentration profile, and (b) the temperature profile along the hydraulic fracture at different thermochemical fluid concentrations.

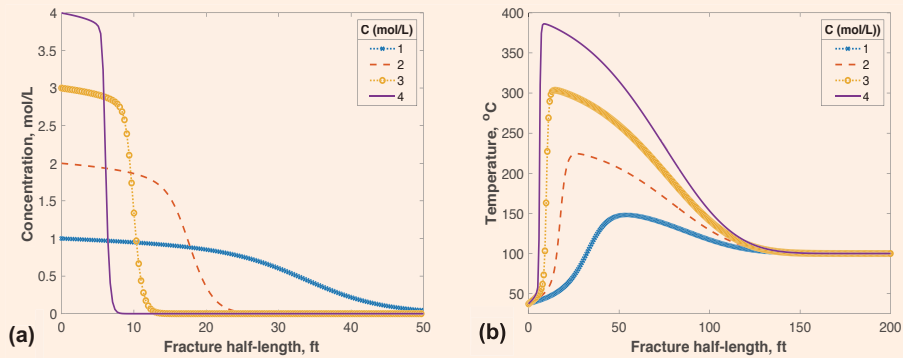
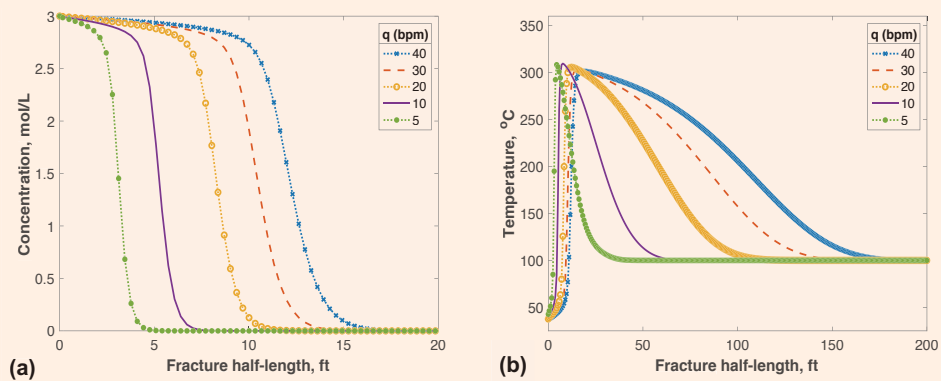


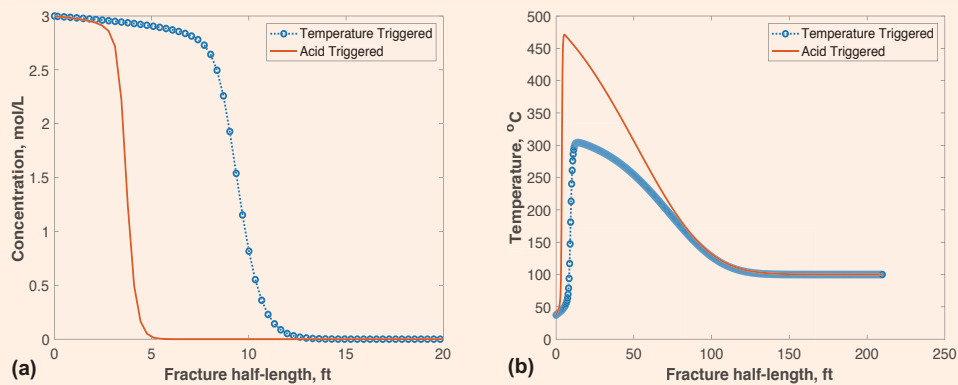
Fig. 19 (a) The concentration profile, and (b) the temperature profile along the hydraulic fracture at different injection rates.



the fracture, Fig. 19b. A higher injection rate leads to less fluid leakoff, and therefore, the hot fluids could reach longer distances. For the low injection rate, heat propagation within the reservoir matrix surrounding the fracture is higher.

Notice that the fracture half-length was less than 50 ft for the 5 bpm injection case while it was larger than 150 ft for the 40 bpm as the fracture length was not constant. Lower injection rates could be targeted if cleaning near the wellbore zone is required.

**Fig. 20** (a) The concentration profile, and (b) the temperature profile along the hydraulic fracture for acid and temperature triggered thermochemical fluids.



**Acid Impacts.** Triggering the thermochemical reaction with acid has significantly different results compared to the temperature triggered reactions. The acid reacts with the carbonate minerals and releases heat, which speeds the reaction of thermochemical fluids. Figure 20a shows that the penetration distance of the thermochemical fluids triggered with acid is shorter. Figure 20b shows that higher temperature magnitudes could be reached if the thermochemical reaction was initiated with acid. The reaction within a shorter distance combined with the heat released from an acid/rock reaction resulted in more efficient heating per unit volume.

## Conclusions

This research showed that thermochemical fluids are a viable option to stimulate unconventional formations. The study combined both experimental and mathematical methods to understand thermochemical reactive behaviors and outcomes. It is observed that the thermochemical fluids could generate synthetic sweet spots by creating multiple microfractures around the region of the wellbore. That helped to reduce the breakdown pressure from 2,167 psia to 900 psia as compared to conventional methods.

Triggering the thermochemical fluids with acid helped to create etching along the fracture surfaces. Therefore, fracture conductivity was maintained at high closure stresses as compared to the thermochemical reaction without acid. The coreflooding experiments on Kentucky sandstone and Indiana limestone with acid activating thermochemical fluid suggested that core permeability cannot decrease under different overburden pressures.

A lab model was created to match the pressure pulse behavior and then validated against experimental data. A field-scale thermochemical reactive transport model was also developed to perform sensitivity analysis. It was found that thermochemical concentration is the key factor to control pressure and temperature magnitudes. The higher concentration, temperature,

and lower injection rates resulted in shorter thermochemical penetration within the hydraulic fracture. Acid triggered thermochemical fluids result in a larger temperature increase and short thermochemical fluids penetration.

## Acknowledgments

A version of this article was previously published in the *Journal of Natural Gas Science and Engineering*, Vol. 85, 2020, <https://doi.org/10.1016/j.jngse.2020.103606>.

## References

- Soliman, M.Y., Daal, J. and East, L.: "Fracturing Unconventional Formations to Enhance Productivity," *Journal of Natural Gas Science and Engineering*, Vol. 8, September 2012, pp. 52-67.
- Beugelsdijk, L.J.L., de Pater, C.J. and Sato, K.: "Experimental Hydraulic Fracture Propagation in a Multifractured Medium," SPE paper 59419, presented at the SPE Asia Pacific Conference on Integrated Modeling for Asset Management, Yokohama, Japan, April 25-26, 2000.
- Dai, C., Xue, L., Wang, W. and Li, X.: "Analysis of the Influencing Factors on the Well Performance in Shale Gas Reservoir," *Geofluids*, Vol. 2017, Issue 11, December 2017, pp. 1-12.
- Leimkuhler, J. and Leveille, G.: "Unconventional Resources," *The Way Ahead*, Vol. 8, Issue 1, February 2012, pp. 27-28.
- Wang, L., Yao, B., Cha, M., Alqahtani, N.B., et al.: "Waterless Fracturing Technologies for Unconventional Reservoirs — Opportunities for Liquid Nitrogen," *Journal of Natural Gas Science and Engineering*, Vol. 35, Part A, September 2016, pp. 160-174.
- Moghadasi, R., Rostami, A. and Hemmati-Sarapardeh, A.: "Application of Nanofluids for Treating Fines Migration during Hydraulic Fracturing: Experimental Study and Mechanistic Understanding," *Advances in Geo-Energy Research*, Vol. 5, Issue 2, 2019, pp. 198-206.
- Cuderman, J.F.: "Multiple Fracturing Experiments — Propellant and Borehole Considerations," SPE/DOE paper 10845, presented at the SPE/DOE Unconventional Gas Recovery Symposium, Pittsburgh, Pennsylvania, May 16-18, 1982.

8. Cuderman, J.F. and Northrop, D.A.: "A Propellant-Based Technology for Multiple Fracturing Wellbores to Enhance Gas Recovery: Application and Results in Devonian Shale," *SPE Production Engineering*, Vol. 1, Issue 2, March 1986, pp. 97-105.
9. Malhotra, S., Rijken, P. and Sanchez, A.: "Experimental Investigation of Propellant Fracturing in a Large Sandstone Block," *SPE Drilling and Completion*, Vol. 35, Issue 2, pp. 87-99.
10. McSpadden, H.W., Tyler, M.L. and Velasco, T.T.: "In Situ Heat and Paraffin Inhibitor Combination Prove Cost-Effective in NPR #5, Casper, Wyoming," SPE paper 15098, presented at the SPE California Regional Meeting, Oakland, California, April 2-4, 1986.
11. Khalil, C.N., Neumann, L.F., Linard, C.A. and Santos, I.G.: "Thermochemical Process to Remove Paraffin Deposits in Subsea Production Lines," OTC paper 7575, presented at the Offshore Technology Conference, Houston, Texas, May 2-5, 1994.
12. Amin, R.A.M., Halim, N.H., Rosli, K.A., Ali, M.I., et al.: "Production Profile of Wells before and after Treatment Using Novel Thermochemical Technique," SPE paper 107663, presented at the European Formation Damage Conference, Scheveningen, the Netherlands, May 30-June 1, 2007.
13. Singh, K., Mohamed, A.S., Alian, S.S., Ismail, M., et al.: "Thermochemical in Situ Heat Generation Technique to Remove Organic Solid Deposition: Effective Tool for Production Enhancement and Flow Assurance," OTC paper 25953, presented at the Offshore Technology Conference, Houston, Texas, May 6-9, 2015.
14. Al-Nakhli, A.R.: "Chemically Induced Pressure Pulse: A New Fracturing Technology for Unconventional Reservoirs," SPE paper 172551, presented at the SPE Middle East Oil and Gas Show and Conference, Manama, Kingdom of Bahrain, March 8-11, 2015.
15. Wang, F., Chen, H., Alzobaidi, S. and Li, Z.: "Application and Mechanisms of Self-Generated Heat Foam for Enhanced Oil Recovery," *Energy Fuels*, Vol. 52, Issue 9, August 2018, pp. 9095-9105.
16. Tariq, Z., Mahmoud, M., Abdulraheem, A., Al-Nakhli, A.R., et al.: "An Experimental Study to Reduce the Breakdown Pressure of the Unconventional Carbonate Rock by Cyclic Injection of Thermochemical Fluids," *Journal of Petroleum Science and Engineering*, Vol. 187, December 2019.
17. Tariq, Z., Mahmoud, M., Abdulraheem, A., Al-Nakhli, A.R., et al.: "An Experimental Study to Reduce the Fracture Pressure of High Strength Rocks Using a Novel Thermochemical Fracturing Approach," *Geofluids*, Vol. 2019, August 2019.
18. Rocha, N.O., Khalil, C.N., Leite, L.C.F. and Bastos, R.M.: "A Thermochemical Process for Wax Damage Removal," SPE paper 80266, presented at the SPE International Symposium on Oil Field Chemistry, Houston, Texas, February 5-7, 2005.
19. Mahmoud, M.: "Well Clean-Up Using a Combined Thermochemical/Chelating Agent Fluids," *Journal of Energy Resources Technology*, Vol. 141, Issue 10, October 2019.
20. Alade, O.S., Mahmoud, M., Hassan, A., Al-Shehri, D., et al.: "Evaluation of Kinetics and Energetics of Thermochemical Fluids for Enhanced Recovery of Heavy Oil and Liquid Condensate," *Energy Fuels*, Vol. 33, Issue 6, April 2019, pp. 5538-5545.
21. Rocha, N.O., Khalil, C.N., Leite, L.F. and Ferreira, A.M.G.: "Thermochemical Process to Remove Sludge from Storage Tanks," SPE paper 105765, presented at the International Symposium on Oil Field Chemistry, Houston, Texas, February 28-March 2, 2007.
22. Al-Nakhli, A.R., BaTaweel, M., Mustafa, A., Tariq, Z., et al.: "Novel Methodology to Reduce the Strength of High Stress Tight Gas Reservoirs Using Thermochemical," paper presented at the 53<sup>rd</sup> U.S. Rock Mechanics/Geomechanics Symposium, New York City, New York, June 25-26, 2019.
23. Mustafa, A., Tariq, Z., Abdulraheem, A., Mahmoud, M., et al.: "Increasing Stimulated Reservoir Volume SRV in Unconventional Reservoirs: Microstructural and Rock Mechanical Study," SPE paper 192808, presented at the Abu Dhabi International Petroleum Exhibition and Conference, Abu Dhabi, UAE, November 12-15, 2018.
24. Mahmoud, M., Alade, O.S., Hamdy, M., Patil, S., et al.: "In Situ Steam and Nitrogen Gas Generation by Thermochemical Fluid Injection: A New Approach for Heavy Oil Recovery," *Energy Conversion and Management*, Vol. 202, December 2019.
25. Aljawad, M.S., Schwalbert, M.P., Zhu, D. and Hill, A.D.: "Optimizing Acid Fracture Design in Calcite Formations: Guidelines Using a Fully Integrated Model," *SPE Production and Operations*, Vol. 55, Issue 1, February 2020, pp. 161-177.
26. Aljawad, M.S.: "Identifying Formation Mineralogy Composition in Acid Fracturing from Distributed Temperature Measurements," *SPE Reservoir Evaluation and Engineering*, Vol. 25, Issue 1, February 2020, pp. 200-211.

---

## About the Authors

### Dr. Zeeshan Tariq

*Ph.D. in Petroleum Engineering,  
King Fahd University of Petroleum  
and Minerals*

Dr. Zeeshan Tariq is an Associate Professor working at the King Fahd University of Petroleum and Minerals (KFUPM). His areas of research interests are geomechanics, hydraulic fracturing, artificial intelligence, and petrophysics.

Zeeshan has published more than 20 peer-reviewed journal articles and filed several patents.

He is an active member of various societies,

such as the Society of Petroleum Engineers (SPE), the Society of Petrophysicists and Well Log Analysts (SPWLA), the Society of Exploration Geophysicists (SEG), and the American Rock Mechanics Association (ARMA).

Zeeshan received his M.S. degree in Petroleum Engineering from KFUPM, Dhahran, Saudi Arabia. He received his Ph.D. degree at the College of Petroleum Engineering and Geosciences, KFUPM.

### Dr. Murthadha S. Al-Jawad

*Ph.D. in Petroleum Engineering,  
Texas A&M University*

Dr. Murthadha S. Al-Jawad is an Assistant Professor in the Department of Petroleum Engineering at King Fahd University of Petroleum and Minerals (KFUPM), Dhahran, Saudi Arabia. He was instrumental in the development of a concentration in unconventional hydrocarbon resources. Also, Murthadha established a fully equipped, state-of-the-art lab to study acid stimulation and hydraulic fracturing.

He has been actively involved in research projects regarding acid stimulation, hydraulic fracturing, and unconventional reservoirs.

Since joining KFUPM in 2018, Murthadha has been a member of several internally and

externally funded projects. He has taught several undergraduate and graduate courses in Petroleum Engineering.

Murthadha has published several technical papers and reports on various areas of research. He is a technical reviewer for several different prestigious journals.

Murthadha received his B.S. degree in Chemical Engineering from KFUPM, and his M.S. degree in Petroleum Engineering from Texas A&M University, College Station, TX. In 2018, Murthadha received his Ph.D. degree in Petroleum Engineering, also from Texas A&M University.

### Dr. Mohamed Mahmoud

*Ph.D. in Petroleum Engineering,  
Texas A&M University*

Dr. Mohamed Mahmoud is an Associate Professor working in the Petroleum Engineering Department with King Fahd University of Petroleum and Minerals (KFUPM), Dhahran, Saudi Arabia. Prior to assuming this position in 2016, he had been a Research Assistant in the same department since 2008.

From 2004 to 2008, Mohamed worked as a Petroleum Engineer at Belayim Petroleum Co. in Egypt. During the period from 2001 to 2004, he

was a Drilling Engineer at Magawish Petroleum Co., Egypt.

Mohamed's research interests are varied and cover several subjects, including well simulation, enhanced oil recovery, and multiphase flow in vertical and horizontal wells.

He received his Ph.D. degree in Petroleum Engineering from Texas A&M University, College Station, TX, in 2011

### Dr. Abdulazeez Abdulaheem

*Ph.D. in Geotechnical  
Engineering,  
University of Oklahoma*

Dr. Abdulazeez Abdulaheem is an Associate Professor in the Department of Petroleum Engineering at King Fahd University of Petroleum and Minerals (KFUPM), Dhahran, Saudi Arabia. His focus is mainly on geomechanics and the applications of artificial intelligence in different areas of petroleum engineering.

Prior to joining the department, Abdulazeez worked as a Research Engineer in the Research Institute at KFUPM for almost 18 years, addressing field challenges in areas such as

wellbore instability, sand production, and experimental rock mechanics.

He has published/presented almost 200 journal and conference papers in the area of geomechanics and the application of artificial intelligence in petroleum engineering.

Abdulazeez received his M.S. degree in Structural Engineering from the Indian Institute of Science, Bangalore, India. He received his Ph.D. degree in Geotechnical Engineering from the University of Oklahoma, Norman, OK.

### Ayman R. Al-Nakhli

*M.S. in Entrepreneurship for  
New Business Development,  
Open University Malaysia*

Ayman R. Al-Nakhli is a Petroleum Scientist in Saudi Aramco's Exploration and Petroleum Engineering Center – Advanced Research Center (EXPEC ARC), where he leads the research program on thermochemicals and develops technologies related to conventional and unconventional reservoirs such as pulse fracturing, stimulation, diverting agents, and heavy oil.

Ayman has developed and field deployed several novel technologies, with four of them being commercialized with international service

companies. He received the World Oil Award for Best Production Chemical in 2015.

Ayman has filed more than 20 patents, published 35 journal papers, and 40 conference papers.

He received his B.S. degree in Industrial Chemistry from King Fahd University of Petroleum and Minerals (KFUPM), Dhahran, Saudi Arabia, and an M.S. degree in Entrepreneurship for New Business Development from Open University Malaysia, Bahrain.

# New Catalyst-free Polycrystalline Diamond with Industry Record Wear Resistance

*Dr. Guodong Zhan, Dr. Bodong Li, Timothy E. Moellendick, Dr. Duanwei He and Dr. Jianhui Xu*

## Abstract /

Polycrystalline diamond compact (PDC) drill bits are key drilling tools for oil and gas exploration and drilling. As semiconductor chips are key components for the manufacturing of high performance electronics, PDC cutters are key drilling components of PDC drill bits. Subsequently, drilling very hard and highly abrasive formations poses a big challenge for today's PDC drill bits. The weakness in the current technology is due to the unavoidable use of metallic catalysts to bond the diamond grains that comprise the PDC cutters. The thermal expansion of the metallic catalysts resulting from high frictional heat at the cutter/rock interface during drilling operation breaks the PDC cutters. Development of catalyst-free PDC cutters would be a game changing technology for drill bits by delivering a significant increase in performance, durability, and drilling economics.

In this study, an innovative ultra high-pressure and high temperature (UHPHT) technology was developed through a two-stage multi-anvil apparatus capable of generating ultra high-pressures up to 35 GPa — seven times higher than current PDC cutter technology — to make ultra-strong and catalyst-free PDC cutting materials.

Here, we report a new type of catalyst-free PDC cutting material, synthesized under an ultra high-pressure of 16 GPa. The new material breaks all single crystal diamond indenters in Vickers hardness testing, and sets a new world record as the hardest diamond material to date. The material also possesses the highest thermal stability in the family of diamonds in air at 1,200 °C, which is about 600 °C higher than current PDC cutters. More importantly, the new material exhibited industry recorded wear resistance, 300% higher than current PDC cutters.

All of these demonstrated a breakthrough in PDC cutter technology development and presented a feasibility for the goal of “One Run to Total Depth” game changing drilling technology.

## Introduction

Polycrystalline diamond compact (PDC) drill bits are key drilling tools for oil and gas exploration and drilling in most of formations, with a market of more than \$4.5 billion per year. PDC cutters are the primary and critical components in the PDC drill bits to cut these formations, due to their outstanding properties such as high hardness, thermal conductivity, and impact and wear resistance. Subsequently, there is a significant challenge for PDC drill bits in the market when drilling very hard and abrasive formations<sup>1-3</sup>. Currently available PDC cutters in the market do not provide sufficient wear resistance, impact resistance, or thermal stability to survive this challenging drilling environment. The low rate of penetration and short bit life push the use of multiple bits to drill a single interval, which is not optimal for well economics<sup>4-6</sup>.

The main weakness in the current technology comes from the unavoidable use of metallic catalyst (typically cobalt) during the manufacturing of the PDC cutters<sup>4</sup>. Traditionally, due to the metallic catalyst, PDC cutters can be manufactured at relatively lower pressure and temperature, which are approximately 5.5 GPa and 1,400 °C, respectively. Consequently, these metallic binders reduce the hardness of the polycrystalline diamond (PCD) material to approximately 50 GPa to 70 GPa<sup>7</sup>.

More severely, the metallic catalyst binder in the diamond can adversely assist to convert the diamond back to graphite when high heat is generated from drilling operations. In addition, the cutting and drilling process exposes the PCD material to high stress, where the PDC cutting edges with cobalt binders tend to produce microcracks and diamond particle falling/chipping when the stress is greater than the bonding strength of the diamond grains within the PDC compact at the specific temperature.

The reason can be explained by the differences of elastic modulus and thermal expansion coefficients between the cobalt metallic binder and diamond, which can lead to mismatched volume changes between the diamond and the binder in the operating environment with high stress and high temperature. As a result, large stresses would be produced inside the PDC materials to cause early failure.

Development of a catalyst-free PDC cutter for drill bits would be an ideal and game changing technical solution to potentially realize the goal of “One Run to Total Depth” in drilling technology. The ultra high-pressure and



high temperature (UHPHT) technology makes this possibility true. UHPHT technology is a cutting-edge technology for research and development of many advanced superhard materials. At present, the technology is mainly focused on the study of nanocrystalline diamonds, however, their industrial applications are limited by the small size and/or high cost.

Irifune et al. (2003)<sup>8</sup> made use of a Kawai-type 2-6-8 large cavity static pressure device to successfully achieve a high-pressure of about 15 GPa in synthesizing millimeter-grade nanocrystalline PDC material. Since then, the size of synthetic nanocrystalline PDC was successfully increased to a centimeter level after nearly 10 years of further development<sup>9</sup>. Larger tonnage high-pressure devices are required to obtain larger sample sizes and to ensure reasonable high-pressure efficiency. The high-pressure efficiency is mainly affected by the load loss in the transmission process in the anvil design where the structural design of the anvil assembly and the anvil material strength of the final stage matters the most.

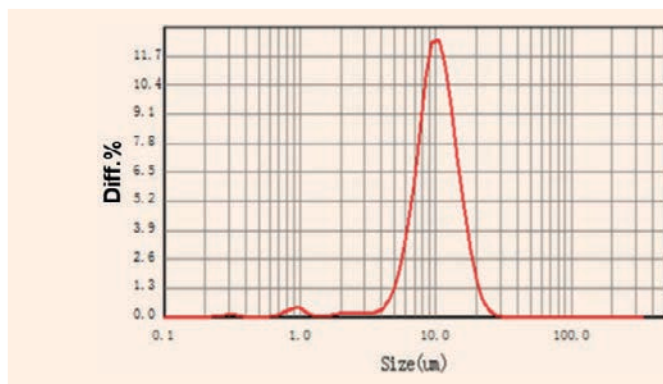
In this study, we applied a newly developed UHPHT technology to generate ultra high-pressures up to 35 GPa for the first time<sup>10-12</sup>. Using this newly developed UHPHT technology, we successfully synthesized catalyst-free PDC materials to a centimeter size under an ultra high-pressure of 16 GPa and ultra high temperature of 2,300 °C. The physical and mechanical properties of the newly synthesized catalyst-free PDC (CFPCD) compact materials are systematically evaluated, including wear resistance, hardness, and thermal stability.

The material shows great thermal stability in air at 1,200 °C, which is about 600 °C higher than current PDC cutters. Also, it is found that the wear resistance of the CFPCD material is 300% more than that of the commercially available PDC cutters currently used in the industry using the industry standard granite turning test method. As is commonly known, it usually takes a decade to increase wear resistance of PDC cutters by 30% to 50%. At such a conversion rate, our development will reduce technology investment by 50 years.

## Experimental Procedures and Materials Characterization

We used diamond powder as the starting material. Figure 1 shows the diamond powder particle size distribution. The diamond powder with average grain sizes of 10 μm were first treated in a vacuum furnace at  $2 \times 10^{-4}$  Torr and 1,200 °C, with a rate of temperature increase by 15 °C/min. After a certain time of maintaining the peak temperature, the sample was cooled to room temperature in the furnace. Next, the treated powder was packed into cylindrical capsules with a diameter of 13 mm and thickness of 6.3 mm. They were then put in the newly developed two-stage multi-anvil large volume high-pressure apparatus based on a DS6X25 MN cubic press to be sintered at a pressure of 16 GPa and temperature of 2,300 °C<sup>4</sup>. More details can be found in Li et al. (2020)<sup>12</sup>.

**Fig. 1** The particle size distribution of the starting material of diamond powder.



An X-ray diffractometer (XRD) was then applied to determine the phases of the starting diamond powder, CFPCD, and commercial PDC materials<sup>12</sup>. The grain structures of the CFPCD material and commercially available PDC materials were investigated using a scanning electron microscope (SEM). The hardness of polished specimens was tested with different loading forces up to 9.8 N and a fixed dwell time of 15 seconds by a Vickers hardness tester. A numerical control lathe was used to carry out the wear resistance performance tests. The thermal stability and oxidation resistance were evaluated under a high temperature in situ XRD ( $\lambda = 0.15406$  nm) at different temperatures, from room temperature to 1,400 °C.

## Results and Discussions

In our study, we successfully achieved the CFPCD samples with dimensions of ~11 mm in diameter and up to 6 mm in thickness for the first time, Fig. 2. These are large enough to be used to make parts and components for a wide range of industrial applications, including drill bits. Previously, all research and industry developments by using UHPHT technology were only able to make miniature samples that limit their use in many potential applications. Our success is attributed to the novel structural design of the anvil assembly and the anvil material strength of the final stage. A lot of effort has been invested to make it work.

SEM images showed that the diamond grain sizes are approximately 10 μm in both the CFPCD material,

**Fig. 2** The world's hardest catalyst-free PDCs made by an ultra high-pressure of 16 GPa and an ultra high temperature of 2,300 °C. The dimension of 11 mm in diameter and 6 mm in thickness could be large enough for drill bit application and other industrial applications.

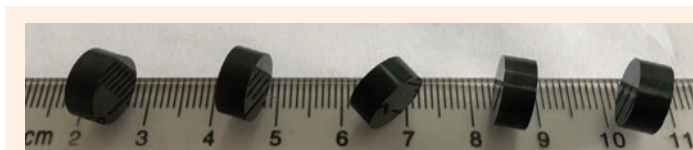


Fig. 3a, and the commercial PDC materials, Fig. 3b. The similar grain sizes are purposely designed in the comparison in this study to eliminate the effect of grain size on the properties. Therefore, the difference of the properties between these tested samples are mainly attributed to the different manufacturing processes.

The XRD results indicate that both the starting material and sintered CFPCD material are pure and well crystallized diamonds<sup>12</sup>. On the other hand, the commercial PDC material contains not only diamond phase but also a cobalt binder, as is well expected. The cobalt catalyst is dispersed at the diamond grain boundaries in the commercial PDC material. It can break the diamond-diamond bonds during harsh cutting or drilling in high temperature and high stress environments.

Hardness is a key performance index of materials, and is mainly tested by the indentation method. The Vickers hardness indentations were performed on the polished samples of these materials under an applied load of up to 9.8 N and a dwelling time of 15 seconds.

Figures 4a and 4b show the Vickers hardness indenters before testing with a standard indenter made of single crystal diamond, and the damaged indenter after it is pressed into the CFPCD sample. We repeated the tests on four different specimens, and all the four new indenters made of the single crystal diamond were broken in the same pattern as Fig. 4b.

It was found that even if the load is increased from 1 N to 9.8 N, the Vickers indentations on the polished CFPCD samples are too small to be accurately measured. As a good comparison, the standard diamond indenter was still in good condition after the test of the commercial PDC sample. The comparison results show that the hardness of the CFPCD sample exceeds the Vickers hardness limit of a single crystal diamond (120 GPa)<sup>13</sup>, indicating the hardest material in the world, so far. The hardness of the commercial PDC material is only about 64 GPa. The higher hardness observed in the CFPCD samples can be attributed to nanostructure defects caused by high-pressure work hardening, such as stacked nanolamellae, stacked faults, and twin microstructures<sup>4</sup>.

**Fig. 3** (a) A SEM secondary electron image shows the microstructure of the polished CFPCD sample prepared under 16 GPa and 2,300 °C, and (b) a SEM backscatter electron image shows the microstructure of the commercial PDC cutter. The dark gray region in Fig. 3 (b) is diamond and the bright region is cobalt catalyst.

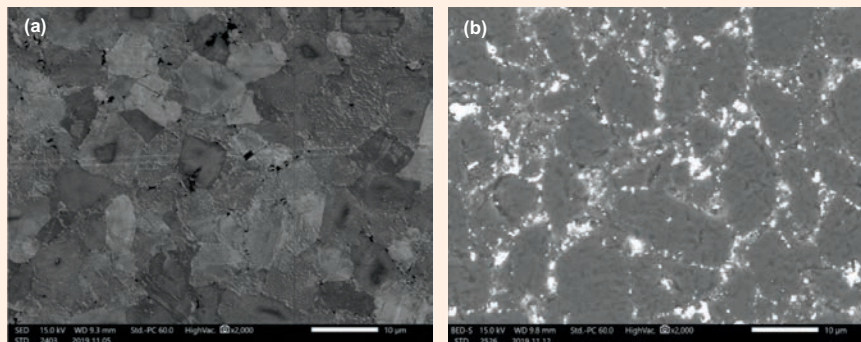
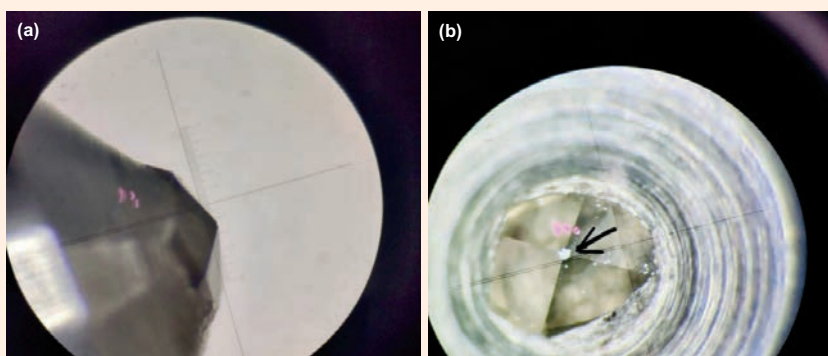


**Fig. 4** The optical images of single crystal diamond indenters (a) before the hardness testing, and (b) after the testing on CFPCD material, showing the hardness of the CFPCD material is higher than single crystal diamond (120 GPa). The arrow in Fig. 4b indicates the damage on the indenter tip.



The cutting performance of the samples were evaluated by cutting a turning granite log in a numerically controlled lathe, which is the most widely used method. The granite has high hardness and wear resistance, and low thermal conductivity. The cutting parameters utilized for the granite log turning test were as follows: cutting speed of 100 m/min, depth of cut of 0.5 mm, and feed rate ( $f$ ) of 0.4 mm/revolution. The CFPCD and the commercial PDC samples were processed into cylindrical cutting tools with a diameter of 11 mm and height of 6 mm.

Figures 5a and 5b shows the optical images of the cutting edges of the CFPCD sample and the commercial PDC sample when the cutting length is 1,260 m, respectively. We can clearly see that the wear areas of the commercial PDC sample are uneven and significantly larger than those of the CFPCD sample, especially when the turning length reaches 1,260 m.

The wear resistance of the CFPCD and commercial PDC samples is quantified using the abrasion wear ratio,  $E$ , and the wear rate or ratio is calculated using the following equation:

$$E = \frac{V_1}{V_2} \quad 1$$

where  $E$  is abrasion ratio;  $V_1$  is the volume loss from granite, ( $\text{mm}^3$ ); and  $V_2$  is the volume loss from cutting tools ( $\text{mm}^3$ ). The higher  $E$  means the higher wear resistance of the material.

It was found that the average abrasion ratio of the CFPCD sample is more than four times that of the commercial PDC sample, which is the best diamond materials currently used in the industry. The CFPCD sample is at a stable level with the increase of cutting length, as there is no falling off of diamond blocks in the process of turning granite testing. The extraordinary wear resistance of the CFPCD material is directly related to its ultra high hardness, which is because of the fact that it is catalyst free.

The wearing surfaces of the CFPCD and commercially available PDC materials were also inspected by SEM after each stop before finishing the total test up to 1,260 m of cutting<sup>12</sup>. The commercial PDC sample

suffered serious breakage and chipping damage after 1,260 minutes of cutting, and there are also many microcracks and grain falling in the cutting edge of the sample. This could be because of the large mismatch of the elastic modulus and thermal expansion coefficient between the diamond grains and cobalt catalyst, and the graphitization of the diamond by reaction under high temperature and with the existence of cobalt catalyst, owing to the increasing temperature and high stress at the cutting point.

Consequently, the CFPCD sample shows very durable wear surfaces, demonstrating unprecedented wear resistance. It is also worth noting that the wear resistance of a cutter is a combination property coming from hardness and toughness. If the material has good hardness, but inferior toughness, it is not able to survive the intensive wear test; or otherwise. Therefore, the toughness of this newly developed material should be very high too, even though no metallic catalyst is used in the manufacturing. It is echoed by the observation in the hardness indentation measurement where we did not observe the cracking at the corners of the indented marks. A further and direct test using  $K_{Ic}$  methodology is still ongoing now, and will be published when available.

A further impact test on the CFPCD sample exhibits intragranular grain failure mode on the fracture surfaces, showing an extremely strong diamond-diamond bond<sup>12</sup>. It is another indication of high toughness of the newly developed CFPCD material.

High temperature thermal stability and oxidation resistance are important to the applications, especially in hard and abrasive formation drilling in the oil and gas industry. The thermal stability and oxidation resistance tests were carried out under in situ XRD at various temperatures from room temperature to 1,400 °C. For comparison, a commercial PDC material was also tested.

Figure 6a shows that the starting oxidation temperature of the commercial PDC is severe at approximately 806 °C. On the other hand, the new CFPCD material does not show oxidation at 1,000 °C, Fig. 6b. In another

**Fig. 5** The wear surfaces at the cutting edges of the commercial PCD compact (a), and (b) the CFPCD compact. The turning length on the granite log is 1,260 m. The pictures are taken at the same distance from the optical microscope.

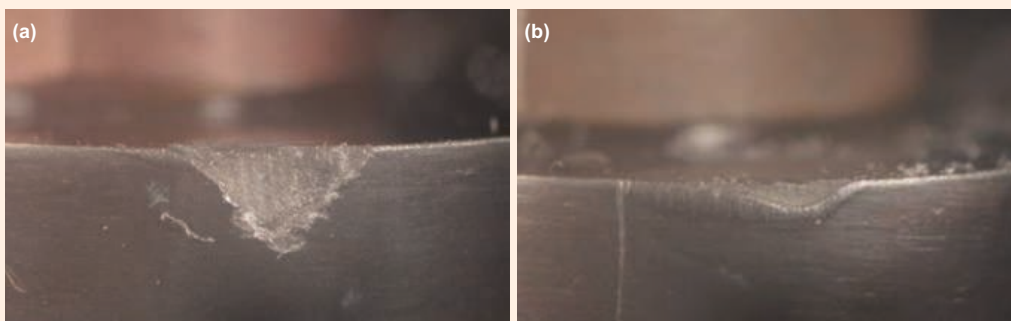
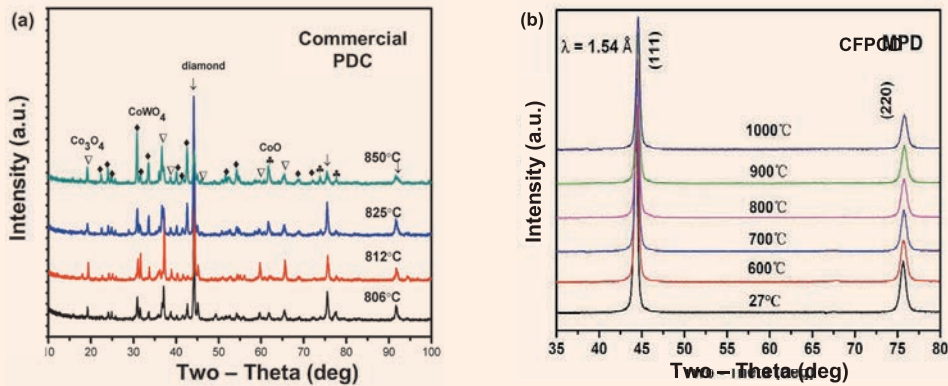


Fig. 6 The high temperature in situ XRD spectra of: (a) a commercial PDC material, and (b) a UHPHT CFPCD material at temperatures up to 1,000 °C.



article<sup>12</sup>, it was tested up to 1,400 °C and found that it is even stable at 1,200 °C — the highest recorded in the industry, which is much higher than those of natural diamond (~800 °C)<sup>14</sup>, nano-grained diamond (~680 °C)<sup>9</sup>, nanotwinned diamond (~1,056 °C)<sup>14</sup>, and commercial PDC (~600 °C)<sup>4</sup>.

## Conclusions

With an extremely high-pressure of 16 GPa and an ultra high temperature of 2,300 °C, a centimeter-sized CFPCD compact has been successfully synthesized. The wear resistance, hardness, and thermal stability were symmetrically evaluated. The results show that the newly developed material has extremely high wear resistance — four times that of the best commercial PDC materials used in the industry. The material also broke all the indenters during the Vickers hardness tests, indicating that it is by far the hardest material in the world. In addition, the material has the highest thermal stability in an oxygen containing environment, with a temperature up to 1,200 °C.

The new CFPCD material has the superior combination of the highest hardness, unprecedented wear resistance, and maximum thermal stability in the diamond family. It is expected to play an important role in scientific research as well as in the oil and gas exploration and drilling industries. The PDC cutters made of these ultra-strong, CFPCD materials in this study bring forward a breakthrough in the oil and gas drilling industry. Further research has been continuing to produce UHPHT cutting materials in larger sizes and implement these full-sized cutters on the drill bits for field-testing, with the targeted goal to achieve a “One Run to Total Depth” game changing drill bit technology.

## Acknowledgments

This article was prepared for presentation at the Middle East Oil and Gas Show and Conference, Manama, Kingdom of Bahrain, November 28-December 1, 2021.

## References

1. Scott, D.E.: “The History and Impact of Synthetic Diamond Cutters and Diamond Enhanced Inserts on the Oil and Gas Industry,” *Industrial Diamond Review*, Vol. 66, Issue 1, January 2006.
2. Bruton, G., Crockett, R., Taylor, M. and DenBoer, D.: “PDC Bit Technology for the 21<sup>st</sup> Century,” *Oilfield Review*, Vol. 26, Issue 2, June 2014, pp. 48-57.
3. Bellin, F., Dourfaye, A., King, W. and Thigpen, M.: “The Current State of PDC Bit Technology,” *World Oil*, September 2010, pp. 41-46.
4. Zhan, G., Patin, A., Pillai, R., Gilleylen, R., et al.: “In-Situ Analysis of the Microscopic Thermal Fracture Behavior of PDC Cutters Using Environmental Scanning Electron Microscope,” SPE paper 168004, presented at the IADC/SPE Drilling Conference and Exhibition, Fort Worth, Texas, March 4-6, 2014.
5. Zhan, G., Moellendick, T.E., Li, B., Gooneratne, C., et al.: “New Ultra-Strong and Catalyst-Free PDC Cutting Element Technology,” IPTC paper 19764, presented at the International Petroleum Technology Conference, Dhahran, Saudi Arabia, January 15-15, 2020.
6. Rassenfoss, S.: “Seeking Ways to Make Better Diamonds by Tending to the Tiniest Details,” *Journal of Petroleum Technology*, Vol. 66, Issue 6, June 2014, pp. 58-47.
7. Wilks, J. and Wilks, E.: *Properties and Applications of Diamond*, Butterworth-Heinemann, Oxford, 1991, 525 p.
8. Irifune, T., Kurio, A., Sakamoto, S., Inoue, T., et al.: “Ultrahard Polycrystalline Diamond from Graphite,” *Nature*, Vol. 421, February 2005, pp. 599-600.
9. Shatskiy, A., Katsura, T., Litasov, K.D., Shcherbakova, A.V., et al.: “High Pressure Generation Using Scaled Up Kawai-Cell,” *Physics of the Earth and Planetary Interiors*, Vol. 189, Issue 1-2, November 2011, pp. 92-108.
10. Liu, J., Zhan, G., Wang, Q., Yan, X., et al.: “Superstrong Micro-Grained Polycrystalline Diamond Compact through Work Hardening under High Pressure,” *Applied Physics Letters*, Vol. 112, Issue 6, February 2018.
11. Liu, Y., Zhan, G., Wang, Q., He, D., et al.: “Hardness of Polycrystalline Wurtzite Boron Nitride (wBN) Compacts,” *Scientific Reports*, Vol. 9, Issue 1, July 2019.



12. Li, Q., Zhan, G., Li, D., He, D., et al.: "Ultrastrong Catalyst-Free Polycrystalline Diamond," *Scientific Reports*, Vol. 10, December 2020.
13. Brookes, C.A. and Brookes, E.J.: "Diamond in Perspective: A Review of Mechanical Properties of Natural Diamond," *Diamond and Related Materials*, Vol. 1, Issue 1, August 1991, pp. 15-17.
14. Huang, Q., Yu, D., Xu, B., Hu, W., et al.: "Nanotwinned Diamond with Unprecedented Hardness and Stability," *Nature*, Vol. 510, June 2014, pp. 250-255.

---

#### About the Authors

##### **Dr. Guodong "David" Zhan**

*Ph.D. in Metallurgical Engineering, Huazhong University of Science and Technology*

Dr. Guodong "David" Zhan is a Science Specialist and the Team Leader of the Advanced Drilling Tools team in the Drilling Technology Division at Saudi Aramco's Exploration and Petroleum Engineering Center – Advanced Research Center (EXPEC ARC). David is a world-renowned materials scientist and expert in advanced drilling tools/technology. He has over 25 years of experience in industrial R&D and managerial positions, including positions as Chief Engineer and R&D Manager at top oil/gas and semiconductor global companies, such as Schlumberger, NOV, and Applied Materials.

Additionally, David has held academic positions at the University of London and the University of Colorado at Boulder, and staff scientist positions at the Japan National Institute for Materials Science.

He is an active member of the Society of Petroleum Engineers (SPE) where he serves on several conferences such as the SPE Internation-

al Petroleum Technology Conference and the Asia Pacific Drilling Technology Conference/ International Association of Drilling Contractors as co-chair and technical committee member. David is also serving as an editorial board member and reviewer for a number of international scientific journals published by The Minerals, Metals and Materials Society and the Material Research Society.

He has published 95 peer-reviewed articles in journals such as *Nature Materials* and *Nature Scientific Reports*, 98 conference proceedings, and has more than 100 filed/published/granted U.S. patents, with an H-index of 37.

In 1994, David received his Ph.D. in Metallurgical Engineering from Huazhong University of Science and Technology, Wuhan, China, and completed a postdoctoral fellowship in Nanomaterials and Nanotechnology at the University of California at Davis.

**Dr. Bodong Li**

*Ph.D. in Electrical Engineering,  
King Abdullah University of  
Science and Technology*

Dr. Bodong Li joined Saudi Aramco in 2015. He is the Technology Leader on Internet-of-Things (IoT) and Robotics at Saudi Aramco's Upstream Advanced Research Center. Bodong is also a member of the Drilling Technology Division focusing on research and development of advanced drilling tools.

He has 12 granted U.S. patents, and has authored and coauthored numerous articles published in scientific journals and conference papers covering the areas of sensing and

downhole technologies.

Bodong is an active member of the Society of Petroleum Engineers (SPE) and the Institute of Electrical and Electronics Engineers.

He received the Discovery Scholarship and Fellowship from King Abdullah University of Science and Technology (KAUST).

Bodong received his M.S. degree in Mechanical Engineering and his Ph.D. degree in Electrical Engineering, both from KAUST, Thuwal, Saudi Arabia.

**Timothy E. Moellendick**

*B.S. in Petroleum Engineering,  
Marietta College*

Timothy E. Moellendick is the Chief Technologist for the Drilling Technology Division at Saudi Aramco's Exploration and Petroleum Engineering Center – Advanced Research Center (EXPEC ARC). Timothy is considered the industry expert in casing and liner drilling applications and engineering.

In his previous role as Director of Technology for Schlumberger, he was responsible for growing the technical and operational knowledge base used to develop, plan, and execute this technology worldwide. Timothy has also held drilling operations and engineering

positions, including Senior Drilling Engineer, Drilling Manager for North America, Senior Field Engineer/Directional Driller and Operations Coordinator for the Gulf Coast of Mexico.

With more than 25 years of oil and gas industry experience, he leads a team of world-class researchers in developing the next generation of drilling technology required by Saudi Aramco's Drilling and Workover stakeholders.

In 1996, Timothy received his B.S. degree in Petroleum Engineering from Marietta College, Marietta, OH.

**Dr. Duanwei He**

*Ph.D. in Condensed Matter  
Physics,  
Institute of Physics*

Dr. Duanwei He is a Professor at the Institute of Atomic and Molecular Physics, Sichuan University. He is a world-renowned scientist and expert in hard materials and high pressure physics.

Duanwei's current research interests include advanced superhard materials and bulk nanostructured ceramics, development of technology for large volume high-pressure systems, and elastic and plastic behavior of strong materials under high pressure.

He has also held several positions as a Senior Research Engineer at Schlumberger MegaDiamond, Research Staff from Los Alamos National Institute for Materials Research, and Princeton University.

Duanwei has published 150 journal papers with an H-index of 32, and holds 15 granted patents.

He received his Ph.D. degree in Condensed Matter Physics from the Institute of Physics, Chinese Academy of Sciences, Shanghai, China.

**Dr. Jianhui Xu**

*Ph.D. in Materials Science and  
Engineering,  
University of Kentucky*

Dr. Jianhui Xu is a Materials Engineer with the Drilling Technology Division at Saudi Aramco's Exploration and Petroleum Engineering Center – Advanced Research Center (EXPEC ARC). He joined Saudi Aramco in 2019. Prior to that, Jianhui worked at Schlumberger as a Materials Engineer for 6 years and at the CNPC USA Corporation as a Senior Materials Engineer/ Group Lead for another 6 years.

His research interests are smart materials, nano-technologies, hard materials, degradable materials, coating materials, and process. Jianhui is an expert in the material and process solutions for applications to work in specialty and hostile environments within the oil and gas

industry, including drilling tools and completion tools.

He has published 25 scientific publications and holds 20 patents and applications. Jianhui has been serving as a reviewer for several internationally prestigious journals, including *Materials Science and Engineering* and *Philosophical Magazine Letters*. He is an active member of The Minerals, Metals and Materials Society (TMS) and the Society of Petroleum Engineers (SPE).

In 2008, Jianhui received his Ph.D. degree in Materials Science and Engineering from the University of Kentucky, Lexington, KY.



# Design Optimization for Hydraulically Driven Agitation Tool in Extended Coiled Tubing Reach Application

Hussain A. Al-Saood, Laurie S. Duthie, Ahmed H. Albaqshi and Muhammad Ahsan

## Abstract /

As the boundaries are pushed with the increased length of horizontal wells, coiled tubing (CT) well intervention capabilities are challenged requiring new technologies to expand existing capabilities. When utilizing CT, standard best practice is to first utilize CT modeling software to optimize the size and weight for maximum reach. After choosing the right CT size, the next and most critical factor to address in extending the reach is to drag the frictional forces between the CT and the wellbore. Reducing friction and delaying helical buckling will significantly increase the reach. Several versions have been created utilizing various pressure pulse tools in the CT bottom-hole assembly to accomplish this task.

These tools work by creating vibration or pressure pulses that allow for a delay in the onset of the helical buckling of the CT, and are widely utilized and accepted as solutions, however, existing agitation tool limitations have been reached. A newly designed and developed hydraulically driven agitation tool (HDAT) to extend CT reach delivers continuous frequency pressure waves along the entire length of the CT. The HDAT provides a reduction in static friction and converts that to a dynamic friction form along the CT string. The continuous hydraulic agitation reduces the onset of helical buckling, and thereby reduces CT helical contact points, resulting in a lower resistance force.

The development, design, and lab testing for the HDAT has been through extensive development stages resulting in three generations of the tool, with each version providing an incrementally improved performance. The latest generation HDAT has been designed to function at optimum operational frequencies and produce excitation that works on a longer section of the CT. The performance advancement of the newly designed HDAT generation was achieved after extensive lab testing with a field run reaching a total depth of 24,500 ft over a 4,600 ft open hole lateral section.

The new HDAT was redesigned to improve performance and reliability to achieve an effective matrix acid stimulation treatment. The lessons learned from previous generations were imbedded to extend the reach of the CT in the most challenging extended reach wells.

## Introduction

The global pressure on oil and gas demand has pushed the development of new concepts to increase the operational efficiency and to decrease the production cost. With this demand, the drilled well profiles became more complex with time. This added complexity makes the drilling and intervention operations more challenging, requiring continuous enhancement and optimization of the technologies used.

This article will study the technology, design enhancement, and performance optimization for the multiple hydraulically driven agitation tool (HDAT) generations used with coiled tubing (CT) to perform intervention jobs, and the challenges faced in operations. The subjected applications are focused mainly on three methodologies that were followed in the design for the well profiles. The HDAT was used where the wells were drilled with extended reach multilateral and horizontal profiles.

### Extended Reach Wells

The number of extended reach wells has increased rapidly because of their benefits and value. Extended reach applications are technically challenging, costly, and in some cases, will require the use of special techniques and equipment to reach the targets. Subsequently, with the right planning and execution of the drilling and intervention operations, designing the well with extended reach profiles can add value.

By drilling an extended reach well, the long length of the drilled hole will capitalize on the increased reservoir interval exposed, enhance the production rate, improve reservoir control and management, and reduce the drilled well count, optimizing producing field's economics.

From the standard oil field criteria, any well with the ratio of measured depth (MD) to the true vertical depth that is greater than 2.0 will be considered an extended reach well. From the definition, the extended reach well can have a long MD and relatively short and shallow vertical depth<sup>1</sup>.

### Multilateral Wells

Drilling a multilateral well is another method that is used to reduce the cost and optimize the return on investment for oil and gas wells. In general, multilateral wells are more effective economically when they target low to moderate permeable reservoirs rather than high permeability reservoirs. Multilateral wells can be defined as wells with additional sections drilled from a motherbore, Fig. 1.

Multilateral sections can be as simple as an open hole sidetrack or can be more complicated with a junction that is cased and has pressure isolation and reentry capabilities. Multilaterals allow production to be incrementally increased with less capital costs. Multilaterals can also be used to place additional horizontal wells in a reservoir to cover more of the production zones in the same well<sup>2</sup>.

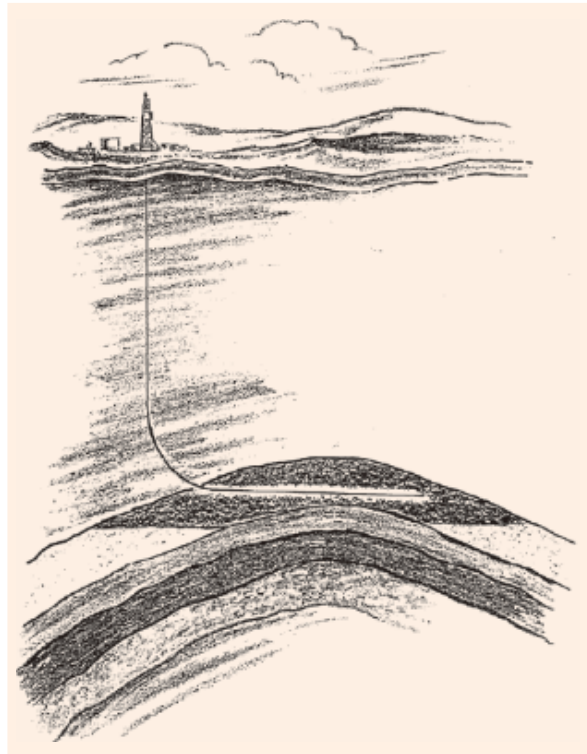
### Horizontal Wells

Some individual sources consider a well to be a horizontal well profile when the well trajectory has an inclination greater than 75°. Other sources use 85° inclination as a minimum inclination to describe a horizontal well. In this article, the horizontal wellbore is considered for the wells that were drilled at an inclination greater than 80° through the production formations. The horizontal section length will be the portion of the MD after the well inclination has increased to 80°. Any part of the well interval prior to reaching 80° will not be considered as part of the horizontal section length.

Since the early 1980s, horizontal well profiles have been commonly used in the oil and gas industry. The primary purpose of planning a well with a horizontal profile is to improve the reservoir production. Horizontal well profiles are planned to target and produce from thin oil zones. The horizontal well has to be optimally located in the oil leg of the reservoir, Fig. 2. Because of the increased amount of production zones exposed to the wellbore in horizontal wells, the oil can be produced at higher rates with less pressure drawdown.

Horizontal wells are used to enhance production from reservoirs that are not being drained by vertical wells efficiently, where they may have permeability streaks in combination with natural fractures. The

Fig. 2 A horizontal well cross-section view.



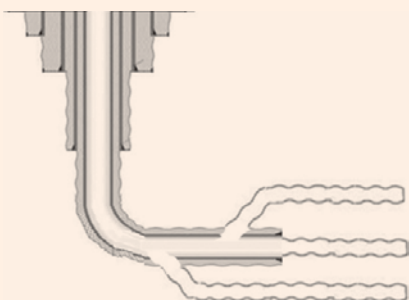
horizontal well can link the zones of the reservoir that are productive in a single wellbore<sup>2</sup>.

### Application Overview

The CT deployment in extended reach wells for stimulation and intervention applications is becoming more challenging with the growing complexity of wellbores. The limitation to deploy CT into relatively deep intervals has been challenging for conducting acid stimulation to restore the injectivities of these wells after drilling and completion<sup>5</sup>. It is important to run the CT as deep as possible to achieve uniform distribution of stimulation fluids over the length of the open hole.

The objective of the stimulation treatment process is to remove and bypass the formation damages resulting from the drilling mud, and to enhance the production zones. Stimulation fluids are normally bullheaded through the CT from lockup depth to the remaining uncovered section of the extended reach well. This type of treatment potentially jeopardizes the ultimate objective of the stimulation treatment. Bullheading is typically conducted after multiple attempts to run the CT to the desired depth of stimulation treatment. Bullheading is a process to pump treatment fluids at higher flow rates to forcibly pump the fluids into the formation. Consequently, bullheading the stimulation treatment does not guarantee a proper placement of fluids across the open hole, because the fluids will typically travel toward the least resistive paths, usually the most permeable zone, which may not require

Fig. 1 An example of horizontal trilateral well profile.



any treatment<sup>†</sup>. Maximizing the reach of the open hole interval is essential for a successful stimulation treatment.

The challenges related to limited CT reach for stimulation fluids placement have been widely addressed through the use of various techniques. These techniques include the use of nitrogen through the CT to make it lighter and more buoyant, the use of larger diameter CT, the use of friction reducing fluids, and the use of friction reduction tools.

### Challenges

One of the most significant problems related to extended reach or horizontal wells are frictional force and drag, which are caused by the friction between the CT and the walls of the wellbore. The magnitude of the drag is determined by the extent with which the CT contacts the borehole and the friction between the wall and the CT.

The friction coefficient depends on the type of fluid in the wellbore and the roughness of the wellbore's walls. The cased hole will mostly show a lower friction coefficient than the open hole and a higher fluid density will yield a higher friction coefficient due to the presence of higher solid contents.

One of the challenges during intervention for CT is reaching the maximum depth in extended reach wells. The factors that contribute to this challenge are well depth, horizontal lateral length, open hole interval, drag/friction between the wellbore and the CT, hole size, and the limitation of the CT size, due to the minimum restriction in the wellbore. As the depth of the well increases, the friction between the CT and wellbore increases. This increased friction first induces sinusoidal buckling that progresses to helical buckling as the CT is being pushed further in the wellbore.

This helical buckling ultimately leads to lockup, where no further advancement to the depth can be achieved, Fig. 3. The helical buckling plays the most important part in the development of the lockup stage when it is attempted to run the CT deeper in the well. Therefore, delaying of helical buckling by utilizing a friction reduction system to reduce the friction between the wellbore and the CT will prevent lockup in the early stages, enabling the CT to reach the desirable deeper depths.

The targeted wells had higher friction coefficients due

to the presence of denser fluids or components such as tar and asphaltenes. This refers to the increased resistance for the CT to run in such wellbore conditions. Another major challenge is to reach target depth while running a smaller size of CT due to the minimum restriction in the wellbore. Bigger open hole sizes, i.e., 6⅞" and 8½", also contribute to the struggle to reach targeted depths to conduct acid stimulation operation. The presence of hydrogen sulfide also limits the use of available resources and technologies to address the challenges for extended reach application.

Long multilateral and horizontal sections are the other challenges associated with the CT runs. A larger open hole size with the open hole section ranging from 8,000 ft to 9,500 ft adds to the complication of deploying the CT to the maximum targeted depth.

### HDAT Technology Principle

In such applications, the amount of friction and drag will limit the reachability of the CT to the final target well depth. The cumulative friction and drag will cause the CT to buckle at early stages, contributing to lockup. The buckling state of the CT string can be eliminated or delayed by reducing the induced friction due to the CT string and wellbore contact area.

The HDAT is used as a friction reduction tool to reduce the drag and frictional forces between the wellbore and the CT string while running in the hole. The HDAT working principle is to break the static friction and convert it to a lower amount of friction in a dynamic form. This is accomplished by generating continuous pressure pulses while pumping fluid through the tool. The CT string will be reacting with these traveling excitation waves as continuous mechanical motions. The friction will be reduced in the part of the string where the pressure waves are traveling through the system. This friction reduction mechanism will result in improved weight transfer, faster CT tripping in speed, delayed CT buckling occurrence, and extending the CT reach.

The HDAT consists of two main sections: a power section and a valve assembly. The tool is activated by pumping a fluid through it and both tool sections work together converting the hydraulic energy to produce a series of pressure fluctuation waves that travel up and down in the coil.

When the pumped fluid is passing through the tool, the rotor inside the power section rotates. The rotor's

**Fig. 3** How helical buckling of the CT can lead to lockup development.

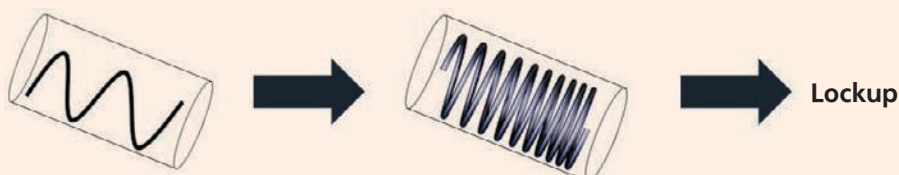
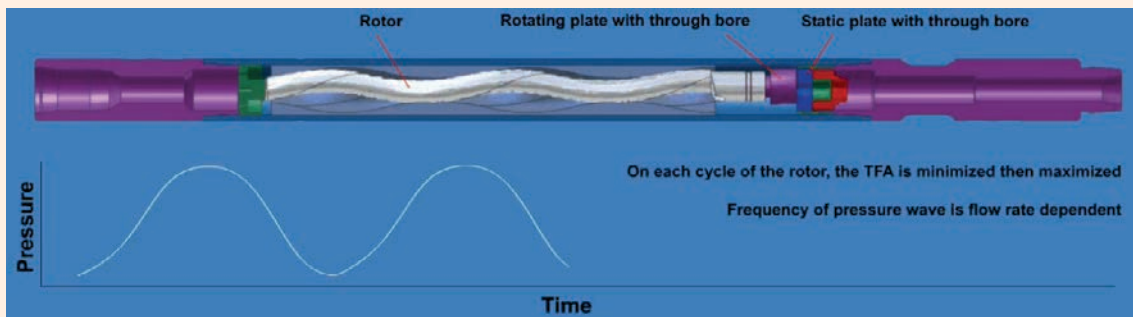


Fig. 4 The HDAT schematic and cyclic pressure waves signature.



rotation, which occurs at a frequency proportional to the flow rate, will drive the oscillation valve plate in a continuous dynamic track relative to a stationary valve plate. This movement creates cyclic variation of the fluid's total flow area. This total flow area variation initiates a series of repetitive pressure pulses that are carried by the pumped fluid, Fig. 4.

### Demand for Performance and Optimization

The HDAT has been run to aid extending the reach and to improve CT placement in the reservoir in wells that have open hole intervals ranging from 3,500 ft MD to 9,500 ft MD lengths, and with 12,000 ft to 25,000 ft target depths.

Because of the challenges experienced to extend the CT reach, multiple application studies and laboratory prototype trial tests were implemented. This resulted in three design improvement phases; all three generations were introduced to optimize the results and to achieve the main objectives of extending the reach.

The main objective of the three tool design generations was to meet the latest application challenges. This objective was achieved, resulting in a tool with higher energy output, greater reduction of friction forces, a streamlined manufacturing process, an increased torsional and tensile capacities, and overall increased tool reliability.

#### HDAT: First-Generation

The first-generation of the HDAT design technology was built based on the legacy tool structure with more enhanced friction reduction rates. The first-generation of the HDAT has a single lobe power section configuration that delivers high frequency rates — up to 18 Hz. The valve assembly section was redesigned in a way to allow setting the tool with a wider range of pressure pulse values and more controlled performance options. Based on the application requirements, the HDAT was adjusted to generate the desired pressure waves at the specific pumped flow rates.

#### HDAT: Second-Generation

The development continued, resulting in the introduction of the second-generation of the HDAT with the

purpose of providing more energized technology to aid in extending the CT reach in the same application.

The power section was reconfigured with a multi-lobe design in the second-generation, which facilitated higher flow rates with the same differential pressure and pressure pulses. The multi-lobe power section design enables slower rotor rotational speed at the same flow rates, improving performance by allowing better pressure pulse frequency control and optimum operation of the valve system. The valve assemblies were designed to create higher excitation that work on a longer length of the CT string.

#### HDAT: Third-Generation

With the growing complexity of wellbores, the third-generation of the HDAT was introduced to address the challenges of long laterals and extreme doglegs. The newly designed third-generation tool's stronger and more reliable design was the result of the data gathered and experience gained from runs of the previous generations.

The third-generation of the HDAT tool was designed after full research and observation of the tool's behavior/performance with different activation flow rates, variable differential pressure across the system, as well as with different cyclic wave speed.

During the design phase, a series of prototypes and testing regimes were implemented to enhance the optimization process.

The resulting tool design incorporated a multi-lobe power section configuration and a redesigned valve assembly, which reduced the differential pressure across the tool, and increased while increasing efficiency and power. The new tool design was allowed to customize the parameters to fit the application requirements, achieving up to 100% more energy output compared to the previous generations.

#### Research and Development Laboratory Testing

As part of the in-house research and development of the technology, a horizontal test rig was used to perform multiple cycles of different designs to achieve the desired functionality of the tool.

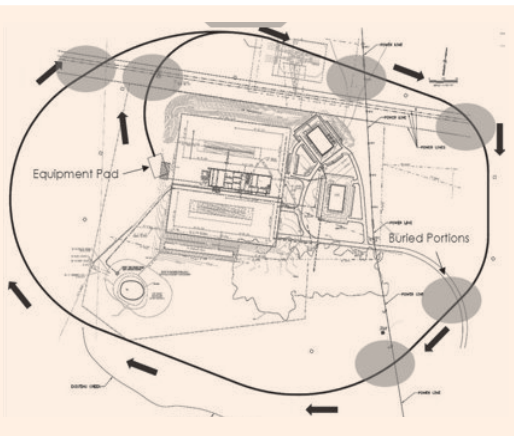
The horizontal test rig, Fig. 5, was set to simulate the



**Fig. 5** The horizontal test rig equipment.



**Fig. 6** The closed research and development test loop.



closest possible conditions and environment to that in the real-time application. In testing the horizontal test rig, the tool was run in the string and activated by pumping fluid through the system. Several measurement devices were connected to monitor the output parameters, which were used to compare the test results of each tool's design improvement and to verify the design modifications.

A closed test loop with 20,000 ft of metallic tubular, Fig. 6, was attached to the horizontal test rig unit and oriented horizontally to simulate the challenges that the tool would be run in. This allowed for a better understanding of the theory and provided wider capabilities for the research and development process.

**Service Center Testing**

With every new tool assembly, a function test of the tool is conducted using a dynamometer, Fig. 7a. During the

**Fig. 7** The dynamometer stand (a), and the dynamometer parameter control panel (b).

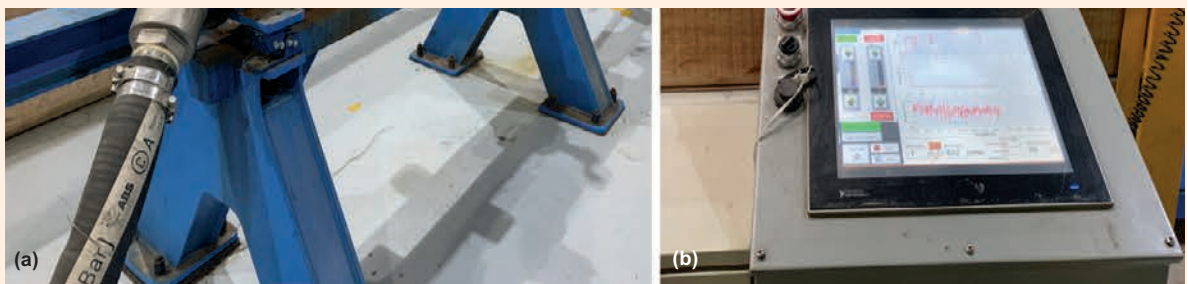


**Fig. 7** The dynamometer stand (a), and the dynamometer parameter control panel (b).

**Fig. 8** The performance of the first-generation HDAT from relatively low to high challenging applications.

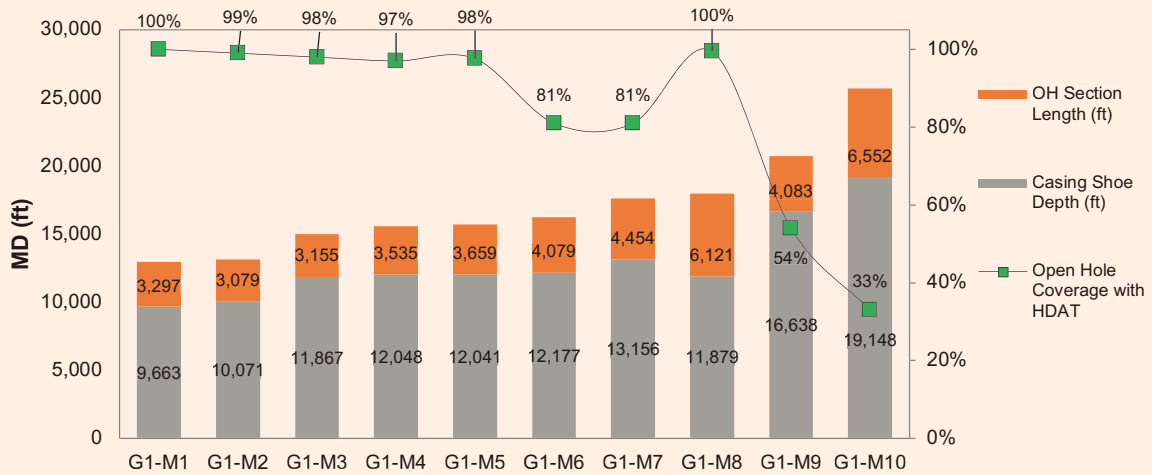


**Fig. 9** The performance of the first-generation HDAT, as the tool enabled the CT to cover an average 83% open hole interval in 10 runs.

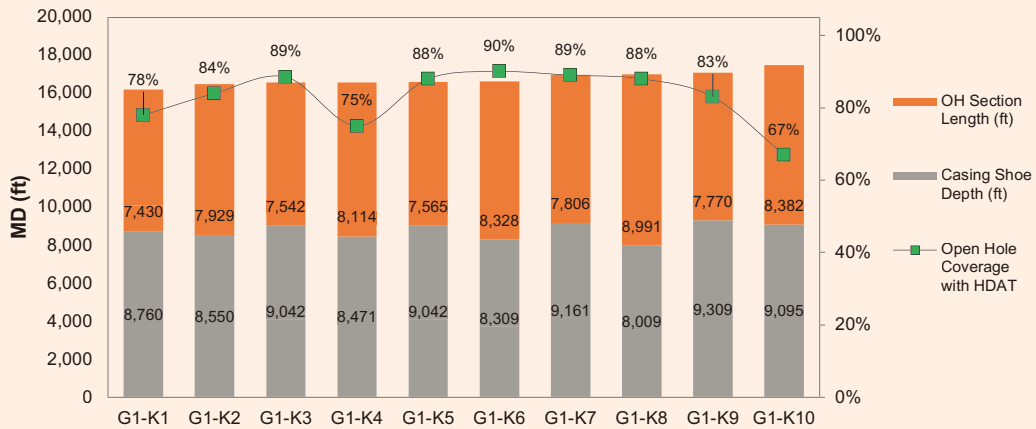


**Fig. 10** The HDAT exhibited notable performance covering 89% and 100% of the open hole interval, respectively, in two runs.

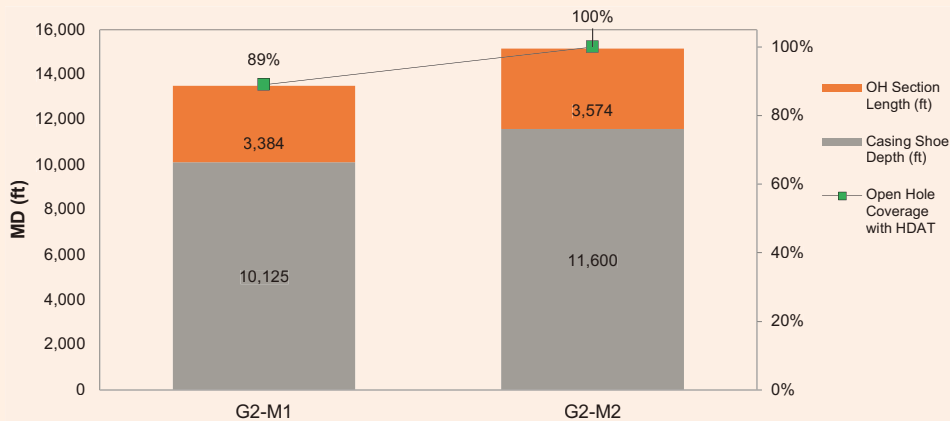




**Fig. 11** The performance development for the three runs using the second-generation HDAT.

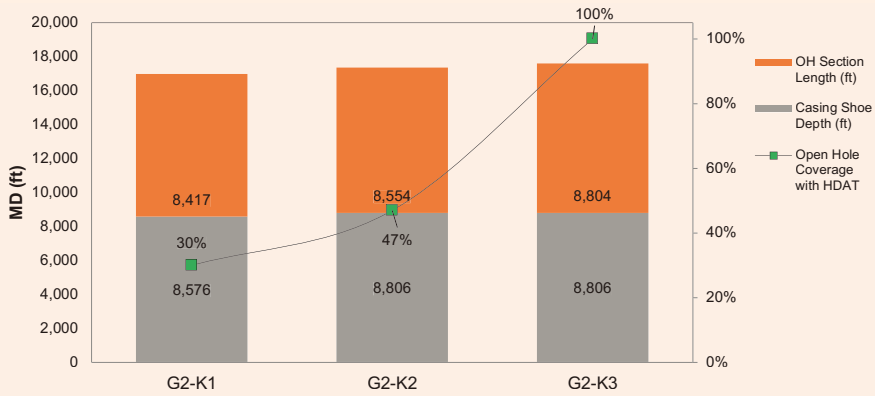


**Fig. 12** The third-generation of the HDAT delivered exceptional performance in covering 100% of the open hole in most of the runs while reaching more than 24,500 ft MD in one of the runs.

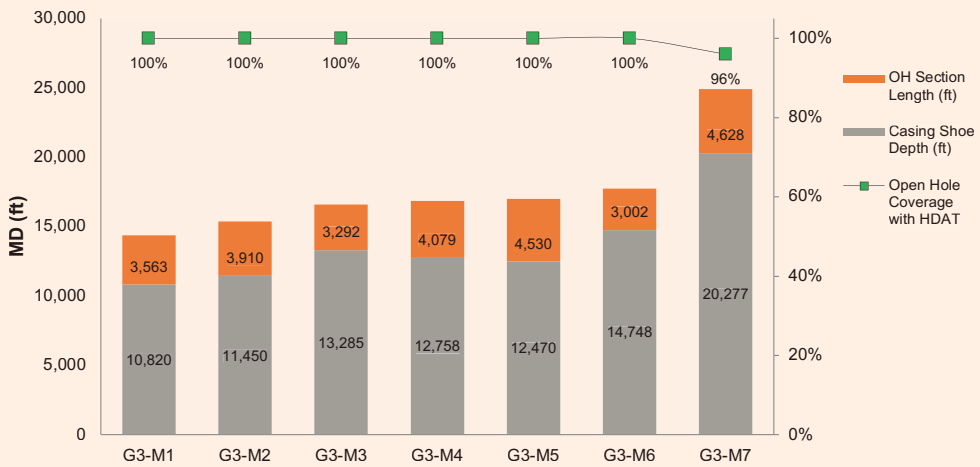
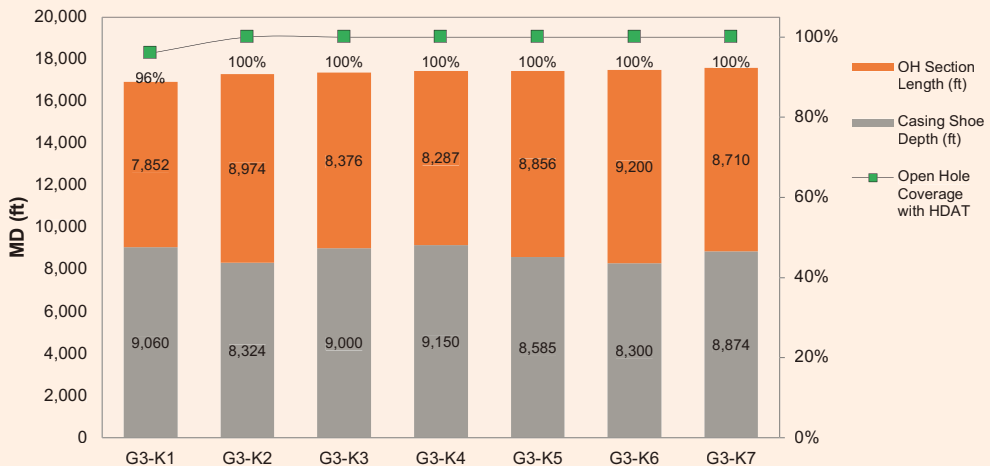


**Fig. 13** The consistent high performance for the third-generation HDAT, overcoming the challenge of a long lateral and big open hole size while reaching target depth in most of the runs.



dynamometer test, the tool is assembled into a closed loop flow system that continuously pumps through the tool at various controlled flow rates. The parameters measured during the dynamometer test allow for optimal setup of the tool, which is not achievable without the dynamometer parameter control panel, Fig. 7b.

#### First-Generation Runs

The first-generation of the HDAT was designed considering the need for reaching target depths with a relatively less challenging application at that time. The tool still achieved the desired results, meeting the target depth in most of the runs. Figure 8 shows the performance of the first-generation tool from relatively low to high challenging applications. The tool achieved average a 98% open hole coverage in the first five runs. But as the well depth increased with the length of the open hole section, the need for a more robust tool was realized to meet the target depth.

Figure 9 shows the performance of the first-generation tool, as the tool enabled the CT to cover an average 83% open hole interval in 10 runs. While the application became more challenging, it was required to optimize the tool to work for more challenging applications.

#### Second-Generation Runs

The HDAT exhibited notable performance covering 89% and 100% of the open hole interval, respectively, in two runs, Fig. 10. Consequently, the slow running in hole speed for the CT recognized the requirement for a stronger tool that could generate a higher energy and increase the CT running in hole speed.

Figure 11 shows performance development for the three runs using the second-generation HDAT. The chart shows an average 39% open hole coverage in the first two runs, and 100% open hole coverage in the third run for the similar interval.

#### Third-Generation Runs

The third-generation of the HDAT delivered exceptional performance in covering 100% of the open hole in most of the runs while reaching more than 24,500 ft MD in one of the runs, Fig. 12. During these runs, the third-generation HDAT improved weight transfer and run in hole speed as compared to the previous generations.

Figure 13 shows the consistent high performance for the third-generation HDAT, overcoming the challenge of a long lateral and big open hole size while reaching target depth in most of the runs.

### Conclusions

Many challenges were experienced during the execution of the acid stimulation jobs that limited the CT reach. Field research and lab testing were conducted to optimize the performance and achieving the objectives. The HDAT went through a series of design improvements that helped to address the application's challenges.

The latest HDAT was redesigned to improve performance and reliability to achieve an effective matrix acid stimulation treatment. The newly developed HDAT

has repeatedly proven to be an efficient solution for CT extended reach applications. The recent consistent and exceptional performance is the testimony that the tool has overcome the challenges associated with extended reach and frictional forces. The tool achieved total depth in most of the runs to effectively acid stimulate the pay zones.

### Acknowledgments

This article was presented at the virtual SPE/ICoTA Virtual Well Intervention Conference and Exhibition, March 22-25, 2021.

### References

1. Bhalla, K.: "Coiled Tubing Extended Reach Technology," SPE paper 30404, presented at the SPE Offshore Europe Conference, Aberdeen, U.K., September 5-8, 1995.
2. Carden, R.S. and Grace, R.D.: *Horizontal and Directional Drilling*, Petroskills LLC, 2007, 409 p.
3. Al-Meshal, F., Sabut, B., Bawaked, W., Beheiri, F., et al.: "Enhanced Coiled Tubing Intervention Practices on Extended Reach Open Hole Completion in a Field in Saudi Arabia," SPE paper 156946, presented at the SPE/DGS Saudi Arabia Section Technical Symposium and Exhibition, al-Khobar, Saudi Arabia, April 4-7, 2010.
4. Al-Najim, A., Zahedi, A., Al-Khonaini, T., Al-Sharqawi, A.I., et al.: "A New Methodology for Stimulation of a High Water Cut Horizontal Oil Well through the Combination of a Smart Chemical System with Real-Time Temperature Sensing: A Case Study of South Umm Gudair Field, PZ Kuwait," SPE paper 154387, presented at the SPE/ICoTA Coiled Tubing and Well Intervention Conference and Exhibition, The Woodlands, Texas, March 27-28, 2012.

---

### About the Authors

#### **Hussain A. Al-Saood**

*B.S. in Petroleum Engineering,  
University of Oklahoma*

Hussain A. Al-Saood is a Production Engineer working in the Manifa Production Engineering Division of Saudi Aramco's Northern Area Production Engineering and Well Services Department. He joined Saudi Aramco as a Petroleum Engineer, but has also held several drilling and reservoir engineering positions, covering several onshore and offshore fields. Hussain's areas of interest include rigless intervention with coiled tubing (CT), wireline, and hydraulic workover operations.

Throughout his career, he has worked on multiple projects, including the change out of electric submersible pumps utilizing the hydraulic workover unit, and developing downhole equipment to enhance the CT reach, i.e., CT tractors and pulsation tools, in extended reach wells for stimulation and logging applications.

Hussain received his B.S. degree in Petroleum Engineering from the University of Oklahoma, Norman, OK.

#### **Laurie S. Duthie**

*M.S. in Petroleum Engineering,  
University of New South Wales*

Laurie S. Duthie joined Saudi Aramco in 2011 as a Petroleum Engineer and works in the Manifa Production Engineering Unit of the Northern Area Production Engineering Department. His focus is on the development and production of a large offshore field in the Northern Area.

Laurie started his career in 1986 working on offshore installations in the U.K. North Sea as a Field Engineer in well testing and wireline operations. He has a strong background in reservoir surveillance, well intervention, acid

stimulation, well testing, completions, and cased hole logging. Laurie has gained extensive operational experience in diverse remote onshore and offshore locations — across Africa, Central Asia, the former Soviet Union, Asia Pacific, and in the Middle East region — since 2009.

In 2005, Laurie received his M.S. degree in Petroleum Engineering from the University of New South Wales, Sydney, Australia.

#### **Ahmed H. Albaqshi**

*B.S. in Applied Mechanical  
Engineering,  
King Fahd University of  
Petroleum and Minerals*

Ahmed H. Albaqshi joined National Oilwell Varco in Dhahran, Saudi Arabia in 2014 as a Drilling Solutions Engineer and joined the International Development Training Program with an intensive focus on drilling and intervention operations. During his training, Ahmed worked with product design engineering, operations technical support, and manufacturing teams in Dubai, Aberdeen, and Houston.

Ahmed's interests are in drilling, fishing and coiled tubing tools and accessories design and

optimization in the oil and gas industry. He is currently involved in downhole tools operation planning, analyzing, and field execution in Saudi Arabia's oil and gas operations.

Ahmed is a member of the Society of Petroleum Engineers (SPE) and actively participates in different workshops and conferences.

He received his B.S. degree in Applied Mechanical Engineering from King Fahd University of Petroleum and Minerals (KFUPM), Dhahran, Saudi Arabia.

#### **Muhammad Ahsan**

*B.S. in Petroleum  
and Gas Engineering,  
University of Engineering  
and Technology*

Muhammad Ahsan joined National Oilwell Varco in 2019 as a Sales Engineer for coiled tubing (CT) and intervention tools. He has more than 7 years of experience in CT and stimulation operations in multiple locations.

Muhammad is handling the CT downhole tools account and provides technical support for

CT and well intervention operations in Saudi Arabia.

He received his B.S. degree in Petroleum and Gas Engineering from the University of Engineering and Technology (UET), Lahore, Pakistan.

# A New Aramco Record in Patents

Michael J. Ives

Saudi Aramco continued to accelerate the growth of its patent portfolio in 2020, receiving 1,588 granted patents globally, including 683 from the U.S. Patent & Trademark Office, a significant increase on the 524 patents granted in 2019, Fig. 1. Approximately 62% of these U.S. granted patents originated from new ideas, with the remainder from continuation or divisional of previous patents.

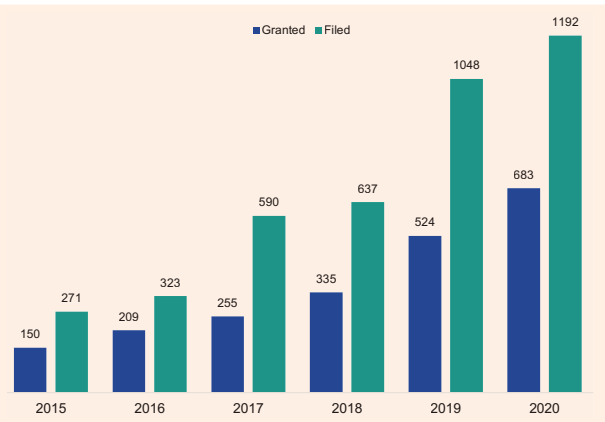
Our Upstream business continues to receive the largest portion of granted U.S. patents with 65%. This is driven by the technology domains of Drilling, Production and Reservoir Engineering.

A total of 1,192 new patent filings were made with 79% originating from new ideas. Our Upstream business also leads new filings with 65%. Analysis of the technology domains shows carbon management within the top 10 for new filed patents.

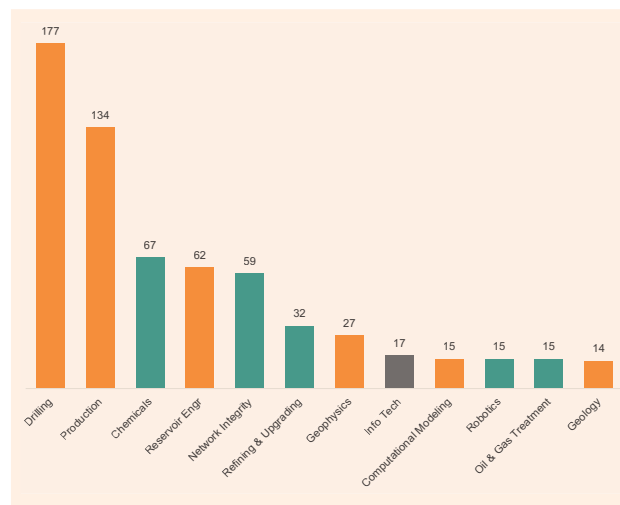
Figure 2 compares the 2020 U.S. granted patents among international oil companies and shows Saudi Aramco having a leading position with 683 granted patents. ExxonMobil follows with 367, followed by Shell with 121.

Figure 3 shows the top technology domain distribution of the granted U.S. patents in 2020 for Saudi Aramco with upstream technology domains of drilling and production leading.

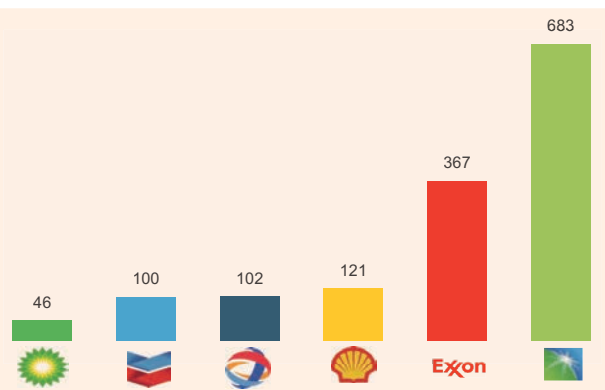
**Fig. 1** Saudi Aramco filed and granted patent numbers (2015-2020).



**Fig. 3** Saudi Aramco's 2020 U.S. granted patents by technology domain.



**Fig. 2** A comparison of the U.S. granted patents in 2020 between the leading international oil companies.



## 2020 Granted Patents

### Polymer Blended Membranes for Sour Gas Separation

*Granted Patent: U.S. Patent 10,525,406,  
Grant Date: January 7, 2020*  
Junyan Yang

### Processing Systems for Produced Water and Methods for Recovering Organic Compounds from the Produced Water

*Granted Patent: U.S. Patent 10,525,415,  
Grant Date: January 7, 2020*  
Regis Vilagines and Guillaume Raynel

### Gellable, Non-Aqueous Oil Well Treatment Fluids Comprising Elastomeric Maleic Anhydride Copolymers

*Granted Patent: U.S. Patent 10,526,458,  
Grant Date: January 7, 2020*  
B. Raghava Reddy and Matthew G. Hilfiger

### Anti-Bit Balling Drilling Fluids, and Methods of Making and Use Thereof

*Granted Patent: U.S. Patent 10,526,520,  
Grant Date: January 7, 2020*  
Abdullah S. Al-Yami, Ahmed A. Bahamdan, Saleh A. Haidary, Vikrant B. Wagle, Hussain Al-Bahrani, Ali M. Al-Safran, Nasser Al-Hareth and Abdulla H. Awadh

### Invert Emulsion Drilling Fluids with Fatty Acid and Fatty Diol Rheology Modifiers

*Granted Patent: U.S. Patent 10,526,521,  
Grant Date: January 7, 2020*  
Vikrant B. Wagle and Abdullah S. Al-Yami

### Cement Having Cross-Linked Polymers

*Granted Patent: U.S. Patent 10,526,522,  
Grant Date: January 7, 2020*  
Elizabeth Q. Contreras

### Settable, Form-Filling Loss Circulation Control Compositions Comprising In Situ Foamed Non-Hydraulic Sorel Cement Systems and Method of Use

*Granted Patent: U.S. Patent 10,526,524,  
Grant Date: January 7, 2020*  
B. Raghava Reddy

### Systems and Methods for Cracking Hydrocarbon Streams Utilizing Cracking Catalysts

*Granted Patent: U.S. Patent 10,526,546,  
Grant Date: January 7, 2020*  
Anas Aqeeli and Aaron Akah

### Upgrading of Heavy Oil for Steam Cracking Process

*Granted Patent: U.S. Patent 10,526,552,  
Grant Date: January 7, 2020*  
Ki-Hyouk Choi, Bander M. Alotaibi, Mazin M. Fathi and Muneef F. Alqarzouh

### Characterizing Crude Oil Using Laser Induced Ultraviolet Fluorescence Spectroscopy

*Granted Patent: U.S. Patent 10,527,546,  
Grant Date: January 7, 2020*  
Omer R. Koseoglu, Adnan Al-Hajji and Ezzat M. Hegazi

### Dual Catalyst System for Propylene Production

*Granted Patent: U.S. Patent 10,532,347,  
Grant Date: January 14, 2020*  
Sohel Shaikh, Sulaiman S. Al-Khattaf, Arudra Palani, Tazul I. Bhuiyan, Mohammad N. Akhtar, Abdullah M. Aitani and Mohammed A. Al-Yami

### Method for Traversing Surface with Magnetic Omni-Wheel

*Granted Patent: U.S. Patent 10,532,609,  
Grant Date: January 14, 2020*  
Ali Outa, Brian J. Parrott, Pablo Carrasco Zanini, Fadl H. Abdel Latif and Hassane A. Trigui

### Modular Thru-Tubing Subsurface Completion Unit

*Granted Patent: U.S. Patent 10,533,393,  
Grant Date: January 14, 2020*  
Muhammad Arsalan and Mohamed N. Noui-Mehidi

### Centrifugal Pump with Adaptive Pump Stages

*Granted Patent: U.S. Patent 10,533,558,  
Grant Date: January 14, 2020*  
Rafael A. Lastra and Chidirim E. Ejim

### Nuclear Magnetic Resonance Gas Isotherm Technique to Evaluate Reservoir Rock Wettability

*Granted Patent: U.S. Patent 10,533,933,  
Grant Date: January 14, 2020*  
Hyung T. Kwak and Ahmad M. Al Harbi

### Cloud-Based Machine Learning System and Data Fusion for the Prediction and Detection of Corrosion under Insulation

*Granted Patent: U.S. Patent 10,533,957,  
Grant Date: January 14, 2020*  
Ayman Amer, Ali Al Shehri, Ser Nam Lim, Mustafa Uzunbas, Ahmad Aldabbagh, Muhammad Ababtain and Vincent Cunningham

### Systems and Methods for Mapping Hydrocarbon Reservoirs Using Electromagnetic Transmissions

*Granted Patent: U.S. Patent 10,534,103,  
Grant Date: January 14, 2020*  
Howard K. Schmidt, Jesus M. Felix-Servin and Erika S. Ellis

### Method and Apparatus for Promoting Droplets Coalescence in Oil Continuous Emulsions

*Granted Patent: U.S. Patent 10,537,850,  
Grant Date: January 21, 2020*  
Abderrazak Traidia, Sebastien A. Duval, Simone Less and Regis Vilagines

### Protection System for Sulfur Storage Apparatus

*Granted Patent: U.S. Patent 10,538,383,  
Grant Date: January 21, 2020*  
Mohammed Al-Mehthel, Saleh Al-Idi, Mohammed Maslehuddin, Mohammed Shameem and Mohammed Ibrahim

### Butyl Ionomer Blends

*Granted Patent: U.S. Patent 10,538,650,  
Grant Date: January 21, 2020*  
Dana K. Adkinson and Jon Bielby

### Development of Anti-Bit Balling Fluids

*Granted Patent: U.S. Patent 10,538,692,  
Grant Date: January 21, 2020*  
Abdullah S. Al-Yami, Ahmed A. Bahamdan, Saleh A. Haidary, Vikrant B. Wagle, Hussain Al-Bahrani, Ali M. Al-Safran, Nasser Al-Hareth and Abdulla H. Awadh

### Stabilization of Petroleum Surfactants for Enhancing Oil Recovery

*Granted Patent: U.S. Patent 10,538,693,  
Grant Date: January 21, 2020*  
Yun Chang

### Determining a Mud Weight of Drilling Fluids for Drilling through Naturally Fractured Formations

*Granted Patent: U.S. Patent 10,539,014,  
Grant Date: January 21, 2020*  
Younane Abouseiman, Yanhui Han, Chao Liu and Shawn Rimassa

### High-Pressure/High Temperature Dynamic Multiphase Corrosion Erosion Simulator

*Granted Patent: U.S. Patent 10,539,498,  
Grant Date: January 21, 2020*  
Turki A. Al-Khaldi and Yahya T. Al-Janabi

### Systems and Methods for Mapping Hydrocarbon Reservoirs Using Electromagnetic Transmissions

*Granted Patent: U.S. Patent 10,539,704,  
Grant Date: January 21, 2020*  
Howard K. Schmidt, Jesus M. Felix-Servin and Erika S. Ellis

### Supercritical Reactor Systems and Processes for Petroleum Upgrading

*Granted Patent: U.S. Patent 10,543,468,  
Grant Date: January 28, 2020*  
Ki-Hyouk Choi, Abdullah T. Al-Abdullah and Mohammed A. Al-Abdullah

### Systems and Methods for Configuring Field Devices Using a Configuration Device

*Granted Patent: U.S. Patent 10,543,594,  
Grant Date: January 28, 2020*  
Brian J. Parrott and Pablo Carrasco Zanini

### Functionalized Copolymer Rubber Containing Nitrile Groups

*Granted Patent: U.S. Patent 10,544,234,  
Grant Date: January 28, 2020*  
Susanna Lieber, Karola Schneiders, Christoph Kins and Werner Obrecht

### Methods and Systems for Neutralizing Hydrogen Sulfide during Drilling

*Granted Patent: U.S. Patent 10,544,344,  
Grant Date: January 28, 2020*  
Ossama Sehsah and Ihab Elhabrouk

### Flaky Date Fruit CAP for Moderate to Severe Loss Control

*Granted Patent: U.S. Patent 10,544,345,  
Grant Date: January 28, 2020*  
Md Amanullah

### Fracturing Fluids Comprising Alkanolamine Borates as Crosslinkers for Polysaccharides

*Granted Patent: U.S. Patent 10,544,347,  
Grant Date: January 28, 2020*  
B. Raghava Reddy, Feng Liang and Leiming Li

### Systems and Methods for Sealing a Wellbore

*Granted Patent: U.S. Patent 10,544,648,  
Grant Date: January 28, 2020*  
Victor Costa de Oliveira, Ramon Rodriguez  
and Khaled Abouelnaaj

### Multiphase Flow Meter with Tuning Fork

*Granted Patent: U.S. Patent 10,544,674,  
Grant Date: January 28, 2020*  
Brett W. Bouldin, Robert Turner, Frode  
Hveding and Mohamed N. Noui-Mehidi

### Spectacle Blinds Swinging Device

*Granted Patent: U.S. Patent 10,544,867,  
Grant Date: January 28, 2020*  
Bandar B. Al-Harbi and Fahad A. Al-Harhi

### Flow Line Insert with Indentations

*Granted Patent: U.S. Patent 10,545,057,  
Grant Date: January 28, 2020*  
Lahdan F. Al-Faihan

### Estimating Formation Properties Using Saturation Profiles

*Granted Patent: U.S. Patent 10,545,105,  
Grant Date: January 28, 2020*  
Jun Gao, Hyung T. Kwak and Ahmad M.  
Al Harbi

### Distributed Agent to Collect Input and Output Data along with Source Code for Scientific Kernels of Single-Process and Distributed Systems

*Granted Patent: U.S. Patent 10,545,740,  
Grant Date: January 28, 2020*  
Mazen A. Al-Hagri

### Multiple Stage Catalyst System for Self-Metathesis with Controlled Isomerization and Cracking

*Granted Patent: U.S. Patent 10,550,048,  
Grant Date: February 4, 2020*  
Noor A. Sulais, Faisal H. Alshafei, Munir  
D. Khokhar, Mohammed R. Alalouni and  
Sohel Shaikh

### Acryloyl-Based Copolymers, Terpolymers, and Use as Hydrate Inhibitors

*Granted Patent: U.S. Patent 10,550,215,  
Grant Date: February 4, 2020*  
Khalid Majnouni, Abdullah R. Al-Malki,  
Mohamed S. Elanany, Manal Al-Eid,  
Mohammed Al-Daous and Shaikh A. Ali

### Sulfur Asphalt in Roofing, Damp-Proofing and Water Proofing

*Granted Patent: U.S. Patent 10,550,267,  
Grant Date: February 4, 2020*  
Mohammed H. Al-Mehthel, Saleh H. Al-  
Idif, Ibnelwaleed A. Hussein and Hamad I.  
Al-Abdulwahhab

### Encapsulated Nanocompositions for Increasing Hydrocarbon Recovery

*Granted Patent: U.S. Patent 10,550,510,  
Grant Date: February 4, 2020*  
Yun Chang

### Encapsulated Nanocompositions for Increasing Hydrocarbon Recovery

*Granted Patent: U.S. Patent 10,550,511,  
Grant Date: February 4, 2020*  
Yun Chang

### Oil Recovery Process Using an Oil Recovery Composition of Aqueous Salt Solution and Dilute Polymer for Carbonate Reservoirs

*Granted Patent: U.S. Patent 10,550,512,  
Grant Date: February 4, 2020*  
Subhash C. Ayirala, Abdulkareem M. Al-  
Sofi and Ali A. Yousef

### High Temperature Fracturing Fluids with Nanoparticles

*Granted Patent: U.S. Patent 10,550,514,  
Grant Date: February 4, 2020*  
Feng Liang, Ghaithan A. Al-Muntasheri  
and Leiming Li

### Downhole Chemical Injection Method and System for Use in ESP Applications

*Granted Patent: U.S. Patent 10,550,678,  
Grant Date: February 4, 2020*  
Jinjiang Xiao and Hattan Banjar

### Supercritical CO<sub>2</sub> Cycle Coupled to Chemical Looping Arrangement

*Granted Patent: U.S. Patent 10,550,753,  
Grant Date: February 4, 2020*  
Mourad Younes, Aadesh Harale and Aqil  
Jamal

### Integrated Ultrasonic Testing and Cathodic Protection Measurement Probe

*Granted Patent: U.S. Patent 10,551,296,  
Grant Date: February 4, 2020*  
Hassane A. Trigui, Sahejad Patel, Ali Outa,  
Ayman Amer, Fadl H. Abdel Latif, Ameen  
Obedan and Hamad Al-Saiari

### Thermography Image Processing with Neural Networks to Identify Corrosion under Insulation (CUI)

*Granted Patent: U.S. Patent 10,551,297,  
Grant Date: February 4, 2020*  
Ayman Amer, Ali Alshehri, Brian J. Parrott  
and Muhammad Sarraj

### Geochemical Water Analysis Element Concentration Prediction for Oil Field Waters

*Granted Patent: U.S. Patent 10,551,567,  
Grant Date: February 4, 2020*  
Ibrahim El-Zefzafy and Mohammed H.  
Al-Hanabi

### Apparatus and Methods of Evaluating Rock Properties while Drilling Using Acoustic Sensors Installed in the Drilling Fluid Circulation System of a Drilling Rig

*Granted Patent: U.S. Patent 10,551,516,  
Grant Date: February 4, 2020*  
Yunlai Yang

### Wellbore Non-Retrieval Sensing System

*Granted Patent: U.S. Patent 10,551,800,  
Grant Date: February 4, 2020*  
Bodong Li, Chinthaka P. Gooneratne and  
Shaohua Zhou

### Capillary Pressure Analysis for Petrophysical Statistical Modeling

*Granted Patent: U.S. Patent 10,552,553,  
Grant Date: February 4, 2020*  
David Forsyth, Yusuf Pamukcu and Nasr-  
Eddine Hammou

### Integrated PCS Functional Competency Assessment

*Granted Patent: U.S. Patent 10,554,625,  
Grant Date: February 4, 2020*  
Fouad M. Al-Khabbaz

### System for Tail Gas Treatment of Sulfur Recovery Units

*Granted Patent: U.S. Patent 10,556,805,  
Grant Date: February 11, 2020*  
Mourad Younes, Maytham Musawi and  
Aadesh Harale

### Cement Slurries, Cured Cement and Methods of Making and Use of These

*Granted Patent: U.S. Patent 10,556,829,  
Grant Date: February 11, 2020*  
B. Raghava Reddy

### Diluent for the Production of Butyl Rubber

*Granted Patent: U.S. Patent 10,556,977,  
Grant Date: February 11, 2020*  
Steven J. Teertstra and Gilles Arsenault

### Nanosilica Dispersion Well Treatment Fluid

*Granted Patent: U.S. Patent 10,557,071,  
Grant Date: February 11, 2020*  
Vikrant B. Wagle and Abdullah S. Al-Yami

### Loss Circulation Compositions (LCM) Having Portland Cement Clinker

*Granted Patent: U.S. Patent 10,557,076,  
Grant Date: February 11, 2020*  
B. Raghava Reddy

### Systems and Methods for Pipe Concentricity, Zonal Isolation, and Stuck Pipe Prevention

*Granted Patent: U.S. Patent 10,557,317,  
Grant Date: February 11, 2020*  
Abdulaziz S. Al-Qasim and Ahmed Y.  
Bukhamseen

### Systems and Methods for Stuck Pipe Mitigation

*Granted Patent: U.S. Patent 10,557,326,  
Grant Date: February 11, 2020*  
Abdulaziz S. Al-Qasim, Raed A. Alouhali  
and Sunil L. Kokal

### Interchangeable Wellbore Cleaning Modules

*Granted Patent: U.S. Patent 10,557,350,  
Grant Date: February 11, 2020*  
Victor Costa de Oliveira, Mario Rivas,  
Khaled Abouelnaaj and Ossama Sehsah.

### Estimating Measures of Formation Flow Capacity and Phase Mobility from Pressure Transient Data under Segregated Oil and Water Flow Conditions

*Granted Patent: U.S. Patent 10,557,333,  
Grant Date: February 11, 2020*  
Hasan A. Nooruddin and Noor M. Anisur  
Rahman

### Flow Meter Well Tool

*Granted Patent: U.S. Patent 10,557,334,  
Grant Date: February 11, 2020*  
Rafael A. Lastra



### Downhole Centrifugal Separation and Removal of Sand from Wells Using Progressing Cavity Pump

*Granted Patent: U.S. Patent 10,557,537,  
Grant Date: February 11, 2020*  
Muhammad Ayub and Rafael A. Lastra Melo

### Systems and Methods to Predict and Inhibit Broken-Out Drilling-Induced Fractures in Hydrocarbon Wells

*Granted Patent: U.S. Patent 10,557,545,  
Grant Date: February 11, 2020*  
Mohammed S. Ameen

### Locally Actuated Partial Stroke Testing System

*Granted Patent: U.S. Patent 10,557,564,  
Grant Date: February 11, 2020*  
Fawaz A. Al-Sahan

### Flexible Strap Antenna Arrays for Tank Volume Calibration and Resonance Frequency Shift Measuring Methods Using Same

*Granted Patent: U.S. Patent 10,557,698,  
Grant Date: February 11, 2020*  
Brian J. Parrott, Ali Alshehri and Ayman Amer

### Alternating Magnetic Field Flow Meters with Embedded Quality Assurance and Control

*Granted Patent: U.S. Patent 10,557,750,  
Grant Date: February 11, 2020*  
Fouad M. Alkhabbaz and Maatoug Al-Maatoug

### Modeling Angle Domain Common Image Gathers from Reverse Time Migration

*Granted Patent: U.S. Patent 10,557,954,  
Grant Date: February 11, 2020*  
Thierry-Laurent D. Tonellot and Vincent Etienne

### Logging Tool with Electric Dipole Source and Magnetic Sensor for Forward and Lateral Imaging

*Granted Patent: U.S. Patent 10,557,961,  
Grant Date: February 11, 2020*  
Teruhiko Hagiwara

### Method for Measurement of Hydrocarbon Content of Tight Gas Reservoirs

*Granted Patent: U.S. Patent 10,557,962,  
Grant Date: February 11, 2020*  
Jin-Hong Chen, Stacey M. Althaus, Daniel T. Georgi and Hui-Hai Liu

### Directional Sensitive Fiber Optic Cable Wellbore System

*Granted Patent: U.S. Patent 10,558,105,  
Grant Date: February 11, 2020*  
Damian P. San-Roman-Alerigi and Frode Hveding

### Role-Based Locking System for Plants Unattended Premises

*Granted Patent: U.S. Patent 10,559,146,  
Grant Date: February 11, 2020*  
Fouad M. Alkhabbaz, Hussain Al-Salem, Zakarya A. Abu Al Saud and Nabil Ouchn

### High Temperature Downhole Power Generating Device

*Granted Patent: U.S. Patent 10,560,058,  
Grant Date: February 11, 2020*  
Chinthaka P. Gooneratne, Bodong Li and Shaohua Zhou

### Harvesting Energy from Fluid Flow

*Granted Patent: U.S. Patent 10,560,059,  
Grant Date: February 11, 2020*  
Talha J. Ahmad, Muhammad Arsalan, Michael J. Black and Mohamed N. Noui-Mehidi

### Harvesting Energy from Fluid Flow

*Granted Patent: U.S. Patent 10,560,040,  
Grant Date: February 11, 2020*  
Talha J. Ahmad, Muhammad Arsalan, Michael J. Black and Mohamed N. Noui-Mehidi

### Methods of Using Drilling Fluid Compositions with Enhanced Rheology

*Granted Patent: U.S. Patent 10,563,110,  
Grant Date: February 18, 2020*  
Hussain Al-Bahrani, Abdullah S. Al-Yami, Ali M. Al-Safran and Abdulaziz Alhelal

### Removal of Barite Weighted Mud

*Granted Patent: U.S. Patent 10,563,113,  
Grant Date: February 18, 2020*  
Mubarak A. Al-Dhufairi and Saif A. Al-Thabi

### Methods for Producing Seawater-Based, High Temperature Viscoelastic Surfactant Fluids with Low Scaling Tendency

*Granted Patent: U.S. Patent 10,563,119,  
Grant Date: February 18, 2020*  
Leiming Li, Feng Liang and Tao Chen

### Method for Optimizing Catalyst Loading for Hydrocracking Process

*Granted Patent: U.S. Patent 10,563,158,  
Grant Date: February 18, 2020*  
Omer R. Koseoglu, Adnan Al-Hajji, Hendrik Muller, Masaru Ushio and Koji Nakano

### Conversion of Crude Oil to Petrochemicals

*Granted Patent: U.S. Patent 10,563,141,  
Grant Date: February 18, 2020*  
Lianhui Ding, Essam Sayed, Duhaiman U. Al-Yami, Abdennour Bourane, Alberto L. Ballesteros and Ibrahim A. Abba

### Collecting Drilling Microchips

*Granted Patent: U.S. Patent 10,563,469,  
Grant Date: February 18, 2020*  
Mohammad S. Al-Badran and Bodong Li

### Collecting Drilling Microchips

*Granted Patent: U.S. Patent 10,563,470,  
Grant Date: February 18, 2020*  
Mohammad S. Al-Badran and Bodong Li

### Sealing a Portion of a Wellbore

*Granted Patent: U.S. Patent 10,563,475,  
Grant Date: February 18, 2020*  
Shaohua Zhou

### Thru-Tubing Retrievable Subsurface Completion System

*Granted Patent: U.S. Patent 10,563,478,  
Grant Date: February 18, 2020*  
Muhammad Arsalan and Mohamed N. Noui-Mehidi

### Determining a Rock Formation Content

*Granted Patent: U.S. Patent 10,563,504,  
Grant Date: February 18, 2020*  
Anas Al-Marzoug

### Flow Distribution Device and Method

*Granted Patent: U.S. Patent 10,563,527,  
Grant Date: February 18, 2020*  
Farooq N. Al-Jwsem

### Rotary Contactor for Vehicle Carbon Dioxide Capture

*Granted Patent: U.S. Patent 10,563,555,  
Grant Date: February 18, 2020*  
Esam Z. Hamad

### Tool-Less Spring Attachment to C-Channel and Method of Using Same

*Granted Patent: U.S. Patent 10,563,686,  
Grant Date: February 18, 2020*  
Brian J. Parrott, Ali Shehri and Pablo Carrasco Zanini

### Analyzing Drilling Fluid Rheology at a Drilling Site

*Granted Patent: U.S. Patent 10,564,083,  
Grant Date: February 18, 2020*  
Hermann F. Spoerker

### Apparatus and Method for Nondestructively Inspecting Fiberglass and Nonmetallic Pipes

*Granted Patent: U.S. Patent 10,564,108,  
Grant Date: February 18, 2020*  
Ahmed S. Al-Omari

### Systems and Methods for Core Data Shifting

*Granted Patent: U.S. Patent 10,564,109,  
Grant Date: February 18, 2020*  
Marwah Al Ismail, Mokhles Mezghani and Abdullah Qasem

### Quantifying Organic and Inorganic Sulfur Components

*Granted Patent: U.S. Patent 10,564,142,  
Grant Date: February 18, 2020*  
Harry D. Oduru

### Processing Methodology for Full Waveform Sonic Wavefield Separation

*Granted Patent: U.S. Patent 10,564,304,  
Grant Date: February 18, 2020*  
Xuekai Sun, Christopher Ayadiuno and Carlos Planchart

### Membrane-Based Process for Butanols Production from Mixed Butenes

*Granted Patent: U.S. Patent 10,570,071,  
Grant Date: February 25, 2020*  
Marwah Al Ismail, Mokhles Mezghani and Abdullah Qasem

### Emulsifier Compositions for Invert Emulsion Fluids and Methods of Using the Same

*Granted Patent: U.S. Patent 10,570,524,  
Grant Date: February 25, 2020*

Vikrant B. Wagle and Abdullah S. Al-Yami

### Invert Emulsion Drilling Fluids with Fatty Acid and Fatty Amine Rheology Modifiers

*Granted Patent: U.S. Patent 10,570,526,  
Grant Date: February 25, 2020*

Vikrant B. Wagle and Abdullah S. Al-Yami

### Thru-Tubing Retrievable Intelligent Completion System

*Granted Patent: U.S. Patent 10,570,696,  
Grant Date: February 25, 2020*

Muhammad Arsalan and Mohamed N. Noui-Mehidi

### Insulating Fluid for Thermal Insulation

*Granted Patent: U.S. Patent 10,570,699,  
Grant Date: February 25, 2020*

Vikrant B. Wagle, Abdullah S. Al-Yami and Abdullah Awadh

### Parallel Processing of Invasion Percolation for Large-Scale, High-Resolution Simulation of Secondary Hydrocarbon Migration

*Granted Patent: U.S. Patent 10,570,706,  
Grant Date: February 25, 2020*

Suha N. Kayum and Larry S. Fung

### Protecting a Hydrocarbon Fluid Piping System

*Granted Patent: U.S. Patent 10,570,712,  
Grant Date: February 25, 2020*

Pedro A. Mujica and Herman Cipriano

### Controlling Hydrocarbon Production

*Granted Patent: U.S. Patent 10,570,716,  
Grant Date: February 25, 2020*

Huseyin O. Balan, Anuj Gupta, Ali Al-Khatib and Alberto F. Marsala

### Data Processing System for Mapping Fracture Length Using Downhole Ground Penetrating Radar

*Granted Patent: U.S. Patent 10,570,727,  
Grant Date: February 25, 2020*

Jesus M. Felix-Servin, Erika S. Ellis, Ersan Turkoglu and Howard K. Schmidt

### Methods and Systems for Determining Gas Permeability of a Subsurface Formation

*Granted Patent: U.S. Patent 10,571,584,  
Grant Date: February 25, 2020*

Hui-Hai Liu, Bitao Lai, Jilin J. Zhang, Daniel T. Georgi and Xinwo Huang

### Sensor for Monitoring for the Presence and Measurement of Aqueous Aldehyde Biocides

*Granted Patent: U.S. Patent 10,571,401,  
Grant Date: February 25, 2020*

Mohammed A. Al-Moniee, Naim Akmal and Peter F. Sanders

### Characterization of Crude Oil by High-Pressure Liquid Chromatography

*Granted Patent: U.S. Patent 10,571,452,  
Grant Date: February 25, 2020*

Omer R. Koseoglu, Adnan Al-Hajji and Saroj Kumar Panda

### False Image Removal in Reverse Time Migration

*Granted Patent: U.S. Patent 10,571,586,  
Grant Date: February 25, 2020*

Jiarui Yang, Tong W. Fei and Yi Luo

### Electrical Submersible Pump Monitoring and Failure Prediction

*Granted Patent: U.S. Patent 10,571,590,  
Grant Date: February 25, 2020*

Mohamed N. Noui-Mehidi and Ahmed Y. Bukhamseen

### Two-Dimensional Reservoir Pressure Estimation with Integrated Static Bottom-Hole Pressure Survey Data and Simulation Modeling

*Granted Patent: U.S. Patent 10,571,604,  
Grant Date: February 25, 2020*

Omar A. Al-Nahdi, Ali A. Al-Turki, Badr M. Al-Harbi and Sami A. Al-Nuaim

### Directional Sensitive Fiber Optic Cable Wellbore System

*Granted Patent: U.S. Patent 10,571,775,  
Grant Date: February 25, 2020*

Damian P. San-Roman-Alerigi and Frode Hveding

### Automated Safety KPI Enhancement

*Granted Patent: U.S. Patent 10,572,796,  
Grant Date: February 25, 2020*

Zakarya Abu Al Saud, Fouad Alkhabbaz, Soloman M. Almadi and Abduladhim H. Al-Abdullatif

### Harvesting Energy from Fluid Flow

*Granted Patent: U.S. Patent 10,574,157,  
Grant Date: February 25, 2020*

Talha J. Ahmad, Muhammad Arsalan, Michael J. Black and Mohamed N. Noui-Mehidi

### Harvesting Energy from Fluid Flow

*Granted Patent: U.S. Patent 10,574,158,  
Grant Date: February 25, 2020*

Talha J. Ahmad, Muhammad Arsalan, Michael J. Black and Mohamed N. Noui-Mehidi

### Synthesis of Sodium Formate and Drilling Fluid Comprising the Same

*Granted Patent: U.S. Patent 10,577,500,  
Grant Date: March 5, 2020*

Abdullah S. Al-Yami, Vikrant B. Wagle, Zainab Alsaihati, Ali Alsafran, Nasser Alhareth and Abdulaziz Alhelal

### Loss Circulation Material Composition Having an Acidic Nanoparticle-Based Dispersion and Polyamine

*Granted Patent: U.S. Patent 10,577,526,  
Grant Date: March 5, 2020*

Vikrant B. Wagle, Abdulaziz Alhelal, Abdullah S. Al-Yami and Zainab Alsaihati

### Waste Vegetable Oil-Based Emulsifier for Invert Emulsion Drilling Fluid

*Granted Patent: U.S. Patent 10,577,527,  
Grant Date: March 5, 2020*

Jothibasu Ramasamy, Md Amanullah and Mujtaba M. Al-Saihati

### Flash Point Adjustment of Wettability Alteration Chemicals in Hydrocarbon Solvents

*Granted Patent: U.S. Patent 10,577,528,  
Grant Date: March 5, 2020*

Mohammed Ali Ibrahim Sayed and Ghaithan A. Al-Muntasheri

### Systems and Processes for Deasphalting Oil

*Granted Patent: U.S. Patent 10,577,546,  
Grant Date: March 5, 2020*

Ki-Hyouk Choi, Mazin M. Fathi and Abdullah T. Alabdulhadi

### Apparatus for Mapping Fracture Length Using Downhole Ground Penetrating Radar

*Granted Patent: U.S. Patent 10,577,925,  
Grant Date: March 5, 2020*

Jesus M. Felix-Servin, Erika S. Ellis, Ersan Turkoglu and Howard K. Schmidt

### Detecting Subterranean Structures

*Granted Patent: U.S. Patent 10,577,926,  
Grant Date: March 5, 2020*

Andrey Bakulin, Pavel Golikov and Ilya Silvestrov

### Modified Goswami Cycle-Based Conversion of Gas Processing Plant Waste Heat into Power and Cooling

*Granted Patent: U.S. Patent 10,577,981,  
Grant Date: March 5, 2020*

Mahmoud B. Noureldin and Akram H. Kamel

### Wellbore Debris Handler for Electric Submersible Pumps

*Granted Patent: U.S. Patent 10,578,111,  
Grant Date: March 5, 2020*

Jinjiang Xiao, Chidirim E. Ejim and Randall A. Shepler

### Decontaminating Rock Samples by Thermovaporization

*Granted Patent: U.S. Patent 10,578,600,  
Grant Date: March 5, 2020*

Sedat Inan

### Secure Enterprise Emergency Notification and Managed Crisis Communications

*Granted Patent: U.S. Patent 10,580,285,  
Grant Date: March 5, 2020*

Rashed Al-Yami

### Dual Catalyst System for Propylene Production

*Granted Patent: U.S. Patent 10,583,425,  
Grant Date: March 10, 2020*

Sohel Shaikh, Sulaiman S. Al-Khattaf, Arudra Palani, Tazul I. Bhuiyan, Mohammad N. Akhtar, Abdullah M. Aitani and Mohammed A. Al-Yami

### Ultra-Pure Rubber

*Granted Patent: U.S. Patent 10,584,195,  
Grant Date: March 10, 2020*

David Thompson

### Pulverulent Mixtures Containing Low Emission Nitrile Rubbers

*Granted Patent: U.S. Patent 10,584,226,  
Grant Date: March 10, 2020*

Andreas Kaiser, Sven Brandau and Robert Staber

### In Situ Generation of Glass-Like Materials Inside Subterranean Formation

Granted Patent: U.S. Patent 10,584,274,  
Grant Date: March 10, 2020

Mohammed A. Bataweel, Prasad B. Karadkar, Ayman Al-Mohsen and Haitham A. Othman

### Process to Produce Blown Asphalt

Granted Patent: U.S. Patent 10,584,285,  
Grant Date: March 10, 2020

Mazin M. Fathi and Ki-Hyouk Choi

### Subsurface Hanger for Umbilical Deployed Electrical Submersible Pump

Granted Patent: U.S. Patent 10,584,545,  
Grant Date: March 10, 2020

Rafael A. Lastra

### Oil Swellable, Surface Treated Elastomeric Polymer and Methods of Using the Same for Controlling Losses of Non-Aqueous Wellbore Treatment Fluids to the Subterranean Formation

Granted Patent: U.S. Patent 10,584,547,  
Grant Date: March 10, 2020

B. Raghava Reddy

### Oil Swellable, Surface Treated Elastomeric Polymer and Methods of Using the Same for Controlling Losses of Non-Aqueous Wellbore Treatment Fluids to the Subterranean Formation

Granted Patent: U.S. Patent 10,584,548,  
Grant Date: March 10, 2020

B. Raghava Reddy

### Thru-Tubing Subsurface Completion Unit Employing Detachable Anchoring Seals

Granted Patent: U.S. Patent 10,584,556,  
Grant Date: March 10, 2020

Muhammad Arsalan and Mohamed N. Noui-Mehidi

### In Situ Reservoir Depletion Management-Based on Surface Characteristics of Production

Granted Patent: U.S. Patent 10,584,577,  
Grant Date: March 10, 2020

Meftah Tiss, Amjad Ashri, Abdullah Al-Utaibi, Abdulrahman Al-Nutaifi and Bestman Somairi

### Equal Walled Gerotor Pump for Wellbore Applications

Granted Patent: U.S. Patent 10,584,702,  
Grant Date: March 10, 2020

Rafael A. Lastra and Jinjiang Xiao

### Processing Methodology for Full Waveform Sonic Wavefield Separation

Granted Patent: U.S. Patent 10,585,200,  
Grant Date: March 10, 2020

Xuekai Sun, Christopher Ayadiuno and Carlos Planchart

### Additives for Gas Phase Oxidatives Desulfurization Catalysts

Granted Patent: U.S. Patent 10,589,259,  
Grant Date: March 17, 2020

Omer R. Koseoglu, Yaming Jin, Zinifer Ismagilov, Svetlana Yashnik, Mikhail Kerzhentsev and Valentin Parmon

### Underwater Pipeline Inspection Crawler

Granted Patent: U.S. Patent 10,589,452,  
Grant Date: March 17, 2020

Fadl H. Abdel Latif, Ali Outa, Ammar Al-Nahwi and Ihsan Al-Taie

### Underwater Pipeline Inspection Crawler

Granted Patent: U.S. Patent 10,589,453,  
Grant Date: March 17, 2020

Fadl H. Abdel Latif, Ali Outa, Ammar Al-Nahwi and Ihsan Al-Taie

### Spacer Fluid Compositions that Include Surfactants

Granted Patent: U.S. Patent 10,590,525,  
Grant Date: March 17, 2020

Hussain Al-Bahrani, Abdullah S. Al-Yami and Vikrant B. Wagle

### Storable Gas Generating Compositions

Granted Patent: U.S. Patent 10,590,526,  
Grant Date: March 17, 2020

B. Raghava Reddy

### Removal of Barite Weighted Mud

Granted Patent: U.S. Patent 10,590,528,  
Grant Date: March 17, 2020

Mubarak A. Al-Dhufairi and Saif A. Al-Thabit

### Oil Recovery Process Using an Oil Recovery Composition of Aqueous Salt Solution and Dilute Polymer for Carbonate Reservoirs

Granted Patent: U.S. Patent 10,590,529,  
Grant Date: March 17, 2020

Subhash C. Ayirala, Abdulkareem M. Al-Sofi and Ali A. Yousef

### Oil Recovery Process Using an Oil Recovery Composition of Aqueous Salt Solution and Dilute Polymer for Carbonate Reservoirs

Granted Patent: U.S. Patent 10,590,530,  
Grant Date: March 17, 2020

Subhash C. Ayirala, Abdulkareem M. Al-Sofi and Ali A. Yousef

### Automated Preventive and Predictive Maintenance of Downhole Valves

Granted Patent: U.S. Patent 10,590,752,  
Grant Date: March 17, 2020

Al-Waleed A. Al-Gouhi, Soliman Almadi and Obiomalotao L. Isichei

### Methods for Analyzing Natural Gas Flow in Subterranean Reservoirs

Granted Patent: U.S. Patent 10,591,599,  
Grant Date: March 17, 2020

Hui-Hai Liu, Bitao Lai, Jin-Hong Chen and Daniel T. Georgy

### Emu Impulse Antenna

Granted Patent: U.S. Patent 10,591,626,  
Grant Date: March 17, 2020

Howard K. Schmidt, Jesus M. Felix-Servin, Erika S. Ellis, Mazen Kanj and Abdullah Al Shehri

### Wellbore Non-Retrieval Sensing System

Granted Patent: U.S. Patent 10,591,874,  
Grant Date: March 17, 2020

Bodong Li, Chinthaka P. Gooneratne and Shaohua Zhou

### Cored Rock Analysis Planning through CT Images

Granted Patent: U.S. Patent 10,593,107,  
Grant Date: March 17, 2020

Sinan Caliskan and Abdullah Shebatalhamd

### Systems and Methods Comprising Smart Auto Cleaning Pipe Screen for Drilling Operations

Granted Patent: U.S. Patent 10,596,496,  
Grant Date: March 24, 2020

Ossama Sehsah, Victor Costa de Oliveira and Mario Rivas

### Catalyst to Attain Low Sulfur Gasoline

Granted Patent: U.S. Patent 10,596,555,  
Grant Date: March 24, 2020

Ki-Hyouk Choi, Sameer A. Al-Ghamdi, Ali H. Al-Shareef and Ali H. Al-Hamadah

### Enriched Acid Gas for Sulfur Recovery

Granted Patent: U.S. Patent 10,597,297,  
Grant Date: March 24, 2020

Nasser A. Al-Qahtani

### Coupling Photovoltaic, Concentrated Solar Power, and Wind Technologies for Desalination

Granted Patent: U.S. Patent 10,597,509,  
Grant Date: March 24, 2020

Yazeed S. Alshahrani

### Chlorination Assisted Coagulation Processes for Water Purification

Granted Patent: U.S. Patent 10,597,515,  
Grant Date: March 24, 2020

Guillaume Raynel and Regis Vilagines

### Cross-Linking Agents Containing Isocyanate Groups for Nitrile Rubbers

Granted Patent: U.S. Patent 10,597,467,  
Grant Date: March 24, 2020

Sven Brandau, Michael Klimpel and Hans Magg

### Loss Circulation Material for Seepage to Moderate Loss Control

Granted Patent: U.S. Patent 10,597,572,  
Grant Date: March 24, 2020

Jothibasu Ramasamy and Md Amanullah

### Date Tree Trunk-Based Superfine Fibrous Materials for Seepage Loss Control

Granted Patent: U.S. Patent 10,597,575,  
Grant Date: March 24, 2020

Md Amanullah and Jothibasu Ramasamy

### Drilling with a Whipstock System

Granted Patent: U.S. Patent 10,597,962,  
Grant Date: March 24, 2020

Ossama Sehsah, Victor Costa de Oliveira and Mario Rivas

### Systems and Methods for Operating Downhole Inflow Control Valves

Granted Patent: U.S. Patent 10,597,988,  
Grant Date: March 24, 2020

Mohammed D. Al-Ajmi and Nasser M. Al-Hajri

### Heat Exchanger Configuration for Adsorption-Based Onboard Octane On-Demand and Cetane On-Demand

*Granted Patent: U.S. Patent 10,598,100, Grant Date: March 24, 2020*

Eman Tora, Amer A. Amer, Junseok Chang and Esam Z. Hamad

### Measuring Source Rock Potential Using Terahertz Analysis

*Granted Patent: U.S. Patent 10,598,814, Grant Date: March 24, 2020*

Sebastian Csutak

### Cogen-mom Integration Using Tabulated Information Recognition

*Granted Patent: U.S. Patent 10,602,099, Grant Date: March 24, 2020*

Hussain Al-Salem, Fouad Alkhabbaz and Srinidhi Mallur

### Nano-Sized Zeolite Supported Catalysts and Methods for Their Production

*Granted Patent: U.S. Patent 10,605,657, Grant Date: March 31, 2020*

Lianhui Ding, Essam Sayed, Manal Al-Eid and Hanaa Habboubi

### Method and Apparatus for Smart Electromagnetic Screen System for Use in Drilling Operations

*Granted Patent: U.S. Patent 10,605,607, Grant Date: March 31, 2020*

Ossama Sehsah, Victor Costa de Oliveira and Mario Rivas

### Reversible Amino Gel Compositions, Methods, and Use

*Granted Patent: U.S. Patent 10,604,691, Grant Date: March 31, 2020*

Peter J. Boul, B. Raghava Reddy, Matthew G. Hilfiger and Carl J. Thaemlitz

### Activating a Well System Tool

*Granted Patent: U.S. Patent 10,605,054, Grant Date: March 31, 2020*

Michael Affleck

### System and Method for Isolating a Wellbore Zone for Rigless Hydraulic Fracturing

*Granted Patent: U.S. Patent 10,605,041, Grant Date: March 31, 2020*

Mohamed N. Noui-Mehidi

### Multi-Vector Engineering Methods and Apparatus for Isolated Process Control Systems

*Granted Patent: U.S. Patent 10,606,249, Grant Date: March 31, 2020*

Fouad M. Al-Khabbaz and Osama Bahwal

### Evaluating Well Stimulation to Increase Hydrocarbon Production

*Granted Patent: U.S. Patent 10,606,967, Grant Date: March 31, 2020*

Karam S. Yateem, Mubarak Dhufairi, Saleh Ghamdi and Ramy Ahmed

### Subsurface Reservoir Model with 3D Natural Fractures Prediction

*Granted Patent: U.S. Patent 10,607,045, Grant Date: March 31, 2020*

Otto E. Meza Camargo, Tariq Mahmood and Khalid Hawas

### Adjusting a Fuel On-Board a Vehicle

*Granted Patent: U.S. Patent 10,611,258, Grant Date: April 7, 2020*

Esam Z. Hamad and Abdullah S. Alramadan

### Heteroatom Containing Modified Diene Polymers

*Granted Patent: U.S. Patent 10,611,855, Grant Date: April 7, 2020*

Heike Kloppenburg and Thomas Ruenzi

### Anti-Agglomerants for the Rubber Industry

*Granted Patent: U.S. Patent 10,611,886, Grant Date: April 7, 2020*

David Thompson and Clinton Lund

### Functionalized Nanosilica as Shale Inhibitor in Water-Based Fluids

*Granted Patent: U.S. Patent 10,611,942, Grant Date: April 7, 2020*

Peter J. Boul, Carl J. Thaemlitz and B. Raghava Reddy

### Acid-Soluble Plug Forming Rapidly Dehydrating Loss Control Slurry

*Granted Patent: U.S. Patent 10,611,945, Grant Date: April 7, 2020*

Md Amanullah

### Acid-Soluble Plug Forming Rapidly Dehydrating Loss Control Slurry

*Granted Patent: U.S. Patent 10,611,944, Grant Date: April 7, 2020*

Md Amanullah

### Acid-Soluble Plug Forming Rapidly Dehydrating Loss Control Slurry

*Granted Patent: U.S. Patent 10,611,945, Grant Date: April 7, 2020*

Md Amanullah

### Acid-Soluble Plug Forming Rapidly Dehydrating Loss Control Slurry

*Granted Patent: U.S. Patent 10,611,946, Grant Date: April 7, 2020*

Md Amanullah

### Pyrolysis to Determine Hydrocarbon Expulsion Efficiency of Hydrocarbon Source Rock

*Granted Patent: U.S. Patent 10,611,967, Grant Date: April 7, 2020*

Sedat Inan

### Smart Skidding System for Land Operations

*Granted Patent: U.S. Patent 10,612,515, Grant Date: April 7, 2020*

Ibrahim Ghamdi, Ossama Sehsah and Mahmoud Alqurashi

### Stimulating U-Shape Wellbores

*Granted Patent: U.S. Patent 10,612,555, Grant Date: April 7, 2020*

Khalid M. Alruwaili and Mohamed N. Noui-Mehidi

### Ring Assembly for Measurement while Drilling, Logging while Drilling and Well Intervention

*Granted Patent: U.S. Patent 10,612,560, Grant Date: April 7, 2020*

Abdulaziz S. Al-Qasim and Alberto F. Marsala

### Coiled Tubing Multifunctional Quad-Axial Visual Monitoring and Recording

*Granted Patent: U.S. Patent 10,612,562, Grant Date: April 7, 2020*

Mohammed Alshehri and Ossama Sehsah

### Detecting Landing of a Tubular Hanger

*Granted Patent: U.S. Patent 10,612,566, Grant Date: April 7, 2020*

Monty Gilleland and Michael Affleck

### Open Smart Completion

*Granted Patent: U.S. Patent 10,612,570, Grant Date: April 7, 2020*

Brett W. Bouldin, Rob Turner and Jonathan Brown

### Internal Combustion Engines Which Utilize Multiple Fuels and Methods for the Operation of Such

*Granted Patent: U.S. Patent 10,612,476, Grant Date: April 7, 2020*

Yoann Viollet, Kai J. Morganti and Robert A. Head

### Water Injection to Increase Hydrogen Production by On-Board Reforming of Fuel for Automotive Internal Combustion Engines

*Granted Patent: U.S. Patent 10,612,497, Grant Date: April 7, 2020*

Alexander K. Voice and Vincent S. Costanzo

### Determining Structural Tomographic Properties of a Geologic Formation

*Granted Patent: U.S. Patent 10,612,968, Grant Date: April 7, 2020*

Howard K. Schmidt, Jesus M. Felix-Servin, Frode Hveding and Daniele Colombo

### Determining Structural Tomographic Properties of a Geologic Formation

*Granted Patent: U.S. Patent 10,612,969, Grant Date: April 7, 2020*

Howard K. Schmidt, Jesus M. Felix-Servin, Frode Hveding and Daniele Colombo

### Electrophoresis Analysis to Identify Tracers in Produced Water at a Wellhead

*Granted Patent: U.S. Patent 10,615,055, Grant Date: April 7, 2020*

Al-Waleed A. Al-Gouhi and Mohamed N. Noui-Mehidi

### Systems and Methods for Real-Time Spectrophotometric Quantification of Crude Oil

*Granted Patent: U.S. Patent 10,615,074, Grant Date: April 7, 2020*

Dmitry Kosynkin and Mohammed Al-Askar

### Intelligent Distributed Industrial Facility Safety System

*Granted Patent: U.S. Patent 10,615,505, Grant Date: April 7, 2020*

Mohammed Al-Juaid

### Halogenated Polyisolefins with Reduced Halogenated Oligomers

*Granted Patent: U.S. Patent 10,618,985, Grant Date: April 14, 2020*

Dana K. Adkinson and Sarah Elliott



### Nanosilica Dispersion Lost Circulation Material (LCM)

*Granted Patent: U.S. Patent 10,619,085,  
Grant Date: April 14, 2020*

Vikrant B. Wagle, Abdullah S. Al-Yami and Nassar Al-Hareth

### Material Design for the Encapsulation of Additives and Release

*Granted Patent: U.S. Patent 10,619,085,  
Grant Date: April 14, 2020*

Elizabeth Q. Contreras

### Compositions of and Methods for Using Hydraulic Fracturing Fluid for Petroleum Production

*Granted Patent: U.S. Patent 10,619,089,  
Grant Date: April 14, 2020*

Fakuen F. Chang, Paul D. Berger and Christie H. Lee

### Fracturing Fluid Compositions having Portland Cement Clinker and Methods of Use

*Granted Patent: U.S. Patent 10,619,090,  
Grant Date: April 14, 2020*

B. Raghava Reddy and Feng Liang

### Hydrocracking and Hydrotreating Catalytic Compositions Comprising Zeolite and Regenerated, Spent Catalyst and Uses Thereof

*Granted Patent: U.S. Patent 10,619,110,  
Grant Date: April 14, 2020*

Omer R. Koseoglu and Robert P. Hodgkins

### Process and System for Conversion of Crude Oil to Petrochemicals and Fuel Products Integrating Vacuum Gas Oil Hydrotreating and Steam Cracking

*Granted Patent: U.S. Patent 10,619,112,  
Grant Date: April 14, 2020*

Mohammad S. Al-Ghamdi

### Oil Swellable, Surface Treated Elastomeric Polymer and Methods of Using the Same for Controlling Losses of Non-Aqueous Wellbore Treatment Fluids to the Subterranean Formation

*Granted Patent: U.S. Patent 10,619,432,  
Grant Date: April 14, 2020*

B. Raghava Reddy

### ARC Perm-Squeeze RDF — A Permeable Plug Forming Rapidly Dehydrating Fluid

*Granted Patent: U.S. Patent 10,619,433,  
Grant Date: April 14, 2020*

Md Amanullah

### Hydraulic Fracturing in Kerogen-Rich Unconventional Formations

*Granted Patent: U.S. Patent 10,619,469,  
Grant Date: April 14, 2020*

Yanhui Han, Leiming Li, Ghaithan A. Al-Muntasheri, Younane N. Abousleiman, Katherine L. Hull and David Jacobi

### Remotely Operated Inflow Control Valve

*Granted Patent: U.S. Patent 10,619,474,  
Grant Date: April 14, 2020*

Kenechukwu O. Ofondu, Auda K. Al-Dulajian and Ali A. Al-Hajji

### Systems and Methods for Wirelessly Monitoring Well Conditions

*Granted Patent: U.S. Patent 10,619,475,  
Grant Date: April 14, 2020*

Chinthaka P. Gooneratne, Bodong Li and Shaohua Zhou

### Incorporate Wall Thickness Measurement Sensor Technology into Aerial Visual Inspection Intrinsically Safe Drones

*Granted Patent: U.S. Patent 10,620,002,  
Grant Date: April 14, 2020*

Saad A. Al-Jabr

### Microwave Horn Antennas-Based Transducer System for CUI Inspection without Removing the Insulation

*Granted Patent: U.S. Patent 10,620,115,  
Grant Date: April 14, 2020*

Ali Shehri and Ayman Amer

### Systems and Methods for Real-Time Spectrophotometric Quantification of Crude Oil

*Granted Patent: U.S. Patent 10,620,183,  
Grant Date: April 14, 2020*

Dmitry Kosynkin and Mohammed Al-Askar

### Three-Dimensional Elastic Frequency-Domain Iterative Solver for Full Waveform Inversion

*Granted Patent: U.S. Patent 10,621,266,  
Grant Date: April 14, 2020*

Belonovos Mikhail, Dmitriev Maxim, Cheverda Vladimir and Neklyudov Dmitry

### Method and System for Capturing High-Purity CO<sub>2</sub> in a Hydrocarbon Facility

*Granted Patent: U.S. Patent 10,622,656,  
Grant Date: April 14, 2020*

Ali Shakir Al-Hunaidy and Stamatios Souentie

### Removing Debris from a Hydrocarbon Fluid

*Granted Patent: U.S. Patent 10,625,181,  
Grant Date: April 21, 2020*

Aslan Bulekbay, Mustafa Al-Zaid, Manaf Al-Aithan and Khalid Al-Khamed

### Butyl Rubber with New Sequence Distribution

*Granted Patent: U.S. Patent 10,626,201,  
Grant Date: April 21, 2020*

Steven J. Teertstra

### Double Emulsified Acids and Methods for Producing and Using the Same

*Granted Patent: U.S. Patent 10,626,323,  
Grant Date: April 21, 2020*

Mohammed H. Al-Khaldi and Tariq A. Al-Mubarak

### Double Emulsified Acids and Methods for Producing and Using the Same

*Granted Patent: U.S. Patent 10,626,324,  
Grant Date: April 21, 2020*

Mohammed H. Al-Khaldi and Tariq A. Al-Mubarak

### Cement Squeeze Well Tool

*Granted Patent: U.S. Patent 10,626,698,  
Grant Date: April 21, 2020*

Ahmed Al-Mousa and Ahmed Al-Ramadhan

### Steam Driven Submersible Pump

*Granted Patent: U.S. Patent 10,626,709,  
Grant Date: April 21, 2020*

Faisal M. Al-Dossary

### Natural Gas Liquid Fractionation Plant Waste Heat Conversion to Power Using Dual Turbines Organic Rankine Cycle

*Granted Patent: U.S. Patent 10,626,756,  
Grant Date: April 21, 2020*

Mahmoud B. Noureldin and Akram H. Kamel

### Characterization of Crude Oil by Near Infrared Spectroscopy

*Granted Patent: U.S. Patent 10,627,545,  
Grant Date: April 21, 2020*

Omer R. Koseoglu and Adnan Al-Hajji

### Systems and Methods for Acquiring and Employing Resiliency Data for Leadership Development

*Granted Patent: U.S. Patent 10,628,770,  
Grant Date: April 21, 2020*

Samantha Horseman and Brent Mattson

### Compositions and Methods to Recover Irreducible Water for Enhanced formation Evaluation

*Granted Patent: U.S. Patent 10,633,574,  
Grant Date: April 28, 2020*

Shouxiang M. Ma and Nedhal Musharfi

### Double Emulsified Acids and Methods for Producing and Using the Same

*Granted Patent: U.S. Patent 10,633,577,  
Grant Date: April 28, 2020*

Mohammed H. Al-Khaldi and Tariq A. Al-Mubarak

### Removing Submerged Piles of Offshore Production Platforms

*Granted Patent: U.S. Patent 10,633,817,  
Grant Date: April 28, 2020*

Prakasha Kuppalli

### Mitigation of Sand Production in Sandstone Reservoir Using Thermally Expandable Beads

*Granted Patent: U.S. Patent 10,633,954,  
Grant Date: April 28, 2020*

Yanhui Han, Mohammad H. Haque and Feng Liang

### Hybrid Distributed Acoustic Testing

*Granted Patent: U.S. Patent 10,634,553,  
Grant Date: April 28, 2020*

Frode Hveding, Islam Ashry, Mao Yuan, Mohd S. Bin Alias, Boon Siew Ooi and Muhammad Arsalan

### Water Crest Monitoring Using Electromagnetic Transmissions

*Granted Patent: U.S. Patent 10,634,809,  
Grant Date: April 28, 2020*

Jesus M. Felix-Servin and Howard K. Schmidt

### Cored Rock Analysis Planning through CT Images

*Granted Patent: U.S. Patent 10,636,204,  
Grant Date: April 28, 2020*

Sinan Caliskan and Abdullah Shebatalhamd

### Compositions and Methods of Making of Shale Inhibition Fluids

*Granted Patent: U.S. Patent 10,640,694,  
Grant Date: May 5, 2020*

Abdullah S. Al-Yami, Vikrant B. Wagle, Hussain Al-Bahrani, Ali Al-Safran and Naser Al-Hareth

### Dispersant in Cement Formulations for Oil and Gas Wells

*Granted Patent: U.S. Patent 10,640,695,  
Grant Date: May 5, 2020*

Abdullah S. Al-Yami, Hussain Al-Bahrani, Vikrant B. Wagle and Ali Al-Safran

### Oil-Based Drilling Fluids for High-Pressure and High Temperature Drilling Operations

*Granted Patent: U.S. Patent 10,640,696,  
Grant Date: May 5, 2020*

Mona Al Batal, John A. Hall, Andrew Whiting, Gasan Alabedi, Hugh C. Greenwell, Musarrat H. Mohammed and Michael Hodder

### High Temperature Cross-Linked Fracturing Fluids

*Granted Patent: U.S. Patent 10,640,700,  
Grant Date: May 5, 2020*

Ghaithan A. Al-Muntasheri, Leiming Li, Feng Liang and B. Raghava Reddy

### Supercritical Reactor Systems and Processes for Petroleum Upgrading

*Granted Patent: U.S. Patent 10,640,715,  
Grant Date: May 5, 2020*

Ki-Hyouk Choi, Abdullah T. Alabdulhadi and Mohammed A. Alabdullah

### Reverse Circulation Well Tool

*Granted Patent: U.S. Patent 10,641,052,  
Grant Date: May 5, 2020*

Shaohua Zhou

### Apparatus and Method for In Situ Stabilization of Unconsolidated Sediment in Core Samples

*Granted Patent: U.S. Patent 10,641,055,  
Grant Date: May 5, 2020*

Nikolaos A. Michael, Maher I. Marhoon and Peng Lu

### Thru-Tubing Retrievable Subsurface Completion System

*Granted Patent: U.S. Patent 10,641,060,  
Grant Date: May 5, 2020*

Muhammad Arsalan and Mohamed N. Noui-Mehidi

### Consolidated Material to Equalize Fluid Flow into a Wellbore

*Granted Patent: U.S. Patent 10,641,071,  
Grant Date: May 5, 2020*

Abdulrahman A. Al-Mulhem

### Isolation Techniques for Fracturing Rock Formations in Oil and Gas Applications

*Granted Patent: U.S. Patent 10,641,074,  
Grant Date: May 5, 2020*

Ali H. Alabdulmuhsin, Jon E. Hansen and Hamad F. Al-Kulaib

### Solidifying Filler Material for Well Integrity Issues

*Granted Patent: U.S. Patent 10,641,079,  
Grant Date: May 5, 2020*

Mohammad Aljubran, Hussain Al-Bahrani, Sameeh I. Batareseh and Timothy E. Moellendick

### Systems and Methods for Wirelessly Monitoring Well Conditions

*Granted Patent: U.S. Patent 10,641,085,  
Grant Date: May 5, 2020*

Chinthaka P. Gooneratne, Bodong Li and Shaohua Zhou

### Pre-Processing Characterization of Residual Oil

*Granted Patent: U.S. Patent 10,641,759,  
Grant Date: May 5, 2020*

Omer R. Koseoglu

### Devices, Methods and Computer Medium to Provide Real Time 3D Visualization Bio-Feedback

*Granted Patent: U.S. Patent 10,642,955,  
Grant Date: May 5, 2020*

Samantha Horseman and Linda Gilligan

### Machine Learning System and Data Fusion for Optimization of Deployment Conditions for Detection of Corrosion under Insulation

*Granted Patent: U.S. Patent 10,643,324,  
Grant Date: May 5, 2020*

Ali Al Shehri, Ser Nam Lim, Ayman Amer, Mustafa Uzunbas, Ahmad Aldabbagh, Muhammad Ababtain, Vincent Cunningham, John Boot and Godine Chan

### System and Method for Image Processing and Feature Recognition

*Granted Patent: U.S. Patent 10,643,325,  
Grant Date: May 5, 2020*

Enrico Bovero

### Novel Anti-Agglomerants for Elastomeric Ethylene/A-Olefin Copolymers

*Granted Patent: U.S. Patent 10,647,842,  
Grant Date: May 12, 2020*

David Thompson and Clinton Lund

### Oil-Based Drilling Fluid Compositions Which Include Layered Double Hydroxides as Rheology Modifiers and Amino Amides as Emulsifiers

*Granted Patent: U.S. Patent 10,647,905,  
Grant Date: May 12, 2020*

Andrew Whiting, Michael Hodder, Mona Al Batal, Musarrat H. Mohammed, Hugh C. Greenwell, Manohara G. Veerabhadrapa, John A. Hall and Gasan Alabedi

### Hydraulic Fracturing Fluid

*Granted Patent: U.S. Patent 10,647,909,  
Grant Date: May 12, 2020*

Leiming Li, Feng Liang, Ghaithan A. Al-Muntasheri and Amy J. Cairns

### Desulfurization of Hydrocarbon Feed Using Gaseous Oxidant

*Granted Patent: U.S. Patent 10,647,926,  
Grant Date: May 12, 2020*

Abdenmour Bourane and Omer R. Koseoglu

### Wellbore Parted Casing Access Tool

*Granted Patent: U.S. Patent 10,648,278,  
Grant Date: May 12, 2020*

Adib A. Al-Mumen, Ibrahim A. Al-Obaidi, Nelson O. Pinero Zambrano and Abdullah E. Al-Noaimi

### Polyurethane Foamed Annular Chemical Packer

*Granted Patent: U.S. Patent 10,648,280,  
Grant Date: May 12, 2020*

Prasad B. Karadkar and Mohammed A. Bataweel

### Systems and Methods for Carbonated Water Flooding of Hydrocarbon Reservoirs

*Granted Patent: U.S. Patent 10,648,305,  
Grant Date: May 12, 2020*

Subhash Ayirala, Ali Yousef, Sultan Al-Enezi and Ahmed Al-Eidan

### Multiphase Flow Meter Combining Extended Throat Venturi with Microwave Resonators

*Granted Patent: U.S. Patent 10,648,841,  
Grant Date: May 12, 2020*

Muhammad A. Karimi, Atif Shamim and Muhammad Arsalan

### Evaluating Black Powder Formation of Hydrocarbon Gas Flowed through Pipelines

*Granted Patent: U.S. Patent 10,648,891,  
Grant Date: May 12, 2020*

Yufeng He and Rohit Patwardhan

### Power Management of Computing and Communications Systems during Power Fluctuation and Sudden Power Failure Events

*Granted Patent: U.S. Patent 10,649,515,  
Grant Date: May 12, 2020*

Khalid K. Al-Aqeel and Syed K. Javaid

### Hydrocarbon Migration and Accumulation Methods and Systems

*Granted Patent: U.S. Patent 10,650,175,  
Grant Date: May 12, 2020*

Larry S. Fung and Shouhong Du

### Self-Healing Durable Cement

*Granted Patent: U.S. Patent 10,655,044,  
Grant Date: May 19, 2020*

Abdullah S. Al-Yami, Vikrant B. Wagle, Hussain Albahrani, Zainab Alsayhathi, Antonio Santagati, Mohammad Al-Alqam, Ali Alsafran, Abdulaziz Alhelal, Nasser Alhareth and Abdullah Al-Awadh

### Self-Healing Durable Cement

*Granted Patent: U.S. Patent 10,655,045,  
Grant Date: May 19, 2020*

Abdullah S. Al-Yami, Vikrant B. Wagle, Hussain Albahrani, Zainab Alsayhathi, Antonio Santagati, Mohammad Al-Alqam, Ali Alsafran, Abdulaziz Alhelal, Nasser Alhareth and Abdullah Al-Awadh

### Cement Having Cross-Linked Polymers

*Granted Patent: U.S. Patent 10,655,046,  
Grant Date: May 19, 2020*

Elizabeth Q. Contreras



### Method and Materials to Convert a Drilling Mud into a Solid Gel-Based Lost Circulation Material

*Granted Patent: U.S. Patent 10,655,049,  
Grant Date: May 19, 2020*

Vikrant B. Wagle, Rajendra A. Kalgaonkar and Abdullah S. Al-Yami

### Method and Materials to Convert a Drilling Mud into a Solid Gel-Based Lost Circulation Material

*Granted Patent: U.S. Patent 10,655,050,  
Grant Date: May 19, 2020*

Vikrant B. Wagle, Rajendra A. Kalgaonkar and Abdullah S. Al-Yami

### Methods and Compositions for Diversion during Enhanced Oil Recovery

*Granted Patent: U.S. Patent 10,655,053,  
Grant Date: May 19, 2020*

Ahmed N. Rizq and Badr H. Zahrani

### Methods and Materials for Treating Subterranean Formations Using a Three-Phase Emulsion-Based Fracturing Fluid

*Granted Patent: U.S. Patent 10,655,057,  
Grant Date: May 19, 2020*

Rajendra A. Kalgaonkar

### Well Bit Assembly

*Granted Patent: U.S. Patent 10,655,400,  
Grant Date: May 19, 2020*

Ahmad M. Al-Abduljabbar

### Vehicle Mounted Blowout Preventer Equipment

*Granted Patent: U.S. Patent 10,655,419,  
Grant Date: May 19, 2020*

Mohammad Al-Badran

### Thru-Tubing Retrievable Intelligent Completion System

*Granted Patent: U.S. Patent 10,655,429,  
Grant Date: May 19, 2020*

Muhammad Arsalan and Mohamed N. Noui-Mehidi

### Pulsed Hydraulic Fracturing with Geopolymer Precursor Fluids

*Granted Patent: U.S. Patent 10,655,445,  
Grant Date: May 19, 2020*

Ahmed M. Goma, Khalid R. Noaimi and Ghaithan A. Muntasheri

### Systems, Apparatuses, and Methods for Downhole Water Separation

*Granted Patent: U.S. Patent 10,655,446,  
Grant Date: May 19, 2020*

Muhammad Ayub

### Measuring Source Rock Potential Using a Quantum Electronic Scanner

*Granted Patent: U.S. Patent 10,656,108,  
Grant Date: May 19, 2020*

Sebastian Csutak

### Generating a Velocity Model Using Subsurface Azimuth and Reflection Angle Dependent Full Waveform Inversion

*Granted Patent: U.S. Patent 10,656,294,  
Grant Date: May 19, 2020*

Constantinos X. Tsingas, Woodon Jeong and Young S. Kim

### Maintaining a Solar Power Module

*Granted Patent: U.S. Patent 10,658,970,  
Grant Date: May 19, 2020*

James C. Hassell and Luiz Do Val

### Method and System for Blending Wellbore Treatment Fluids

*Granted Patent: U.S. Patent 10,661,256,  
Grant Date: May 26, 2020*

Mohamed N. Noui-Mehidi

### Zeolite Composite Catalysts for Conversion of Heavy Reformate to Xylenes

*Granted Patent: U.S. Patent 10,661,260,  
Grant Date: May 26, 2020*

Syed A. Ali, Sulaiman S. Al-Khattaf, Rabin dran J. Balasamy, Raed Abudawoud and Abdullah M. Aitani

### Molten Metal Anode Solid Oxide Fuel Cell for Transportation-Related Auxiliary Power Units

*Granted Patent: U.S. Patent 10,661,756,  
Grant Date: May 26, 2020*

Nadimul H. Faisal, Rehan Ahmed, Matheus Goosen, Sai P. Katikaneni and Stamatios Souentia

### Two-Stage Adsorption Process for Claus Tail Gas Treatment

*Granted Patent: U.S. Patent 10,662,061,  
Grant Date: May 26, 2020*

Yuguo Wang, Rashid M. Othman and Georgios Lithoxoos

### Catalysts and Methods for Polymer Synthesis

*Granted Patent: U.S. Patent 10,662,211,  
Grant Date: May 26, 2020*

Geoffrey W. Coates, Robert E. Lapointe, Chris A. Simoneau, Scott D. Allen, Anna E. Cherian, Jay J. Farmer and Alexei A. Gridnev

### Reversible Amino Gel Compositions, Methods, and Use

*Granted Patent: U.S. Patent 10,662,562,  
Grant Date: May 26, 2020*

Peter J. Boul, B. Raghava Reddy, Matthew G. Hilfiger, Carl J. Thaemlitz and Diana Rasner

### Lubricants for Water-Based Drilling Fluids

*Granted Patent: U.S. Patent 10,662,565,  
Grant Date: May 26, 2020*

Abdullah S. Al-Yami, Hussain Al-Bahrani, Vikrant B. Wagle, Ali M. Al-Safran, Nasser Al-Hareth, Abdulaziz Alhelal and Abdulla H. Awadh

### Cement Having Cross-Linked Polymers

*Granted Patent: U.S. Patent 10,662,567,  
Grant Date: May 26, 2020*

Elizabeth Q. Contreras

### Method and Apparatus for Stuck Pipe Mitigation

*Granted Patent: U.S. Patent 10,662,728,  
Grant Date: May 26, 2020*

Ali Hajji and Ossama Sehsah

### Evaluation of Cased Hole Perforations in Under-Pressured Gas Sand Reservoirs with Stoneley Wave Logging

*Granted Patent: U.S. Patent 10,662,761,  
Grant Date: May 26, 2020*

Mohammed S. Ameen

### Casing System Having Sensors

*Granted Patent: U.S. Patent 10,662,762,  
Grant Date: May 26, 2020*

Faisal N. Al-Nughaimish, Jonathan M. Jimenez and Ossama R. Sehsah

### Measuring Transmissivity of Wells from Multiple Logs

*Granted Patent: U.S. Patent 10,662,763,  
Grant Date: May 26, 2020*

Mohammed H. Alshawaf, Mickey Warlick and Fahad A. Al-Ajmi

### Natural Gas Liquid Fractionation Plant Waste Heat Conversion to Power Using Organic Rankine Cycle

*Granted Patent: U.S. Patent 10,662,824,  
Grant Date: May 26, 2020*

Mahmoud B. Noureldin and Akram H. Kamel

### Staged Chemical Looping Process with Integrated Oxygen Generation

*Granted Patent: U.S. Patent 10,663,163,  
Grant Date: May 26, 2020*

Tidjani Niass and Mourad V. Younes

### Natural Gas Liquid Fractionation Plant Waste Heat Conversion to Simultaneous Cooling Capacity and Potable Water Using Kalina Cycle and Modified Multi-Effect Distillation System

*Granted Patent: U.S. Patent 10,663,254,  
Grant Date: May 26, 2020*

Mahmoud B. Noureldin and Akram H. Kamel

### Combining Multiple Geophysical Attributes Using Extended Quantization

*Granted Patent: U.S. Patent 10,663,609,  
Grant Date: May 26, 2020*

Saleh A. Al-Dossary and Jinsong Wang

### High Integrity Protection System for Hydrocarbon Flow Lines

*Granted Patent: U.S. Patent 10,663,988,  
Grant Date: May 26, 2020*

Mohammad R. Al-Khunaizi, Rashid D. Al-Hajri, Anthony E. Kakpovbia and Fahad A. Al-Hindas

### Cement Having Cross-Linked Polymers

*Granted Patent: U.S. Patent 10,669,469,  
Grant Date: June 2, 2020*

Elizabeth Q. Contreras

### Additives to Minimize Viscosity Reduction for Guar/Borate System under High Pressure

*Granted Patent: U.S. Patent 10,669,472,  
Grant Date: June 2, 2020*

Feng Liang, Ghaithan A. Al-Muntasheri and Abdulrahman F. Al-Harbi

### Integrated Process for Producing Anode Grade Coke

*Granted Patent: U.S. Patent 10,669,485,  
Grant Date: June 2, 2020*  
Omer R. Koseoglu

### Method to Mitigate a Stuck Pipe during Drilling Operations

*Granted Patent: U.S. Patent 10,669,798,  
Grant Date: June 2, 2020*  
Abdulaziz S. Al-Qasim, Mohammed K. Al-Arfaj and Sunil L. Kokal

### Swellable Seals for Well Tubing

*Granted Patent: U.S. Patent 10,669,806,  
Grant Date: June 2, 2020*  
Ahmad M. Al-Abduljabbar and Kamal E. Aghazada

### Controlling Water Inflow in a Wellbore

*Granted Patent: U.S. Patent 10,669,810,  
Grant Date: June 2, 2020*  
Peter Egbe and Fawaz AlShuraim

### In Situ Heating Fluids with Electromagnetic Radiation

*Granted Patent: U.S. Patent 10,669,814,  
Grant Date: June 2, 2020*  
Sameeh I. Batarseh and Mohamed N. Noui-Mehidi

### Using Electromagnetic Waves to Remove Near Wellbore Damages in a Hydrocarbon Reservoir

*Granted Patent: U.S. Patent 10,669,829,  
Grant Date: June 2, 2020*  
Jin-Hong Chen, Hui-Hai Liu, Feng Liang and Rajesh K. Saini

### Apparatus, Computer Readable Medium, and Program Code for Evaluating Rock Properties While Drilling Using Downhole Acoustic Sensors and a Downhole Broadband Transmitting System

*Granted Patent: U.S. Patent 10,669,846,  
Grant Date: June 2, 2020*  
Yunlai X. Yang

### Methods and Systems of Fluid Flow Rate Measurement Based on Magnetization

*Granted Patent: U.S. Patent 10,670,456,  
Grant Date: June 2, 2020*  
Juan D. Escobar

### Method for Determining Unconventional Liquid Imbibition in Low Permeability Materials

*Granted Patent: U.S. Patent 10,670,506,  
Grant Date: June 2, 2020*  
Hui-Hai Liu, Bitao Lai and Jin-Hong Chen

### Impedance-Based Flow Line Water Cut Measurement System

*Granted Patent: U.S. Patent 10,670,544,  
Grant Date: June 2, 2020*  
Jana M. Al-Jindan and Mohamed N. Noui-Mehidi

### History Matching of Time-Lapse Crosswell Data Using Ensemble Kalman Filtering

*Granted Patent: U.S. Patent 10,670,753,  
Grant Date: June 2, 2020*  
Fabio Ravanelli and Ibrahim Hoteit

### Gas Assisted Chemical Injection System

*Granted Patent: U.S. Patent 10,671,099,  
Grant Date: June 2, 2020*  
Nisar Ansari, Samusideen Salu, Talal Al-Zahrani and Mohamed Soliman

### Silicone Rubber Foam Brush

*Granted Patent: U.S. Patent 10,673,576,  
Grant Date: June 2, 2020*  
Pablo Carrasco Zanini, Brian J. Parrott and Ali Alshehri

### Interface for Integration of Radio Systems

*Granted Patent: U.S. Patent 10,674,524,  
Grant Date: June 2, 2020*  
Mustafa Jar, Naif Daafas and Mohammed Kharafi

### Advanced Heat Integration in Sulfur Recovery Unit — Safarclaus

*Granted Patent: U.S. Patent 10,676,556,  
Grant Date: June 9, 2020*  
Yazeed S. Al-Shahrani

### Oil-Based Drilling Fluids for High-Pressure and High Temperature Drilling Operations

*Granted Patent: U.S. Patent 10,676,658,  
Grant Date: June 9, 2020*  
Andrew Whiting, Musarrat H. Mohammed, Hugh C. Greenwell, Michael Hodder, Mona Al Batal, John A. Hall and Gasan Alabedi

### Downhole In Situ Heat Generation to Remove Filter Cake

*Granted Patent: U.S. Patent 10,677,001,  
Grant Date: June 9, 2020*  
Pubudu Gamage and Matthew G. Hilfiger

### Downhole In Situ Heat Generation to Remove Filter Cake

*Granted Patent: U.S. Patent 10,677,002,  
Grant Date: June 9, 2020*  
Pubudu Gamage and Matthew G. Hilfiger

### Apparatus and Method Employing Retrivable Landing Base with Guide for Same Location Multiple Perforating Gun Firings

*Granted Patent: U.S. Patent 10,677,025,  
Grant Date: June 9, 2020*  
Alwaleed A. Al-Gouhi

### Click Together Electrical Submersible Pump

*Granted Patent: U.S. Patent 10,677,050,  
Grant Date: June 9, 2020*  
Abdullah M. Al-Zahrani

### Integrated Pump and Compressor and Method of Producing Multiphase Well Fluid Downhole and at Surface

*Granted Patent: U.S. Patent 10,677,051,  
Grant Date: June 9, 2020*  
Jinjiang Xiao and Randall Shepler

### Controlling Hydrocarbon Production

*Granted Patent: U.S. Patent 10,677,054,  
Grant Date: June 9, 2020*  
Huseyin O. Balan, Anuj Gupta, Daniel T. Georgi, Ali Al-Khatib and Alberto F. Marsala

### Controlling Hydrocarbon Production

*Granted Patent: U.S. Patent 10,677,055,  
Grant Date: June 9, 2020*  
Huseyin O. Balan, Anuj Gupta, Daniel T. Georgi, Ali Al-Khatib and Alberto F. Marsala

### Natural Gas Liquid Fractionation Plant Waste Heat Conversion to Simultaneous Power, Cooling, and Potable Water Using Integrated Mono-Refrigerant Triple Cycle and Modified Multi-Effect Distillation System

*Granted Patent: U.S. Patent 10,677,104,  
Grant Date: June 9, 2020*  
Mahmoud B. Noureldin and Akram H. Kamel

### Smart Drilling Jar

*Granted Patent: U.S. Patent 10,677,009,  
Grant Date: June 9, 2020*  
Victor Costa de Oliveira, Mario Rivas and Khaled Abouelnaaj

### Method for Sealing a Wellbore Liner Hanger Tie-Back System

*Granted Patent: U.S. Patent 10,677,011,  
Grant Date: June 9, 2020*  
Ahmad M. Al-Abduljabbar and Kamal E. Aghazada

### Removing Scale from a Wellbore

*Granted Patent: U.S. Patent 10,677,020,  
Grant Date: June 9, 2020*  
Aslan Bulekbay, Sultan Attiah, Talal Al-Mutairi and Abdulrahman Al-Sousy

### Removing Scale from a Wellbore

*Granted Patent: U.S. Patent 10,677,021,  
Grant Date: June 9, 2020*  
Aslan Bulekbay, Sultan Attiah, Talal Al-Mutairi and Abdulrahman Al-Sousy

### Characterization of Crude Oil by Near Infrared Spectroscopy

*Granted Patent: U.S. Patent 10,677,718,  
Grant Date: June 9, 2020*  
Omer R. Koseoglu and Adnan Al-Hajji

### Generating Unconstrained Voronoi Grids in a Domain Containing Complex Internal Boundaries

*Granted Patent: U.S. Patent 10,677,960,  
Grant Date: June 9, 2020*  
Xiang Y. Ding, Larry S. Fung and Ali H. Dogru

### Multilayer Aromatic Polyamide Thin-Film Composite Membranes for Separation of Gas Mixtures

*Granted Patent: U.S. Patent 10,682,606,  
Grant Date: June 16, 2020*  
Seung-Hak Choi, Mohammad S. Al-Qahtani and Eyad A. Qasem

### Reversible Amino Gel Compositions, Methods, and Use

*Granted Patent: U.S. Patent 10,683,445,  
Grant Date: June 16, 2020*  
Peter J. Boul, B. Raghava Reddy, Matthew G. Hilfiger and Carl J. Thaeamlitz

### Reversible Amino Gel Compositions, Methods, and Use

*Granted Patent: U.S. Patent 10,685,446,  
Grant Date: June 16, 2020*

Peter J. Boul, B. Raghava Reddy, Matthew G. Hilfiger and Carl J. Thaeamlitz

### Invert Emulsion-Based Drilling Fluid and Methods of Using Same

*Granted Patent: U.S. Patent 10,685,447,  
Grant Date: June 16, 2020*

Vikrant B. Wagle, Abdullah S. Al-Yami and Nasser Al-Hareth

### Alkyl Ester Spotting Fluid Compositions for Differential Sticking

*Granted Patent: U.S. Patent 10,685,448,  
Grant Date: June 16, 2020*

Md Amanullah

### Cement Having Cross-Linked Polymers

*Granted Patent: U.S. Patent 10,685,450,  
Grant Date: June 16, 2020*

Elizabeth Q. Contreras

### Cement Compositions Comprising Aqueous Latex Containing Dispersed Solid and Liquid Elastomer Phases

*Granted Patent: U.S. Patent 10,685,451,  
Grant Date: June 16, 2020*

B. Raghava Reddy

### Nanosilica Dispersion for Thermally Insulating Packer Fluid

*Granted Patent: U.S. Patent 10,685,452,  
Grant Date: June 16, 2020*

Vikrant B. Wagle, Abdullah S. Al-Yami, Zainab Alsayhathi and Abdulaziz Alhelal

### Curing a Lost Circulation Zone in a Wellbore

*Granted Patent: U.S. Patent 10,685,724,  
Grant Date: June 16, 2020*

Sergey Kozodeev and Pavel Golikov

### Isolation Polymer Packer

*Granted Patent: U.S. Patent 10,685,726,  
Grant Date: June 16, 2020*

Abdulrahman A. Al-Mulhem and Ayman M. Almohsin

### Caliper Steerable Tool for Lateral Sensing and Accessing

*Granted Patent: U.S. Patent 10,685,752,  
Grant Date: June 16, 2020*

Abdulrahman A. Al-Mulhem

### Natural Gas Liquid Fractionation Plant Waste Heat Conversion to Simultaneous Power and Cooling Capacities Using Modified Goswami System

*Granted Patent: U.S. Patent 10,684,079,  
Grant Date: June 16, 2020*

Mahmoud B. Noureldin and Akram H. Kamel

### Characterization of Crude Oil by NMR Spectroscopy

*Granted Patent: U.S. Patent 10,684,259,  
Grant Date: June 16, 2020*

Omer R. Koseoglu, Adnan Al-Hajji, Mohammed A. Al-Ghamdi and Alexander Rebrov

### Generating Target Oriented Acquisition Imprint-Free Prestack Angle Gathers Using Common Focus Point Operators

*Granted Patent: U.S. Patent 10,684,582,  
Grant Date: June 16, 2020*

Hongwei Liu and Mustafa Al-Ali

### Simultaneous Cement Enhancement and Carbon Dioxide Utilization by Mounting a Carbon Dioxide Capture System Onboard a Concrete Mixer Vehicle

*Granted Patent: U.S. Patent 10,688,686,  
Grant Date: June 23, 2020*

Ahmad D. Hammad, Issam T. Amr, Bandar A. Fadhel and Rami Bamagain

### Cement Slurries, Cured Cement and Methods of Making and Use of These

*Granted Patent: U.S. Patent 10,689,293,  
Grant Date: June 23, 2020*

B. Raghava Reddy

### Manufacturing Polymers of Thiophene, Benzothiophene, and their Alkylated Derivatives

*Granted Patent: U.S. Patent 10,689,466,  
Grant Date: June 23, 2020*

Abdullah R. Al-Malki

### Flexible Durable Cement

*Granted Patent: U.S. Patent 10,689,559,  
Grant Date: June 23, 2020*

Abdullah S. Al-Yami, Vikrant B. Wagle, Hussain Albahrani, Zainab Alsayhathi, Antonio Santagati, Mohammad Al-Alqam, Ali Alsafran, Abdulaziz Alhelal, Nasser Alhareth and Abdullah Al-Awadh

### Flexible Durable Cement

*Granted Patent: U.S. Patent 10,689,560,  
Grant Date: June 23, 2020*

Abdullah S. Al-Yami, Vikrant B. Wagle, Hussain Albahrani, Zainab Alsayhathi, Antonio Santagati, Mohammad Al-Alqam, Ali Alsafran, Abdulaziz Alhelal, Nasser Alhareth and Abdullah Al-Awadh

### ARC Perm-Squeeze RDF — A Permeable Plug Forming Rapidly Dehydrating Fluid

*Granted Patent: U.S. Patent 10,689,561,  
Grant Date: June 23, 2020*

Md Amanullah

### ARC Perm-Squeeze RDF — A Permeable Plug Forming Rapidly Dehydrating Fluid

*Granted Patent: U.S. Patent 10,689,562,  
Grant Date: June 23, 2020*

Md Amanullah

### Systems and Methods for Processing Heavy Oils

*Granted Patent: U.S. Patent 10,689,585,  
Grant Date: June 23, 2020*

Kareemuddin M. Shaik, Lianhui Ding, Mazin Tamimi, Ibrahim A. Abba and Abdenour Bourane

### Systems and Processes for Conversion of Crude Oil

*Granted Patent: U.S. Patent 10,689,587,  
Grant Date: June 23, 2020*

Abdenour Bourane, Essam Al-Sayed, Lianhui Ding, Alberto L. Ballesteros, Omer R. Koseoglu and Furquan Al Jumah

### Supporting a String within a Wellbore with a Smart Stabilizer

*Granted Patent: U.S. Patent 10,689,915,  
Grant Date: June 23, 2020*

Victor Costa de Oliveira, Mario Rivas, Khaled Abouelnaaj and Bader S. Zahrani

### Opening a Wellbore with a Smart Hole Opener

*Granted Patent: U.S. Patent 10,689,914,  
Grant Date: June 23, 2020*

Victor Costa de Oliveira, Mario Rivas, Khaled Abouelnaaj and Bader S. Zahrani

### Lost Circulation Zone Isolating Liner

*Granted Patent: U.S. Patent 10,689,926,  
Grant Date: June 23, 2020*

Shaohua Zhou

### Method for Determining Gelation Time in a Core Plug

*Granted Patent: U.S. Patent 10,689,978,  
Grant Date: June 23, 2020*

Abdulkareem M. Al-Sofi, Jinxun Wang and Hassan W. Al Hashim

### Natural Gas Liquid Fractionation Plant Waste Heat Conversion to Simultaneous Power and Potable Water Using Organic Rankine Cycle and Modified Multi-Effect Distillation Systems

*Granted Patent: U.S. Patent 10,690,407,  
Grant Date: June 23, 2020*

Mahmoud B. Noureldin and Akram H. Kamel

### Piezoelectric Alternating Magnetic Field Flow Meters

*Granted Patent: U.S. Patent 10,690,551,  
Grant Date: June 23, 2020*

Fouad M. Alkhabbaz, Maatoug Al-Maatoug and Luay H. Al-Awami

### Method and Device for Testing a Material Sample in a Standard Test for in-Plane Fracture Toughness Evaluation

*Granted Patent: U.S. Patent 10,690,575,  
Grant Date: June 23, 2020*

Abderrazak Traidia, Mustapha Jouiad and Elias Chatzidouros

### Giant Dielectric Nanoparticles as High Contrast Agents for Electromagnetic (EM) Fluids Imaging in an Oil Reservoir

*Granted Patent: U.S. Patent 10,690,798,  
Grant Date: June 23, 2020*

Erika S. Ellis, Howard K. Schmidt and Jesus Manuel Felix-Servin

### Directional Sensitive Fiber Optic Cable Wellbore System

*Granted Patent: U.S. Patent 10,690,871,  
Grant Date: June 23, 2020*

Frode Hveding

### Building Flexible Relationships between Reusable Software Components and Data Objects

*Granted Patent: U.S. Patent 10,691,426,  
Grant Date: June 23, 2020*

Abdullah K. Ibrahim

### End-To-End IT Service Performance Monitoring

*Granted Patent: U.S. Patent 10,695,751,  
Grant Date: June 23, 2020*

Hamed A. Al-Shafei, Baher Al-Ramady,  
Nawaf I. Al-Dossary and Hussain Al-Nasser

### Providing Secure Data Transfer between Networks

*Granted Patent: U.S. Patent 10,695,906,  
Grant Date: June 23, 2020*

Abdulmajeed A. Al-Abdulhadi and Saleem  
E. Al-Harhi

### Oil Field Well Downhole Drone

*Granted Patent: U.S. Patent 10,696,365,  
Grant Date: June 30, 2020*

Mohammed Al-Dabbous and David R.  
Lewis

### Integrated Process for Maximizing Production of Para-Xylene from Full Reformate

*Granted Patent: U.S. Patent 10,696,609,  
Grant Date: June 30, 2020*

Qi Xu and Raed Abudawoud

### Lost Circulation Material Compositions and Methods of Isolating a Lost Circulation Zone of a Wellbore

*Granted Patent: U.S. Patent 10,696,888,  
Grant Date: June 30, 2020*

Abdullah S. Al-Yami, Ali Alsafran, Vikrant  
B. Wagle and Zainab Alsaihati

### Enhancements of Gelled Hydrocarbon Systems

*Granted Patent: U.S. Patent 10,696,892,  
Grant Date: June 30, 2020*

Sehmus Ozden, Leiming Li, Ghaithan A.  
Al-Muntasheri and Feng Liang

### Systems and Methods for Processing Heavy Oils by Oil Upgrading Followed by Steam Cracking

*Granted Patent: U.S. Patent 10,696,909,  
Grant Date: June 30, 2020*

Kareemuddin M. Shaik, Lianhui Ding,  
Mazin Tamimi, Ibrahim A. Abba and  
Abdenour Bourane

### Systems and Methods for Processing Heavy Oils by Oil Upgrading Followed by Distillation

*Granted Patent: U.S. Patent 10,696,910,  
Grant Date: June 30, 2020*

Kareemuddin M. Shaik, Lianhui Ding,  
Mazin Tamimi, Ibrahim A. Abba and  
Abdenour Bourane

### Methods, Systems, and Computer Medium Having Computer Programs Stored Thereon to Optimize Reservoir Management Decisions Based on Reservoir Properties

*Granted Patent: U.S. Patent 10,697,283,  
Grant Date: June 30, 2020*

Ghazi D. Al-Qahtani, Abdulhameed A.  
Faleh, Khalid A. Nasser, Fouad F. Abouheit  
and Cihan Alan

### Adjusting a Fuel On-Board a Vehicle

*Granted Patent: U.S. Patent 10,697,380,  
Grant Date: June 30, 2020*

Esam Z. Hamad and Ibrahim M. Al-  
Gunaibet

### Onboard Fuel Separation for Octane-On-Demand Using Membrane Distillation

*Granted Patent: U.S. Patent 10,697,412,  
Grant Date: June 30, 2020*

Esam Z. Hamad and Husain A. Baaqel

### Self-Calibrating Base Station for Offset Measurements

*Granted Patent: U.S. Patent 10,697,820,  
Grant Date: June 30, 2020*

Sahejad Patel, Brian J. Parrott, Abdullah  
Arab, Fadl H. Abdel Latif and Pablo  
Carrasco Zanini

### Two-Stage Corrosion under Insulation Detection Methodology and Modular Vehicle with Dual Locomotion Sensory Systems

*Granted Patent: U.S. Patent 10,697,955,  
Grant Date: June 30, 2020*

Ayman Amer, Ali Shehri and Brian J.  
Parrott

### Produced Water Treatment Process at Crude Oil and Natural Gas Processing Facilities

*Granted Patent: U.S. Patent 10,705,644,  
Grant Date: July 7, 2020*

Mourad Younes, Regis Vilagines and  
Guillaume Raynel

### Highly Pure Halogenated Rubbers

*Granted Patent: U.S. Patent 10,705,865,  
Grant Date: July 7, 2020*

Gilles J. Arsenault, David Thompson and  
Clinton Lund

### Development of Retarded Acid System

*Granted Patent: U.S. Patent 10,705,957,  
Grant Date: July 7, 2020*

Abdullah S. Al-Yami, Vikrant B. Wagle and  
Ali Al-Safran

### Methods and Systems for Proactively Monitoring Crude Quality Assurance

*Granted Patent: U.S. Patent 10,705,987,  
Grant Date: July 7, 2020*

Emad F. Al-Seraihi, Adeb H. Bukhari,  
Saad Y. Mousa and Khaled K. Al-Yousef

### System to Remove Sulfur and Metals from Petroleum

*Granted Patent: U.S. Patent 10,705,988,  
Grant Date: July 7, 2020*

Ki-Hyouk Choi, Ashok K. Punetha and  
Muneef F. Al-Qarzouh

### Conserving Fresh Wash Water Usage in Desalting Crude Oil

*Granted Patent: U.S. Patent 10,705,989,  
Grant Date: July 7, 2020*

Vilas S. Koleshwar and Saif F. Albluwi

### Catalytic Demetallization and Gas Phase Oxidative Desulfurization of Residual Oil

*Granted Patent: U.S. Patent 10,705,998,  
Grant Date: July 7, 2020*

Omer R. Koseoglu

### Integrated Supercritical Water and Steam Cracking Process

*Granted Patent: U.S. Patent 10,705,999,  
Grant Date: July 7, 2020*

Ki-Hyouk Choi, Abdullah T. Alabdulhadi,  
Mohammed A. Alabdullah, Essam Al-  
Sayed, Gonzalo Martinez and Ali M.  
Alsomali

### Preventing Hydrate Formation in a Flow Line

*Granted Patent: U.S. Patent 10,704,005,  
Grant Date: July 7, 2020*

Jana M. Aljindan

### Reverse Circulation Well Tool

*Granted Patent: U.S. Patent 10,704,348,  
Grant Date: July 7, 2020*

Shaohua Zhou

### Zonal Isolation of a Subterranean Wellbore

*Granted Patent: U.S. Patent 10,704,354,  
Grant Date: July 7, 2020*

Saad Hamid and Scott F. Ashby

### Simultaneous Injection and Fracturing Interference Testing

*Granted Patent: U.S. Patent 10,704,369,  
Grant Date: July 7, 2020*

Mohamed Larbi Zeghlache and Mark  
Proett

### Polymeric Tracers

*Granted Patent: U.S. Patent 10,704,381,  
Grant Date: July 7, 2020*

Jason R. Cox

### Polymeric Tracers

*Granted Patent: U.S. Patent 10,704,382,  
Grant Date: July 7, 2020*

Jason R. Cox

### Choke Valve with Internal Sleeve for Erosion Protection

*Granted Patent: U.S. Patent 10,704,702,  
Grant Date: July 7, 2020*

Abdullah A. Al-Salam

### Capacitive Electromagnetic Formation Surveillance Using Passive Source

*Granted Patent: U.S. Patent 10,705,240,  
Grant Date: July 7, 2020*

Daniele Colombo, Gary W. McNeice and  
Bouldin W. Brett

### Process Scheme for the Production of Optimal Quality Distillate for Olefin Production

*Granted Patent: U.S. Patent 10,711,208,  
Grant Date: July 14, 2020*

Vinod Ramaseshan, Bruce R. Beadle,  
Marcus J. Killingworth and Abdulaziz S.  
Al-Ghamdi

### Traversing Across a Wash-Out Zone in a Wellbore

*Granted Patent: U.S. Patent 10,711,548,  
Grant Date: July 14, 2020*

Frode Hveding and Saeed M. AlMubarak

### Milling Downhole Tubulars

*Granted Patent: U.S. Patent 10,711,551,  
Grant Date: July 14, 2020*

Ahmed A. Al-Ramadhan

### Wellbore Cementing System

*Granted Patent: U.S. Patent 10,711,566,  
Grant Date: July 14, 2020*

Ziyad Alsahlawi and Ossama R. Sehsah

### Well Debris Handling System

*Granted Patent: U.S. Patent 10,711,575,  
Grant Date: July 14, 2020*

Chidirim E. Ejim and Jinjiang Xiao



### Real-Time On-site Mechanical Characterization of Wellbore Cuttings

*Granted Patent: U.S. Patent 10,711,606,  
Grant Date: July 14, 2020*  
Katherine L. Hull and Younane N. Abousleiman

### Salinated Wastewater for Enhancing Hydrocarbon Recovery

*Granted Patent: U.S. Patent 10,711,582,  
Grant Date: July 14, 2020*  
Mohammed J. Al-Shakhs and Anthony R. Kovscek

### Optomechanical Part for Parabolic Mirror Fine Rotation and On-Axis Linear Positioning

*Granted Patent: U.S. Patent 10,712,269,  
Grant Date: July 14, 2020*  
Ezzat M. Hegazi, Vincent Cunningham, Christoph Stamm and Christof Brunner

### Frequency-Based Horizon Interpretation Based on Seismic Data

*Granted Patent: U.S. Patent 10,712,459,  
Grant Date: July 14, 2020*  
Mohammed Bin Gubair and Maher Al Marhoon

### Iterative and Repeatable Workflow for Comprehensive Data and Processes Integration for Petroleum Exploration and Production Assessments

*Granted Patent: U.S. Patent 10,715,598,  
Grant Date: July 14, 2020*  
Mokhles Mezghani, Nazih Najjar, Mahdi AbuAli, Rainer Zuhlke, Sedat Inan and Conrad Allen

### Cored Rock Analysis Planning through CT Images

*Granted Patent: U.S. Patent 10,715,845,  
Grant Date: July 14, 2020*  
Sinan Caliskan and Abdullah Shebatalhamd

### Multi-Pollutant Exhaust Treatment Using Seawater for Marine Applications

*Granted Patent: U.S. Patent 10,717,044,  
Grant Date: July 21, 2020*  
Christos M. Kalamaras and Esam Z. Hamad

### Composition and Method for Stimulation of Sandstone Wells

*Granted Patent: U.S. Patent 10,717,922,  
Grant Date: July 21, 2020*  
Abdullah M. Al-Dhafaeri and Nader M. Obeid

### Supercritical Carbon Dioxide Emulsified Acid

*Granted Patent: U.S. Patent 10,717,924,  
Grant Date: July 21, 2020*  
Bader G. Al-Harbi, Fawaz M. Al-Otaibi and Mohammed H. Al-Khaldi

### Process and System for Conversion of Crude Oil to Petrochemicals and Fuel Products Integrating Steam Cracking and Fluid Catalytic Cracking

*Granted Patent: U.S. Patent 10,717,941,  
Grant Date: July 21, 2020*  
Bader Bahammam, Naif Al Osaimi, Sami Barnawi and Mohammad S. Al-Ghamdi

### Thermochemical Method for Removing Organic and Inorganic Deposits from a Wellbore

*Granted Patent: U.S. Patent 10,718,184,  
Grant Date: July 21, 2020*  
Abdullah M. Al Harith

### Dynamic Contact Angle Measurement

*Granted Patent: U.S. Patent 10,718,702,  
Grant Date: July 21, 2020*  
Amar J. Alshehri and Abdulkarim M. Al-Sofi

### Systems and Methods Comprising Smart Sample Catcher for Drilling Operations

*Granted Patent: U.S. Patent 10,722,819,  
Grant Date: July 28, 2020*  
Ossama Sehsah, Victor Costa de Oliveira and Mario Rivas

### Water Separation in Flow Lines or Trunk Lines

*Granted Patent: U.S. Patent 10,722,854,  
Grant Date: July 28, 2020*  
Alwaleed A. Al-Gouhi, Nabil S. Al-Khanaifer, Abdullah M. Al-Zahrani, Mutaz A. Al-Daas, Riyad S. Al-Anazi, Yaseen A. Bokhamseen, Abdullah S. Al-Saddah and Jana M. Aljindan

### Preparation of Electrodes on CFRP Composites with Low Contact Resistance Comprising Laser-Based Surface Pre-Treatment

*Granted Patent: U.S. Patent 10,722,984,  
Grant Date: July 28, 2020*  
Khaled H. Al-Muhammadi, Gilles H. Fernard Lubineau, Marco F. Alfano and Ulrich Buttner

### Methods of Producing Composite Zeolite Catalysts for Heavy Reformate Conversion into Xylenes

*Granted Patent: U.S. Patent 10,725,650,  
Grant Date: July 28, 2020*  
Mohamed Elanany, Raed Abudawoud, Avelino Corma Canos, M. Teresa Portilla, Vincente J. Margarit Benavent, M. Teresa Navarro Villalba, M. Cristina Martinez, Ibrahim M. Al-Zahrani and Khalid Ali Al-Majnouni

### Methods of Producing Composite Zeolite Catalysts for Heavy Reformate Conversion into Xylenes

*Granted Patent: U.S. Patent 10,725,651,  
Grant Date: July 28, 2020*  
Raed Abudawoud, Vincente J. Margarit Benavent, M. Teresa Navarro Villalba, M. Cristina Martinez, Ibrahim M. Al-Zahrani, Avelino Corma Canos and M. Teresa Portilla

### Capsule Design for the Capture of Reagents

*Granted Patent: U.S. Patent 10,725,952,  
Grant Date: July 28, 2020*  
Elizabeth Q. Contreras

### Capsule Design for the Capture of Reagents

*Granted Patent: U.S. Patent 10,725,953,  
Grant Date: July 28, 2020*  
Elizabeth Q. Contreras

### Oil Recovery Process Using an Oil Recovery Composition of Aqueous Salt Solution and Dilute Polymer for Carbonate Reservoirs

*Granted Patent: U.S. Patent 10,725,957,  
Grant Date: July 28, 2020*  
Subhash C. Ayirala, Abdulkareem M. Al-Sofi and Ali A. Yousef

### Production of Upgraded Petroleum by Supercritical Water

*Granted Patent: U.S. Patent 10,725,962,  
Grant Date: July 28, 2020*  
Ki-Hyouk Choi, Joo-Hyeong Lee, Mohammad S. Garhoush and Ali H. Alshareef

### Integrated Residuum Hydrocracking and Hydrofinishing

*Granted Patent: U.S. Patent 10,725,963,  
Grant Date: July 28, 2020*  
Vinod Ramaseshan, Yufeng He, Hiren Shethna and Mohammed Wohaibi

### Thru-Tubing Retrievable Subsurface Completion System

*Granted Patent: U.S. Patent 10,724,529,  
Grant Date: July 28, 2020*  
Muhammad Arsalan and Mohamed N. Noui-Mehidi

### Sphere-Shaped Lost Circulation Material (LCM) having Hooks and Latches

*Granted Patent: U.S. Patent 10,724,527,  
Grant Date: July 28, 2020*  
Raed A. Alouhali, Timothy E. Moellendick, Md Amanullah, Mohammed K. Al-Arfaj and Mohammed Al Rashead

### Rapidly Cooling a Geologic Formation in which a Wellbore is Formed

*Granted Patent: U.S. Patent 10,724,537,  
Grant Date: July 28, 2020*  
Aslan Bulekbay, Abdulkareem Harbi and Abdullah Khamees

### Rapidly Cooling a Geologic Formation in which a Wellbore is Formed

*Granted Patent: U.S. Patent 10,724,538,  
Grant Date: July 28, 2020*  
Aslan Bulekbay, Abdulkareem Harbi and Abdullah Khamees

### Multi-Fuel Internal Combustion Engines and Methods for their Operation

*Granted Patent: U.S. Patent 10,724,448,  
Grant Date: July 28, 2020*  
Yoann Viollet, Junseok Chang and Amer A. Amer

### Single Actuation Probe or Tool Deployment Mechanisms for in-Pipe Applications

*Granted Patent: U.S. Patent 10,724,669,  
Grant Date: July 28, 2020*  
Abdoulelah Al-Hannabi, Mohamed Abdelkader, Hassane A. Trigui, Sahejad Patel and Fadl H. Abdel Latif

### Plugging a Heat Exchanger Tube

*Granted Patent: U.S. Patent 10,724,808,  
Grant Date: July 28, 2020*  
Ridha Alhassan, Jalal Ramdhan, Shadi Hazmi and Abdullah Al-Otaibi

### Method and Apparatus for CT Scanning of Longer Whole Cores

*Granted Patent: U.S. Patent 10,724,972,  
Grant Date: July 28, 2020*  
Sinan Caliskan and Abdullah Shebatalhamd

### Determining Chemical Oxygen Demand

*Granted Patent: U.S. Patent 10,725,011,  
Grant Date: July 28, 2020*  
Nasir Ullattampoyil and Abdulaziz M. Rueshed

### Characterization of Crude Oil by Fourier Transform Ion Cyclotron Resonance Mass Spectrometry

*Granted Patent: U.S. Patent 10,725,013,  
Grant Date: July 28, 2020*  
Omer R. Koseoglu, Adnan Al-Hajji, Hendrik Muller and Hanadi H. Jawad

### Salt Analyzer for Crude Oil

*Granted Patent: U.S. Patent 10,725,014,  
Grant Date: July 28, 2020*  
Fahad A. Al-Amri

### Determining Permeability Variation

*Granted Patent: U.S. Patent 10,725,198,  
Grant Date: July 28, 2020*  
Hassan W. Al Hashim, Jinxun Wang, Abdulkareem M. Al-Sofi and Amar J. Alshehri

### Hybrid Particle Mix for Seal and Plug Quality Enhancement

*Granted Patent: U.S. Patent 10,751,068,  
Grant Date: August 4, 2020*  
Md Amanullah, Mohammed K. Al-Arfaj and Turki T. Alsubaie

### Well Treatment Fluid Having an Acidic Nanoparticle-Based Dispersion and a Polyamine

*Granted Patent: U.S. Patent 10,751,069,  
Grant Date: August 4, 2020*  
Vikrant B. Wagle, Rajendra A. Kalgaonkar, Abdullah S. Al-Yami and Zainab Alsaihati

### Systems and Methods for Stuck Drill String Mitigation

*Granted Patent: U.S. Patent 10,751,432,  
Grant Date: August 4, 2020*  
Krzysztof Machocki and Michael Affleck

### Induced Cavitation to Prevent Scaling on Wellbore Pumps

*Granted Patent: U.S. Patent 10,751,441,  
Grant Date: August 4, 2020*  
Jinjiang Xiao

### Laser-Induced Plasma Tool

*Granted Patent: U.S. Patent 10,751,450,  
Grant Date: August 4, 2020*  
Damian P. San-Roman-Alerigi and Sameeh I. Batarseh

### Wellbore Analysis Using Tm01 and Te01 Mode Radar Waves

*Granted Patent: U.S. Patent 10,751,457,  
Grant Date: August 4, 2020*  
Sunder Ramachandran and Aydin Babakhani

### Apparatus and Method for the Nondestructive Measurement of Hydrogen Diffusivity

*Granted Patent: U.S. Patent 10,752,163,  
Grant Date: August 4, 2020*  
Mohamed Shibly, Kaamil Ur Rahman, Abderrazak Traidia and Abdullah Enezi

### Assessment of Inaccessible Pore Volume for Polymer Flooding

*Granted Patent: U.S. Patent 10,752,516,  
Grant Date: August 4, 2020*  
Ahmad M. Alharbi, Hyung T. Kwak and Jun Gao

### Electronic Document Workflow

*Granted Patent: U.S. Patent 10,753,178,  
Grant Date: August 4, 2020*  
Majid Al-Roqaie

### Power Control System

*Granted Patent: U.S. Patent 10,754,821,  
Grant Date: August 4, 2020*  
Mohamed Y. Haj-Maharsi and Altalhi A. Abdulaziz

### Invert Emulsion Drilling Fluids

*Granted Patent: U.S. Patent 10,758,250,  
Grant Date: August 11, 2020*  
Vikrant B. Wagle and Abdullah S. Al-Yami

### Pressure Pulse Assisted Injection WaterFlooding Processes for Carbonate Reservoirs

*Granted Patent: U.S. Patent 10,758,253,  
Grant Date: August 11, 2020*  
Ali Yousef and Subhash Ayirala

### High Temperature Fracturing Fluids with Nano-Crosslinkers

*Granted Patent: U.S. Patent 10,758,256,  
Grant Date: August 11, 2020*  
Ghaithan A. Al-Muntasheri, Feng Liang, Hooisweng Ow, Jason Cox and Martin E. Poitzsch

### Drilling a Rock Formation with a Drill Bit Assembly with Electrodes

*Granted Patent: U.S. Patent 10,758,536,  
Grant Date: August 11, 2020*  
Scott Fraser and Ben Bamford

### Repulsion Force Systems and Methods for Metal Fish Retrieval

*Granted Patent: U.S. Patent 10,758,554,  
Grant Date: August 11, 2020*  
Ali Al-Safwany

### Apparatus and Method for Producing Oil and Gas Using Buoyancy Effect

*Granted Patent: U.S. Patent 10,758,572,  
Grant Date: August 11, 2020*  
Mari H. Alqahtani

### Methods of Using a Laser-Induced Plasma Tool

*Granted Patent: U.S. Patent 10,758,579,  
Grant Date: August 11, 2020*  
Sameeh I. Batarseh and Damian P. San-Roman-Alerigi

### Monitoring Operating Conditions of a Rotary Steerable System

*Granted Patent: U.S. Patent 10,758,587,  
Grant Date: August 11, 2020*  
Ossama Sehsah and Mohammed Al-Khowaildi

### In Situ Thermal Response Fluid Characterization

*Granted Patent: U.S. Patent 10,758,602,  
Grant Date: August 11, 2020*  
Mohamed N. Noui-Mehidi and Sameeh I. Batarseh

### Locally Actuated Partial Stroke Testing System

*Granted Patent: U.S. Patent 10,758,912,  
Grant Date: August 11, 2020*  
Fawaz A. Al-Sahan

### Analyzing a Rock Sample

*Granted Patent: U.S. Patent 10,759,326,  
Grant Date: August 11, 2020*  
David Jacobi, John Longo, Quishi Sun and Jordan Kone

### Controlling Flow of Black Powder in Hydrocarbon Pipelines

*Granted Patent: U.S. Patent 10,744,514,  
Grant Date: August 18, 2020*  
James C. Hassell

### Apparatus and Method for In Situ Cathodic Protection of Piggable Water Pipelines

*Granted Patent: U.S. Patent 10,744,543,  
Grant Date: August 18, 2020*  
Husain M. Al-Mahrous

### Oil-Based Drilling Fluid Compositions Which Include Layered Double Hydroxides as Rheology Modifiers

*Granted Patent: U.S. Patent 10,745,606,  
Grant Date: August 18, 2020*  
Andrew Whiting, Michael Hodder, Manohara G. Veerabhadrapa, John A. Hall, Musarrat H. Mohammed, Hugh C. Greenwell and Gasan Alabedi

### Method and Composition for Sealing a Subsurface Formation

*Granted Patent: U.S. Patent 10,745,610,  
Grant Date: August 18, 2020*  
Rajendra A. Kalgaonkar and Vikrant B. Wagle

### Formation Fracturing Using Heat Treatment

*Granted Patent: U.S. Patent 10,746,005,  
Grant Date: August 18, 2020*  
Khaled A. Al-Buraik

### Weight on Bit Calculations with Automatic Calibration

*Granted Patent: U.S. Patent 10,746,008,  
Grant Date: August 18, 2020*  
Hermann F. Spoerker

### Weight on Bit Calculations with Automatic Calibration

*Granted Patent: U.S. Patent 10,746,010,  
Grant Date: August 18, 2020*  
Hermann F. Spoerker



### Smart Coating Device for Storage Tank Monitoring and Calibration

*Granted Patent: U.S. Patent 10,746,554,  
Grant Date: August 18, 2020*  
Ali Outa, Ihsan Al-Taie and Enrico Bovero

### RFID Triangulated Tank Gauging and Inventory Management System

*Granted Patent: U.S. Patent 10,746,866,  
Grant Date: August 18, 2020*  
Fouad M. Alkhabbaz

### Systems and Methods for Preventing Damage to Unseen Utility Assets

*Granted Patent: U.S. Patent 10,748,427,  
Grant Date: August 18, 2020*  
Muhammad Al-Juaid, Mazen A. Baragaba and Marek Ziderk

### Methods for Producing Mesoporous Zeolite Multifunctional Catalysts for Upgrading Pyrolysis Oil

*Granted Patent: U.S. Patent 10,751,709,  
Grant Date: August 25, 2020*  
Veera Venkata R Tammana, Ke Zhang and Miao Sun

### Methods for Producing Multifunctional Catalysts for Upgrading Pyrolysis Oil

*Granted Patent: U.S. Patent 10,751,710,  
Grant Date: August 25, 2020*  
Miao Sun

### Processes for Fracturing Using Shape Memory Alloys

*Granted Patent: U.S. Patent 10,752,828,  
Grant Date: August 25, 2020*  
Ahmed M. Gomaa, Khalid M. Alruwaili and Ghaithan A. Al-Muntasher

### Integrated Hydrothermal Process to Upgrade Heavy Oil

*Granted Patent: U.S. Patent 10,752,847,  
Grant Date: August 25, 2020*  
Ali S. Al-Nasir, Ki-Hyoun Choi, Mazin M. Fathi and Bader M. Al-Otaibi

### Forming Mineral in Fractures in a Geological Formation

*Granted Patent: U.S. Patent 10,753,190,  
Grant Date: August 25, 2020*  
Desmond Schipper, Katherine L. Hull and Mohammad H. Haque

### Systems and Methods to Identify and Inhibit Spider Web Borehole Failure in Hydrocarbon Wells

*Granted Patent: U.S. Patent 10,753,205,  
Grant Date: August 25, 2020*  
Mohammed S. Ameen

### Photonic Sensing Analytical Device

*Granted Patent: U.S. Patent 10,753,729,  
Grant Date: August 25, 2020*  
Enrico Bovero, Hawraa Bin Saad, Tim Briggs and Dan Linehan

### Smart High Integrity Protection System

*Granted Patent: U.S. Patent 10,753,852,  
Grant Date: August 25, 2020*  
Pedro A. Mujica

### Physical Reservoir Rock Interpretation in a 3D Petrophysical Modeling Environment

*Granted Patent: U.S. Patent 10,753,918,  
Grant Date: August 25, 2020*  
Roger R. Sung

### Methods and Systems of Upgrading Heavy Aromatics Stream to Petrochemical Feedstock

*Granted Patent: U.S. Patent 10,759,725,  
Grant Date: September 1, 2020*  
Omer R. Koseoglu and Robert P. Hodgkins

### Cationic Polymers and Porous Materials

*Granted Patent: U.S. Patent 10,759,881,  
Grant Date: September 1, 2020*  
Yu Han, Wei Xu, Miao Sun, Qiwei Tian, Xinglong Dong, Zhaohui Liu, Jean-Marie Basset, Youssef Saih and Sohel Shaikh

### Rapidly Dehydrating Lost Circulation Material (LCM)

*Granted Patent: U.S. Patent 10,759,984,  
Grant Date: September 1, 2020*  
Md Amanullah

### Loss Circulation Material Composition having Alkaline Nanoparticle-Based Dispersion and Water-Soluble Hydrolysable Ester

*Granted Patent: U.S. Patent 10,759,986,  
Grant Date: September 1, 2020*  
Vikrant B. Wagle, Rajendra A. Kalgaonkar, Abdullah S. Al-Yami and Zainab Alsaihati

### System for Conversion of Crude Oil to Petrochemicals and Fuel Products Integrating Vacuum Gas Oil Hydrocracking and Steam Cracking

*Granted Patent: U.S. Patent 10,760,011,  
Grant Date: September 1, 2020*  
Mohammad S. Al-Ghamdi

### System for Conversion of Crude Oil to Petrochemicals and Fuel Products Integrating Steam Cracking and Conversion of Naphtha into Chemical Rich Reformate

*Granted Patent: U.S. Patent 10,760,012,  
Grant Date: September 1, 2020*  
Bader Bahammam, Naif Al Osaimi, Sami Barnawi and Mohammad S. Al-Ghamdi

### Preventing Hydrate Formation in a Flow Line

*Granted Patent: U.S. Patent 10,760,025,  
Grant Date: September 1, 2020*  
Jana M. Aljindan

### System and Method for Subsurface Cable Insertion for the Protection of Underground Assets

*Granted Patent: U.S. Patent 10,760,244,  
Grant Date: September 1, 2020*  
Thibault Villette, Iqbal Hussain and Waheed Alrafai

### Conditioning a Subterranean Formation

*Granted Patent: U.S. Patent 10,760,395,  
Grant Date: September 1, 2020*  
Jilin J. Zhang, Feng Liang, Leiming Li and Bitao Lai

### Using Radio Waves to Fracture Rocks in a Hydrocarbon Reservoir

*Granted Patent: U.S. Patent 10,760,396,  
Grant Date: September 1, 2020*  
Jin-Hong Chen, Daniel T. Georgi, Hui-Hai Liu and Davis L. Arthur

### Solvent-Based Adsorbent Regeneration for Onboard Octane On-Demand and Cetane On-Demand

*Granted Patent: U.S. Patent 10,760,507,  
Grant Date: September 1, 2020*  
Esam Z. Hamad, Eman Tora, Amer A. Amer and Junseok Chang

### Fluid Evaluation Devices for Oil and Gas Applications

*Granted Patent: U.S. Patent 10,760,955,  
Grant Date: September 1, 2020*  
Fahad S. Al-Namasi

### Fabricating Calcite Nanofluidic Channels

*Granted Patent: U.S. Patent 10,761,428,  
Grant Date: September 1, 2020*  
Dong Kyu Cha, Mohammed B. Al-Otaibi and Ali A. Al-Yousef

### Parallel Solution for Fully Coupled Fully Implicit Wellbore Modeling in Reservoir Simulation

*Granted Patent: U.S. Patent 10,762,258,  
Grant Date: September 1, 2020*  
Larry S. Fung

### Helium Recovery from Gaseous Streams

*Granted Patent: U.S. Patent 10,765,995,  
Grant Date: September 8, 2020*  
Feras Hamad, Taib Abang, Sebastien A. Duval, Megat A. Ritahuddeen and Milind Vaidya

### Reusable Buoyancy Modules for Buoyancy Control of Underwater Vehicles

*Granted Patent: U.S. Patent 10,766,147,  
Grant Date: September 8, 2020*  
Hassane A. Trigui, Ali H. Outa, Fadl H. Abdel Latif and Sahejad Patel

### Ultrafiltration of Polyisooolefin Copolymers and Polyisooolefin Copolymers with Reduced Oligomer Content

*Granted Patent: U.S. Patent 10,766,974,  
Grant Date: September 8, 2020*  
Conrad Siegers

### Nanosilica Dispersion Well Treatment Fluid

*Granted Patent: U.S. Patent 10,767,094,  
Grant Date: September 8, 2020*  
Vikrant B. Wagle and Abdullah S. Al-Yami

### Hybrid Particle Mix for Seal and Plug Quality Enhancement

*Granted Patent: U.S. Patent 10,767,095,  
Grant Date: September 8, 2020*  
Md Amanullah, Mohammed K. Al-Arfaj and Turki T. Alsubaie

### Date Tree Waste-Based Binary Fibrous Mix for Moderate to Severe Loss Control

*Granted Patent: U.S. Patent 10,767,096,  
Grant Date: September 8, 2020*  
Md Amanullah

### Invert Emulsion Drilling Fluids with Fatty Acid and Fatty Diol Rheology Modifiers

Granted Patent: U.S. Patent 10,767,097,  
Grant Date: September 8, 2020

Vikrant B. Wagle and Abdullah S. Al-Yami

### Compositions and Methods for Sealing off Flow Channels in Contact with Wet Cement

Granted Patent: U.S. Patent 10,767,099,  
Grant Date: September 8, 2020

B. Raghava Reddy and Matthew G. Hilfiger

### Enhanced Light Olefin Yield via Steam Catalytic Downer Pyrolysis of Hydrocarbon Feedstock

Granted Patent: U.S. Patent 10,767,117,  
Grant Date: September 8, 2020

Muased S. Al-Ghrami, Wei Xu and Aaron Akah

### Simultaneous Crude Oil Dehydration, Desalting, Sweetening and Stabilization

Granted Patent: U.S. Patent 10,767,121,  
Grant Date: September 8, 2020

Mohamed Soliman

### Liner Installation with Inflatable Packer

Granted Patent: U.S. Patent 10,767,452,  
Grant Date: September 8, 2020

Muhammad Arsalan, Henrik W. Clayborough, Jarl A. Fellinghaug and Brett W. Bouldin

### Characterization of Crude Oil-Water Interfacial Film Rigidity to Enhance Oil Recovery

Granted Patent: U.S. Patent 10,767,458,  
Grant Date: September 8, 2020

Subhash Ayirala and Ali Yousef

### Systems and Methods for Detection of Induced Micro Fractures

Granted Patent: U.S. Patent 10,767,473,  
Grant Date: September 8, 2020

Jilin J. Zhang, Hui-Hai Liu and Gary Eppler

### Recovery and Reuse of Waste Energy in Industrial Facilities

Granted Patent: U.S. Patent 10,767,952,  
Grant Date: September 8, 2020

Mahmoud B. Noureldin and Hani M. Al-Saed

### Thermography Image Processing with Neural Networks to Identify Corrosion under Insulation (CUI)

Granted Patent: U.S. Patent 10,768,094,  
Grant Date: September 8, 2020

Ayman Amer, Ali Alshehri, Brian J. Parrott and Muhammad Sarraj

### Parallel Solution for Fully Coupled Fully Implicit Wellbore Modeling in Reservoir Simulation

Granted Patent: U.S. Patent 10,769,526,  
Grant Date: September 8, 2020

Larry S. Fung

### Robotic Solar Panel Cleaning System

Granted Patent: U.S. Patent 10,771,008,  
Grant Date: September 8, 2020

Abdullah M. Al-Otaibi

### Maintaining a Solar Power Module

Granted Patent: U.S. Patent 10,771,009,  
Grant Date: September 8, 2020

James C. Hassell and Luiz Do Val

### Zeolites, the Production Thereof, and Their Uses for Upgrading Heavy Oils

Granted Patent: U.S. Patent 10,773,248,  
Grant Date: September 15, 2020

Essam Al-Sayed, Lianhui Ding, Kareemuddin M. Shaik, Abdennour Bourane and Manal Al-Eid

### Process for Epoxidation of Unsaturated Polymer

Granted Patent: U.S. Patent 10,774,158,  
Grant Date: September 15, 2020

Brianna Binder, Sarah Elliott, Gregory J.E. Davidson and Sharon Guo

### Polymer Gel with Nanocomposite Crosslinker

Granted Patent: U.S. Patent 10,774,211,  
Grant Date: September 15, 2020

Ayman Al-Mohsin, Mohammed A. Bataweel, Faheem Ahmed and Edreese Al-Sharaeh

### High Performance Brine Viscosifier

Granted Patent: U.S. Patent 10,774,255,  
Grant Date: September 15, 2020

Peter J. Boul

### Multistage Fractionation of FCC Naphtha with Post Treatment and Recovery of Aromatics and Gasoline Fractions

Granted Patent: U.S. Patent 10,774,276,  
Grant Date: September 15, 2020

Ali H. Alshareef

### Apparatus and Method for In Situ Stabilization of Unconsolidated Sediment in Core Samples

Granted Patent: U.S. Patent 10,774,605,  
Grant Date: September 15, 2020

Nikolaos A. Michael, Maher I. Marhoon and Peng Lu

### Method and System for Microannulus Sealing by Galvanic Deposition

Granted Patent: U.S. Patent 10,774,611,  
Grant Date: September 15, 2020

Atallah N. Harbi

### Systems and Methods for Extinguishing Oil and Gas Wells

Granted Patent: U.S. Patent 10,774,616,  
Grant Date: September 15, 2020

Mohammad S. Al-Badran

### Method of Producing from a Hydrocarbon Bearing Zone with Laterals Extending from an Inclined Main Bore

Granted Patent: U.S. Patent 10,774,625,  
Grant Date: September 15, 2020

Mohamed N. Noui-Mehidi and Fakuen F. Chang

### Anisotropy and Dip Angle Determination Using Electromagnetic (EM) Impulses from Tilted Antennas

Granted Patent: U.S. Patent 10,774,656,  
Grant Date: September 15, 2020

Teruhiko Hagiwara

### Multiphase Production Boost Method and System

Granted Patent: U.S. Patent 10,774,822,  
Grant Date: September 15, 2020

Jinjiang Xiao and Shoubo Wang

### Nano-Indentation Test to Determine Mechanical Properties of Reservoir Rock

Granted Patent: U.S. Patent 10,775,560,  
Grant Date: September 15, 2020

Yanhui Han, Younane N. Abousleiman, Katherine L. Hull and Ghaithan A. Al-Muntasheri

### Simultaneous Wavefield Reconstruction and Receiver De-Ghosting of Seismic Streamer Data Using an L1 Inversion

Granted Patent: U.S. Patent 10,775,524,  
Grant Date: September 15, 2020

Yimin Sun and Dirk J. Verschuur

### Systems and Methods for Detecting Obfuscated Malware in Obfuscated Just-in-Time (JIT) Compiled Code

Granted Patent: U.S. Patent 10,776,487,  
Grant Date: September 15, 2020

Aminullah S. Tora, Faisal A. Al-Mansour, Faisal S. Al-Ghamdi and Rana Y. Al-Nujaidi

### Aerosol Processing Method for Controlled Coating of Surface Species to Generate Catalysts

Granted Patent: U.S. Patent 10,780,421,  
Grant Date: September 22, 2020

Michele L. Ostraat and Maxim Bukhovich

### Oxidized Disulfide Oil Solvent Compositions

Granted Patent: U.S. Patent 10,781,168,  
Grant Date: September 22, 2020

Omer R. Koseoglu, Robert P. Hodgkins, Adnan Al-Hajji, Hendrik Muller, Nadrah A. Alawani, Frederick M. Adam and Qaseem Saleem

### Polymer Compositions Having a Halo-Containing Polymer with a Multifunctional Phosphine Linkage

Granted Patent: U.S. Patent 10,781,501,  
Grant Date: September 22, 2020

Mark Ingratta, Sharon Guo, Phil Magill and Gregory J.E. Davidson

### Date Tree Waste-Based Compound Fibrous LCMs

Granted Patent: U.S. Patent 10,781,554,  
Grant Date: September 22, 2020

Md Amanullah

### Cement Slurries, Cured Cement and Methods of Making and Use Thereof

Granted Patent: U.S. Patent 10,781,556,  
Grant Date: September 22, 2020

Zainab Alsaihati, Abdullah S. Al-Yami, Vikrant B. Wagle, Abdullah Al-Awadh, Abdulaziz Alhelal and Nasser Alhareth

### Kerogen and Organic Matter Degrading Additive for Hydraulic Fracturing Fluids

Granted Patent: U.S. Patent 10,781,560,  
Grant Date: September 22, 2020

Katherine L. Hull, Younane N. Abousleiman, Ghaithan A. Al-Muntasheri and David Jacobi

### Stabilized Nanoparticle Compositions Comprising Ions

*Granted Patent: U.S. Patent 10,781,561, Grant Date: September 22, 2020*  
 Jason R. Cox, Hooisweng Ow and Dmitry Kosynkin

### Oil Recovery Process Using an Oil Recovery Composition of Aqueous Salt Solution and Dilute Polymer for Carbonate Reservoirs

*Granted Patent: U.S. Patent 10,781,562, Grant Date: September 22, 2020*  
 Subhash C. Ayirala, Abdulkareem M. Al-Sofi and Ali A. Yousef

### Self-Adjusting Downhole Motor

*Granted Patent: U.S. Patent 10,781,659, Grant Date: September 22, 2020*  
 Peter I. Egbe

### Thixotropic Cement Slurry and Placement Method to Cure Lost Circulation

*Granted Patent: U.S. Patent 10,781,648, Grant Date: September 22, 2020*  
 Joseph M. Shine Jr.

### Thru-Tubing Retrievable Intelligent Completion System

*Granted Patent: U.S. Patent 10,781,660, Grant Date: September 22, 2020*  
 Muhammad Arsalan and Mohamed N. Noui-Mehidi

### Systems and Methods for Optimizing Rate of Penetration in Drilling Operations

*Granted Patent: U.S. Patent 10,781,682, Grant Date: September 22, 2020*  
 Mohammad M. Al-Rubaii, Ossama Sehsah and Eno Itam Omini

### Smoothing Seismic Data

*Granted Patent: U.S. Patent 10,782,451, Grant Date: September 22, 2020*  
 Saleh Al-Dossary, Jinsong Wang and Bander Jumah

### Seismic Image Orientation Using 3D Integration Operations

*Granted Patent: U.S. Patent 10,783,693, Grant Date: September 22, 2020*  
 Saleh Al-Dossary and Jinsong Wang

### Composition of Encapsulated Chemical Additives and Methods for Preparation of the Same

*Granted Patent: U.S. Patent 10,787,600, Grant Date: September 29, 2020*  
 Elizabeth Q. Contreras and B. Raghava Reddy

### Modified USY-Zeolite Catalyst for Reforming Hydrocarbons

*Granted Patent: U.S. Patent 10,787,618, Grant Date: September 29, 2020*  
 Omer R. Koseoglu, Robert P. Hodgkins, Ali H. Al-Shareef, Koji Uchida, Mitsunori Watabe and Kenji Nita

### Magnetic Proppants for Enhanced Fracturing

*Granted Patent: U.S. Patent 10,787,893, Grant Date: September 29, 2020*  
 Sameeh I. Batarseh

### Sampling Techniques to Detect Hydrocarbon Seepage

*Granted Patent: U.S. Patent 10,787,903, Grant Date: September 29, 2020*  
 Mahdi AbuAli, Maher Marhoon and Khaled Aroui

### Gelation Characterization in Slim Tubes

*Granted Patent: U.S. Patent 10,788,410, Grant Date: September 29, 2020*  
 Jinxun Wang, Abdulkareem M. Al-Sofi and Amar J. Alshehri

### Generating a Reflectivity Model of Subsurface Structures

*Granted Patent: U.S. Patent 10,788,597, Grant Date: September 29, 2020*  
 Young Seo Kim, Ali A. Almomin, Woodon Jeong and Constantine Tsingas

### Solid Oxide Fuel Cell Stack with Reduced Leakage Unit Cells

*Granted Patent: U.S. Patent 10,790,519, Grant Date: September 29, 2020*  
 Sai P. Katikaneni, Inyong Kang, Jinwoo Park, Hyumdal Song, Hyunbae Park and Byungwook Park

### Modification of Bentonite Properties for Drilling Fluids

*Granted Patent: U.S. Patent 10,793,760, Grant Date: October 6, 2020*  
 Mansour A. Al-Shafei, Akram A. Alflow, Awadh M. Al-Mofleh, Jamal M. Al-Aamri, Syed Rehan Ahmad Zaidi and Amer A. Al-Tuwailib

### Layered Double Hydroxides for Oil-Based Drilling Fluids

*Granted Patent: U.S. Patent 10,793,762, Grant Date: October 6, 2020*  
 Andrew Whiting, Michael Hodder, Manohara G. Veerabhadrapa, John A. Hall, Musarrat H. Mohammed, Hugh C. Greenwell and Gasan Alabedi

### Stabilized Foams with Tailored Water Chemistry for Mobility Control in Gas Injection Processes

*Granted Patent: U.S. Patent 10,793,767, Grant Date: October 6, 2020*  
 Zuhair AlYousif, Subhash Ayirala and Mustafa Alkhowaildi

### Solvent for Use in Aromatic Extraction Process

*Granted Patent: U.S. Patent 10,793,782, Grant Date: October 6, 2020*  
 Omer R. Koseoglu, Robert P. Hodgkins, Adnan Al-Hajji, Hendrik Muller and Nadrah A. Alawani

### Systems and Methods for the Conversion of Heavy Oils to Petrochemical Products

*Granted Patent: U.S. Patent 10,793,792, Grant Date: October 6, 2020*  
 Lianhui Ding, Sherif Mohamed, Ibrahim Al-Nutaifi, Alberto L. Ballesteros, Ibrahim A. Abba and Essam Al-Sayed

### Process and System for Conversion of Crude Oil to Petrochemicals and Fuel Products Integrating Solvent Deasphalting of Vacuum Residue

*Granted Patent: U.S. Patent 10,793,794, Grant Date: October 6, 2020*  
 Bader Bahammam, Naif Al Osaimi, Sami Barnawi and Mohammad S. Al-Ghamdi

### Well Debris Handling System

*Granted Patent: U.S. Patent 10,794,151, Grant Date: October 6, 2020*  
 Chidirim E. Ejim and Jinjiang Xiao

### Downhole Tool for Fracturing a Formation Containing Hydrocarbons

*Granted Patent: U.S. Patent 10,794,164, Grant Date: October 6, 2020*  
 Sameeh I. Batarseh and Haitham A. Othman

### Smart System for Selection of Wellbore Drilling Fluid Loss Circulation Material

*Granted Patent: U.S. Patent 10,794,170, Grant Date: October 6, 2020*  
 Hugo Cuellar, Rafael Pino Rojas, Victor Costa de Oliveira and Khaled Abouelnaaj.

### Contact Angle Measurement with Sonication

*Granted Patent: U.S. Patent 10,794,807, Grant Date: October 6, 2020*  
 Mohammed Al-Geer and Amar Al-Shehri

### Dynamically Determining a Rock Wettability Alteration

*Granted Patent: U.S. Patent 10,794,812, Grant Date: October 6, 2020*  
 Ahmed Gmira and Mohammed El Geer

### Characterization of Crude Oil by Ultraviolet Visible Spectroscopy

*Granted Patent: U.S. Patent 10,794,821, Grant Date: October 6, 2020*  
 Omer R. Koseoglu, Adnan Al-Hajji and Gordon Jamieson

### Combined Water Cut and Salinity Meter

*Granted Patent: U.S. Patent 10,794,846, Grant Date: October 6, 2020*  
 Michael J. Black and Mohamed N. Noui-Mehidi

### Combined Water Cut and Salinity Meter

*Granted Patent: U.S. Patent 10,794,847, Grant Date: October 6, 2020*  
 Michael J. Black and Mohamed N. Noui-Mehidi

### Date Tree Waste-Based Compound Fibrous LCMs

*Granted Patent: U.S. Patent 10,800,959, Grant Date: October 13, 2020*  
 Md Amanullah

### Date Tree Leaflet-Based Flaky Lost Circulation Material

*Granted Patent: U.S. Patent 10,800,960, Grant Date: October 13, 2020*  
 Md Amanullah

### System for Conversion of Crude Oil to Petrochemicals and Fuel Products Integrating Delayed Coking of Vacuum Residue

*Granted Patent: U.S. Patent 10,800,977,  
Grant Date: October 15, 2020*

Bader Bahammam, Naif Al Osaimi, Sami Barnawi and Mohammad S. Al-Ghamdi

### Non-Solvent Asphaltene Removal from Crude Oil Using Solid Heteropoly Compounds

*Granted Patent: U.S. Patent 10,800,979,  
Grant Date: October 15, 2020*

Miao Sun, Faisal M. Melebari and Mohammed Al-Daous

### Non-Solvent Asphaltene Removal from Crude Oil Using Solid Heteropoly Compounds

*Granted Patent: U.S. Patent 10,800,980,  
Grant Date: October 15, 2020*

Miao Sun, Faisal M. Melebari and Mohammed Al-Daous

### Process for Producing Diesel Fuel from Olefinic Refinery Feedstreams

*Granted Patent: U.S. Patent 10,800,981,  
Grant Date: October 15, 2020*

Omer R. Koseoglu

### System for Conversion of Crude Oil to Petrochemicals and Fuel Products Integrating Vacuum Residue Conditioning and Base Oil Production

*Granted Patent: U.S. Patent 10,800,985,  
Grant Date: October 15, 2020*

Bader Bahammam, Naif Al Osaimi, Sami Barnawi and Mohammad S. Al-Ghamdi

### Adsorbent Circulation for Onboard Octane on-Demand and Cetane on-Demand

*Granted Patent: U.S. Patent 10,801,422,  
Grant Date: October 15, 2020*

Esam Z. Hamad, Eman Tora, Amer A. Amer and Junseok Chang

### Multiphase Production Boost Method and System

*Granted Patent: U.S. Patent 10,801,482,  
Grant Date: October 15, 2020*

Jinjiang Xiao and Shoubo Wang

### Recovery and Reuse of Waste Energy in Industrial Facilities

*Granted Patent: U.S. Patent 10,801,785,  
Grant Date: October 15, 2020*

Mahmoud B. Noureldin and Hani M. Al-Saed

### Method of Synthesis of Nano-Sized Beta Zeolites Containing Mesopores and Uses Thereof

*Granted Patent: U.S. Patent 10,807,078,  
Grant Date: October 20, 2020*

Manal Eid, Lianhui Ding and Kareemuddin Shaik

### Controlled Catalytic Oxidation of MEROX Process Byproducts in Integrated Refinery Process

*Granted Patent: U.S. Patent 10,807,947,  
Grant Date: October 20, 2020*

Omer R. Koseoglu and Robert P. Hodgkins

### Rubber Composition

*Granted Patent: U.S. Patent 10,808,115,  
Grant Date: October 20, 2020*

Martin Van Duin, Victor F. Quiroga Norambuena and Maria Alvarez-Grima

### Date Tree Waste-Based Binary Fibrous Mix for Moderate to Severe Loss Control

*Granted Patent: U.S. Patent 10,808,160,  
Grant Date: October 20, 2020*

Md Amanullah

### Ecofriendly Emulsifier Synthesis from Esterified Waste Vegetable Oil for Wellbore Drilling Fluids

*Granted Patent: U.S. Patent 10,808,161,  
Grant Date: October 20, 2020*

Jothibasu Ramasamy and Md Amanullah

### Integrated Gas Oil Separation Plant for Crude Oil and Natural Gas Processing

*Granted Patent: U.S. Patent 10,808,180,  
Grant Date: October 20, 2020*

Mohamed Soliman, Samusideen Salu, Talal Al-Zahrani and Nisar Ansari

### Systems and Methods for Separation and Extraction of Heterocyclic Compounds and Polynuclear Aromatic Hydrocarbons from a Hydrocarbon Feedstock

*Granted Patent: U.S. Patent 10,808,186,  
Grant Date: October 20, 2020*

Ahmad Hammad, Alberto L. Ballesteros and Zaki Yusuf

### System for Conversion of Crude Oil to Petrochemicals and Fuel Products Integrating Vacuum Residue Hydroprocessing

*Granted Patent: U.S. Patent 10,808,187,  
Grant Date: October 20, 2020*

Bader Bahammam, Naif Al Osaimi, Sami Barnawi and Mohammad S. Al-Ghamdi

### Modeling Intersecting Faults and Complex Wellbores in Reservoir Simulation

*Granted Patent: U.S. Patent 10,808,501,  
Grant Date: October 20, 2020*

Larry S. Fung, Xiang Y. Ding and Ali H. Dogru

### Self-Winding Power Generating Systems and Methods for Downhole Environments

*Granted Patent: U.S. Patent 10,808,504,  
Grant Date: October 20, 2020*

Chinthaka P. Gooneratne and Bodong Li

### Surface Logging Wells Using Depth Tagging of Cuttings

*Granted Patent: U.S. Patent 10,808,529,  
Grant Date: October 20, 2020*

Hooisweng Ow, Jason R. Cox, Martin E. Poitzsch, Daniel Georgi and Alberto F. Marsala

### Photoacoustic Gas Detection

*Granted Patent: U.S. Patent 10,809,229,  
Grant Date: October 20, 2020*

Weichang Li, Sebastian Csutak, Angelo Sampedro and Gregory D. Ham

### Apparatus and Method for the Nondestructive Measurement of Hydrogen Diffusivity

*Granted Patent: U.S. Patent 10,809,241,  
Grant Date: October 20, 2020*

Abderrazak Traidia, Mohammed Al-Shahrani and Sebastien A. Duval

### System and Method for Using a Unidirectional Watermark for Information Leak Identification

*Granted Patent: U.S. Patent 10,811,018,  
Grant Date: October 20, 2020*

Peter Magdina, Hussain A. Al-Nasser, Kashif Khawaja and Abdullah Al-Makki

### Attachment Mechanisms for Stabilization of Subsea Vehicles

*Granted Patent: U.S. Patent 10,814,495,  
Grant Date: October 27, 2020*

Fadl H. Abdel Latif, Ali Outa, Sahejad Patel, Hassane A. Trigui and Abdullah Arab

### Nanocomposite Comprising a Layer Silicate and a Rubber

*Granted Patent: U.S. Patent 10,815,359,  
Grant Date: October 27, 2020*

Thomas Fruh, Nadine Gottlieb, Alex Lucassen, Andreas Bischoff, Robert Hans Schuster and Marion Schellenberg

### Sealing Gels, Process for Production Thereof and Use Thereof in Sealing Compounds for Self-Sealing Tires

*Granted Patent: U.S. Patent 10,815,364,  
Grant Date: October 27, 2020*

Christopher Kohl, Udo Schmidt, Jiawen Zhou, Thomas Fruh and Alex Lucassen

### Systems and Processes for Power Generation

*Granted Patent: U.S. Patent 10,815,454,  
Grant Date: October 27, 2020*

Ki-Hyoun Choi, Muneef F. Al-Qarzouh, Abdullah T. Alabdulhadi and Mohannad H. Alabisi

### Wellbore Parted Casing Access Tool

*Granted Patent: U.S. Patent 10,815,751,  
Grant Date: October 27, 2020*

Adib A. Al-Mumen, Ibrahim A. Al-Obaidi, Nelson O. Pinero Zambrano and Abdullah E. Al-Noaimi

### Unicode Conversion with Minimal Downtime

*Granted Patent: U.S. Patent 10,817,649,  
Grant Date: October 27, 2020*

Alaa Tashkandi, Fayez Soufyani and Abdulaziz Mulhim

### Butyl Rubber Containing Allylic Alcohol

*Granted Patent: U.S. Patent 10,822,439,  
Grant Date: November 3, 2020*

Sarah Elliott, Gregory J.E. Davidson and Sharon Guo

### Retarded Acid Systems, Emulsions, and Methods for Using in Acidizing Carbonate Formations

*Granted Patent: U.S. Patent 10,822,534,  
Grant Date: November 3, 2020*

Abdullah S. Al-Yami, Vikrant B. Wagle and Ali Al-Safran



### Refinery Preheat Train Systems and Methods

*Granted Patent: U.S. Patent 10,822,551, Grant Date: November 3, 2020*  
Mahmoud B. Noureldin and Zeeshan Farooq

### Preventing Hydrate Formation in a Flow Line

*Granted Patent: U.S. Patent 10,822,564, Grant Date: November 3, 2020*  
Jana M. Aljindan

### Laser Tool that Combines Purging Medium and Laser Beam

*Granted Patent: U.S. Patent 10,822,879, Grant Date: November 3, 2020*  
Sameeh I. Batarseh

### Curing a Lost Circulation Zone in a Wellbore

*Granted Patent: U.S. Patent 10,822,916, Grant Date: November 3, 2020*  
Saad S. Al-Shammari

### Determining Pressure Distribution in Heterogeneous Rock Formations for Reservoir Simulation

*Granted Patent: U.S. Patent 10,822,925, Grant Date: November 3, 2020*  
Ali H. Dogru

### Mitigating Corrosion of Carbon Steel Tubing and Surface Scaling Deposition in Oil Field Applications

*Granted Patent: U.S. Patent 10,822,926, Grant Date: November 3, 2020*  
Qiwei Wang and Tao Chen

### Determining Hydrocarbon Gas Maturity

*Granted Patent: U.S. Patent 10,825,716, Grant Date: November 3, 2020*  
Feng Hu Lu

### Intelligent Personal Protective Equipment

*Granted Patent: U.S. Patent 10,824,132, Grant Date: November 3, 2020*  
Samantha J. Horseman, Mohammed Al-Abdrabbuh and Yasser F. Alem

### Spring-Based Magnetic Attachment Method for Crawling Vehicle

*Granted Patent: U.S. Patent 10,829,171, Grant Date: November 10, 2020*  
Brian J. Parrott

### Systems and Processes for Producing Hydrogen from Sour Gases

*Granted Patent: U.S. Patent 10,829,571, Grant Date: November 10, 2020*  
Aadesh Harale, Mourad Younes, Maytham Musawi and Aqil Jamal

### Oxycombustion Systems and Methods with Thermally Integrated Ammonia Synthesis

*Granted Patent: U.S. Patent 10,829,584, Grant Date: November 10, 2020*  
Mourad Younes and Tidjani Niass

### Wellbore Drill Bit Nozzle

*Granted Patent: U.S. Patent 10,850,001, Grant Date: November 10, 2020*  
Ahmad M. Al-Abduljabbar

### In Situ Heating Fluids with Electromagnetic Radiation

*Granted Patent: U.S. Patent 10,850,017, Grant Date: November 10, 2020*  
Sameeh I. Batarseh and Mohamed N. Noui-Mehidi

### System and Method to Evaluate Kerogen-Rich Shale

*Granted Patent: U.S. Patent 10,850,027, Grant Date: November 10, 2020*  
Katherine L. Hull, Younane N. Abousleiman, Shannon L. Eichmann and David Jacobi

### Wet Well Prediction Using Real Time Data

*Granted Patent: U.S. Patent 10,852,152, Grant Date: November 10, 2020*  
Muhammad S. Khakwani, Abbas W. Al-Beshri and Abdullah H. Bar

### Non-Catalytic Hydrogen Generation Process for Delivery to a Hydrodesulfurization Unit and a Solid Oxide Fuel Cell System Combination for Auxiliary Power Unit Application

*Granted Patent: U.S. Patent 10,855,541, Grant Date: November 10, 2020*  
Thang V. Pham, Hasan Imran and Mohamed Daoudi

### Methods for Producing Mesoporous Zeolite Multifunctional Catalysts for Upgrading Pyrolysis Oil

*Granted Patent: U.S. Patent 10,855,894, Grant Date: November 17, 2020*  
Veera Venkata R Tammana, Ke Zhang and Miao Sun

### Polycarbonate Polyol Compositions and Methods

*Granted Patent: U.S. Patent 10,856,859, Grant Date: November 17, 2020*  
Geoffrey W. Coates, Chris A. Simoneau, Scott D. Allen, Anna E. Cherian, Jay J. Farmer and Alexei A. Gridnev

### Method for Improving Cement Toughness

*Granted Patent: U.S. Patent 10,856,950, Grant Date: November 17, 2020*  
Hasmukh A. Patel and Carl Joseph Thaemlitz

### Polysaccharide Coated Nanoparticle Compositions Comprising Ions

*Granted Patent: U.S. Patent 10,856,953, Grant Date: November 17, 2020*  
Jason R. Cox, Hooisweng Ow, Howard K. Schmidt and Shannon L. Eichmann

### Enhancing Acid Fracture Conductivity

*Granted Patent: U.S. Patent 10,856,956, Grant Date: November 17, 2020*  
Aslan Bulekbay and Ahmed M. Gomaa

### Converting Carbon-Rich Hydrocarbons to Carbon-Poor Hydrocarbons

*Granted Patent: U.S. Patent 10,856,967, Grant Date: November 17, 2020*  
Mohammed A. Al-Wohaibi, Vinod Ramaseshan, Marcus J. Killingworth and Hisham T. Al-Bassam

### Liner Hanger System

*Granted Patent: U.S. Patent 10,857,245, Grant Date: November 17, 2020*  
Syed M. Ali and Yassar K. Zia

### Tandem Cement Retainer and Bridge Plug

*Granted Patent: U.S. Patent 10,857,254, Grant Date: November 17, 2020*  
Ahmed A. Al-Mousa, Marius Neacsu and Ahmed A. Al-Ramadhan

### Well Kickoff Systems and Methods

*Granted Patent: U.S. Patent 10,857,267, Grant Date: November 17, 2020*  
Jinjiang Xiao, Rafael A. Lastra and Brian A. Roth

### Determining a Mud Weight of Drilling Fluids for Drilling through Naturally Fractured Formations

*Granted Patent: U.S. Patent 10,857,279, Grant Date: November 17, 2020*  
Younane Abousleiman, Yanhui Han, Chao Liu and Shawn Rimassa

### Generating Images of a Reservoir Based on Introduction of a Polymer-Based Contrast Agent

*Granted Patent: U.S. Patent 10,858,101, Grant Date: November 17, 2020*  
Erika S. Ellis, Howard K. Schmidt, Jason Cox and Jesus M. Felix-Servin

### Paleo Fossil and Sedimentary Structure Data Mining and Datum for Biostratigraphy

*Granted Patent: U.S. Patent 10,858,976, Grant Date: November 17, 2020*  
Roger R. Sung

### Membrane Contactor

*Granted Patent: U.S. Patent 10,845,128, Grant Date: November 24, 2020*  
Seung-Hak Choi, Sebastien A. Duval, Abdulaziz Y. Ammar and Sarah N. Almahfoodh

### Systems and Methods for Synthesis of ZSM-22 Zeolite

*Granted Patent: U.S. Patent 10,845,950, Grant Date: November 24, 2020*  
Emad N. Al-Shafei, Oki Muraza, Anas K. Jamil, Ki-Hyouk Choi and Zain H. Yamani

### Methods and Systems for Producing Para-Xylene from C8-Containing Compositions

*Granted Patent: U.S. Patent 10,845,983, Grant Date: November 24, 2020*  
Zhang Zhonglin, Shaikh Sohel, Tammana V. Venkata R, Abudawoud Raed, Beadle B. Richard, Bassam H. Tawfiq and Bilaus R. Sulaiman

### Compositions Containing NBR-Based Microgels

*Granted Patent: U.S. Patent 10,844,181, Grant Date: November 24, 2020*  
Udo Schmidt, Christopher Kohl, Jiawen Zhou and Thomas Fruh

### Loss Circulation Material for Seepage to Moderate Loss Control

*Granted Patent: U.S. Patent 10,844,265, Grant Date: November 24, 2020*  
Jothibasu Ramasamy and Md Amanullah

### Spacer Fluids and Cement Slurries That Include Surfactants

*Granted Patent: U.S. Patent 10,844,266, Grant Date: November 24, 2020*  
Abdullah S. Al-Yami, Vikrant B. Wagle and Hussain Al-Bahrani

### Cement Slurries, Cured Cement and Methods of Making and Use Thereof

*Granted Patent: U.S. Patent 10,844,271, Grant Date: November 24, 2020*  
Zainab Alsaihati, Abdullah S. Al-Yami, Vikrant B. Wagle, Abdullah Al-Awadh, Abdulaziz Alhelal and Nasser Alhareth

### Cement Slurries, Cured Cement and Methods of Making and Use Thereof

*Granted Patent: U.S. Patent 10,844,272, Grant Date: November 24, 2020*  
Zainab Alsaihati, Abdullah S. Al-Yami, Vikrant B. Wagle, Abdullah Al-Awadh, Abdulaziz Alhelal and Nasser Alhareth

### Chemical Looping Processes for Catalytic Hydrocarbon Cracking

*Granted Patent: U.S. Patent 10,844,289, Grant Date: November 24, 2020*  
Wei Xu, Ibrahim A. Abba, Rodrigo Sandoval Rivera and Ali Ola

### Systems and Processes to Deoxygenate Aromatic-Rich Hydrocarbon Streams

*Granted Patent: U.S. Patent 10,844,295, Grant Date: November 24, 2020*  
Omer R. Koseoglu and Robert P. Hodgkins

### Conversion of Crude Oil to Aromatic and Olefinic Petrochemicals

*Granted Patent: U.S. Patent 10,844,296, Grant Date: November 24, 2020*  
Thamer A. Mohammad, Raed Abudawoud, Alberto L. Ballesteros and Essam Al-Sayed

### Fiber Reinforced and Powered Coil Tubing

*Granted Patent: U.S. Patent 10,844,673, Grant Date: November 24, 2020*  
Rafael A. Lastra, Jinjiang Xiao and Brian A. Roth

### Downhole Ultrasonic Actuator System for Mitigating Lost Circulation

*Granted Patent: U.S. Patent 10,844,689, Grant Date: November 24, 2020*  
Jothibasu Ramasamy and Chinthaka P. Gooneratne

### Self-Powered Miniature Mobile Sensing Device

*Granted Patent: U.S. Patent 10,844,694, Grant Date: November 24, 2020*  
Chinthaka P. Gooneratne, Bodong Li and Shaohua Zhou

### Bypass System and Method for Inverted ESP Completion

*Granted Patent: U.S. Patent 10,844,699, Grant Date: November 24, 2020*  
Jinjiang Xiao and Rafael A. Lastra

### Removing Water Downhole in Dry Gas Wells

*Granted Patent: U.S. Patent 10,844,700, Grant Date: November 24, 2020*  
Alwaleed A. Al-Gouhi

### Balancing Axial Thrust in Submersible Well Pumps

*Granted Patent: U.S. Patent 10,844,701, Grant Date: November 24, 2020*  
Jinjiang Xiao and Chidirim E. Ejim

### Ultrasonic Flow Measurement for Multiphase Fluids Using Swirl Blade Section Causing Vortical Flow for Central Gas Flow Region

*Granted Patent: U.S. Patent 10,845,224, Grant Date: November 24, 2020*  
Mohamed N. Noui-Mehidi

### Method for Correcting Low Permeability Laboratory Measurements for Leaks

*Granted Patent: U.S. Patent 10,845,292, Grant Date: November 24, 2020*  
Daniel T. Georgi, Haungye Chen and Hui-Hai Liu

### Determining Composition of a Sample

*Granted Patent: U.S. Patent 10,845,506, Grant Date: November 24, 2020*  
Ezzat M. Hegazi and Vincent B. Cunningham

### Determining Composition of a Sample

*Granted Patent: U.S. Patent 10,845,507, Grant Date: November 24, 2020*  
Ezzat M. Hegazi and Vincent B. Cunningham

### Relative Valuation Method for Naphtha Streams

*Granted Patent: U.S. Patent 10,845,555, Grant Date: November 24, 2020*  
Omer R. Koseoglu

### Virtual Source Redatuming Using Radiation Pattern Correction

*Granted Patent: U.S. Patent 10,845,494, Grant Date: November 24, 2020*  
Yang Zhao, Roy M. Burnstad and Weichang Li

### Drone-Based Electromagnetics for Early Detection of Shallow Drilling Hazards

*Granted Patent: U.S. Patent 10,845,498, Grant Date: November 24, 2020*  
Daniele Colombo, Ersan Turkoglu and Gary W. McNeice

### Optical Master Unit Alarm Collector and Translator

*Granted Patent: U.S. Patent 10,847,019, Grant Date: November 24, 2020*  
Badie A. Guwaisem and Hassan Al-Helal

### Method and Materials to Convert a Drilling Mud into a Solid Gel-Based Lost Circulation Material

*Granted Patent: U.S. Patent 10,851,279, Grant Date: December 1, 2020*  
Vikrant B. Wagle, Abdullah S. Al-Yami, Rajendra A. Kalgaonkar and Zainab Alsaihati

### Development of Anti-Bit Balling Fluids

*Granted Patent: U.S. Patent 10,851,281, Grant Date: December 1, 2020*  
Abdullah S. Al-Yami, Ahmed A. Bahamdan, Saleh A. Haidary, Vikrant B. Wagle, Hussain Al-Bahrani, Ali M. Al-Safran, Nasser Al-Hareth and Abdulla H. Awadh

### Method to Improve the Efficiency of Pipeline Transportation of Heavy Oils

*Granted Patent: U.S. Patent 10,851,514, Grant Date: December 1, 2020*  
Robert P. Hodgkins and Omer R. Koseoglu

### Conversion of Crude Oil to Aromatic and Olefinic Petrochemicals

*Granted Patent: U.S. Patent 10,851,516, Grant Date: December 1, 2020*  
Thamer A. Mohammad and Raed Abudawoud

### Multi-Level Wellhead Support Platform

*Granted Patent: U.S. Patent 10,851,596, Grant Date: December 1, 2020*  
Brian A. Roth and Jinjiang Xiao

### Wellbore Zonal Isolation

*Granted Patent: U.S. Patent 10,851,612, Grant Date: December 1, 2020*  
Alwaleed A. Al-Gouhi, Mohamed N. Noui-Mehidi, Qais M. Al Hennawi and Fadhil N. Alsayegh

### Polyurethane Foamed Annular Chemical Packer

*Granted Patent: U.S. Patent 10,851,617, Grant Date: December 1, 2020*  
Prasad B. Karadkar and Mohammed A. Bataweel

### Acoustic Testing of Core Samples

*Granted Patent: U.S. Patent 10,851,641, Grant Date: December 1, 2020*  
Yunlai Yang and Maher I Almarhoon

### Natural Gas Liquid Fractionation Plant Waste Heat Conversion to Potable Water Using Modified Multi-Effect Distillation System

*Granted Patent: U.S. Patent 10,851,679, Grant Date: December 1, 2020*  
Mahmoud B. Noureldin and Akram H. Kamel

### Measuring Source Rock Potential Using a Quantum Electronic Scanner

*Granted Patent: U.S. Patent 10,852,260, Grant Date: December 1, 2020*  
Sebastian Csutak

### Refraction-Based Surface Consistent Amplitude Compensation and Deconvolution

*Granted Patent: U.S. Patent 10,852,450, Grant Date: December 1, 2020*  
Daniele Colombo and Diego Rovetta

### Metal Organic Framework Absorbent Platforms for Removal of CO<sub>2</sub> and H<sub>2</sub>S from Natural Gas

*Granted Patent: U.S. Patent 10,857,500, Grant Date: December 8, 2020*  
Mohamed Eddaoudi, Amandine Cadiau, Prashant M. Bhatt, Karim Adil and Youssef Belmabkhout

### Process for the Production of Water and Solvent-Free Nitrile Rubbers

*Granted Patent: U.S. Patent 10,858,455, Grant Date: December 8, 2020*  
Hanns-Ingolf Paul, Paul Wagner, Rolf Feller, Jorg Kirchhoff, John Lovegrove, Florian Forner, Michael Klimpel, Peter Weuta and Sven Brandau



**Gas Generating Compositions**

*Granted Patent: U.S. Patent 10,858,565,  
Grant Date: December 8, 2020*  
B. Raghava Reddy

**Rheology Modifier for Organoclay-Free Invert Emulsion Drilling Fluid Systems**

*Granted Patent: U.S. Patent 10,858,568,  
Grant Date: December 8, 2020*  
Jothibasur Ramasamy, Vikrant B. Wagle  
and Md Amanullah

**Material Design for the Encapsulation of Additives and Release**

*Granted Patent: U.S. Patent 10,858,572,  
Grant Date: December 8, 2020*  
Elizabeth Q. Contreras

**Enhancing Acid Fracture Conductivity**

*Granted Patent: U.S. Patent 10,858,578,  
Grant Date: December 8, 2020*  
Aslan Bulekbay and Ahmed M. Gomaa

**Separation of Fractions in Hydrocarbon Samples Using an Accelerated Solvent Extractor**

*Granted Patent: U.S. Patent 10,858,596,  
Grant Date: December 8, 2020*  
Frederick Adam, Zahra Almisbaa, Mansour  
Alzayer and Faisal Alrasheed

**Core Sampler with Impregnation Windows and Method for Stabilization of Unconsolidated Sediment in Core Samples**

*Granted Patent: U.S. Patent 10,858,899,  
Grant Date: December 8, 2020*  
Nikolaos A. Michael

**Enhancing Reservoir Production Optimization through Integrating Inter-Well Tracers**

*Granted Patent: U.S. Patent 10,858,951,  
Grant Date: December 8, 2020*  
Hsieh Chen and Martin Poitzsch

**Determining Geologic Formation Permeability**

*Granted Patent: U.S. Patent 10,858,956,  
Grant Date: December 8, 2020*  
Stacey Althaus, Jin-Hong Chen and  
Hui-Hai Liu

**Machine Learning-Based Models for Phase Equilibria Calculations in Compositional Reservoir Simulations**

*Granted Patent: U.S. Patent 10,859,750,  
Grant Date: December 8, 2020*  
Vinay Raman and Todd R. Ferguson

**Identifying Network Issues Using an Agentless Probe and End-Point Network Locations**

*Granted Patent: U.S. Patent 10,862,781,  
Grant Date: December 8, 2020*  
Baher Ramady, Marek Zidek, Mawada  
Felemban and Mohammad Muneia

**Multi-Modal Polyisolefin Compositions and Processes Therefor**

*Granted Patent: U.S. Patent 10,865,299,  
Grant Date: December 15, 2020*  
Sharon Guo, Gregory J.E. Davidson and  
Brianna Binder

**Coatings for Corrosion Protection**

*Granted Patent: U.S. Patent 10,865,540,  
Grant Date: December 15, 2020*  
Abdullah A. Al-Shahrani, Gasan Alabedi  
and Ihsan Al-Taie

**Enhanced High Temperature Cross-Linked Fracturing Fluids**

*Granted Patent: U.S. Patent 10,865,542,  
Grant Date: December 15, 2020*  
Leiming Li and Feng Liang

**Downhole Ultraviolet System for Mitigating Lost Circulation**

*Granted Patent: U.S. Patent 10,865,620,  
Grant Date: December 15, 2020*  
Jothibasur Ramasamy and Chinthaka P.  
Gooneratne

**Shrouded Electrical Submersible Pump**

*Granted Patent: U.S. Patent 10,865,627,  
Grant Date: December 15, 2020*  
Abdullah M. Al-Zahrani

**Downhole Tool with CATR**

*Granted Patent: U.S. Patent 10,865,640,  
Grant Date: December 15, 2020*  
Jose O. Alvarez

**Natural Gas Liquid Fractionation Plant Waste Heat Conversion to Simultaneous Power, Cooling, and Potable Water Using Modified Goswami Cycle and New Modified Multi-Effect Distillation System**

*Granted Patent: U.S. Patent 10,865,661,  
Grant Date: December 15, 2020*  
Mahmoud B. Noureldin and Akram H.  
Kamel

**In Situ HIC Growth Monitoring Probe**

*Granted Patent: U.S. Patent 10,866,183,  
Grant Date: December 15, 2020*  
Abderrazak Traidia and Abdelmounam  
Sherik

**Formation Clay Typing from Electromagnetic Measurements**

*Granted Patent: U.S. Patent 10,866,335,  
Grant Date: December 15, 2020*  
Shouxiang M. Ma, Ping Zhang, Wael  
Abdallah and Chengbing Liu

**Configurable System for Resolving Requests Received from Multiple Client Devices in a Network System**

*Granted Patent: U.S. Patent 10,868,751,  
Grant Date: December 15, 2020*  
Mohammad D. Shammari, Adnan O.  
Haidar, Abdullah A. Tamimi, Mohammad  
A. Qahtani, Hussain H. Hajjaj and Sami  
H. Buri

**Processes for Analysis and Optimization of Multiphase Separators, Particularly in Regard to Simulated Gravity Separation of Immiscible Liquid Dispersions**

*Granted Patent: U.S. Patent 10,870,070,  
Grant Date: December 22, 2020*  
Sharon Guo, Gregory J.E. Davidson and  
Brianna Binder

**Methods for Producing Multifunctional Catalysts for Upgrading Pyrolysis Oil**

*Granted Patent: U.S. Patent 10,870,106,  
Grant Date: December 22, 2020*  
Jothibasur Ramasamy and Chinthaka P.  
Gooneratne

**Date Tree Trunk-Based Fibrous Loss Circulation Materials**

*Granted Patent: U.S. Patent 10,870,787,  
Grant Date: December 22, 2020*  
Abdullah M. Al-Zahrani

**Thermally Stable Surfactants for Oil-Based Drilling Fluids**

*Granted Patent: U.S. Patent 10,870,788,  
Grant Date: December 22, 2020*  
Mahmoud B. Noureldin and Akram H.  
Kamel

**High-Severity Fluidized Catalytic Cracking Systems and Processes Having Partial Catalyst Recycle**

*Granted Patent: U.S. Patent 10,870,802,  
Grant Date: December 22, 2020*  
Leiming Li and Feng Liang

**Removal of Olefins from Hydrothermally Upgraded Heavy Oil**

*Granted Patent: U.S. Patent 10,870,805,  
Grant Date: December 22, 2020*  
Jothibasur Ramasamy and Chinthaka P.  
Gooneratne

**Process and System for Conversion of Crude Oil to Petrochemicals and Fuel Products Integrating Steam Cracking, Fluid Catalytic Cracking and Conversion of Naphtha into Chemical Rich Reformate**

*Granted Patent: U.S. Patent 10,870,807,  
Grant Date: December 22, 2020*  
Shouxiang M. Ma, Ping Zhang, Wael  
Abdallah and Chengbing Liu

**Hydraulic Fracturing in Kerogen-Rich Unconventional Formations**

*Granted Patent: U.S. Patent 10,871,060,  
Grant Date: December 22, 2020*  
Abderrazak Traidia and Abdelmounam  
Sherik

**Treatment of Kerogen in Subterranean Zones**

*Granted Patent: U.S. Patent 10,871,061,  
Grant Date: December 22, 2020*  
Mohammad D. Shammari, Adnan O.  
Haidar, Abdullah A. Tamimi, Mohammad  
A. Qahtani, Hussain H. Hajjaj and Sami  
H. Buri

**Flow Testing Wellbores while Drilling**

*Granted Patent: U.S. Patent 10,871,069,  
Grant Date: December 22, 2020*  
Jose O. Alvarez

**Porous Micromodel Network to Simulate Formation Flows**

*Granted Patent: U.S. Patent 10,871,451,  
Grant Date: December 22, 2020*  
Jothibasur Ramasamy and Chinthaka P.  
Gooneratne

**Inspection and Failure Detection of Corrosion under Fireproofing Insulation Using a Hybrid Sensory System**

*Granted Patent: U.S. Patent 10,871,444,  
Grant Date: December 22, 2020*

Abdullah A. Al-Shahrani, Gasan Alabedi and Ihsan Al-Taie

**Real Time Analysis of Fluid Properties for Drilling Control**

*Granted Patent: U.S. Patent 10,871,762,  
Grant Date: December 22, 2020*

Jothibasu Ramasamy and Chinthaka P. Gooneratne

**Systems and Methods for Desalinating Aqueous Compositions through Hetero-Azeotropic Distillation**

*Granted Patent: U.S. Patent 10,874,957,  
Grant Date: December 29, 2020*

Guillaume Jean-François R. Raynel, Regis Didier Alain Vilagines and Duaa J. Al Saeed

**Methods for Preparing Mixed Metal Oxide Diamondoid Nanocomposites and Catalytic Systems including the Nanocomposites**

*Granted Patent: U.S. Patent 10,875,092,  
Grant Date: December 29, 2020*

Hugh C. Greenwell, Manohara G. Veerabhadrapa, John A. Hall, Andrew Whiting and Gasan Alabedi

**Enhanced Filtration Control Packages, Wellbore Servicing Fluids Utilizing the Same, and Methods of Maintaining the Structure of a Wellbore**

*Granted Patent: U.S. Patent 10,876,028,  
Grant Date: December 29, 2020*

Abdullah S. Al-Yami, Vikrant B. Wagle, Hussain Al-Bahrani, Ali M. Al-Safran and Nasser Al-Hareth

**Consolidation of Formation Particulates**

*Granted Patent: U.S. Patent 10,876,037,  
Grant Date: December 29, 2020*

Frank F. Chang and Xiaoyu Tan

**Thermally Stable Surfactants for Oil-Based Drilling Fluids**

*Granted Patent: U.S. Patent 10,876,039,  
Grant Date: December 29, 2020*

Mona Al Batal, John A. Hall, Andrew Whiting, Gasan Alabedi, Hugh C. Greenwell, Musarrat H. Mohammed and Michael Hodder

**Oil Production and Recovery with Supercritical Water**

*Granted Patent: U.S. Patent 10,876,585,  
Grant Date: December 29, 2020*

Abdulrahman A. Al-Mulhem

**Method of Fabricating Smart Photonic Structures for Material Monitoring**

*Granted Patent: U.S. Patent 10,877,192,  
Grant Date: December 29, 2020*

Aziz Fihri, Abdullah A. Al-Shahrani and Enrico Bovero

**Depressurizing a Branch Pipe**

*Granted Patent: U.S. Patent 10,877,494,  
Grant Date: December 29, 2020*

Abdulaziz M. Al-Otaibi

**Simultaneous Distributed Temperature and Vibration Sensing Using Multimode Optical Fiber**

*Granted Patent: U.S. Patent 10,880,007,  
Grant Date: December 29, 2020*

Frode Hveding, Islam Ashry, Mao Yuan, Boon Siew Ooi and Muhammad Arsalan

**Root Cause Analysis for Unified Communications Performance Issues**

*Granted Patent: U.S. Patent 10,880,152,  
Grant Date: December 29, 2020*

Baher Ramady, Zahrah Almousa and Mawada Felemban

---

## Notes

---

---

---

---

---

---

---

---

---

---

---

---

---

---

---

---

---

---

---

---

---

---

---

---



---

## Notes

---

---

---

---

---

---

---

---

---

---

---

---

---

---

---

---

---

---

---

---

---

---

---

---

---

---

# Have an article you would like to publish? Here are our guidelines.

These guidelines are designed to simplify and help standardize submissions. They need not be followed rigorously. If you have any questions, please call us.

## Length

Average of 2,500-4,000 words, plus illustrations/photos and captions. Maximum length should be 5,000 words. Articles in excess will be shortened.

## What to send

Send text in Microsoft Word format via email. Illustrations/photos should be clear and sharp. Editable files are requested for graphs, i.e., editable in Excel.

## Procedure

Notification of acceptance is usually within three weeks after the submission deadline. The article will be edited for style and clarity and returned to the author for review. All articles are subject to the company's normal review. No paper can be published without a signature at the manager level or above.

## Format

No single article need include all of the following parts. The type of article and subject covered will determine which parts to include.

### Working Title

Lorem Ipsum here.

### Abstract

Usually 150-300 words to summarize the main points.

### Introduction

Different from the abstract in that it sets the stage for the content of the article, rather than telling the reader what it is about.

### Main body

May incorporate subtitles, artwork, photos, etc.

### Conclusion/Summary

Assessment of results or restatement of points in introduction.

### Endnotes/References/Bibliography

Use only when essential. Use author/date citation method in the main body. Numbered footnotes or endnotes will be converted. Include complete publication information. Standard is *The Associated Press Stylebook*, 52<sup>nd</sup> ed. and *Webster's New World College Dictionary*, 5<sup>th</sup> ed.

### Acknowledgments

Use to thank those who helped make the article possible.

## Illustration/Tables/Photos and explanatory text

If the files are large, these can be submitted separately, due to email size limits. Initial submission may include copies of originals; however, publication will require the originals. When possible, submit original images. Color is preferable.

## File Format

Illustration files with .EPS extensions work best. Other acceptable extensions are .TIFF/.JPEG/.PICT.

## Permission(s) to reprint, if appropriate

Previously published articles are acceptable but can be published only with written permission from the copyright holder.

## Author(s)/Contributor(s)

Please include a brief biographical statement.

## Submission/Acceptance Procedures

Papers are submitted on a competitive basis and are evaluated by an editorial review board comprised of various department managers and subject matter experts. Following initial selection, authors whose papers have been accepted for publication will be notified by email.

Papers submitted for a particular issue but not accepted for that issue may be carried forward as submissions for subsequent issues, unless the author specifically requests in writing that there be no further consideration.

## Submit articles to:

Editor

*The Saudi Aramco Journal of Technology*

C-10B, Room AN-1080

North Admin Building #175

Dhahran 31311, Saudi Arabia

Tel: +966-013-876-0498

Email: [william.bradshaw.1@aramco.com.sa](mailto:william.bradshaw.1@aramco.com.sa)

## Submission deadlines

Issue	Paper submission deadline	Release date
Winter 2021	August 12, 2021	December 31, 2021
Spring 2022	November 15, 2021	March 31, 2022
Summer 2022	February 8, 2022	June 30, 2022
Fall 2022	May 17, 2022	September 30, 2022



---

## There is more.

### Evaluation of Machine Learning Methods for Prediction of Multiphase Production Rates

*Dr. Anton Gryzlov, Liliya Mironova, Dr. Sergey Safonov and Dr. Muhammad Arsalan*

**Abstract /** Multiphase flow metering is an important tool for production monitoring and optimization. Although there are many technologies available on the market, the existing multiphase meters are only accurate to a certain extent and generally are expensive to purchase and maintain.

Use of virtual flow meters are a low-cost alternative to conventional production monitoring tools, which relies on mathematical modeling rather than the use of hardware instrumentation. Supported by the availability of the data from different sensors and production history, the development of different virtual flow metering systems has become a focal point for many companies.

### SmartWater Synergy with Microsphere Injection for Permeable Carbonates

*Dongqing Cao, Dr. Ming Han, Salah H. Saleh, Dr. Subhash C. Ayirala and Dr. Ali A. Yousef*

**Abstract /** This article presents a laboratory study on the combination of SmartWater with microsphere injection to improve oil production in carbonates, which increases the sweep efficiency and oil displacement efficiency. In this study, the properties of a micro-sized polymeric microsphere were investigated, including size distribution, rheology, and zeta potential in SmartWater, compared with conventional high salinity water (HSW). Coreflooding tests using natural permeable carbonate cores were performed to evaluate flow performance and oil production potential at 95 °C and 3,100 psi pore pressure. The flow performance was evaluated by the injection of 1 pore volume (PV) microspheres, followed by excessive water injection. Oil displacement tests were also performed by injecting 1 PV of microspheres dissolved in SmartWater after conventional waterflooding.

---

To read these articles and others, go to [www.saudiaramco.com/jot](http://www.saudiaramco.com/jot)



Aramco  
Journal  
of Technology

## Liked this issue? Sign up. It's free.

To begin receiving the *Aramco Journal of Technology* please complete this form, scan and send by email to [william.bradshaw.1@aramco.com](mailto:william.bradshaw.1@aramco.com).

### Got questions?

Just give us a call at +966-013-876-0498 and we'll be happy to help!



Scan the QR code to go straight to your email and attach the form!

### Subscription Form



